

POINT SOURCE MODEL
EVALUATION AND DEVELOPMENT
STUDY

prepared by
Allan Fabrick
Ralph Sklarew
John Wilson

Contract A5-058-87

for the
California Air Resources Board
and the
California Energy Resources Conservation
and Development Commission

LIBRARY
AIR RESOURCES BOARD
P. O. BOX 2815
SACRAMENTO, CA 95812



SCIENCE APPLICATIONS, INC.

875 Westlake Blvd., Suite 212, Westlake Village, California 91361
213/889-0514

ADDENDUM

- Page 10 2nd paragraph - This discussion applies to the use of Gaussian models in complex terrain only. The performance of Gaussian models in rolling or flat terrain was not evaluated in this study.
- Page 21 Section 3.1.1 - At the present time there is no general consensus about the height at which σ_{θ} should be measured in order to correctly evaluate the Gaussian horizontal dispersion parameter σ_y .
- Page 23 Table 3-1 - Smith does not indicate the height at which σ_{θ} was measured.
- Page 33 Units of: F are $m^4/sec.^3$ and g are $m/sec.^2$.
- Page 34 Units of S are sec^{-2} .
- Page 78 Section 4.3.2 - Data taken from Smith (1972); σ values are for a height of 30m above ground level and are used for all elevations; for heights greater than 100 meters the turbulence length scale for 100 meters is used.
- Page 79 Section 4.3.3 - Data for this section derived from Intercomp (1975).
- Page 92 First paragraph - change concentrate to concentration.
- Page 102 Second paragraph - Because of the limited resolution of the coastal data, model accuracy for a one-hour averaging time was not investigated. However it is expected to be worse than the accuracy for the three or four hour average.
- Pages 101, 104, 106, 107 Calculations shown in Figures 4-13, 4-14, 4-15, 4-16, and 4-17 were made using the input values given on Pages 98 and 100.
- Page 111 Figure 4-18 is based on data reported in Eschenroeder(1972) for smog chamber experiment 271.
- Page 113 Table 4-9 is based on data reported in Hecht (1974) for smog chamber experiment 348.
- Page 171 First paragraph - The values of the vertical diffusivities in this discussion were taken at one cell height above the terrain, i.e., 133.33 meters.
- Page 173 First paragraph - The selection of a mixing height of 250 meters was based on temperature profile data taken by MRI (Smith 1975) and is consistent with other interpretations (Smith 1975), (Liu 1976). The selection of stability class was based on temperature gradients (see Table 5-7) and is consistent with the use of a local Richardson number as an indicator of atmospheric stability.
- Page 177 The four hydrocarbon chemical mechanism, CHEM15, was not used since the data needed to assign the background hydrocarbon splits was not available. Additional calculations utilizing the CHEM6 mechanism indicate that the inorganic chemical mechanism dominates the portion at least to the point of maximum ground concentration thus the use of CHEM15 should produce results similar to those indicated in Figures 5-26 to 5-29.
- The background values used for the photochemical simulation were obtained from Sklarew (1975).
- Page 179 Table 5-12 - The values of solar insolation were deduced from Eschenroeder (1972) and are consistent with values used for photochemical simulations of the Los Angeles Basin.

ACKNOWLEDGEMENTS

The authors would like to express their appreciation to the following individuals for their encouragement and assistance:

Mr. Andrew Ranzieri and Mr. Charles Ward who provided the Myrup/Ranzieri diffusivity model and monitored this study.

Dr. John L. Wilson who contributed to the discussion of statistical analysis and model validation.

Mr. Gary Phillips who contributed to the analysis and discussion of the wind field models MATHEW and WEST.

Mr. James Taft who assisted in computer programming.

Mr. Fred Laughter who provided most capable editorial assistance.

ABSTRACT

This report provides the results of a study of the comparative attributes of air pollution point source submodels. Submodels were tested against four data bases as well as against analytic solutions. The submodels that were determined to offer the greatest potential were assembled into two distinct models: a generalized Gaussian model, GEM (Gaussian Evaluation Model); and a finite difference model, IMPACT (Integrated Model for Plumes and Atmospherics in Complex Terrain). These final models were then evaluated using actual data taken from four field tests. GEM permits the user to specify options for each of the major parameters. The parameters that were evaluated include horizontal and vertical dispersion, standard deviations, plume rise, and various treatments of terrain and mixing layers. A useful extension of GEM was developed to automatically calculate concentrations over an array of receptors; this model is GEMGAR (GEM with Grided Array of Receptors). IMPACT was developed from the best state-of-the-art modules for wind field, diffusivity field, plume rise, pollutant transport, and chemistry. Field data employed for validation came from the NOAA program in Garfield, Utah; from the ARB programs at three California power plants; and from the Southern California Edison program at Ormond Beach in Ventura County, California. The relative precision, realism, and generality of each model were evaluated.

"The statements and conclusions in this report are those of the Contractor and not necessarily those of the State Air Resources Board. The mention of commercial products, their source or their use in connection with material reported herein is not to be construed as either an actual or implied endorsement of such products."

TABLE OF CONTENTS

	<u>Page</u>
1.0 INTRODUCTION.....	1
1.1 Study Approach.....	3
1.2 Organization of This Report.....	4
2.0 RESULTS, CONCLUSIONS, AND RECOMMENDATIONS.....	7
2.1 Results.....	7
2.2 Conclusions.....	9
2.3 Recommendations.....	14
3.0 THE GAUSSIAN EVALUATION MODEL.....	19
3.1 Review and Analysis of the Options Used in Gaussian Plume Models.....	21
3.1.1 Horizontal Dispersion Standard Deviation, σ_y	21
3.1.2 Vertical Dispersion Standard Deviation, σ_y	26
3.1.3 Plume Rise ΔH	33
3.1.4 Complex Terrain.....	38
3.1.5 Limited Mixing.....	43
3.2 Modification of the Gaussian Evaluation Model for Grided Receptors.....	47
4.0 THE GRID MODEL IMPACT (INTEGRATED MODEL FOR PLUMES AND ATMOSPHERICS IN COMPLEX TERRAIN).....	49
4.1 General Description of IMPACT.....	50
4.2 Review of the Wind Field Module Options.....	53
4.3 Review of Diffusivity Module Options.....	75
4.3.1 Gaussian Dispersion Standard Deviation.....	75
4.3.2 DEPICT Diffusion Coefficient.....	76
4.3.3 Intercomp Diffusion Model.....	79
4.3.4 Myrup/Ranzieri Diffusion Model.....	80
4.3.5 Tensor Diffusivity Model.....	84
4.3.6 Comparison of Diffusivity Formulations.....	84
4.3.7 Variations of Diffusivity With Height.....	88
4.3.8 The Ratio of Horizontal to Vertical Diffusivity.....	88
4.4 Review of Pollutant and Advection/Diffusion Modules.....	92
4.5 Review of Chemistry Options.....	108

TABLE OF CONTENTS (Continued)

5.0	VALIDATION OF DISPERSION MODELS.....	117
5.1	Discussion of Validation Options.....	118
5.1.1	Precision.....	119
5.1.2	Realism.....	123
5.1.3	Generality.....	124
5.2	Field Data Description.....	125
5.2.1	The NOAA Garfield, Utah Field Program Description.....	130
5.2.2	The ARB Point Source Field Program Description.....	135
5.2.3	The SCE Ormond Beach Field Program Description.....	143
5.3	Estimates of Model Precision.....	147
5.3.1	GEM, Gaussian Evaluation Model.....	147
5.3.2	IMPACT, Integrated Model for Plumes and Atmospherics in Complex Terrain.....	162
5.4	Summary of Model Precision, Realism, and Generality.....	182
6.0	REFERENCES.....	189

LIST OF TABLES

Table 2-1.	Summary of Model Precision.....	13
Table 2-2.	Summary of Model Generality.....	13
Table 3-1.	Standard Deviation of Wind Direction Fluctuations σ_θ as a Function of Stability Class.....	23
Table 4-1.	Comparison of Wind Field Models.....	54
Table 4-2.	Summary of Results Comparing MATHEW AND WEST Using Dugway Proving Ground Test Data.....	73
Table 4-3.	Relationship of Land Use, Surface Roughness, Atmospheric Stability, and Monin-Obukhov Length.....	83
Table 4-4.	Comparison of Normalized Eddy Diffusivities as Derived from EPA and Pasquill Vertical Dispersion Standard Deviation σ_z and the DEPICT and M/R Diffusivity Models.....	87
Table 4-5.	Past Comparisons of Advection Methods.....	94
Table 4-6.	Proposed Advection-Diffusion Methods with Uniform Wind Field and Constant Mesh.....	97
Table 4-7.	CHEM6 Reaction Mechanism.....	109
Table 4-8.	CHEM15 Reaction Mechanism.....	112
Table 4-9.	Comparison of Solutions of the Seinfeld- Hecht-Dodge Photochemical Reaction Model.....	113
Table 4-10.	Rate of SO ₂ -Sulfate Conversion as Estimated from the Predictions of the Reactive Plume Model.....	114
Table 5-1.	Summary of Candidate Model Validation Data Bases.....	126
Table 5-2.	Summary of Model Validation Data Bases.....	128
Table 5-3.	Validation Data Base Matrix.....	129
Table 5-4.	One-Hour Averaged SF ₆ CIT Tracer Data for Moss Landing Test No. 2, 11 August 1974.....	142
Table 5-5.	Input Data Used for Gaussian Evaluation Tests.....	148
Table 5-6.	Height of Terrain Matrix for Garfield Test Site.....	149
Table 5-7.	Stability Class as Determined by Temperature Stratification.....	150
Table 5-8.	Garfield Test No. 3.....	151

LIST OF TABLES (Continued)

Table 5-9.	Garfield Test No. 7.....	152
Table 5-10.	Moss Landing Test No. 2.....	153
Table 5-11.	Ormond Beach, 4-Hour Averages.....	154
Table 5-12.	Hourly Data Used in IMPACT Photochemical Simulation of the Ormond Beach Power Plant....	179
Table 5-13.	Summary of Model Precision.....	183
Table 5-14.	Summary of Model Realism by Submodel.....	185
Table 5-15.	Summary of Model Generality.....	187

LIST OF FIGURES

Figure 2-1.	Summary of IMPACT Photochemical Simulation Test.....	12
Figure 3-1.	Correction Factors for Estimating Lateral Spread of a Plume.....	22
Figure 3-2.	Comparison of Alternate Formulation for the Horizontal Dispersion Standard Deviation.....	25
Figure 3-3.	Comparison of Field Data with σ_y Formulations.....	27
Figure 3-4.	Parametric Characterization of Numerical Solution of Vertical Dispersion.....	29
Figure 3-5.	Comparison of σ_z for Rural Areas and Urban Areas.....	30
Figure 3-6.	Comparison of Field Data with σ_z Formulations.....	32
Figure 3-7.	Plume Rise as a Function of Downwind Distance.....	36
Figure 3-8.	Final Plume Rise as a Function of Temperature Gradients for Stable Conditions.....	37
Figure 3-9.	Comparison of Observed and Predicted Plume Rise Parameter.....	39
Figure 3-10.	Plume Centerline Trajectory in Complex Terrain.....	41
Figure 3-11.	Comparison of Various Plume Trajectories Using Data from Two Garfield Tests.....	42
Figure 3-12.	Effective Mixing Height in Complex Terrain...	44
Figure 3-13.	Ground Level Vertical Dilution Term as a Function of Mixing Height, σ_z , and Plume Rise for the Workbook and Reflection Models...	46
Figure 3-14.	Example GEMGAR Grid.....	48
Figure 4-1.	IMPACT Logic Flow.....	52
Figure 4-2.	Two-Dimensional Example of Terrain Representation in WEST and MATHEW.....	67
Figure 4-3.	Computational Cell.....	68
Figure 4-4.	Wind Data from Salt Lake City Rawinsonde at 1200 Z, 18 January 1973.....	70
Figure 4-5.	Observed Wind Vectors at 10 m Height AGL.....	71
Figure 4-6.	Dugway Topography at Two Resolutions.....	72

LIST OF FIGURES (Continued)

Figure 4-7.	Vertical and Horizontal Diffusion Coefficients, Derived Using EPA Workbook Dispersion Standard Deviations.....	77
Figure 4-8.	1/L as a Function of Pasquill Stability Classes.....	78
Figure 4-9.	Comparison of the Myrup/Ranzieri and DEPICT Diffusivities in the Lower Boundary Layer....	85
Figure 4-10.	Comparison of the Vertical Diffusivities Predicted by the DEPICT Model and the M/R Model.....	89
Figure 4-11.	Variation of the Ratio of Horizontal to Vertical Diffusivity as a Function of Atmospheric Stability.....	90
Figure 4-12.	Analytic Solution of a Plume with Wind Shear and Variable Diffusion.....	99
Figure 4-13.	Comparison of Surface Plus Centerline Concentrations for Finite Difference and Random Walk Solutions of a Three-Dimensional Point Source Plume, Uniform Wind and Diffusion Fields.....	101
Figure 4-14.	Comparison of Surface Concentrations for Finite Difference Solutions of a Three-Dimensional Point Source Plume, Vertically Sheared Wind and Diffusion Fields.....	104
Figure 4-15.	Comparison of Perspective and Contour Plots of Surface Concentrations for Finite Difference Solutions of Three-Dimensional Point Source Plume, Vertically Sheared Diffusion Field and Vertically and Horizontally Sheared Wind Field.....	105
Figure 4-16.	Comparison of Surface Concentrations for Finite Difference Solutions of a Three-Dimensional Point Source Plume, Vertically Sheared Diffusion Field and Vertically and Horizontally Sheared Wind Field.....	106
Figure 4-17.	Perspective and Contour Plots Showing the Difference Between the Analytic Solutions Less the ADH and SHASTA Solutions.....	107
Figure 4-18.	Comparison of CHEM6 Model Results, GRC Model Results, and Experimental Data, Experiment 271, Toluene/NO _x	111
Figure 4-19.	SO ₂ Conversion to SO ₄	115

LIST OF FIGURES (Continued)

Figure 5-1.	Illustration of the Problems in Using Statistical Measures in Assessing Model Validation for Point Source Models.....	120
Figure 5-2.	Areas of Uncertainty and Possible Sources of Error Associated with Each Step in the Model Validations Procedure.....	122
Figure 5-3.	Garfield Test Site, Distribution of Ground Level Samplers and Terrain Heights for Tests 1 through 7.....	131
Figure 5-4.	The Garfield Grid, Two Examples.....	132
Figure 5-5.	Representative Plume Trajectories for the Garfield Tests, Illustrated in Relation to the Area's Terrain.....	134
Figure 5-6.	Sampling Locations for Tests Conducted from the Long Beach Power Plants.....	137
Figure 5-7.	Surface Streamline Analysis of the Los Angeles Area, 30 October 1974.....	139
Figure 5-8.	Summary of Meteorological Data Taken at Moss Landing Test Site.....	140
Figure 5-9.	Location of Air Samplers and the Test Grid for the Moss Landing Field Program.....	141
Figure 5-10.	Wind, Pibal, and Air Quality Sites.....	144
Figure 5-11.	Ormond Beach Test, 14 August 1973, Measured 4-hour Average.....	145
Figure 5-12.	Summary of GEM Validation Tests.....	156
Figure 5-13.	Representative GEM Validation Using Garfield Test No. 3 Data.....	157
Figure 5-14.	Representative GEM Validation Using Garfield Test No. 7 Data.....	158
Figure 5-15.	Representative GEM Validation Using Moss Landing Test No. 2 Data.....	159
Figure 5-16.	Representative GEM Validation Using Ormond Beach Data with Brigg's Plume Rise....	160
Figure 5-17.	Representative GEM Validation Using Ormond Beach Data with TVA's Plume Rise.....	161
Figure 5-18.	WEST Validation Test Using Garfield Test No. 3 Data.....	164

LIST OF FIGURES (Continued)

Figure 5-19.	WEST Validation Test Using Los Angeles Data, 0900 Hours, 30 October 1974, Comparing Streamline Patterns as a Function of the Number of Meteorological Inputs.....	165
Figure 5-20.	WEST Validation Test Using Los Angeles Data, 1500 Hours, 30 October 1974, Comparing Streamline Patterns as a Function of the Number of Meteorological Inputs.....	166
Figure 5-21.	WEST Validation Test Using Los Angeles Data Taken at 0900 Hours on 30 October 1974, Comparing Calculated and Observed Data.....	167
Figure 5-22.	WEST Validation Test Using Los Angeles Data Taken at 1500 Hours on 30 October 1974, Comparing Calculated and Observed Data.....	168
Figure 5-23.	Results of IMPACT Validation Using Garfield Test No. 3 Data.....	170
Figure 5-24.	Results of IMPACT Validation Using Garfield Test No. 7 Data.....	172
Figure 5-25.	Results of IMPACT Validation Using Moss Landing Test No. 2 Data.....	174
Figure 5-26.	Results of IMPACT Validation Using Ormond Beach Test Tracer Data.....	176
Figure 5-27.	NO and NO ₂ Concentrations, Comparing 4-Hour Average of Measured and Calculated Values....	178
Figure 5-28.	Hour-Averaged Ozone Contours in Relation to Camarillo APCD Station.....	180
Figure 5-29.	Temporal Variation of Pollutant Concentrations at the Camarillo APCD Station in Ventura County.....	181
Figure 5-30.	Hierarchical Analysis of Air Quality Impact from Point Sources.....	186

1.0 INTRODUCTION

Both the Air Resources Board (ARB) and Energy Resources Conservation and Development Commission (ERCDC) have specific needs for standard point source air quality models. These needs stem from regulations requiring evaluation of fuels, controls, and siting. The current sharp reduction in the availability of natural gas will require evaluation of the air quality impact from utilization of higher sulfur fuels. Remaining natural gas supplies may have to be allocated on the basis of air quality impact, especially during episodic conditions. These require models capable of addressing the parameters of reactive pollutants, coastal meteorology, and winds over complex terrain. Presently proposed controls for NO_x include tuning the air-fuel mixtures for each boiler and load redistribution (requiring multiple source models); for higher sulfur and ash fuels, flue gas removal systems may have to be used as intermittent or continuous controls. Models can provide a basis for the required decisions. Evaluation of new source siting is envisioned as one of the major applications of the models. Urban sites may present the potential of a major photochemical impact on a large populace, while rural sites may degrade areas valued for their pristine condition and for recreational use.

The ARB has a review responsibility in support of the Air Pollution Control Districts (APCD) in their assessment of new source impact on air quality. In this case, "new source" means both new stationary sources and changes in current emissions from stationary sources. The APCD's are charged with analyzing the effect of these new or modified emissions on air quality before granting a permit to operate. The ARB has a review responsibility for these analyses. This assessment procedure would be facilitated by the ARB's undertaking the following:

- Providing the APCD's with standard models with which to perform the analyses,

- Modeling the new source for the APCD's, or
- Using standard models in reviewing APCD analyses.

The ERCDC is charged with preparation and review of energy-related impacts and with development and evaluation of a list of possible electrical generation sites. Specifically, the ERCDC needs standard models to evaluate and review all proposed sites and new facilities to ensure conformance with air quality standards and with air quality implementation and maintenance plans.

The emphasis on "standard" models is used to underscore the need for accepted, user-ready models, each with predetermined applicability and error bounds. The acceptance of a model is based on state-of-the-art techniques, on verification against the most definitive data bases available, and on error bounds associated with clearly defined classes of applications. Thus, this program was designed to select the best available state-of-the-art models, evaluate and verify them with carefully selected data bases, and package them for easy use.

1.1 Study Approach

At the initiation of this program, it was apparent that two distinctly different types of models were required. The common and relatively straightforward Gaussian model (similar to the EPA PTMPT code) with modifications for complex terrain, limited mixing, etc., would be used for simple situations and to screen other sources for potential impact in more complex situations. With regard to the latter application, the Gaussian model could be used to determine if the more complex, finite difference, grid-type model would be required to accurately assess potential impact on air quality. Thus, the decision was made that both these two types of models would be the subject of this study.

Because of the differences in the complexity of the models, two separate approaches were used to select the modules to be incorporated in the final models.

Rather than preselect the various modules of the Gaussian model (i.e., plume rise, plume dispersion parameters, σ_y , σ_z , complex terrain, limited mixing, etc.), a wide range of optional modules were incorporated into a new Gaussian Evaluation Model (GEM). The modules were then compared using parametric and analytic techniques. However, the final evaluation was made by on-line comparison of the various options and combinations with actual field data.

The complexity and cost of running the grid type models necessitated evaluation of the module options singly on the basis of conceptual analysis, historical studies, and performance comparisons with data and analytic solutions. Additionally, a few module options were evaluated on-line using actual data bases in the IMPACT (Integrated Model for Plumes and Atmospherics in Complex Terrain) model.

1.2 Organization of This Report

Section 2 contains a discussion on the evaluation of the proposed module options and summarizes the accuracy and validity of the delivered models. This section also contains recommendations, based on the experience gained in this study, for improvements needed in future field studies, for future investigation into specific modules, and for the need to develop improved methodology in model applications.

Section 3 contains a description of the Gaussian Evaluation Model, GEM, and a review and analysis of the options used in GEM. Included in this section is a description of a variant of the GEM model called GEMGAR which calculates a concentration array over a grid of receptors instead of the specific receptor input required by GEM.

Section 4 contains a description of the grid model IMPACT. Included in this section are review and analysis of the modules (submodels) used for creating the wind field, creating the dispersion or diffusivity field, and for advection or transporting the concentration fields. Also included is a discussion of the photochemistry and sulfate chemistry models included in IMPACT.

Section 5 contains a discussion of the validation efforts. Included in this discussion are:

- The meaning and purpose of model validation
- The validation methodology used
- The approach used for validating GEM, IMPACT, and the wind field module WEST
- A discussion of the field data, including deficiencies and uncertainties
- A discussion of model validity and sensitivity to input parameters.

Section 6 is a listing of the references employed in this study.

Three appendices, published under separate cover, conclude the report:

- Appendix A, User Guide to GEM
- Appendix B, User Guide to GEMGAR
- Appendix C, User Guide to IMPACT.

2.0 RESULTS, CONCLUSIONS, AND RECOMMENDATIONS

2.1 Results

The two air quality simulation models developed for this study provide a basis for the evaluation of the various alternative submodels currently used in other models. Since there are two separate types of deterministic air quality models, both a Gaussian model (GEM) and a finite difference grid model (IMPACT) were required. Numerous submodels for simulating pollutant transport, dispersion, plume rise, and atmospheric chemistry were considered and evaluated. The evaluation of the submodels included theoretical analysis, comparison with field data (e.g., plume rise), and the application of the GEM and IMPACT models to predict surface concentrations for comparison with observations.

Currently available data bases from point source release field programs were reviewed and analyzed to determine the availability of model input parameters, and the resolution and accuracy of measured surface concentrations. Of numerous point source field programs reviewed for consideration as a model validation data base, only three separate programs were found to be conditionally acceptable. The four actual field tests selected from these three programs provided the best available data bases with which to evaluate the accuracy of point source air quality simulation models.

The philosophy and practice of model validation were investigated to provide a basis for an analysis of the accuracy of the models. The results of this investigation showed that a rigorous statistical evaluation of model precision is currently not possible because of the inadequacy of the current field data bases. A discussion of model validity in terms of model precision, realism, and generality showed that general comments on model validity could be based on the current field data and analyses of various submodels. The rationale and requirements

for improvements in the Gaussian and grid models and in future field programs are placed in a conceptual framework to facilitate the prioritization of future research in the area of air quality modeling.

2.2 Conclusions

In spite of the discouraging state of field data vis-à-vis model validation, it is clear that we are on the threshold of an increased use of and reliance on modeling as a tool for air quality management. This study has demonstrated that, as expected, the grid type model is superior to the Gaussian model in terms of precision, realism, and generality. However, due to the increased cost of the grid model compared to the Gaussian model, both are needed for balanced, cost-effective, air quality modeling.

Evaluation of the options available in the Gaussian model indicated that the new formulations for pollutant dispersion standard deviations (σ_y , σ_z) developed by EPA and Pasquill are superior to the commonly used Turner Workbook values. However, due to the limited field data available, it was not possible to select the better of the two newer formulations. After reviewing the limited plume rise data available in the selected field studies, it appears that the newer Briggs plume rise models are superior to other models. The reader is referred to a report by G. A. Briggs (Briggs, 1975) for a thorough discussion of plume rise models. Based on the field data taken at Garfield, Utah, under unstable atmospheric conditions, the ERT complex terrain plume trajectory model is superior to the NOAA, EPA, and Cramer models. Since the field data was taken under unstable atmospheric conditions only, no evaluation of plume trajectory models under stable atmospheric conditions was possible. Coastal regions appeared more difficult for Gaussian models to handle than the complex terrain situations (at least for the test cases considered in this study). Among the factors contributing to this situation are that large sources tested in coastal regions impact large surface areas. Therefore, the Gaussian assumption of constant winds and atmospheric stability may not be valid; unsteady, shifting winds in the coastal region result in curved plume trajectories which cannot be correctly treated by these straight-line

steady state Gaussian models. Under unstable atmospheric conditions, and the complex terrains considered in this study, the plumes appear to have a more-or-less straight trajectory, while meandering in the vertical.

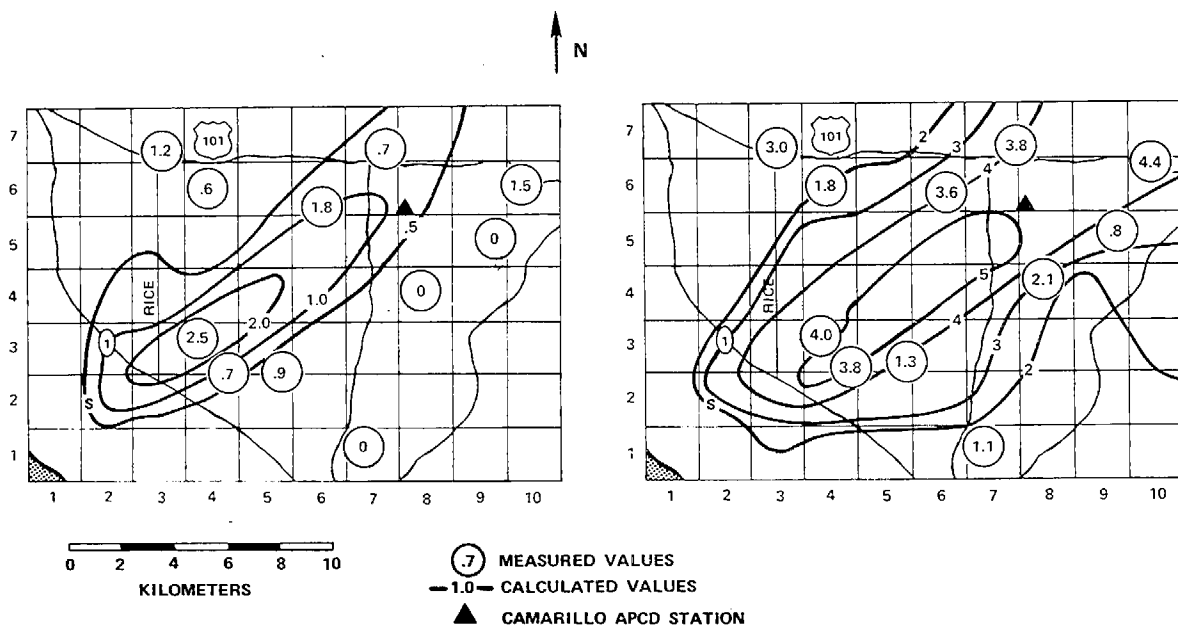
It should be noted that the Gaussian model is not actually applicable to complex terrain situations where high wind shear and strong inversions can result in plume channeling and other effects that produce non-Gaussian concentration profiles. The use of prescriptions for plume trajectory and mixing heights is an ad hoc patch to extend the model into conditions where it is not applicable. Thus, the reader is cautioned that the use of these models in complex terrain is useful, at best, for approximate estimates and may result in large errors under certain applications. After careful review of the Gaussian evaluation tests, one reaches the conclusion that almost any desired result can be obtained, given the range of options for the dispersion parameters, plume trajectory in complex terrain, etc., and the range of experimental uncertainty in the observed wind speed, wind direction, and atmospheric stability. Thus, for each test there were certain sets of options (known only with hindsight) for which the Gaussian model performed adequately in rough terrain and with less precision in the rotating winds of coastal regions.

The evaluation and analysis of options available for inclusion in the finite difference grid model resulted in the selection of the WEST wind field module primarily due to its versatility in treating spatial variability in atmospheric stability, and allowing the predicted velocity at a measurement site to agree with the observed value. The advection/diffusion module selected was a flux-corrected version of Crowely's second-order scheme chosen for its ability to accurately treat localized sources in a shearing, rotating flow field. As no direct data is available from which an evaluation of the various diffusivity modules can be made, the selection of the best diffusivity module is problematic at this time.

The finite difference grid model IMPACT is more deterministic than the Gaussian model with options only for diffusivity and plume rise modules (all other modules were preselected as noted above). The performance of IMPACT was a "factor of two" or better in calculating both the wind field and maximum ground level pollutant concentrations.

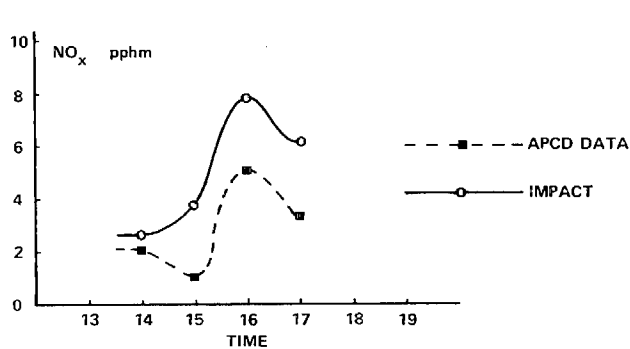
The ability of IMPACT to simulate a photochemically reacting plume in a coastal plain is summarized in Figure 2-1.

Table 2-1 provides a summary of model precision in terms of the ability of the model to predict the maximum observed surface concentrations. Table 2-2 illustrates model generality in terms of the applicability of the model for various time periods, regions, and pollutants.

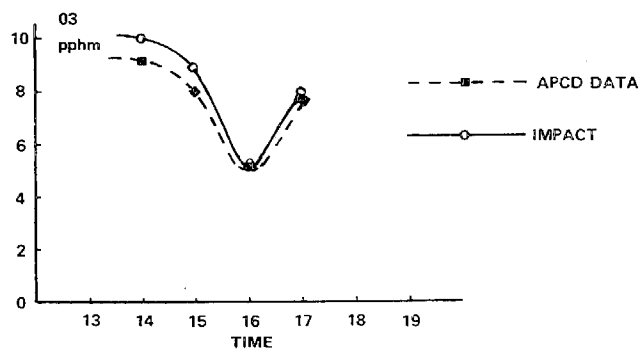


A. COMPARISON OF MEASURED AND CALCULATED NO (pphm), 4-hr AVERAGE

B. COMPARISON OF MEASURED AND CALCULATED NO₂ (pphm), 4-hr AVERAGE



C. NO_x VARIATION AT THE CAMARILLO APCD SITE (HOUR-AVERAGED DATA)



D. OZONE VARIATION AT THE CAMARILLO APCD SITE (HOUR-AVERAGED DATA)

Figure 2-1: Summary of IMPACT Photochemical Simulation Test.

Table 2-1. Summary of Model Precision.

REGION \ AVERAGING PERIOD	1-HOUR	3-HR.	24-HR.	ANNUAL
	1-HOUR	3-HR.	24-HR.	ANNUAL
FLAT OR ROLLING	NOT TESTED IN THIS PROGRAM; SHOULD BE MORE ACCURATE THAN THE OTHER REGIONS HOWEVER			REQUIRES MODIFICATION FOR USING STAR-TYPE DATA OR THE USE OF METEOROLOGICAL REGIME ANALYSIS
COMPLEX TERRAIN	<u>GEM</u> FACTOR OF 2 TO 3 FACTOR OF ~2 <u>IMPACT</u>	NOT TESTED IN THIS PROGRAM	NOT TESTED IN THIS PROGRAM	
COASTAL	NOT EXAMINED IN THIS PROGRAM, BUT LIKELY TO BE WORSE THAN 3-HR AVERAGE	<u>GEM</u> FACTOR OF 3 TO 4 FACTOR OF 2 4-HR AVG <u>IMPACT</u>		

Table 2-2. Summary of Model Generality.

MODEL TYPE		GEM	IMPACT
EVALUATION CRITERIA			
TIME PERIOD	1-HOUR	YES	YES
	3-HOUR	YES	YES
	24-HR.	YES	YES
	ANNUAL	REQUIRES MODIFICATION FOR STAR DATA	REQUIRES THE DEVELOPMENT OF METEOROLOGICAL REGIME METHODOLOGY
REGION	FLAT OR ROLLING	YES	YES
	COMPLEX	FOR INITIAL EVALUATION ONLY	YES
	COASTAL		YES
POLLUTANT TYPE	INERT POLLUTANT	YES	YES
	SULFATES	ONLY WITH EXPONENTIAL DECAY	SIMPLIFIED SO ₂ CONVERSION MODEL
	PHOTOCHEMICAL	NO	YES

2.3 Recommendations

An important result of the analysis and evaluation of the various submodels used in the Gaussian and grid models is a list of recommendations to increase the validity (precision, realism, and generality) of a number of the submodels. The following list of research topics includes the programs that are considered most relevant to increased model validity; however, since the prioritization of this type of research requires the interaction of the user and the modeler, there is no significance to the order of these recommendations.

- Improvements in the plume rise submodel should include an extension of the Briggs model encompassing arbitrary atmospheric stability structure and partial penetration of the plume into an elevated inversion (Briggs, 1975), and/or the use of numerical hydrodynamic models to describe the interaction of a buoyant plume with the ambient atmosphere.
- Improvements in the pollutant transport submodel can be separated into suggestions for improving the treatment of pollutant transport in the Gaussian and grid models. For the Gaussian models, the inclusion of a treatment for curved wind field would enhance the usefulness of the code for longer range impact, particularly in coastal regions. For the grid models, removing the spatial splitting, implicitization and possible utilization of Lagrangian techniques would be natural extensions. Further investigation of other methods for the numerical solution of the pollutant transport equation could result in increased accuracy, and in reductions in computer storage and/or run-time requirements. The incorporation of variable grid resolution would achieve an improvement in model accuracy with minimum additional effort.

- To enhance the validity of the WEST (Winds Extrapolated from Stability and Terrain) submodel, there is a need for the refinement of the terrain channeling parameters through the use of numerical or physical experiments and the inclusion of thermal forcing effects to simulate upslope heating and downslope drainage winds.
- Improvements in the treatment of pollutant dispersion for the Gaussian submodel await the availability of additional field data. However, treatment of eddy diffusivity as a full tensor quantity (Freeman, 1976) could be a significant improvement over current grid model dispersion submodels.
- The development of a capability to provide estimates of emission impact on an annual basis would provide a major increase in model generality. Approaches to this requirement could include adaptation of the Gaussian model to use available summary climatological data (e.g., STAR) as in the U.S. Environmental Protection Agency's Climatological Dispersion Model, CDM, (Busse, 1973), or the development of a rigorous formalism to develop and use meteorological regimes (Fabrick, 1975; Phillips, 1977) in both the Gaussian and grid models.

A significant conclusion of this study is the need for the careful planning of future air quality field programs in order to provide the accurate input parameters and surface concentrations needed for an objective determination of model validity. In addition, future programs need to be planned so that a variety of source types (power plants, industry, etc.), regions (coastal, mountainous, level, rolling, etc.), and meteorologies (unstable, fumigation, stable, surface inversion, neutral, etc.) are encompassed to quantify the applicability of air quality modeling to each situation.

The following procedures are intended to be supplemental to the procedures used in current field programs:

- Multiple plume traverses per hour should be performed to collect averages of the detailed, instantaneous tracer and/or pollutant concentrations for comparison with fixed hour-averaged data. This procedure would allow a direct evaluation of the Gaussian horizontal dispersion standard deviation σ_y and would provide increased detail of pollutant surface concentrations.
- The hourly average standard deviation of the wind vane fluctuations should be compiled since they are needed as an input parameter for σ_y in the Gaussian models.
- There should be increased use of aircraft to develop hourly vertical profiles of temperature and tracer and/or pollutant concentrations. This data is needed to determine the vertical structure of atmospheric stability and to determine plume rise and plume trajectory.

If an objective of the field program is to provide a data base to evaluate a photochemical air quality model, the following data is required in addition to currently measured data:

- Hourly measurement of ultraviolet flux.
- Detailed hydrocarbon measurements, including analysis of selected samples for the evaluation of hydrocarbon breakdown into reactivity classes.
- Accurate determination of background concentrations and relative humidity including vertical, horizontal, and temporal variations.
- Emissions of local sources of hydrocarbons, oxides of nitrogen, carbon monoxide, and sulfur dioxide.

A major deficiency in almost every part of the field programs evaluated was the lack of specific error estimate of each of the measured parameters. Since the evaluation of model accuracy requires a knowledge of the accuracy of the input parameters, this deficiency has proved to be a major impediment to air quality model evaluation. It is therefore recommended that an estimate of the accuracy of each measured parameter be required in future field programs.

Finally, the inclusion of a person or group specifically involved in air quality modeling in the planning of future field programs is strongly recommended to help ensure the relevance of new model validation data bases.

3.0 THE GAUSSIAN EVALUATION MODEL

The Gaussian Evaluation Model was written to provide a mechanism to explore, evaluate, and use the various options that have been proposed as improvements to the basic Gaussian model. The standard Gaussian expression for relating point source emissions to air pollutant concentrations can be written as

$$C = \frac{Q}{2\pi\sigma_y\sigma_z u} e^{-y^2/2\sigma_y^2} \left\{ e^{-(H-z)^2/2\sigma_z^2} + e^{-(H+z)^2/2\sigma_z^2} \right\} \left\{ e^{-\lambda x/u} \right\} \quad (3.1)$$

where

- C = the pollutant concentration at point x,y,z
- Q = the emission rate
- u = the average wind speed
- x = the downwind distance from source to the closest approach to the receptor
- y = the crosswind distance from plume centerline to receptor
- z = the height of the receptor above ground level
- H = the height of the plume above ground level
- σ_y = the horizontal dispersion standard deviation at the downwind distance x
- σ_z = the vertical dispersion standard deviation at the downwind distance x
- λ = the decay constant of the pollutant (if the pollutant half-life is $\tau_{1/2}$, then $\lambda = .6931/\tau_{1/2}$)

This equation can be rearranged and grouped into the following terms:

$$C = \{\text{source term}\} \{\text{horizontal dilution term}\} \{\text{vertical dilution term}\} \{\text{chemistry term}\} \quad (3.2)$$

where

$$\begin{aligned} \{\text{source term}\} &= \frac{Q}{2\pi u} \\ \{\text{horizontal dilution term}\} &= \frac{1}{\sigma_y} e^{-y^2/2\sigma_y^2} \end{aligned}$$

$$\begin{aligned}\{\text{vertical dilution term}\} &= \frac{1}{\sigma_z} \left[e^{-(H-z)^2/2\sigma_z^2} + e^{-(H+z)^2/2\sigma_z^2} \right] \\ \{\text{chemistry term}\} &= e^{-\lambda x/u}\end{aligned}$$

Equation 3.2 can be generalized to represent the concentration at the k^{th} receptor due to a number of point sources averaged over a number of meteorological periods (usually multiple hours).

$$C_k = \frac{1}{n} \sum_{i=1}^n \sum_{j=1}^m \frac{\{\text{source term}\} \{\text{horizontal dilution term}\}}{\{\text{vertical dilution term}\} \{\text{chemistry term}\}} \quad (3.3)$$

where

$i = 1, n$ represents the meteorological periods

$j = 1, m$ represents the various sources

This expression is the basis for the EPA multiple point source Gaussian model PTMPT and is the basis for the model developed for this project, i.e., GEM.

The major options of the GEM model are summarized below:

- Plume Rise: Briggs 1967, Briggs 1974, TVA, specified
- Mixing Height: horizontal, terrain conformal
- Plume Centerline Trajectory: EPA, NOAA, ERT, Cramer
- Plume Dispersion Standard Deviations: Turner, EPA 1976, Pasquill, specified
- Limited Vertical Mixing: Turner, reflection
- Chemistry: exponential decay

For further details on the structure of the GEM model, see Appendix A of this report, entitled "User Guide to the Gaussian Evaluation Model, GEM."

3.1 Review and Analysis of the Options Used in Gaussian Plume Models

Because of its simplicity, the Gaussian plume model has become a standard method for predicting pollutant concentrations resulting from point source emissions. A number of modifications have been suggested to add realism to the basic model, including new horizontal and vertical dispersion parameters (σ_y , σ_z), new plume rise prescriptions, new treatments for plume trajectories in complex terrain (needed to determine the height of the plume), and new treatments for limited mixing (modifications of the vertical dilution term).

Fundamental to the use of the Gaussian model is the prescription of the dispersion parameters σ_y , σ_z . A methodology, which will be referred to as the EPA Workbook prescription, was proposed (Turner, 1970) to standardize the use of these parameters. This prescription has been in wide use for the last decade. However, examinations of the current state-of-the-art (Pasquill, 1974 and 1976) have indicated that new formulations may be preferable to the standard prescription.

3.1.1 Horizontal Dispersion Standard Deviation, σ_y

Recent review of the lateral spreading of plumes in the atmosphere (e.g., Pasquill, 1974 and 1976) have indicated that irrespective of sampling time (within the range of a few minutes to an hour) and irrespective of surface roughness and stability, the lateral spread, σ_y , is roughly equal to the standard deviation of the wind direction, σ_θ , times the downwind distance, x , times a "universal" correction factor, $F(x)$; i.e.,

$$\sigma_y = \sigma_\theta \cdot x \cdot F(x)$$

The σ_y 's proposed by EPA in 1976 (prepared by Pasquill) and the σ_y 's suggested by Pasquill in 1974 both use this formulation. The major difference between the two prescriptions is in the values of the correction factor, $F(x)$, (see Figure 3-1), and the fact that

x(km)	0.1	0.2	0.4	1	2	4	10	>10
F(x), EPA	0.8	0.7	0.65	0.6	0.5	0.4	0.33	$0.33 (10/X)^{1/2}$
F(x), Pasquill	—	—	—	0.85	0.75	0.6	0.40	—

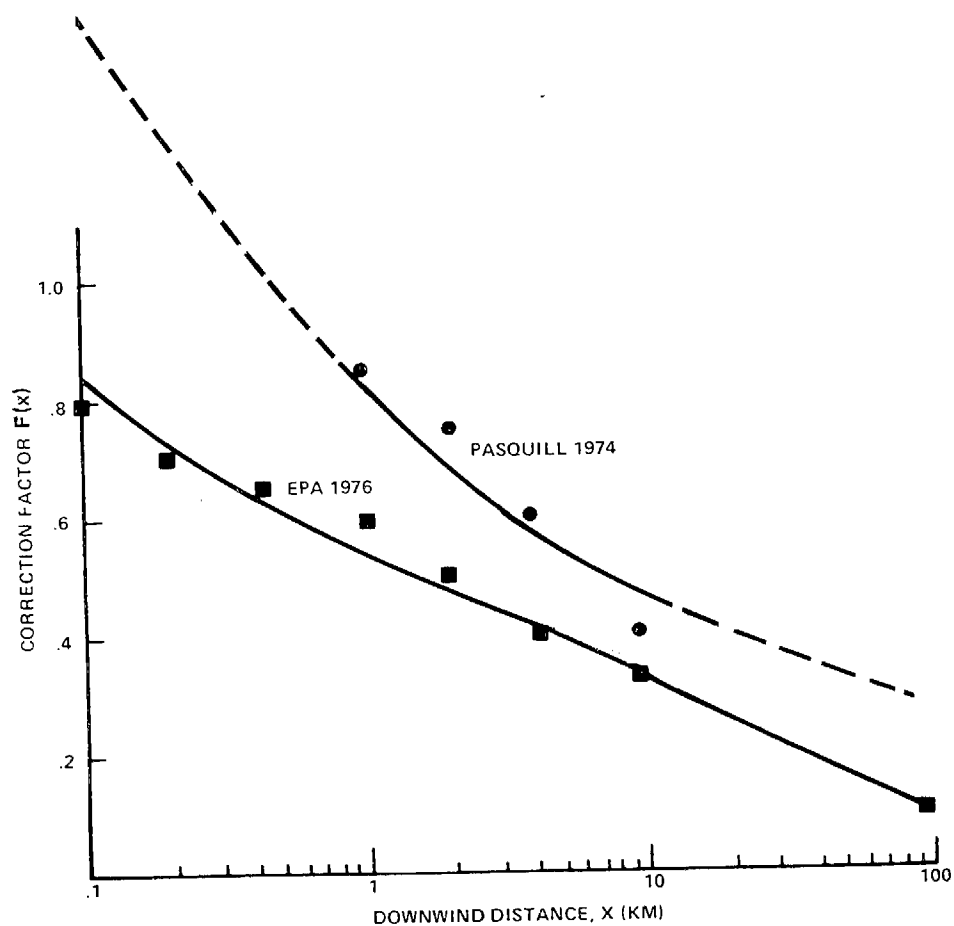


Figure 3-1. Correction Factors for Estimating Lateral Spread of a Plume, (Data Fit as ax^b by Authors).

after 20 km the EPA prescription recommends incorporating another term to include the total change in the mean wind direction over the vertical depth of the plume, $\Delta\theta$ (i.e., $\sigma_y = (\sigma_\theta^2 F(x)^2 x^2 + 0.3 \Delta\theta^2 x^2)^{\frac{1}{2}}$).

EPA Workbook values for σ_y as a function of stability were developed from both wind statistics and tracer studies for flat, smooth (surface roughness parameter, z_0 , between 3 and 30 cm) terrain. To compare the Workbook values with the newer methods, values of σ_θ as a function of stability (and z_0) are needed. This problem will probably be faced by users when only stability data is available; however, as shown in Table 3-1, a rough range of σ_θ as a function of stability was developed (Smith, 1972) and can be used if measured values of σ_θ are not available.

Table 3-1. Standard Deviation of Wind Direction Fluctuations
 σ_θ as a Function of Stability Class, (Smith, 1972).

STABILITY	σ_θ	
	DEGREES	AVERAGE RADIANs
A	> 23°	0.40
B	18-23	0.36
C	13-18	0.27
D	8-13	0.18
E	4-8	0.10
F	< 4	0.065

The average value of σ_θ for each stability class was used to calculate the values of σ_y for the two new methodologies. A comparison of the various formulations of σ_y are shown in Figure 3-2 for stability classes A, D and F.

The slope of the curve for σ_y for the proposed methods is determined by the shape of the correction factor function $F(x)$, while the intercept is determined by the value selected for σ_θ as a function of stability. It is interesting to note that the slope of the σ_y curves of the proposed new methods are less than the Workbook estimates. Thus, both of the proposed formulations suggest that the actual rate of increase in the plume width with increased downwind distance is less than that suggested by the standard Workbook σ_y curves.

Closer examination of the various σ_y curves for all stabilities indicates that the use of any method, given the approximate value σ_θ as a function of stability (Table 3-1), will result in displacement by not more than one stability class from the EPA Workbook values after a downwind distance of a few hundred meters. The new EPA proposed σ_y and the Workbook values are very close, with less than one-half a stability class displacement. Since the designation of atmospheric stability is approximate, the difference in σ_y using the new EPA σ_y 's or the Workbook values is small (when using the average σ_θ values).

It should be noted, however, that even though the differences in the values of σ_y may be small, the resultant differences in the values of the horizontal dilution factor ($\frac{1}{\sigma_y} e^{-y^2/2\sigma_y^2}$) may be large (particularly when $y^2 > \sigma_y^2$).

The increased accuracy in using additional site-specific meteorological data (in addition to wind speed, wind direction, and perhaps mixing height and stability class or lapse rate) makes the two new proposed formulations for σ_y attractive. However, except for a very few limited cases (the St. Louis RAPS program for example), the value of σ_θ is not measured, reduced, or reported in current field measurement programs.

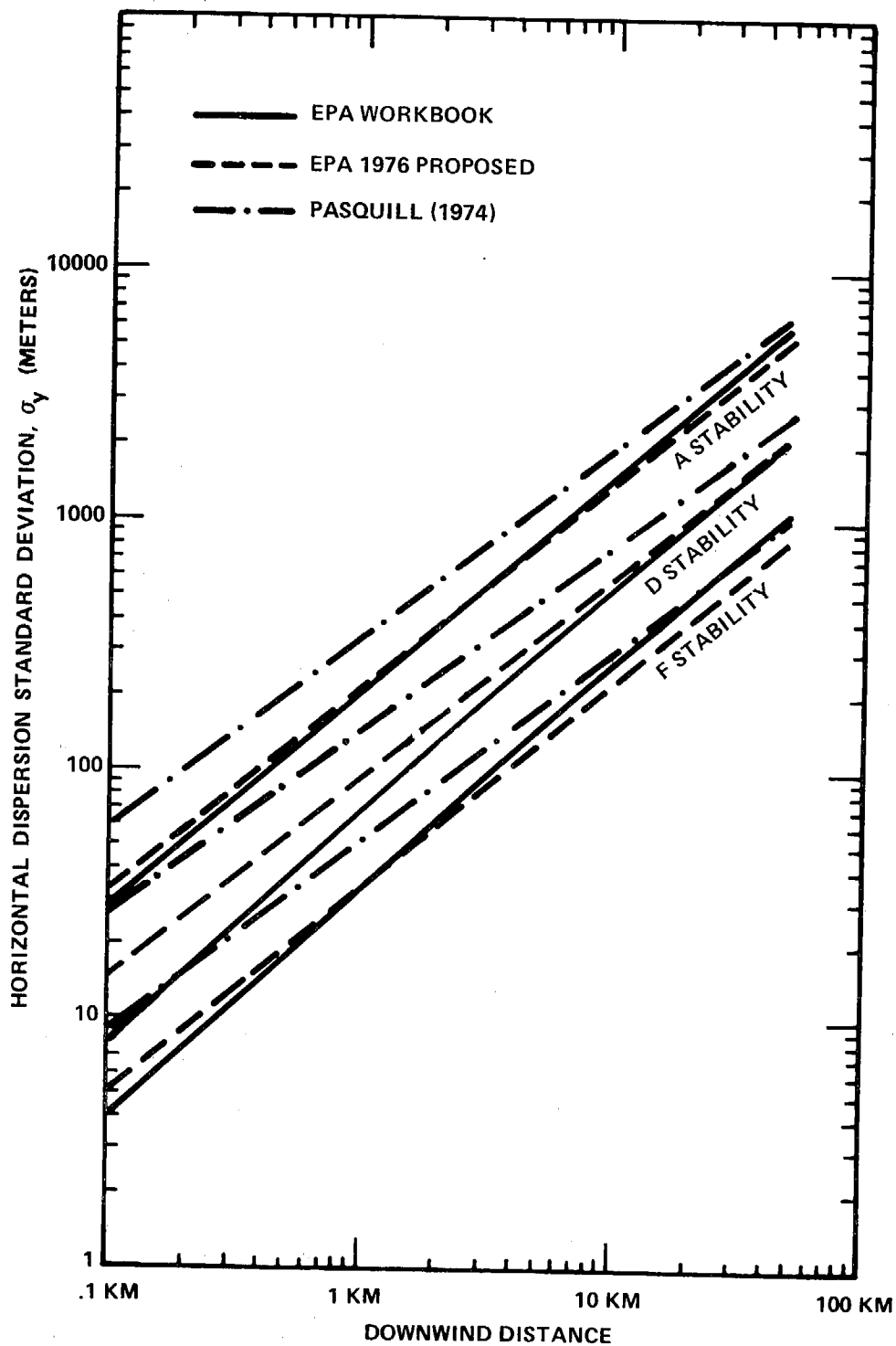


Figure 3-2. Comparison of Alternate Formulation for the Horizontal Dispersion Standard Deviation.

An attempt was made to compare the values of σ_y derived using data taken in selected field programs in complex terrain or on the coast (i.e., NOAA-Garfield tests, and the ARB point source tracer program at Moss Landing and Long Beach) with the various σ_y formulations (using average stability-dependent values for σ_θ). As depicted in Figure 3-3, the results are inconclusive. The large scatter of points and the uncertainty in their values (see section 5.4) indicate that the hourly average data taken at a few locations (5 to 15 sites) may not be sufficient to characterize the plume horizontal dispersion.

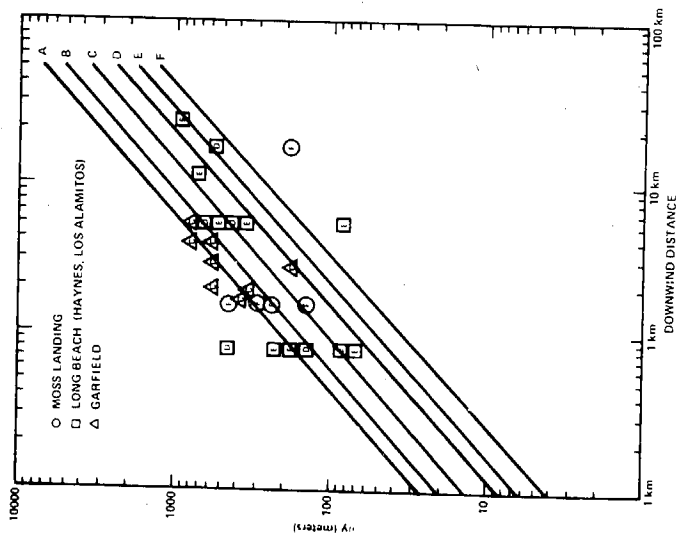
The collection of σ_θ data during future field studies would allow the verification or updating of Table 3-1 and might indicate the characterization of σ_θ as a function of land use (e.g., rural or urban), surface roughness or terrain variation as well as stability class. Additionally, accurate determination of σ_y (with multiple pass traverses as used by Drivas, 1975) would help in the selection of the correct value of the "correction function," i.e.,

$$F(x) = \sigma_\theta \sigma_y^{-1} x^{-1}$$

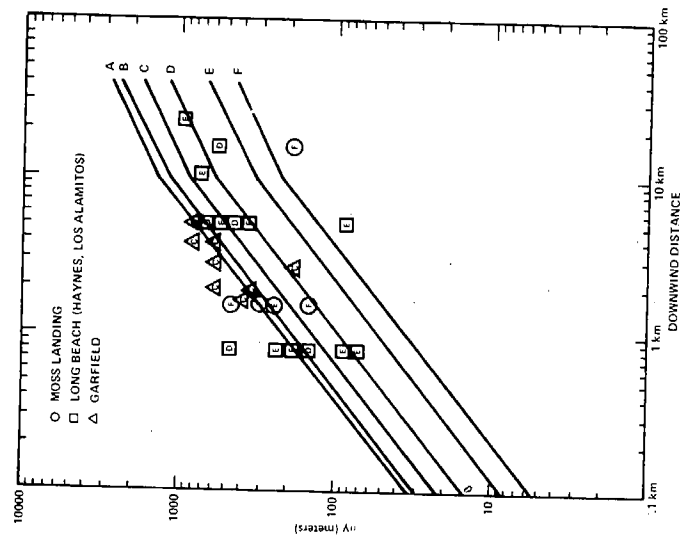
3.1.2 Vertical Dispersion Standard Deviation, σ_z

The EPA Workbook curves for σ_z were developed using a limited amount of tracer dispersion data together with theoretical treatments assuming the properties of the wind profile over smooth surfaces ($z_0 = 3$ cm). The curves were developed for surface point sources only, but were offered as usable for any source height in the mixed layer. Numerical solutions of the diffusion equation by F. B. Smith (Pasquill, 1974), incorporating the effects of surface roughness and atmospheric stability, offer another approach to developing curves for σ_z . The value of σ_z can be calculated as

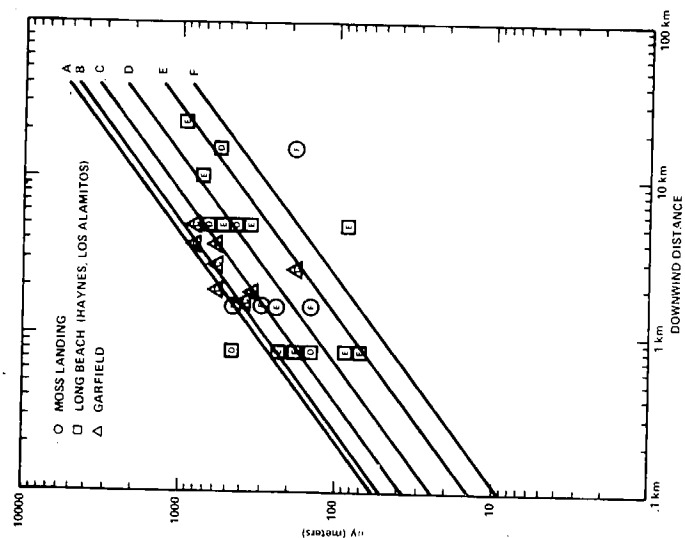
$$\sigma_z = \sigma_{z0}(x) \cdot f(x) \cdot g(x) \quad (3.4)$$



A. EPA WORKBOOK



B. EPA 1976



C. PASQUILL 2ND ED.

Figure 3-3. Comparison of Field Data with σ_y Formulations.

where

- σ_{z0} = the vertical dispersion standard deviation for neutral stability and a surface roughness of 10 cm
- $f(x)$ = the correction factor for other stabilities
- $g(x)$ = the correction factor for other surface roughness heights.

The values of σ_{z0} , $f(x)$, and $g(x)$ are shown in Figure 3-4.

A review of recent theoretical and experimental work by EPA (Pasquill, 1976) has indicated that modifications to the Workbook values for σ_z may be desirable. The modification proposed for the Workbook values can be described as

$$\sigma_z = \left(\sigma_z^0(x)^2 g'(x)^2 + 0.1 \Delta H^2 \right)^{\frac{1}{2}} \quad (3.5)$$

where

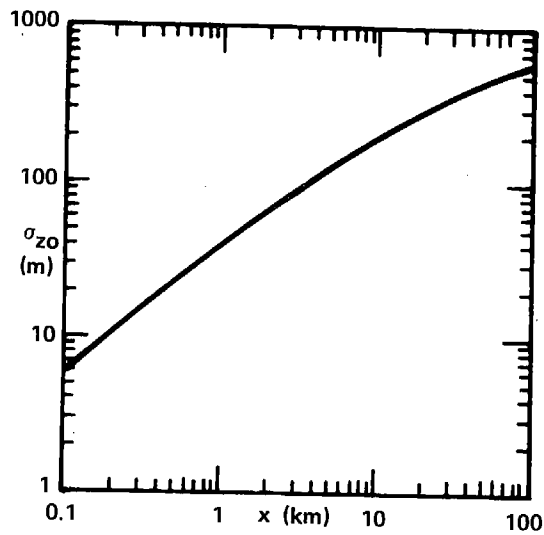
- σ_z^0 = the Workbook vertical dispersion standard deviation
- $g'(x)$ = the correction factor for surface roughness developed by F. B. Smith, $g(x)$, normalized by the value of the correction factor for a surface roughness of 3 cm

ΔH = the buoyant plume rise.

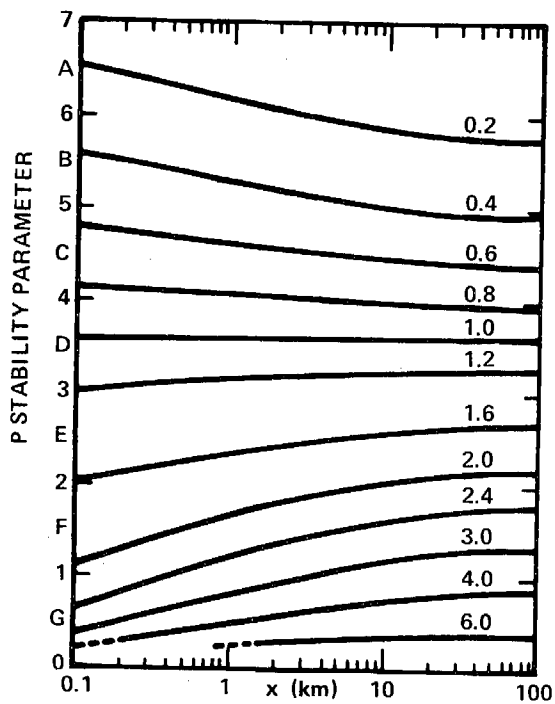
For urban areas, it is suggested that the value of $\sigma_z(x)$ be half of one stability class more unstable (to account for the increased instability due to the urban heat island). Although the type of averaging was not specified by EPA, it seems that in light of the logarithmic nature of the σ_z curves, the geometric mean is the appropriate average, e.g.,

$$\sigma_z \text{ (D stability, urban)} = \sqrt{\sigma_z \text{ (D stability, rural)} \cdot \sigma_z \text{ (C stability, rural)}}$$

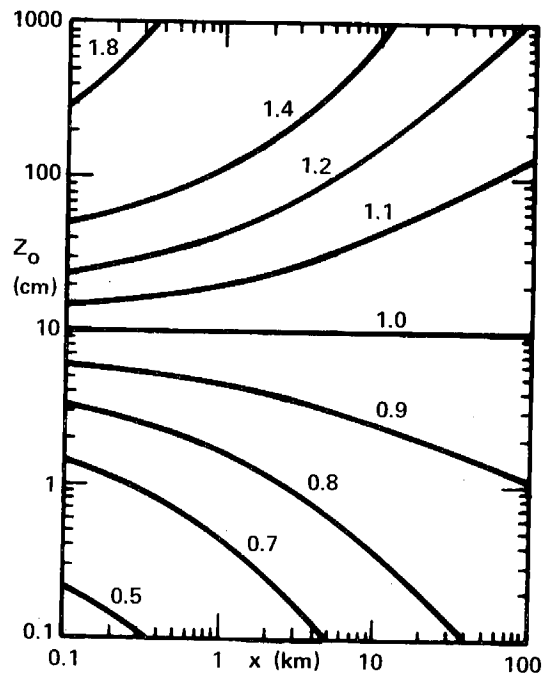
A comparison of the various prescriptions for σ_z over a smooth surface ($z_0 = 3$ cm) for unstable (A) and stable (F) conditions, illustrates the differences between the three approaches (Figure 3-5). Notice that the slope of the σ_z curve suggested by Smith



σ_{z0} FOR $z_0 = 10$ cm, NEUTRAL STABILITY

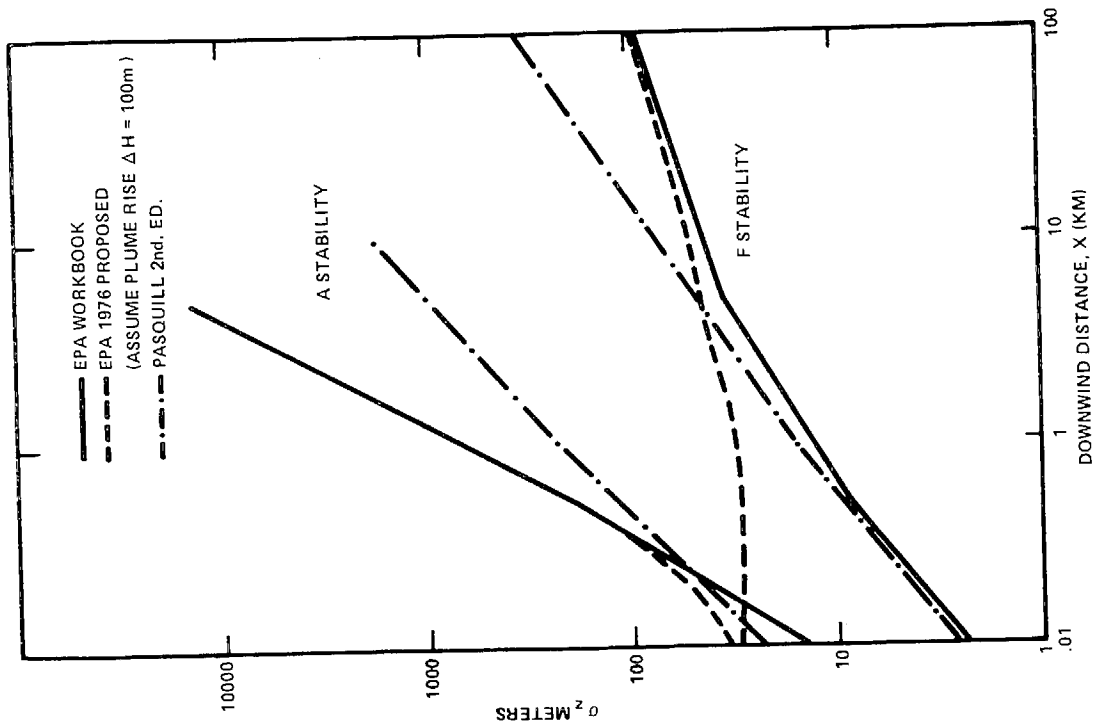


RECIPICAL OF STABILITY CORRECTION FACTOR $f^{-1}(x)$

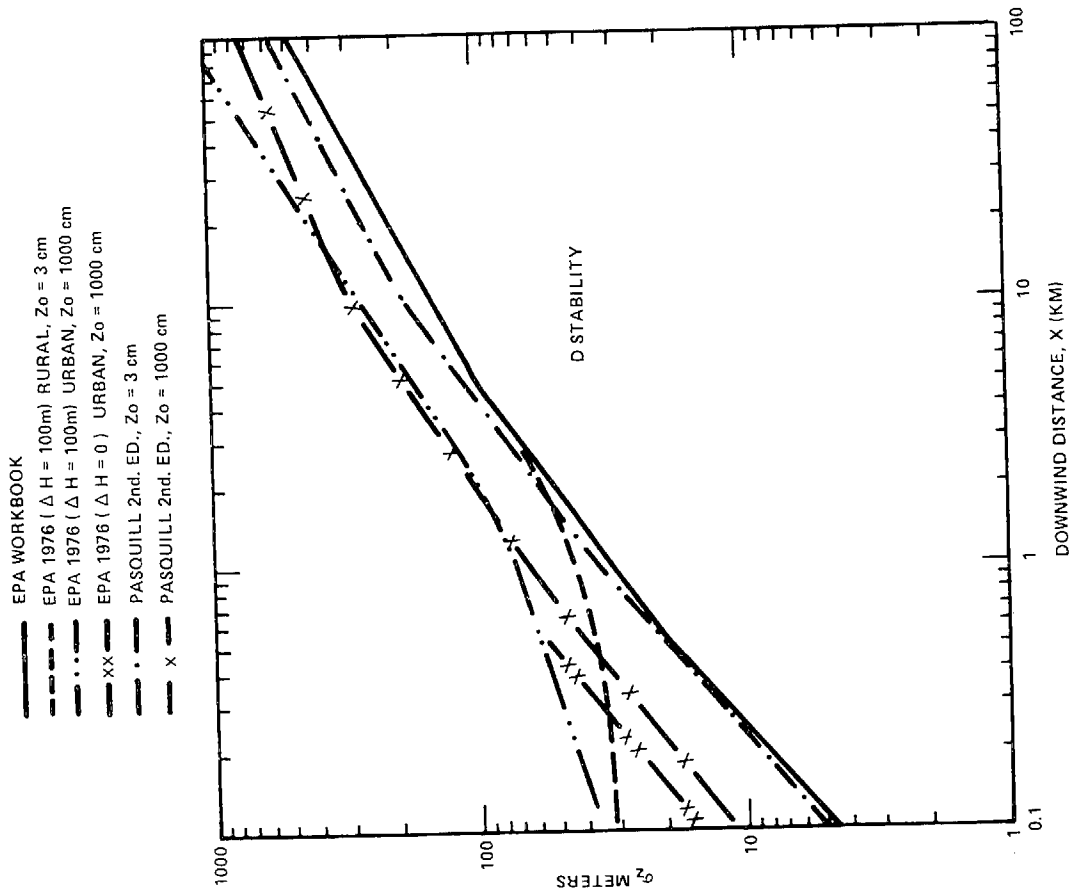


SURFACE ROUGHNESS CORRECTION FACTOR $g(x)$

Figure 3-4. Parametric Characterization of Numerical Solution of Vertical Dispersion, (F. B. Smith, Abstracted by Pasquill, 1974).



A. COMPARISON OF σ_z FOR RURAL AREAS ($Z_o = 3$ cm)



B. COMPARISON OF σ_z FOR RURAL ($Z_o = 3$ cm) AND URBAN AREAS ($Z_o = 1000$ cm)

Figure 3-5. Comparison of σ_z for Rural Areas and Urban Areas.

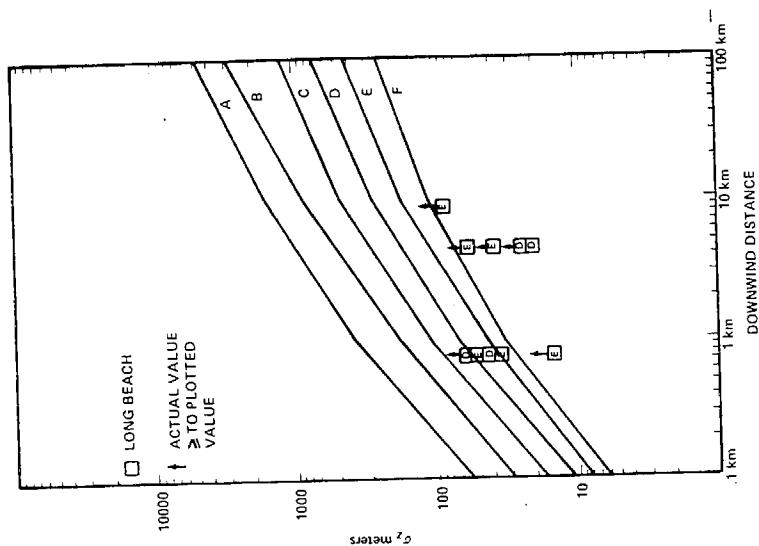
(Pasquill, 1974) is much less steep than the EPA Workbook values. The collection of accurate field data at long range for extremely unstable and stable conditions would help in selecting between the two approaches.

An additional increase to the vertical dispersion, suggested as a modification to the Workbook curves (Pasquill, 1976), is the dispersion caused by buoyant plume rise, Equation 3.5. As illustrated in Figure 3-5, this term is important only for small σ_z , i.e., for stable conditions and for distances less than a few kilometers. Field data from large sources under stable conditions would allow the verification of this theory.

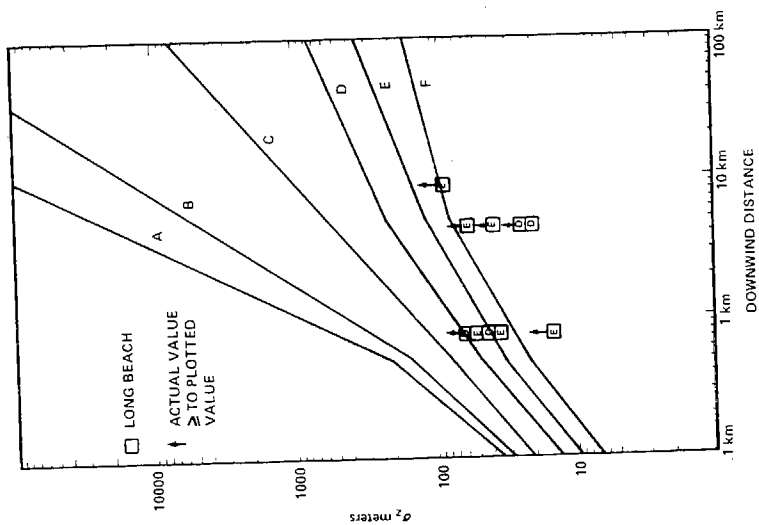
The variation in the values for σ_z for rural and downtown urban conditions is illustrated in Figure 3-5 for neutrally stable atmospheric conditions (stability class D). There is only a small difference between the curves proposed by Smith and the modified EPA curve under neutral conditions (when the buoyant plume rise ΔH is small).

Figure 3-6 provides comparison of the values of σ_z derived using data obtained during the ARB point source tracer program at Long Beach, incorporating the various σ_z formulations (assuming urban conditions and no plume rise). After reviewing this figure it is evident that the data collected during these field programs are not accurate enough nor sufficiently detailed to allow an evaluation of the proposed σ_z formulation.

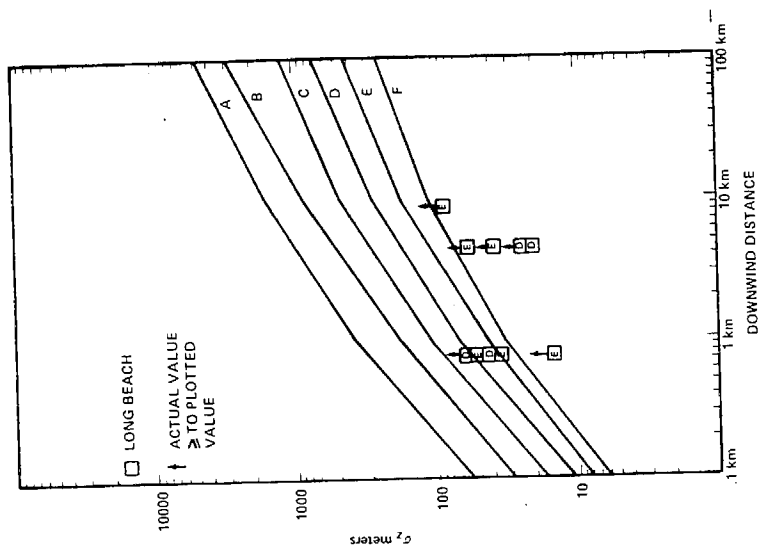
Aside from the prescription of the dispersion parameters, perhaps the most critical and uncertain issue is the prescription for the height of the plume centerline above the surface (i.e., the variable H in the vertical dilution term). This issue can be separated into two separate facets. The first is the calculation of the "effective stack height" or the rise of the hot buoyant plume above the physical height of the stack; the second is the trajectory of the plume centerline in mountainous or "complex" terrain.



A. EPA Workbook



B. EPA 1976



C. Pasquill 2nd Ed.

Figure 3-6. Comparison of Field Data with σ_z Formulations.

3.1.3 Plume Rise ΔH

The rise of the buoyant plume has been the subject of intensive investigation (Briggs, 1969 and 1975; Montgomery, 1974; Carpenter, 1971; Moore, 1974; Moses, 1961). Other approaches used to predict the effective stack height include hybrid analytic, finite difference methods (Winiarski, 1976), and two and three-dimensional solutions of the Navier-Stokes equations (Sklarew, 1970; Liu, 1976). Since this study was limited to the investigation and incorporation of existing methodologies, the latter approaches (which are advanced "state-of-the-art") were not included in our review.

Among the many plume rise formulas currently in use, the ones proposed by Briggs and by the Tennessee Valley Authority (TVA) are the most widely used. The formulas developed by Briggs were derived primarily through theoretical considerations (Briggs, 1975); while the formulas developed by TVA were derived primarily through the use of field data from large, coal-fired power plants (Montgomery, 1974). Our evaluation was restricted to these two approaches.

The formulation originally used by Briggs separated the plume rise phenomenology into two cases corresponding to neutral and unstable atmospheric conditions and to stable conditions which are considered separately.

For the former case, neutral and unstable conditions, Briggs derived the following formula

$$\Delta h = 1.6 \frac{F^{1/3}}{u} x^{2/3} \quad (3.6)$$

where

$F = gV' (T_o - T_a)/T_a$, the buoyancy

$g =$ gravitational acceleration (m^2/sec)

$V' =$ the exhaust volume flux divided by π (V' also equals wr^2 where w is the exit velocity and r is the inside stack radius) (m^3/sec)

T_o = the stack gas temperature ($^{\circ}\text{K}$)
 T_a = the ambient air temperature ($^{\circ}\text{K}$)
 u = the wind speed at the top of the stack (m/sec)
 x = the downwind distance (m)

Based on early experimental evidence, Briggs concluded that the final plume rise occurred at a downwind distance of ten stack heights

$$\text{final } \Delta h = 1.6 \frac{F^{1/3}}{u} (10 h_s)^{2/3} \quad (3.7)$$

However, his later works, based on additional data, conclude that the final plume rise occurs at a downwind distance that is a function of buoyancy

$$\text{final } \Delta h = 1.6 \frac{F^{1/3}}{u} (3.5 x^*)^{2/3} \quad (3.8)$$

where

$$\begin{aligned}
 x^* &= 14 F^{5/8} \quad \text{for } F \leq 55 \\
 x^* &= 34 F^{2/5} \quad \text{for } F > 55
 \end{aligned}$$

Under stable conditions, Briggs derived an expression for the final plume rise as

$$\text{final } \Delta h = (2.6 \text{ to } 2.9) \left(\frac{F}{uS} \right)^{1/3} \quad (3.9)$$

where

$$\begin{aligned}
 S &= \text{the stability parameter; } S = \frac{g}{\theta_a} \frac{\partial \theta_a}{\partial z} \\
 \theta_a &= \text{the potential temperature } (^{\circ}\text{K})
 \end{aligned}$$

The factor of 2.9 was derived as a best fit to initial experimental data; later data and additional theoretical considerations have lead Briggs to recommend the lower value of 2.6.

The plume rise formulations developed by TVA are based on an empirical fit to data taken under adverse meteorological conditions at their large, coal-fired power plants.

For neutral conditions, $-0.017 < \partial T_a / \partial z < -0.0084$ $^{\circ}\text{C/m}$:

$$\Delta h = 2.50 \frac{F^{1/3}}{u} x^{0.56} \quad \text{for } x \leq 3000 \text{ m} \quad (3.10)$$

where

$\frac{\partial T_a}{\partial z}$ is the ambient air temperature gradient ($^{\circ}\text{K/m}$)

For moderately stable conditions, $-0.0084 \leq \partial T_a / \partial z < -0.0030$:

$$\Delta h = 3.75 \frac{F^{1/3}}{u} x^{0.49} \quad \text{for } x \leq 2800 \text{ m} \quad (3.11)$$

For stable conditions, $-0.003 \leq \partial T_a / \partial z < +0.0087$:

$$\Delta h = 13.8 \frac{F^{1/3}}{u} x^{0.26} \quad \text{for } x < 1960 \text{ m} \quad (3.12)$$

TVA has not reported similar expressions for unstable atmospheric conditions. For the final plume rise (at downwind distances greater than 1824 meters), TVA recommends the use of a composite formula

$$\text{final } \Delta h = 173 \frac{F^{1/3}}{u} \exp (-64 \partial \theta_a / \partial z) \quad \text{for } x > 1824 \text{ m} \quad (3.13)$$

for neutral and stable atmospheric conditions.

A comparison of the latter Briggs formulation of plume rise and the TVA plume rise equations are shown in Figure 3-7 as a function of downwind distance. For both formulations the plume rise is proportional to the plume buoyancy to the one-third power ($F^{1/3}$) and inversely proportional to the wind speed (u^{-1}). In the Briggs formulation, the final plume rise is dependent on the initial buoyancy, but this is not the case with the TVA method. Thus, it appears that the Briggs formulation is more general since it treats all ranges of stack buoyancies, whereas the TVA formulation is only valid for large power plants.

The final plume rise predicted by the Briggs and TVA formulations are plotted as a function of potential temperature gradient in Figure 3-8. Notice that there is a disparity between the neutral-unstable Briggs plume rise formulation and his formulation for stable conditions. A calculation of plume rise for slightly stable conditions (Pasquill class D-E) could show large differences depending on the formulation used.

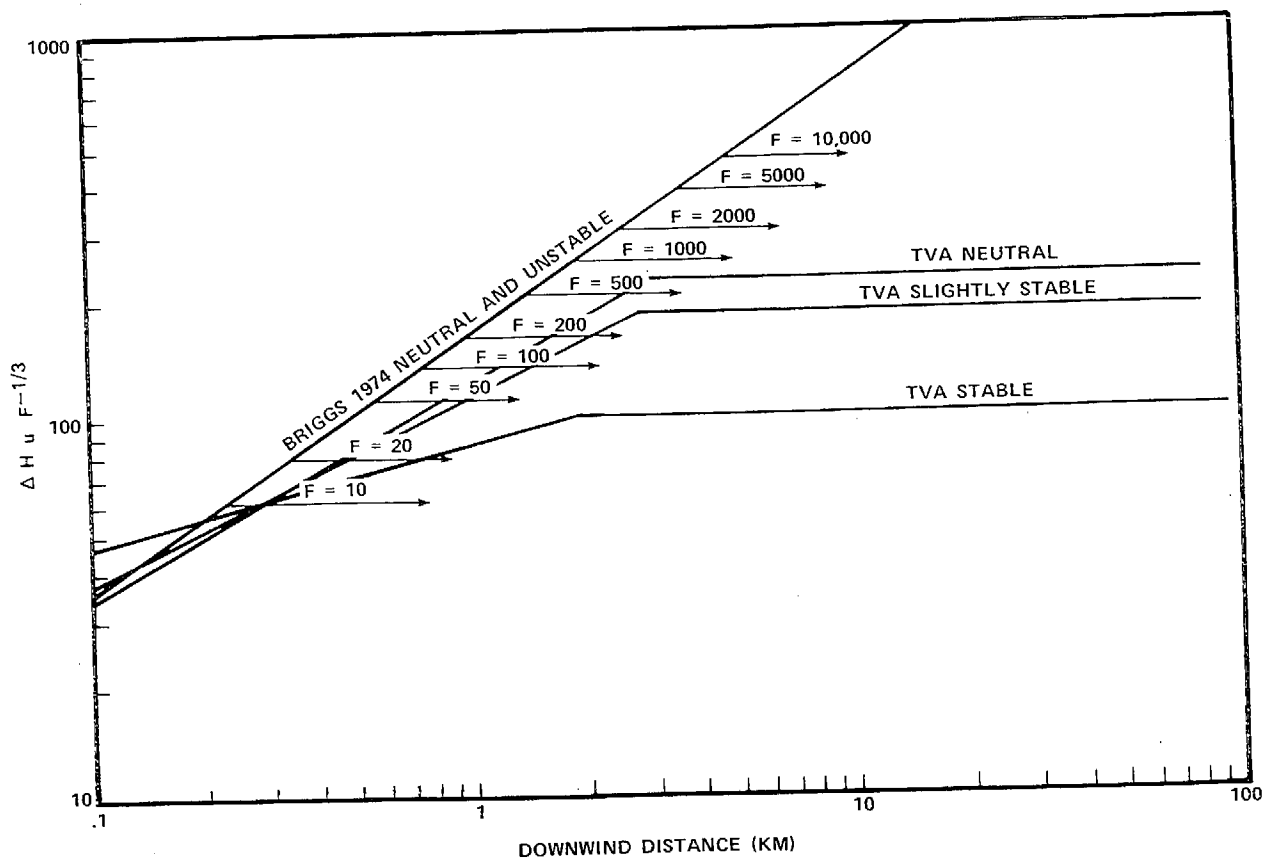


Figure 3-7. Plume Rise as a Function of Downwind Distance.

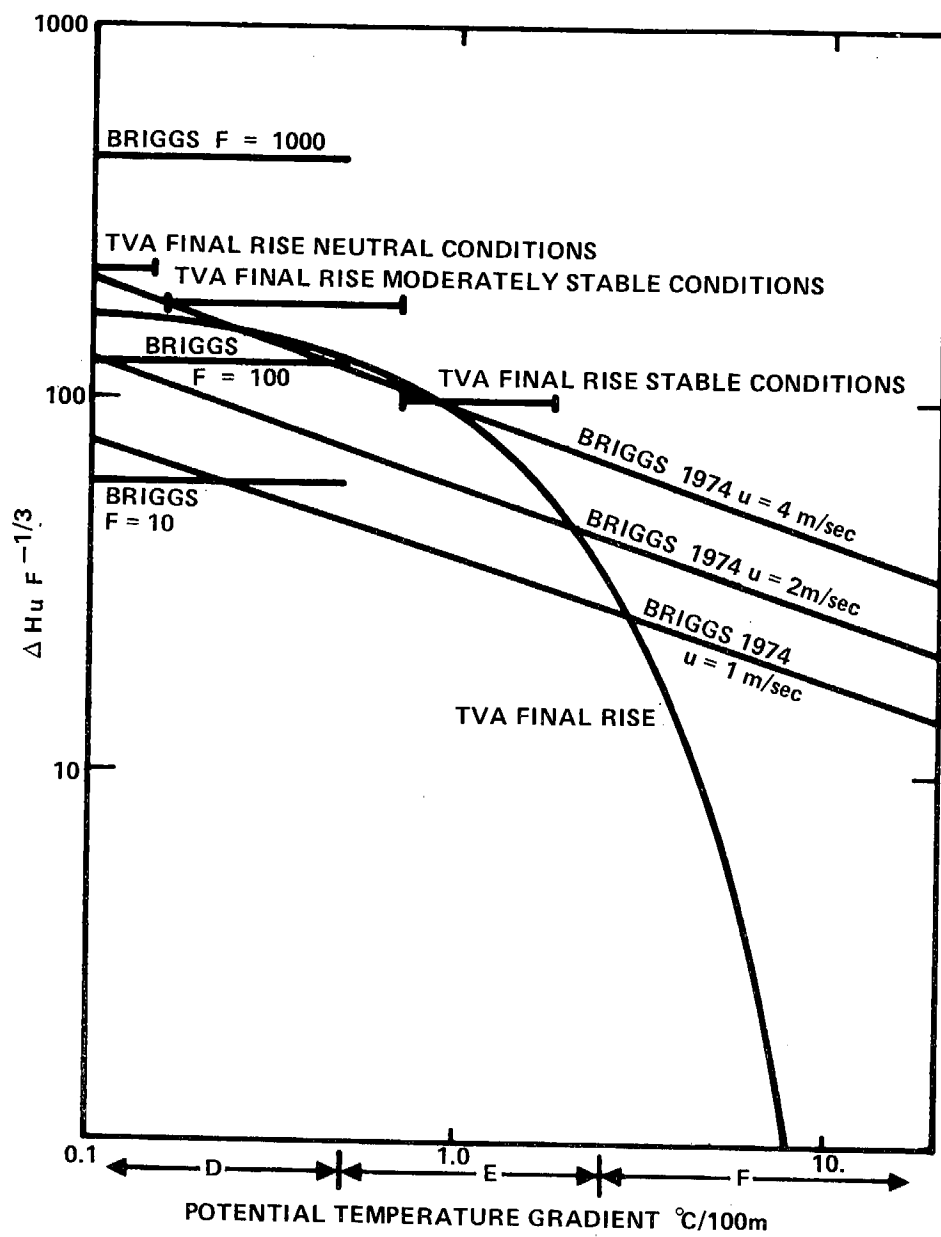


Figure 3-8. Final Plume Rise as a Function of Temperature Gradients for Stable Conditions.

Although both the Briggs and TVA formulations have been subjected to extensive verification, it was felt that it would be instructive to compare the plume rise actually measured in field tests selected for this study with the plume rise equations (Figure 3-9). Data of plume rise under unstable atmospheric conditions were obtained from the Garfield field tests in complex terrain. The range in the observed values is due to the difficulty in separating out the effects of plume rise and the effect of orographic lifting in the projected plume trajectory. The remainder of the data was obtained from the ARB point source tracer program of coastal sites at Moss Landing and Long Beach. The overprediction of all models in the latter tests is believed to be due to the influence of the inversion aloft (typical phenomenon of West Coast meteorology) that restricts the buoyant rise of the plume. Of the formulations considered in this study, none incorporate this effect. From the limited data presented in Figure 3-9, a tentative recommendation could be made to use the Briggs 1974 neutral-unstable formulation for unstable atmospheric conditions and the Briggs 1974 stable formulation for neutral and stable conditions. For a more comprehensive discussion of plume model validation, the reader is referred to Briggs (1975).

3.1.4 Complex Terrain

The Gaussian model was developed originally to predict pollutant concentrations over level or rolling terrain. The only factors incorporated to determine the height of the plume centerline above the surface were the physical height of the stack and the buoyant rise of the plume. In recent years, interest in the impact of pollutant emissions on the air quality in mountainous (complex) terrain has led to the extension of the model to account for the effects of complex terrain. The principal difficulty in applying the model to complex terrain is the determination of the trajectory of the plume and the value of the mixing height. A number of approximations have been developed in an attempt to retain the use of the relatively simple Gaussian model in complex terrain. The major approximations are reviewed below.

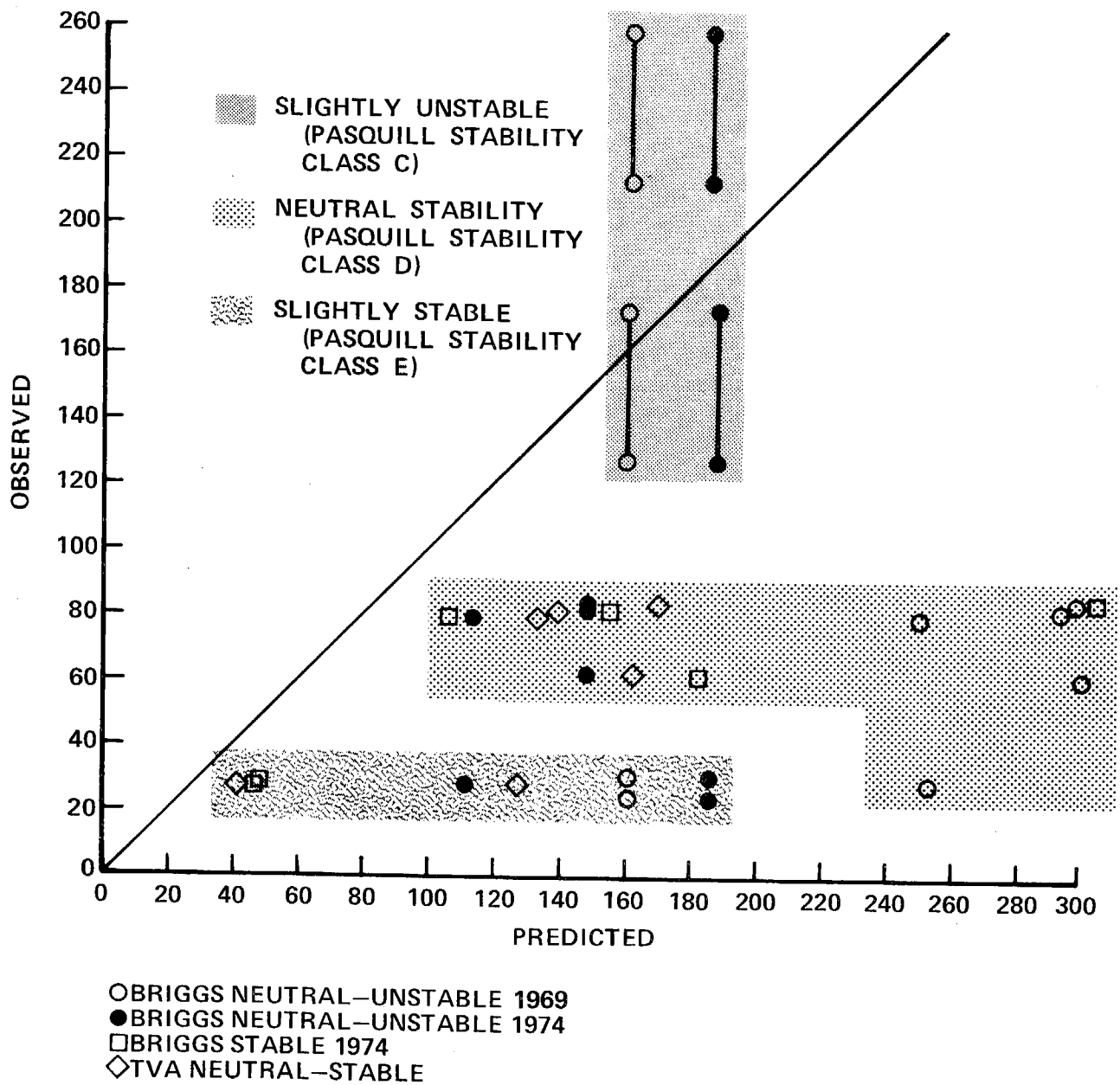


Figure 3-9. Comparison of Observed and Predicted Plume Rise Parameter ($\Delta H_u F^{1/3}$).

Perhaps the two most straightforward assumptions concerning plume trajectory are that either the plume trajectory is conformal with terrain (an assumption used in the EPA C4M3D model and the NOAA model for neutral or unstable conditions) or that the plume trajectory is horizontal regardless of terrain features (an assumption used in the EPA C4M3D model for stable atmospheric conditions (Egan, 1975) and in the Cramer model (Cramer, 1971) for all atmospheric conditions). The assumption of a horizontal plume trajectory can lead to the plume centerline impacting on the surface if the terrain is sufficiently high (see Figure 3-10); such plume impacts can result in unrealistically large predictions for pollutant concentrations. In an attempt to reduce the effects of this plume impact, the NOAA complex terrain model restricts the plume centerline height to a minimum of 10 meters, while assuming a horizontal trajectory under stable atmospheric conditions. Another formulation remotely based on theoretical considerations of potential flow over ridges is the ERT model (Egan, 1975) which assumes an intermediate trajectory halfway between the terrain conformal and horizontal trajectories. Figure 3-10 summarizes the various options discussed above. It is clear that under specific conditions any one of the above descriptions of plume trajectory may be correct; however, the authors have not seen convincing evidence for the use of any particular plume trajectory model. Figure 3-11 compares the field data taken at Garfield during two tests with the various plume trajectories discussed here. After reviewing these results and other test data at the Garfield site (all taken under unstable atmospheric conditions), it is felt that the ERT model for plume trajectory comes closest to predicting the actual trajectory.

Another consideration, directly accounted for only in the Cramer model, is a prescription for effective mixing heights in complex terrain. The Cramer prescription assumes that the mixing height is conformal with terrain except that it is never less than the observed (measured value). Additionally, receptors located on terrain above the observed mixing height are assumed to

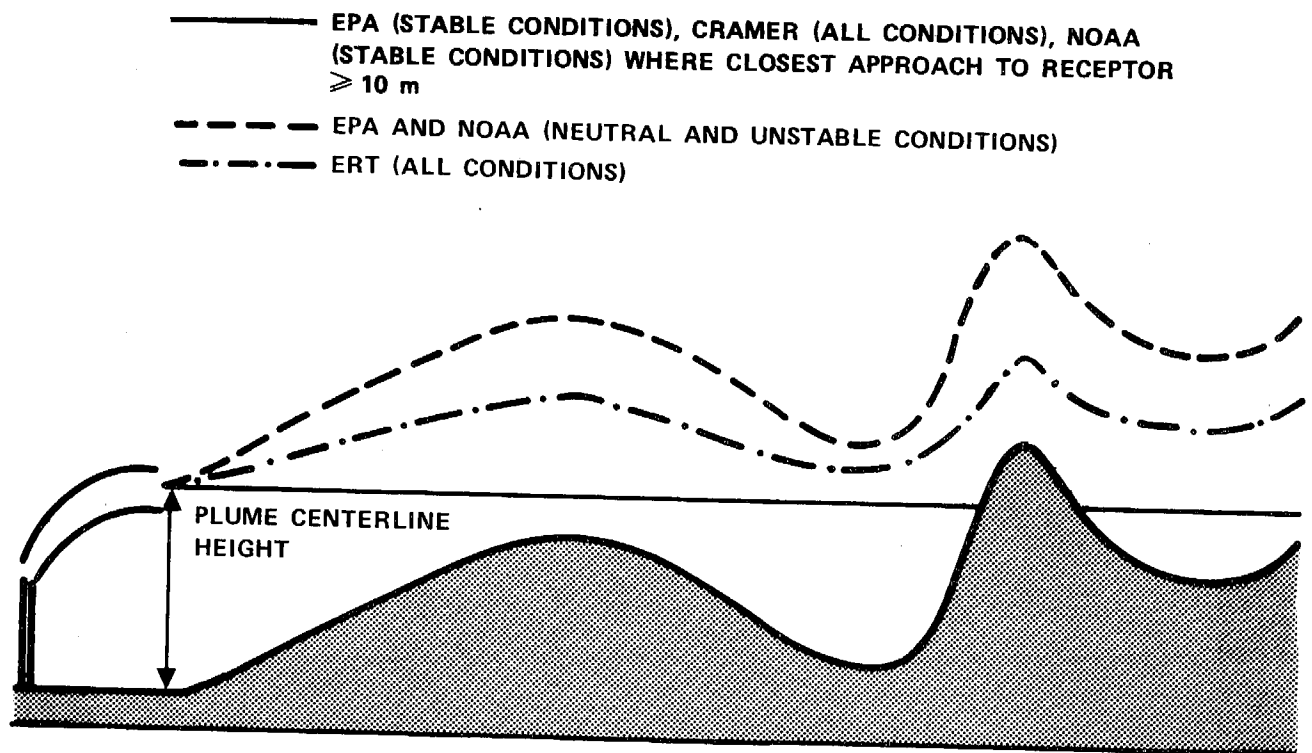


Figure 3-10. Plume Centerline Trajectory in Complex Terrain.

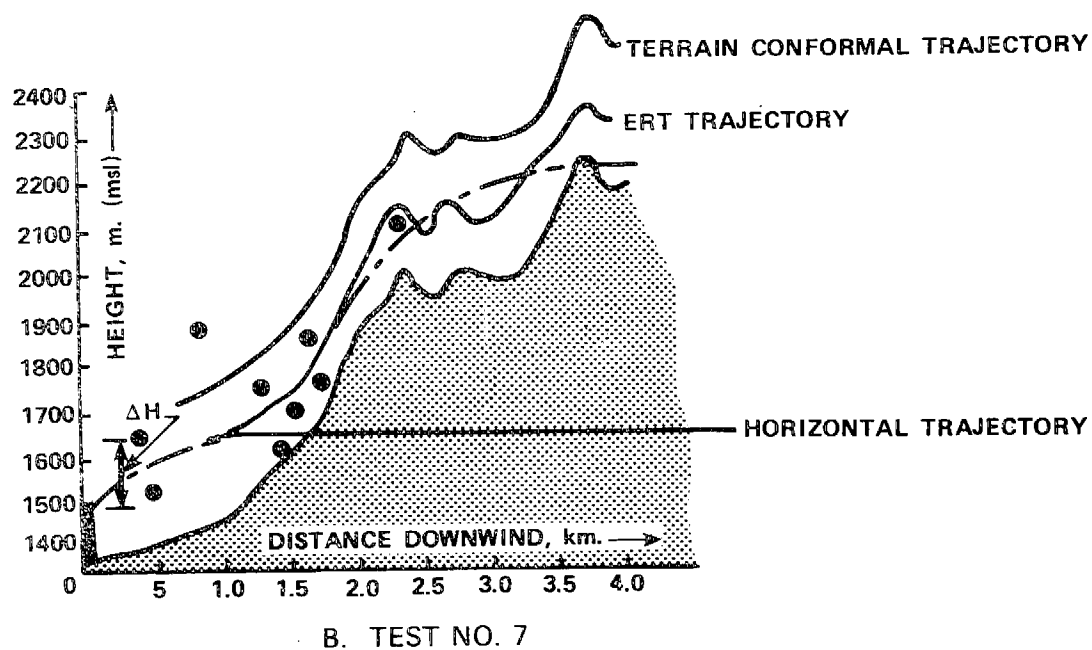
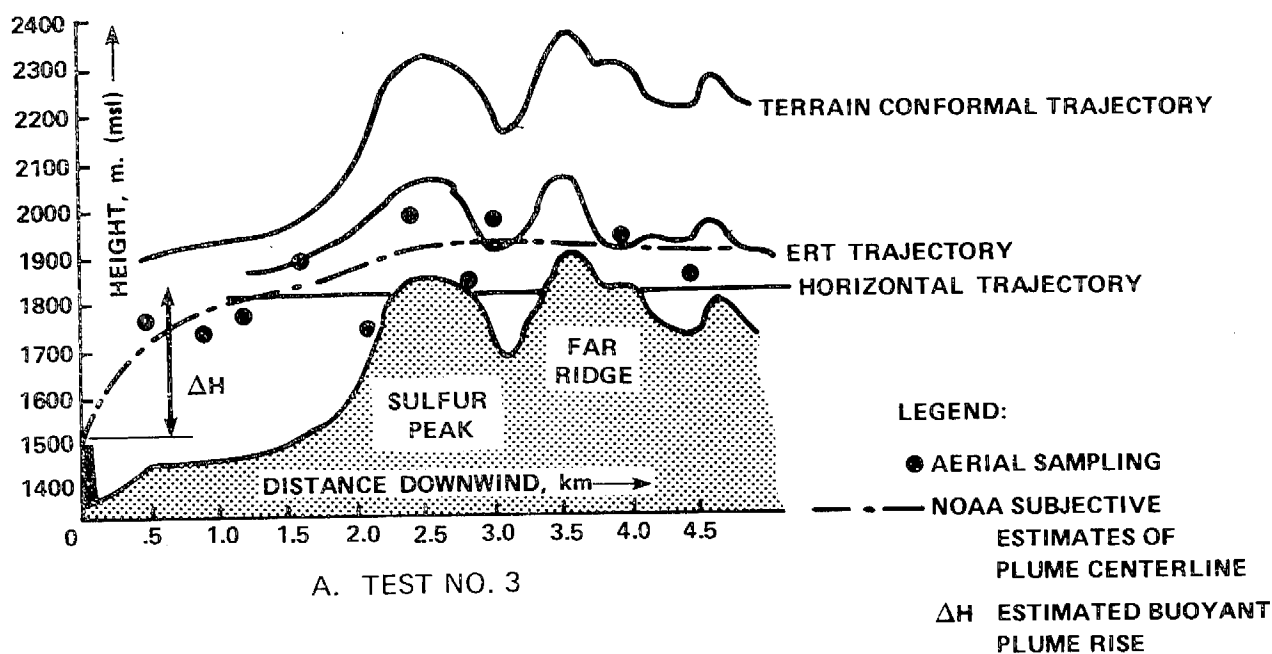


Figure 3-11. Comparison of Various Plume Trajectories Using Data from Two Garfield Tests.

be above the mixing height and thus not impacted by the plume. Other possible prescriptions include a horizontal mixing height or a mixing height completely conformal with terrain. The horizontal prescription is perhaps the most realistic under stable meteorological conditions, but the use of this prescription will result in very high concentrations for receptors on terrain near the top of the mixing layers. A diagram of these various prescriptions is given in Figure 3-12. It should be noted that the Gaussian model is not actually applicable to complex terrain situations where high wind shear and strong inversions can result in plume channeling and other effects that produce non-Gaussian concentration profiles. The use of prescriptions for plume trajectory and mixing heights are at best an ad hoc patch to extend the model into conditions where it may not be applicable. Thus, the reader is cautioned that the use of these models in complex terrain is at best useful for approximate estimates and may result in large errors with certain applications.

3.1.5 Limited Mixing

A frequent situation encountered in plume modeling is the case of a plume trapped below an inversion. In this situation, the vertical spread of the plume is limited between the surface and the height of the mixing layer.

The EPA Workbook (Turner, 1970) suggests that for σ_z less than 0.47 times the mixing height, the normal Gaussian formulation is correct; while for σ_z greater than 0.8 times the mixing height, assume that the plume is uniformly mixed in the vertical. Mathematically, in terms of the vertical dilution factor (Equation 3.1), this can be expressed as

$$\begin{aligned} \{\text{vertical dilution term}\} &= \frac{1}{\sigma_z} \left[e^{-(H+z)^2/2\sigma_z^2} + e^{-(H-z)^2/2\sigma_z^2} \right] \\ &\quad \text{for } \sigma_z < 0.47H \\ &= \frac{2}{0.8H} \quad \text{for } \sigma_z \geq 0.8H \end{aligned} \tag{3.14}$$

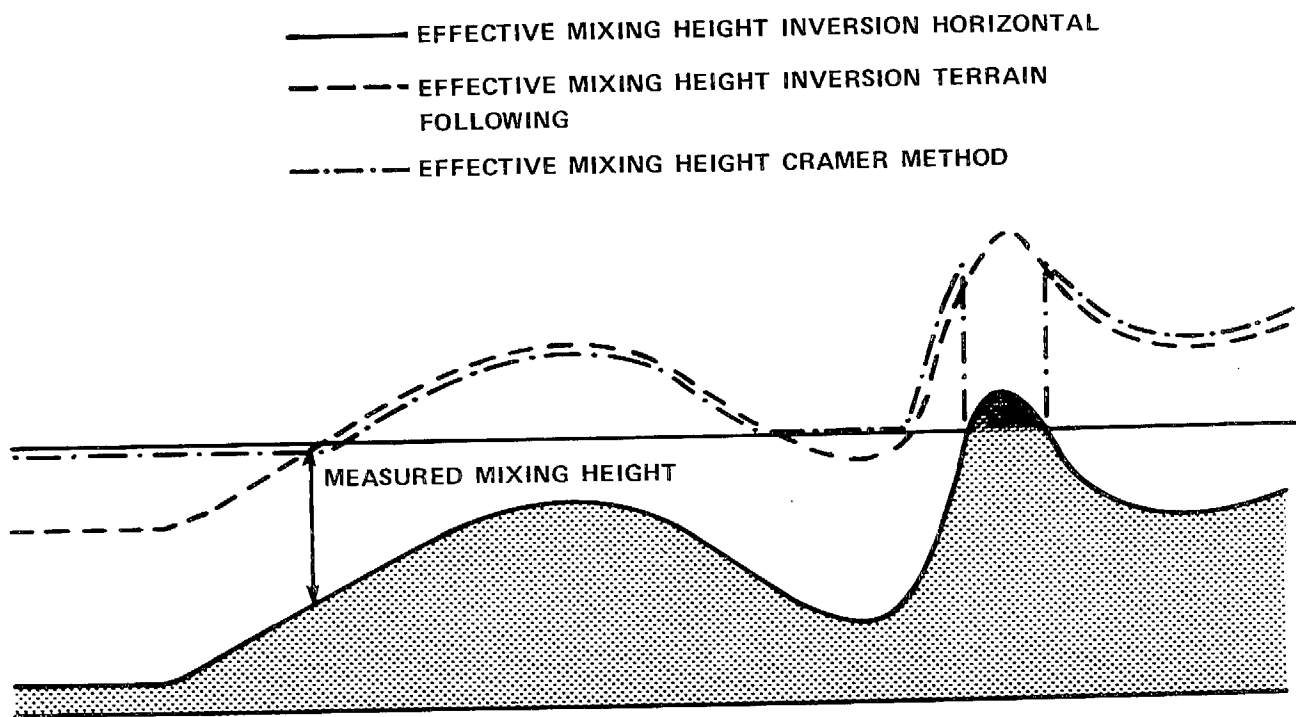


Figure 3-12. Effective Mixing Height in Complex Terrain (i.e., Height of Inversion).

For intermediate values of σ_z ($0.8H > \sigma_z \geq 0.47H$, where H = height of the mixing layer), interpolation between the two solutions is used.

A mathematically more precise solution for the limited mixing situation can be derived using the method of multiple images to satisfy the boundary conditions at the surface and the top of the mixing layer. In principle, an infinite number of image sources are required; however, the importance of each succeeding image source quickly diminishes and the total number of images can be limited (e.g., Cramer, 1971). The vertical dilution term can be represented as

$$\begin{aligned} \{\text{vertical dilution term}\} &= \frac{1}{\sigma_z} \left[\sum_{i=1}^n e^{-(H_i - z)^2 / 2\sigma_z^2} \right. \\ &\quad \left. + \sum_{j=1}^m e^{-(H_j + z)^2 / 2\sigma_z^2} \right] \end{aligned} \quad (3.15)$$

where

$$H_i = H, 2H-H, 2H+H, 4H-H, 4H+H, \dots$$

As the latter terms become larger, the plume becomes uniformly distributed throughout the mixed layer and the vertical dilution term reduces to

$$\{\text{vertical dilution term}\} = \frac{\sqrt{2\pi}}{H} \text{ or } \approx \frac{2}{0.8H}$$

Figure 3-13 presents comparison of the two methods, assuming a ground level receptor ($z = 0$) and a number of effective stack heights which are parameterized as $\beta = H/H$ (i.e., for $\beta = 1$, the plume height is at the top of the mixed layer; for $\beta = 0$, the plume is at ground level). Except for plumes with effective stack height near the top of the mixed layer (i.e., $\beta > 0.8$), both methods result in approximately equivalent values for the vertical dilution factor; while the differences at large β 's are usually less than 10%. Thus, it appears that the two methods are essentially equivalent and the selection of a particular approach is a matter of computational efficiency and convenience.

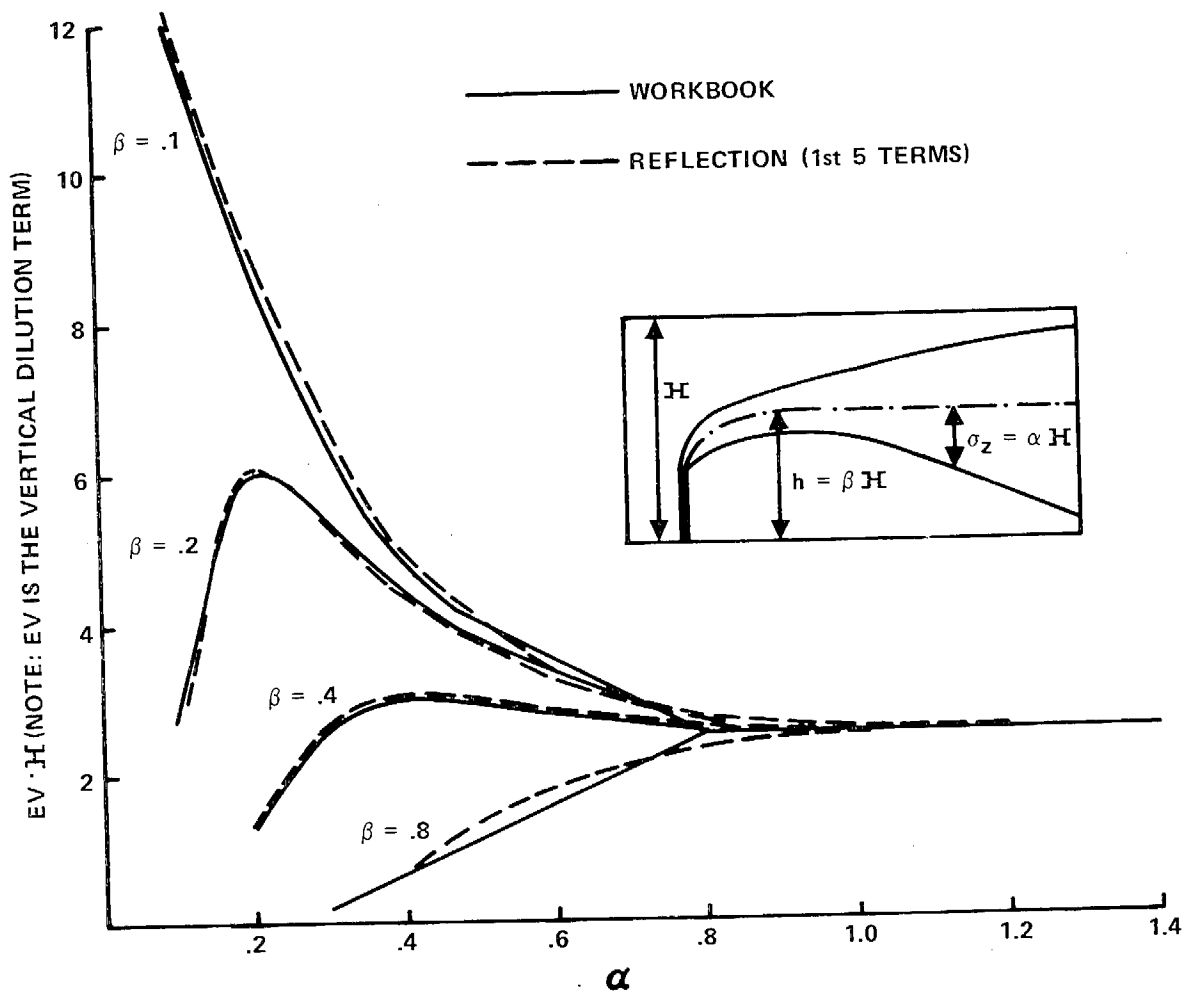


Figure 3-13. Ground Level Vertical Dilution Term as a Function of Mixing Height, σ_z , and Plume Rise for the Workbook and Reflection Models.

3.2 Modification of the Gaussian Evaluation Model for Grided Receptors

The Gaussian evaluation model, GEM, was written as an extension to the EPA PTMPT model, incorporating options that have been proposed as improvements or additions to the basic Gaussian model. In the course of this program it became apparent that a modified version of GEM that would automatically calculate a concentration distribution over an entire region of grided receptors (i.e., similar output to the grid type models) would be useful for model validation and general impact analysis. Thus, the GEM model modified for a grided array of receptors, GEMGAR, was written. Instead of the individual receptor data required by the GEM model, terrain height data must be entered. The values of the grid spacing (DX, DY) and grid size (NX, NY) can also be selected through simple input to the code.

The program output is in the form of a concentration array (in $\mu\text{g}/\text{m}^3$) that is printed from top to bottom in a format that is distortionless on a conventional computer printer so that contour plots, overlays, etc. can be made directly from the printed output. Figure 3-14 is a diagram of the GEMGAR grid. A complete description of the GEMGAR model is given in Appendix B, entitled "User's Guide to GEMGAR."

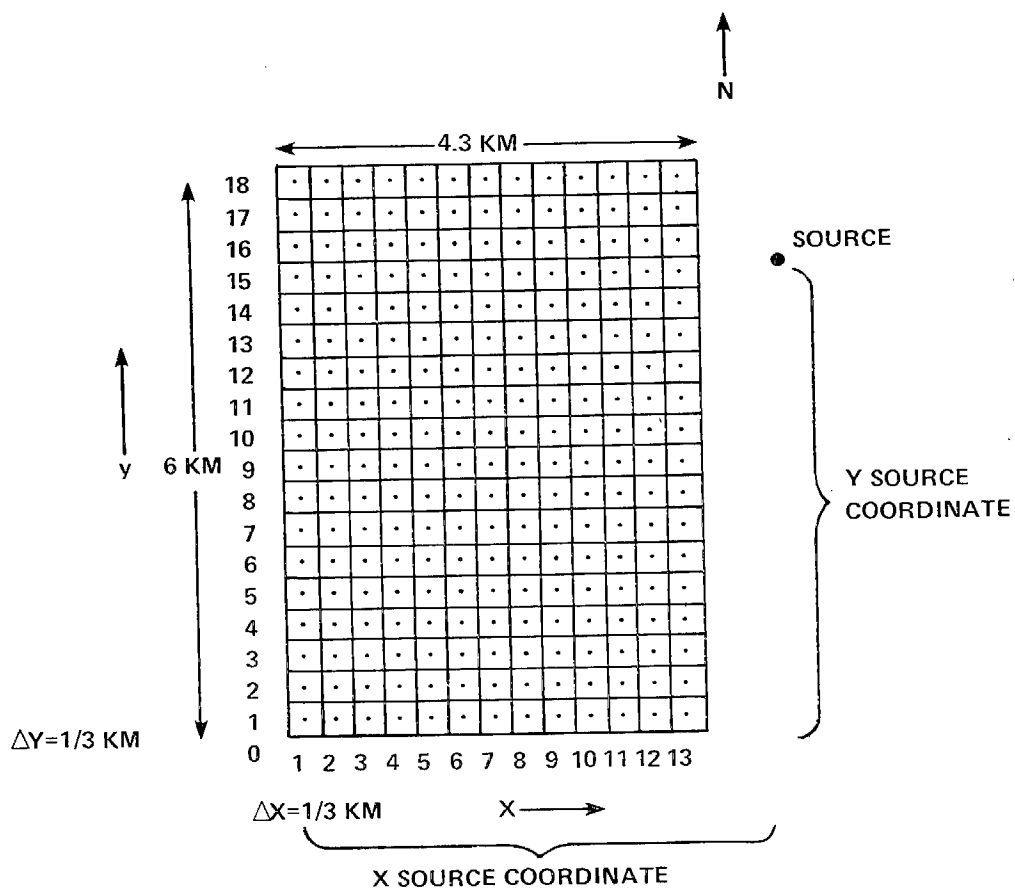


Figure 3-14. Example GEMGAR Grid.

4.0 THE GRID MODEL IMPACT (INTEGRATED MODEL FOR PLUMES AND ATMOSPHERICS IN COMPLEX TERRAIN)

The IMPACT model is designed to serve as a standard advanced point source air quality model for the California Air Resources Board and for the California Energy Resources Conservation and Development Commission. As such, major emphasis was placed on developing a well-structured code with user-oriented input and output. The code was developed in a modular fashion in order that continued improvements in the individual modules can be incorporated without major revision of the entire code.

4.1 General Description of IMPACT

The structure of IMPACT differs from the Gaussian evaluation model since the code is designed to solve the conservation of mass equation

$$\frac{\partial C_i}{\partial t} = - \underbrace{\frac{\partial u C_i}{\partial x} - \frac{\partial v C_i}{\partial y} - \frac{\partial w C_i}{\partial z}}_{\text{advection}} + \underbrace{\frac{\partial}{\partial x} \left(K_x \frac{\partial C_i}{\partial x} \right) + \frac{\partial}{\partial y} \left(K_y \frac{\partial C_i}{\partial y} \right) + \frac{\partial}{\partial z} \left(K_z \frac{\partial C_i}{\partial z} \right)}_{\text{diffusion}} + \underbrace{S_i}_{\text{source term}} + \underbrace{\alpha_{ij} C_j + \beta_{ijk} C_i C_j}_{\text{chemistry}} \quad (4.0)$$

where

- C_i = the i^{th} pollution species
- u, v, w = the three-dimensional wind flow field vectors
- K_x, K_y, K_z = the three-dimensional eddy diffusivity tensor
- S_i = the source term for the i^{th} pollution species
- α, β = the chemical rate constants for first and second-order chemical reactions.

This formulation allows the code to automatically treat single or multiple point or area sources, the effects of arbitrary vertical temperature stratifications (e.g., multiple inversions), shear flows caused by atmospheric boundary layers or by terrain effects, terrain channeling, and chemical transformations (such as those creating photochemical smog). Thus, it provides a more realistic representation of the actual real-world situation than the Gaussian models which are steady state, assume uniform wind and diffusion fields, and can incorporate only simple chemical reactions. The advantages of the grid model come, however, at the expense of larger computer storage and run-time requirements, and increased complexity in coding. Therefore, a major effort must be directed at efficiency in computer storage and speed, as well as overall accuracy.

The basic structure of the model is illustrated in Figure 4-1. The shaded modules represent the major components of the code, with the remainder of the program directing program flow and processing input and output data. The five major modules and available options are as follows:

- Wind field module (WEST) —→ creates u, v, w field
- Diffusivity field module (DIFFUS) —→ creates K_x , K_y , K_z field (options include: M/R, DEPICT)
- Source term module (PLUMER) —→ locates pollutant emissions from point sources (options include: Briggs, 1967; Briggs, 1974; TVA; specified)
- Pollutant advection and diffusion module (ADH) —→ solves the advection and diffusion portion of Equation 4.0
- Chemistry modules (CHEM) —→ solve the chemistry portion of Equation 4.0. (options include: inert, SO_2 conversion, GRC photochemistry, EPA photochemistry).

The remainder of this chapter will discuss the options investigated and tested for each of the modules and the rationale for selecting the particular method(s) in the initial version of IMPACT.

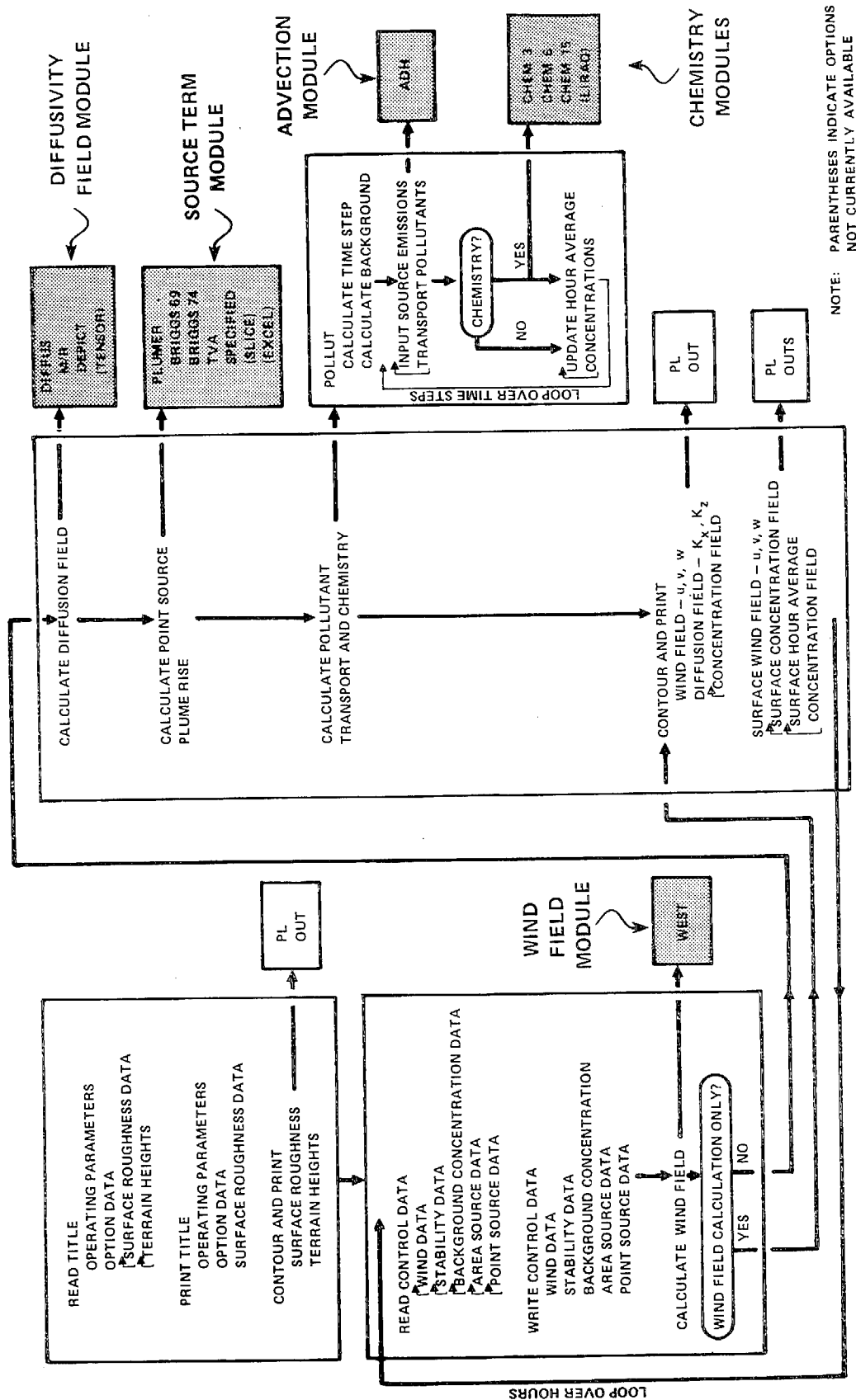


Figure 4-1. IMPACT Logic Flow.

4.2 Review of the Wind Field Module Options

A realistic, accurate treatment of the wind field is essential to any model that seeks to simulate atmospheric phenomena. Thus, a wide range of models have been developed, from the simplistic $1/r^2$ interpolation of measured data to global climatological simulation models. The focus of our investigation is narrowed by the scale of the problem under consideration which is generally thought of as mesoscale meteorology (i.e., roughly a 100 to 1000 km² area). Other criteria used for preliminary review were that the model had to be non-proprietary, user-ready, efficient, and tested to some extent. In other words, the wind module had to be an existing model in the public domain. This initial screening resulted in the list of available wind field modules shown in Table 4-1.

These models were then reviewed and the salient model characteristics evaluated (see Table 4-1). Another level of screening was accomplished by addressing the need of the other modules that interfaced with the wind field module, and the anticipated use of the overall code. From these considerations two criteria were established: the wind module must incorporate terrain effects, and the wind field output must be three-dimensional. These criteria were selected so that the overall model would be capable of modeling flow in complex terrain and be capable of modeling complex atmospheric conditions such as inversions aloft, wind shear, and terrain channeling.

The evaluation of the selected models in Table 4-1 using the above criteria resulted in the narrowing of the wind field module selection to two models: WEST which is a submodel of the DEPICT code (Sklarew, 1976), and MATHEW which was developed by Lawrence Livermore Laboratory as part of their wind energy siting program (Sherman, 1976). The sigma-coordinate models (Fosberg, 1976; Anderson, 1970; Liu's fine grid, 1974) all suffer from a lack of vertical resolution. If versions of these models were developed that feature a three-dimensional wind field, a second look would

Table 4-1. Comparison of Wind Field Models.

MODEL	MODEL CHARACTERISTICS							
	VERTICAL RESOLUTION OF WIND FIELD	TOPOGRAPHY	SURFACE ROUGH- NESS	ATMOSPHERIC STABILITY	CORIOLIS FORCE	SURFACE HEATING	INTERIOR WIND MEASUREMENTS	STEADY STATE
WEST - SKLAREW, WILSON - SCIENCE APPLICATIONS	YES	EXPLICIT	NO (VIA WIND DATA)	YES	NO (VIA WIND DATA)	NO (VIA WIND DATA)	YES	YES
FOSBERG - USDA	NO	SIGMA COORDINATE	YES	VIA PRESSURE & TEMP FIELD	NO	YES	NO	YES
MATHEW - LLL	YES	EXPLICIT	NO (VIA WIND DATA)	YES	NO (VIA WIND DATA)	NO (VIA WIND DATA)	YES	YES
ANDERSON - CENTER FOR ENVIRONMENT AND MAN	NO	SIGMA COORDINATE	NO	NO	NO	YES	NO	YES
COARSE GRID, LIU SYSTEMS APPLICATIONS	YES	NO	NO	YES	YES	YES	NO	NO
FINE GRID, LIU SYSTEMS APPLICATIONS	NO	SIGMA COORDINATE	NO	NO	NO	YES	NO	YES

be warranted since this model class incorporates the effects of surface roughness, atmospheric pressure and temperature, and surface heating in a direct manner. The other model, Liu's coarse grid (Liu, 1974), is essentially an explicit, time-dependent solution of the Navier-Stokes equation; with the incorporation of terrain capability, this model might represent an accurate treatment of wind field physics. However, the expense and complexity of this approach would be so great as to render the overall code impractical as an applications-oriented air quality simulation model.

Both MATHEW and WEST are objective analysis wind field models. Both are three-dimensional and produce terrain-dependent, divergence-free wind fields given observed wind data as input. Both models follow a procedure of extrapolating and interpolating the input data to develop a first estimate of the three-dimensional wind field. The estimated wind field is then adjusted to account for terrain effects and atmospheric stability considerations constrained by the condition that the resulting wind field be nondivergent. The exact procedure for determining each of these steps differs in the two models; a discussion of the structure of the two schemes is given below.

The theoretical basis for MATHEW was developed by Sasaki (1970). A difference functional is defined to minimize the deviation of the adjusted wind field from the estimated field, subject to the constraint that the adjusted wind field be nondivergent. The form of the functional proposed by Lawrence Livermore Laboratory (Sherman, 1976) can be written

$$E(u,v,w,\lambda) = \int_V \left[\alpha_1^2 (u-u^0)^2 + \alpha_2^2 (v-v^0)^2 + \alpha_3^2 (w-w^0)^2 + \lambda \left(\frac{\partial u}{\partial x} + \frac{\partial v}{\partial y} + \frac{\partial w}{\partial z} \right) \right] dV \quad (4.1)$$

where

$$\begin{aligned}
 u, v, w &= \text{the adjusted local velocity components} \\
 u^o, v^o, w^o &= \text{the estimated local velocity components in} \\
 &\quad \text{the } x, y, z \text{ directions} \\
 \lambda = \lambda(x, y, z) &= \text{the Lagrange multiplier} \\
 \alpha_i &= \text{Gaussian precision moduli taken to be} \\
 &\quad \alpha_i^2 = 1/2\sigma_i^2.
 \end{aligned}$$

The values of σ_i represent observational errors and/or deviations of the observed field from the desired adjusted field due to empirical considerations of atmospheric stability.

The associated Euler-Lagrange equations whose solution minimizes Equation 4.1 may be written as

$$\begin{aligned}
 2\alpha_1^2(u-u^o) - \frac{\partial \lambda}{\partial x} &= 0 \\
 2\alpha_2^2(v-v^o) - \frac{\partial \lambda}{\partial y} &= 0 \\
 2\alpha_3^2(w-w^o) - \frac{\partial \lambda}{\partial z} &= 0
 \end{aligned} \tag{4.2}$$

The equation for λ is derived by differentiating the three parts of Equation 4.2, and substituting into the continuity equation

$$\frac{\partial u}{\partial x} + \frac{\partial v}{\partial y} + \frac{\partial w}{\partial z} = 0 \tag{4.3}$$

to obtain

$$\begin{aligned}
 &\left[\frac{1}{2\alpha_1^2} \frac{\partial^2 \lambda}{\partial x^2} + \frac{1}{2\alpha_2^2} \frac{\partial^2 \lambda}{\partial y^2} + \frac{1}{2\alpha_3^2} \frac{\partial^2 \lambda}{\partial z^2} \right] \\
 &\quad + \left[\frac{\partial u^o}{\partial x} + \frac{\partial v^o}{\partial y} + \frac{\partial w^o}{\partial z} \right] = 0
 \end{aligned} \tag{4.4}$$

This is a Poisson equation for λ and may be solved iteratively, subject to the boundary condition

$$A \lambda + B \frac{\partial \lambda}{\partial \hat{n}} = 0 \quad (4.5)$$

where

$A = 1$; $B = 0$, for flow-through boundaries

$A = 0$; $B = 1$, for solid boundaries.

Once λ is determined, it is substituted back into Equation 4.2 to yield the adjusted velocity field.

The WEST adjustment model is mathematically similar to that in MATHEW. However, certain dissimilarities between the two models do exist. The estimated wind field is first adjusted to obtain a global divergence-free field, i.e., the flow through the side boundaries of the computational domain are first adjusted such that the amount of fluid entering the domain is equal to the amount of fluid leaving. This is accomplished by summing the product of the normal velocity component and its cell face area along the boundaries and then dividing by the total boundary area of the sides, i.e.,

$$\delta V_+ = \frac{\sum \vec{V}_{B+} \cdot \vec{\delta A}}{A}$$

$$\delta V_- = \frac{\sum \vec{V}_{B-} \cdot \vec{\delta A}}{A}$$

$\vec{\delta A}$: Outward normal

A : Total area of sides

\vec{V}_{B+} : Velocity at boundary (inflow)

\vec{V}_{B-} : Velocity at boundary (outflow)

and then adjusting the boundary cell normal velocities by

$$\vec{V}_{B+} \cdot \vec{\delta A} = \vec{V}_{B+} \cdot \vec{\delta A} (\delta V_- / \delta V_+)^{\frac{1}{2}}$$

$$\vec{V}_{B-} \cdot \vec{\delta A} = \vec{V}_{B-} \cdot \vec{\delta A} (\delta V_+ / \delta V_-)^{\frac{1}{2}}$$

This procedure is followed primarily to speed convergence and does not significantly effect the final flow field, since all boundaries (except the surface) are unconstrained during the iteration phase.

WEST also requires the local wind field to be nondivergent. The adjusted nondivergent velocity components can be defined by

$$\begin{aligned} u &= u^0 + \bar{u} \\ v &= v^0 + \bar{v} \\ w &= w^0 + \bar{w} \end{aligned} \tag{4.6}$$

where

\bar{u} , \bar{v} , \bar{w} are given by

$$\begin{aligned} \bar{u} &= \tau_x \frac{\partial \phi}{\partial x} \\ \bar{v} &= \tau_y \frac{\partial \phi}{\partial y} \\ \bar{w} &= \tau_z \frac{\partial \phi}{\partial z} \end{aligned} \tag{4.7}$$

Here ϕ is the perturbation velocity potential and τ_x, τ_y, τ_z are transmission coefficients based on temperature profiles obtained from upper air soundings. The present assignment of transmission coefficients was developed on the basis of numerical simulations of idealized test problems and appears to be qualitatively correct. The assignment of transmission coefficients is as follows (note, $\tau_y = \tau_x$):

Atmospheric Stability	A	B	C	D	E	F	G
τ_x/τ_z	.625	.714	.833	1.0	250	833	2500

The requirement that the local wind field is nondivergent is given by Equation 4.3.

Substituting Equations 4.6 and 4.7 into Equation 4.3 leads to a Poisson equation for the perturbation velocity potential

$$\left[\frac{\partial}{\partial x} \left(\tau_x \frac{\partial \phi}{\partial x} \right) + \frac{\partial}{\partial y} \left(\tau_y \frac{\partial \phi}{\partial y} \right) + \frac{\partial}{\partial z} \left(\tau_z \frac{\partial \phi}{\partial z} \right) \right] + \left[\frac{\partial u^0}{\partial x} + \frac{\partial v^0}{\partial y} + \frac{\partial w^0}{\partial z} \right] = 0 \quad (4.8)$$

To demonstrate that the velocity iteration scheme in WEST is a consequence of assuming that the perturbation velocity is derivable from a potential function, we start by assuming a computational domain which consists of N computational cells and is subject to the condition that

$$D_n(u) = (\nabla \cdot \vec{u})_n = 0 \quad n=1, \dots, N \quad (4.9)$$

For simplicity we will assume a two-dimensional Cartesian geometry.

Then $\vec{u} = (u, v)$

with u , the matrix, as follows:

$$u = \begin{bmatrix} u_1 & u_2 & \cdot & \cdot & \cdot & \cdot & u_N \\ v_1 & v_2 & \cdot & \cdot & \cdot & \cdot & v_N \end{bmatrix} .$$

Let $\vec{u} = \vec{u}(\phi)$

with the specific relationship,

$$\vec{u} = \nabla \phi \quad (4.10)$$

Then, Equation 4.9 can be written

$$D_n(\vec{\phi}) = 0 \quad n=1, \dots, N \quad (4.11)$$

where $\vec{\phi}$ is the velocity potential vector whose elements are given by the value of the local velocity potential

$$\vec{\phi} = (\phi_n) \quad n=1, \dots, N$$

To find $\vec{\phi}$ subject to Equation 4.11, we may write

$$D_n(\vec{\phi} + \vec{\delta\phi}) = D_n(\vec{\phi}) + \sum_{m=1}^N [(\phi + \delta\phi)_m - \phi_m] \left(\frac{\partial D_n}{\partial \phi_m} \right)_{\vec{\phi}} + O(\vec{\delta\phi}^2) \quad (4.12)$$

and let

$$D_n(\vec{\phi} + \vec{\delta\phi}) = 0 \quad \text{i.e., } \vec{\delta\phi} \text{ is the change in } \vec{\phi} \text{ required to satisfy Equation 4.10.} \quad (4.13)$$

Substituting Equation 4.13 into Equation 4.12 yields

$$\sum_{m=1}^N [(\phi + \delta\phi)_m - \phi_m] \left(\frac{\partial D_n}{\partial \phi_m} \right)_{\vec{\phi}} = - D_n(\vec{\phi})$$

which can be written

$$\partial \delta\vec{\phi} = - \vec{D} \quad (4.14)$$

where

$$\mathcal{D} \equiv \begin{bmatrix} \partial D_1 / \partial \phi_1 & \partial D_1 / \partial \phi_2 & \dots & \partial D_1 / \partial \phi_N \\ \partial D_2 / \partial \phi_1 & \partial D_2 / \partial \phi_2 & \dots & \partial D_2 / \partial \phi_N \\ \vdots & \vdots & \ddots & \vdots \\ \partial D_N / \partial \phi_1 & \partial D_N / \partial \phi_2 & \dots & \partial D_N / \partial \phi_N \end{bmatrix}$$

$$\vec{D} = (D_n) \quad n=1, \dots, N$$

$$\vec{\delta\phi} = (\delta\phi_n) \quad n=1, \dots, N$$

For N , it is probably not economical to invert the matrix \mathcal{D} . If, however, we make the assumption that $\delta\phi_m$ is most heavily dependent upon $\partial D_m / \partial \phi_m$, we can write Equation 4.14 in the form

$$\vec{\delta\phi} \approx -\vec{D} / \frac{\partial \vec{D}}{\partial \phi} \quad (4.15)$$

where

$$\frac{\partial \vec{D}}{\partial \phi}^T = \left(\frac{\partial D_1}{\partial \phi_1}, \frac{\partial D_2}{\partial \phi_2}, \dots, \frac{\partial D_n}{\partial \phi_n} \right).$$

Since we are taking into account only the local rate of change, we must iterate to allow the signals to propagate through the entire computational domain. To determine $\left(\frac{\partial \vec{D}}{\partial \phi} \right)$, we first write the finite difference analog of Equation 4.9 assuming constant zoning

$$\frac{1}{\delta x} (u_{i+\frac{1}{2}j} - u_{i-\frac{1}{2}j}) + \frac{1}{\delta y} (v_{ij+\frac{1}{2}} - v_{ij-\frac{1}{2}}) = 0 \quad (4.16)$$

where

$$n = (j-1) I + i \quad \text{and} \quad i=1, \dots, I$$

We then calculate $\left(\frac{\partial \vec{D}}{\partial \phi}\right)$ using the chain rule and Equation 4.16

$$\frac{\partial D_{ij}}{\partial \phi_{ij}} = \frac{1}{\delta x} \left\{ \frac{\partial u_{i+\frac{1}{2}j}}{\partial \phi_{ij}} - \frac{\partial u_{i-\frac{1}{2}j}}{\partial \phi_{ij}} \right\} + \frac{1}{\delta y} \left\{ \frac{\partial v_{ij+\frac{1}{2}}}{\partial \phi_{ij}} - \frac{\partial v_{ij-\frac{1}{2}}}{\partial \phi_{ij}} \right\} \quad (4.17)$$

To find the derivatives on the right-hand side of Equation 4.17 we make use of the finite difference analog of Equation 4.10

$$u_{i+\frac{1}{2}j} = \frac{1}{\delta x} (\phi_{i+ij} - \phi_{ij}) ; \quad u_{i-\frac{1}{2}j} = \frac{1}{\delta x} (\phi_{ij} - \phi_{i-ij})$$

$$v_{ij+\frac{1}{2}} = \frac{1}{\delta y} (\phi_{ij+1} - \phi_{ij}) ; \quad v_{ij-\frac{1}{2}} = \frac{1}{\delta y} (\phi_{ij} - \phi_{ij-1})$$

then

$$\begin{aligned} \frac{\partial u_{i+\frac{1}{2}j}}{\partial \phi_{ij}} - \frac{\partial u_{i-\frac{1}{2}j}}{\partial \phi_{ij}} &= - \frac{2}{\delta x} \\ \frac{\partial v_{ij+\frac{1}{2}}}{\partial \phi_{ij}} - \frac{\partial v_{ij-\frac{1}{2}}}{\partial \phi_{ij}} &= - \frac{2}{\delta y} \end{aligned} \quad (4.18)$$

Thus

$$\frac{\partial D_{ij}}{\partial \phi_{ij}} = - \left[\frac{2}{\delta x^2} + \frac{2}{\delta y^2} \right] = - \frac{2\delta y^2 + 2\delta x^2}{\delta x^2 \delta y^2} \quad (4.19)$$

Substituting this relationship into Equation 4.15 leads to

$$\delta\phi_{ij} = \frac{\delta x^2 \delta y^2}{2(\delta y^2 + \delta x^2)} D_{ij} . \quad (4.20)$$

From the finite difference form of the terms in Equations 4.15 we find

$$\begin{aligned} u_{i+\frac{1}{2}j} &= u_{i-\frac{1}{2}j} + \frac{1}{\delta x} \delta\phi_{ij} \\ u_{i-\frac{1}{2}j} &= u_{i+\frac{1}{2}j} - \frac{1}{\delta x} \delta\phi_{ij} \end{aligned} \quad (4.21)$$

$$\begin{aligned} v_{ij+\frac{1}{2}} &= v_{ij-\frac{1}{2}} + \frac{1}{\delta y} \delta\phi_{ij} \\ v_{ij-\frac{1}{2}} &= v_{ij+\frac{1}{2}} - \frac{1}{\delta y} \delta\phi_{ij} . \end{aligned}$$

Substituting for $\delta\phi_{ij}$ from Equation 4.20 leads to

$$u_{u+\frac{1}{2}j}^{k+1} = u_{i+\frac{1}{2}j}^k + \frac{\delta x^2 \delta y^2}{2(\delta y^2 + \delta x^2)} D_{ij}^k . \quad (4.22)$$

If $\delta x = \delta y$, then

$$u_{i+\frac{1}{2}j}^{k+1} = u_{i+\frac{1}{2}j}^k + \frac{\delta x}{4} D_{ij}^k ; \text{ where } k \text{ is the iteration parameter.}$$

The iteration then proceeds as follows: given an initial velocity distribution, calculate

- The velocity change using Equation 4.22.
- Divergence using Equation 4.16

These steps are repeated until the desired convergence criteria are met.

Because the velocity field is selected to be face-centered, the boundary conditions are particularly straightforward. For solid boundaries (terrain cells and the bottom surface of the grid), the velocity is set to zero; for flow-through boundaries (sides and top of the grid), the velocity is adjusted as for any other interior cell (i.e., Equation 4.22).

It should be noted that an additional weighting factor is included in WEST which allows the user to require that the velocity vector at observation stations agrees with the observed value. Following Equation 4.22, the velocity at an observation station is given by:

$$U_{i+\frac{1}{2}j}^{k+1} = \left[(U_{i+\frac{1}{2}j}^k + \frac{\delta x}{4} D_{ij}^k) + W_{i+\frac{1}{2}j}^{\frac{1}{2}} U_{i+\frac{1}{2}j}^o \right] / \left[1.0 + W_{i+\frac{1}{2}j}^{\frac{1}{2}} \right]$$

where

$U_{i+\frac{1}{2}j}^o$ = the observed value at location $i+\frac{1}{2}, j$

$W_{i+\frac{1}{2}j}$ = the weighting factor assigned to the observation
($0 \leq W \leq 1$).

This option is currently not available in MATHEW.

The observed data needed by both WEST and MATHEW are provided by an interpolation-extrapolation scheme using available information at a given site to determine the observed velocity components at each grid point above the topography.

In MATHEW the surface wind data is first extrapolated on a horizontal plane which is conformal to the terrain and located a distance z_o above it.

$$(u_{z_o}, v_{z_o}) \text{ cell faces} = \frac{\sum_{\ell} (U^o, V^o)_{\ell} / r_{\ell}^2}{\sum_{\ell} 1/r_{\ell}^2} \quad (4.23)$$

where

- ℓ = the index of the observation site
- (U^o, V^o) = surface wind components at station ℓ
- r_{ℓ} = the distance from the ℓ th station to the cell face location of (u_{z_o}, v_{z_o}) .

The values of (u_{z_o}, v_{z_o}) are then extrapolated in the vertical using

$$u_{i-\frac{1}{2}jk}^o = \left[(u_{z_o})_{i-\frac{1}{2}j} \cos(\alpha(z_{ij}-z_o)) + (v_{z_o})_{i-\frac{1}{2}j} \sin(\alpha(z_{ij}-z_o)) \right] \left(\frac{z_{ij}}{z_o} \right)^{\beta} \quad (4.24)$$

$$v_{ij-\frac{1}{2}k}^o = \left[-(u_{z_o})_{ij-\frac{1}{2}} \sin(\alpha(z_{ij}-z_o)) + (v_{z_o})_{ij-\frac{1}{2}} \cos(\alpha(z_{ij}-z_o)) \right] \left(\frac{z_{ij}}{z_o} \right)^{\beta}$$

$$w_{ijk-\frac{1}{2}}^o = 0$$

where α and β are obtained from smoothed upper air data.

WEST, on the other hand, uses surface wind data and upper air data directly at each station to obtain u^o, v^o, w^o . That is,

$$u^o_{i-\frac{1}{2}jk} = \frac{\sum_{\ell} (U^o_k, V^o_k)_{\ell} / r_{\ell}^2}{\sum_{\ell} 1/r_{\ell}^2}$$

$$v^o_{ij-\frac{1}{2}k} = \frac{\sum_{\ell} (U^o_k, V^o_k)_{\ell} / r_{\ell}^2}{\sum_{\ell} 1/r_{\ell}^2} \quad (4.25)$$

$$w^o_{ijk-\frac{1}{2}} = 0.$$

Here, $(U^o_k, V^o_k)_{\ell}$ are the actual wind components at the k th level for the ℓ th station as obtained from surface and upper air data. In lieu of upper air data, WEST also extrapolates upwards using surface data in a manner similar to MATHEW and then interpolates using Equation 4.25 to define the initial wind field.

The computational domain in both WEST and MATHEW is a rectangular box set on the Earth's surface with the bottom of the box located at the lowest topographic point in the area. The dimensions of the box are determined by the specific application and computer storage limitations. Within the computation domain, the volume is subdivided into a rectangular grid with intervals $\Delta x, \Delta y, \Delta z$ in the x, y, z directions, respectively. The indices i, j, k in this section denote grid positions along the x, y, z coordinates. The topography is represented by obstacle cells as depicted in Figure 4-2, and represents the true topography within the resolution dictated by the choice of $\Delta x, \Delta y, \Delta z$. The velocity components u, v, w and the transmission coefficient τ_x, τ_y, τ_z are defined at cell faces, while the velocity potential, ϕ , or Lagrange multiplier, λ , are cell-centered quantities. Figure 4-3 diagrammatically presents the components of the computational cell.

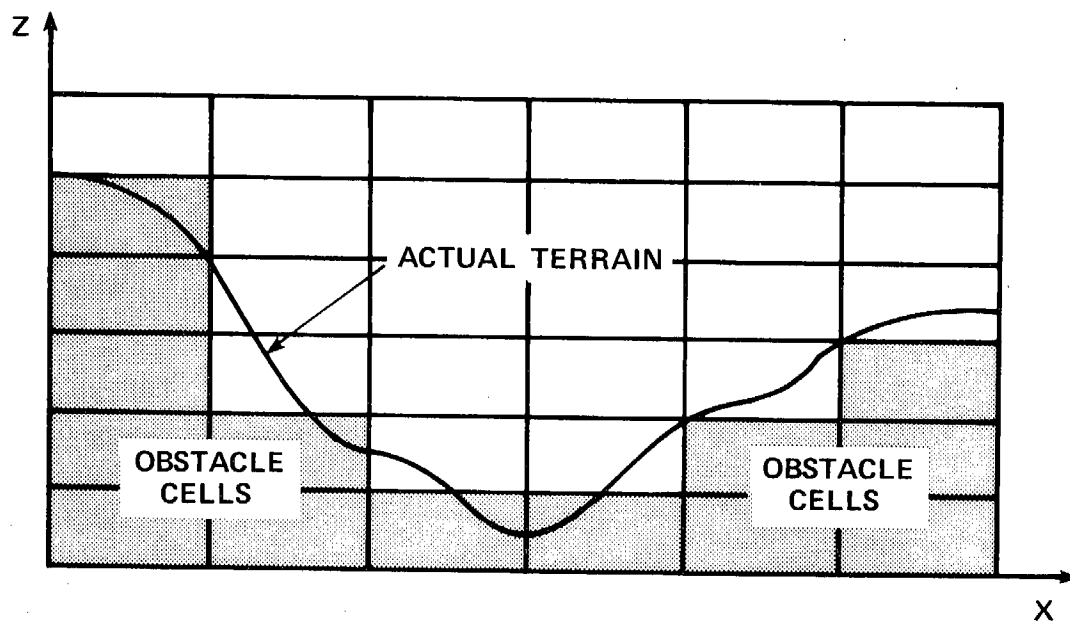


Figure 4-2. Two-Dimensional Example of Terrain Representation in WEST and MATHEW.

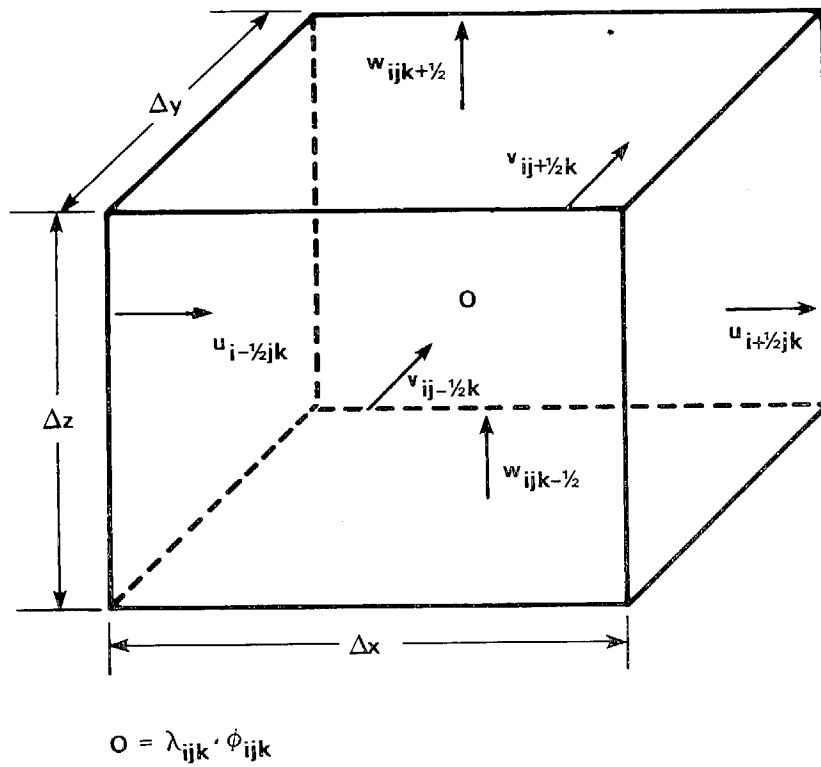


Figure 4-3. Computational Cell.

In summary, both models are mathematically similar. Both interpolate and/or extrapolate observed wind data to obtain an estimated wind field. Both then solve for a perturbation velocity potential (Lagrange multiplier) to obtain corrections to the estimated wind field, taking into account atmospheric stability and the presence of topography subject to the constraint that the resulting wind field be nondivergent. The principal differences between the two methods lie in the treatment of the transmission coefficients which are used to model atmospheric stability, and the particulars of the iteration scheme used to solve the velocity potential. While MATHEW requires that these coefficients remain constant in space, WEST allows for spatial variation. This means that the stability structure of the atmosphere can be accounted for more realistically in WEST.

A comparative calculation was performed using surface wind and upper air sounding data provided by Dugway Proving Ground (DPG) in Utah, and by National Climatic Center (NCC). To initialize both codes, the Rawinsonde at Salt Lake City at 1200 Z (0500 MST) was analyzed along with surface wind speed and direction data for 16 stations situated in and around Rush Valley, which is southwest of Salt Lake City. In Figure 4-4, the wind direction and wind speed as functions of geopotential height are shown. Figure 4-5 is a plot of surface station positions along with their respective wind vector observation.

The Rawinsonde data was parameterized according to Equation 4.24 with $\alpha = 0.03$ and $\beta = 0.046$, and were "hardwired" into WEST so that the initial conditions for MATHEW and WEST would be identical. Neutral stability was assumed for both runs (i.e., $\alpha_1 = \alpha_2 = \alpha_3 = 1$, $\tau_x = \tau_y = \tau_z = 1$). This procedure was followed in order to test the effects of using slightly different adjustment schemes.

Terrain data was digitized from USGS topographic maps on a grid of 2.5 x 2.5 km. Figure 4-6 represents a perspective view

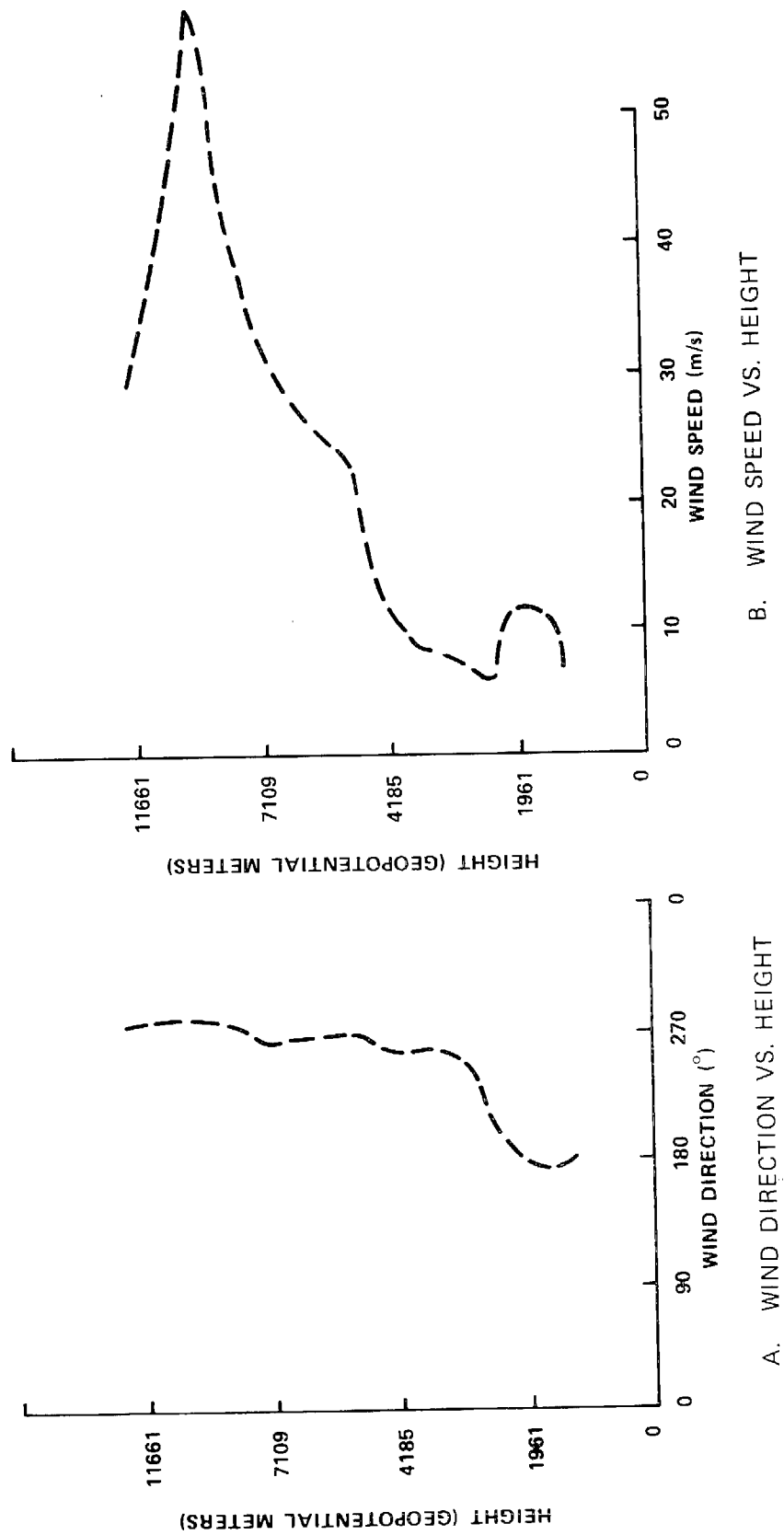


Figure 4-4. Wind Data from Salt Lake City Rawinsonde at
1200 Z, 18 January 1973.

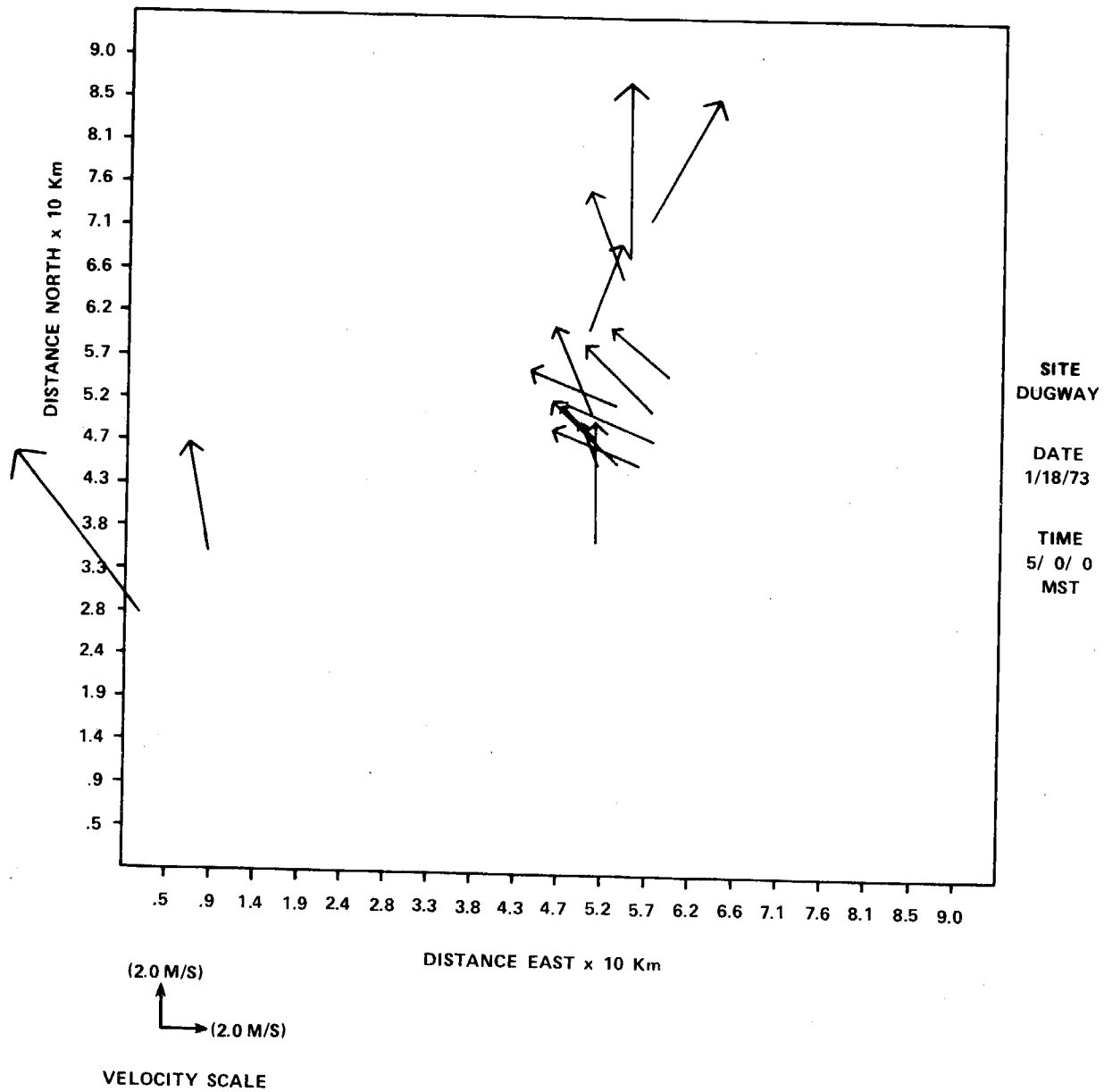
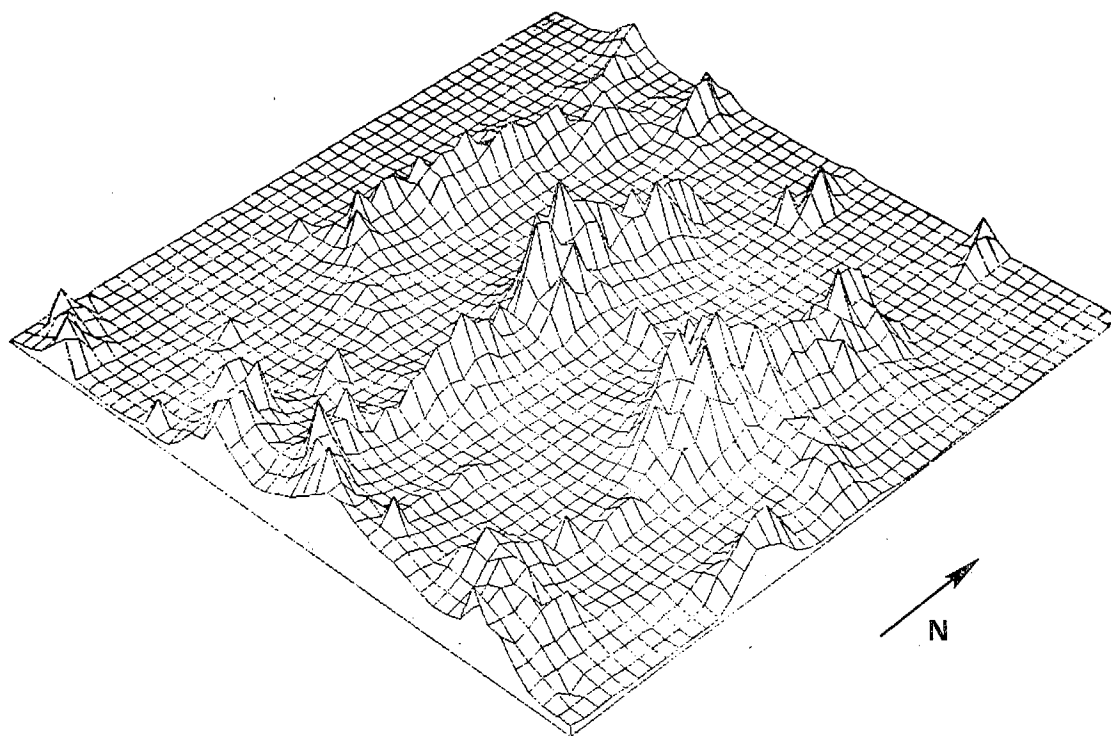
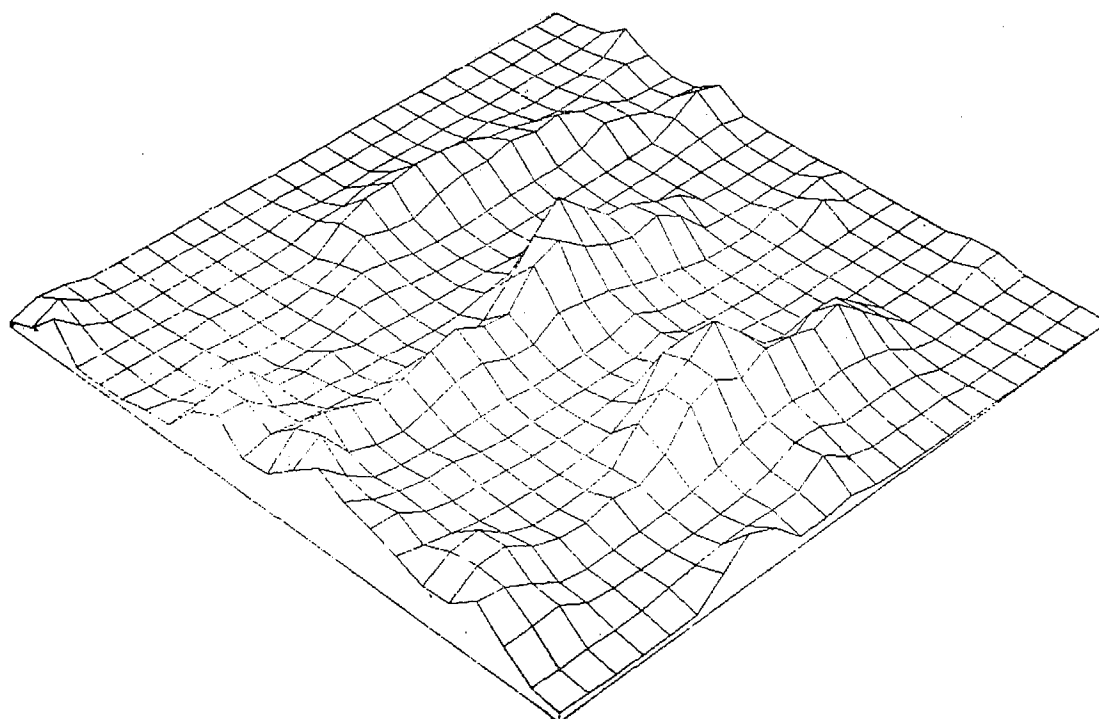


Figure 4-5. Observed Wind Vectors at 10 m Height AGL.



A. 2.5 km RESOLUTION



B. 5 km RESOLUTION

Figure 4-6. Dugway Topography at Two Resolutions.

of the terrain data. To reduce the expense of the calculation, the horizontal resolution was further reduced to 5 x 5 km by performing a four-point smoothing of the data.

The computational domain in both codes was subdivided into a 19 x 19 x 14 mesh with cell dimensions 5 km x 5 km x 200 m in the x, y, and z directions, respectively. Both codes were then run until the residual divergence error was reduced to order 10^{-4} .

The results of this comparison are shown in Table 4-2, where the minimum and maximum values of the v and w components of velocity are shown for the wind field at the surface, middle, and top of the computational domain.

Table 4-2. Summary of Results Comparing
MATHEW and WEST Using Dugway
Proving Ground Test Data.

POSITION IN COMPUTATIONAL DOMAIN		MATHEW		WEST WEIGHTING FACTOR = 0		WEST WEIGHTING FACTOR = 1	
		MIN.	MAX.	MIN.	MAX.	MIN.	MAX.
Top	w velocity	-0.81	1.24	-0.77	1.03	-1.4	2.02
	v velocity	-1.23	8.06	-1.07	9.44	-2.19	9.26
Middle	w velocity	-0.49	0.66	-0.74	0.66	-1.02	0.68
	v velocity	0.0	11.4	0.0	11.6	0.0	12.2
Surface	w velocity	-0.36	0.24	-0.42	0.24	-0.48	0.31
	v velocity	0.0	9.14	0.0	9.43	0.0	9.94

A weighting factor of unity forces the velocity vector components at observation stations to remain unchanged, while a factor of zero allows the vector to change as a result of the adjustment procedure. The latter case most closely approximates the MATHEW algorithm.

As can be seen in Table 4-2, specific values of w and v may differ slightly, but the calculations are essentially the same. These small discrepancies are attributable to the differences previously noted in the adjustment schemes. The WEST results associated with a zero weighting factor are most similar to those produced by MATHEW. This result is not surprising due to the mathematical similarity of the two codes when the transmission coefficients were assumed constant.

As a result of the above analyses, it is felt that WEST will provide greater flexibility, principally through the inclusion of the space-dependent transmission coefficients. While MATHEW could be reformulated to include this spatial dependence, the resulting code would be WEST in a slightly recast form. Therefore, the WEST model was incorporated into the new point source code, IMPACT, and should provide a realistic wind field module suitable for point source calculations.

4.3 Review of Diffusivity Module Options

The dispersion of atmospheric pollutants can be modeled as two separate processes, i.e., dispersion due to advective processes (wind shear, convergence, and divergence) and dispersion due to the turbulent motion of the atmosphere. This section reviews the second process, that of turbulent diffusivity. It should be noted that for point source modeling in complex terrain, it appears that advective dispersion is dominant (Sklarew, 1976). In areas of homogeneous terrain where wind shear, convergence, and divergence phenomena are less important, turbulent dispersion will dominate. Therefore, the development of a point source model applicable to all situations requires an accurate, complete description of both phenomena. Current models of turbulent diffusivity were examined and compared, with particular attention paid to the variability of turbulent diffusivity with wind speed, atmospheric stability, and height. In addition, the ratio of vertical to horizontal diffusivity was examined.

There are several methodologies currently in use for developing diffusivity factors based on available input parameters. A representative sample of the more common approaches are discussed below.

4.3.1 Gaussian Dispersion Standard Deviation

A relationship between the dispersion sigmas used in the Gaussian models and the value of the associated eddy diffusivity can be derived assuming a power law form for sigma, i.e., $\sigma = ax^b$, and a Gaussian solution to the conservation of mass equation (Fabrick, 1974). The eddy diffusivity, K, is equal to:

$$K = Uba^2 x^{2b-1} \text{ (m}^2\text{/sec)}$$

where

U = the average wind speed (m/sec)

x = the downwind distance (meters).

An example of this procedure is shown in Figure 4-7 where vertical and horizontal diffusivities were derived using the EPA Workbook dispersion standard deviations, assuming a 10 mile-per-hour mean wind speed. It should be noted that the diffusivity coefficients derived in this manner are functions of downwind distance only (except for the case where the coefficient $b = \frac{1}{2}$), being independent of height. This is due to the uniform wind field assumption of the Gaussian model which requires dispersion standard deviations to account for the effects of wind shear and other spatial phenomena that cause the plume to spread.

The ratios of vertical to horizontal diffusivities can be written as

$$K_z/K_y = \frac{b_z a_z^2}{b_y a_y^2} x^{2(b_z - b_y)}$$

where

$$\sigma_y = a_y x^{b_y} \quad \text{and} \quad \sigma_z = a_z x^{b_z}.$$

This ratio is independent of mean wind speed but is still a function of downwind distance.

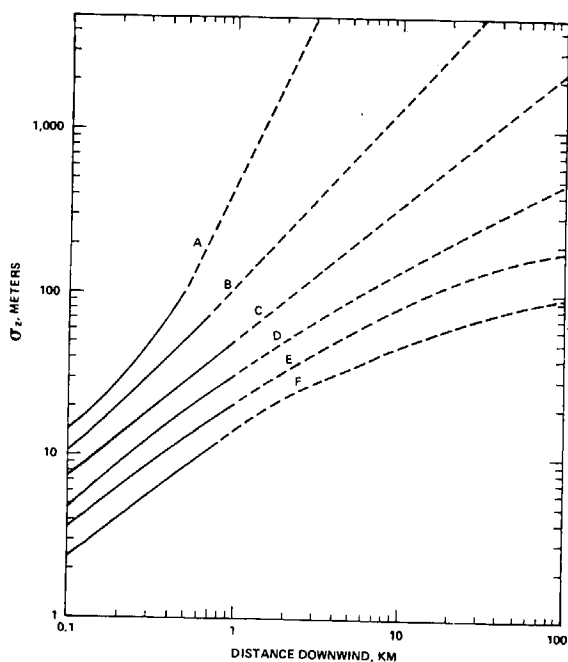
4.3.2. DEPICT Diffusion Coefficient

An approximate method for calculating the eddy diffusivities was developed by T. B. Smith (1972) and adapted by Sklarew and Wilson (1976) for the DEPICT model. The vertical diffusivity is calculated using the following algorithm

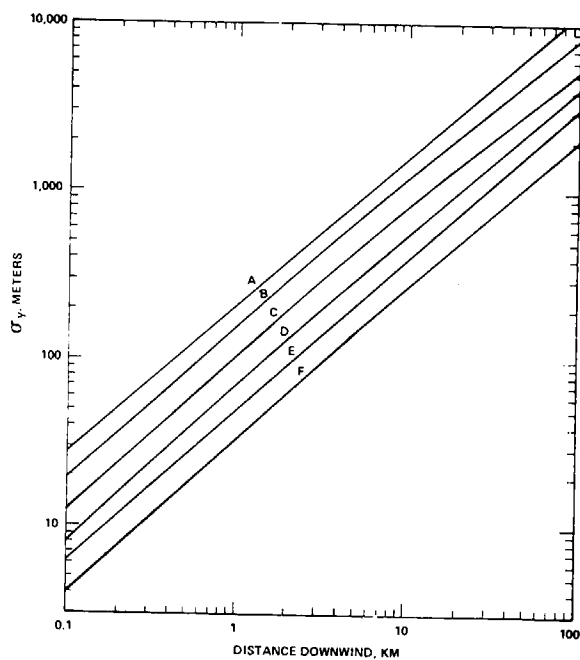
$$K_z = K \bar{U} \sigma_z \ell \quad (\text{m}^2/\text{sec})$$

where

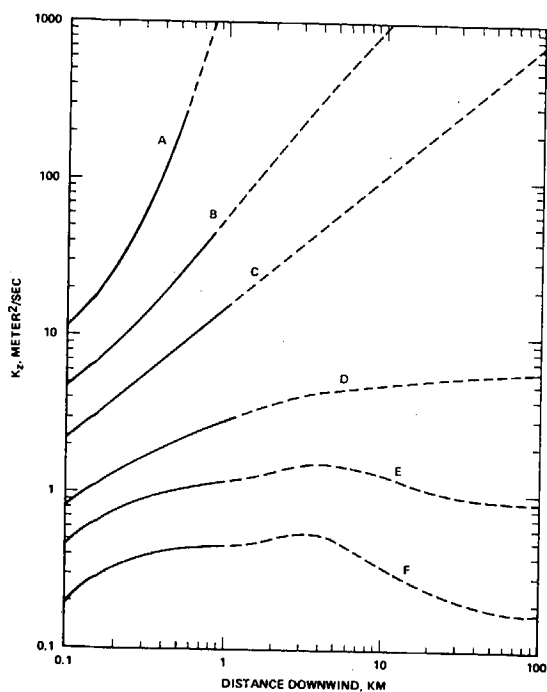
$$\bar{U} = \text{the wind speed at the point of interest (m/sec)}$$



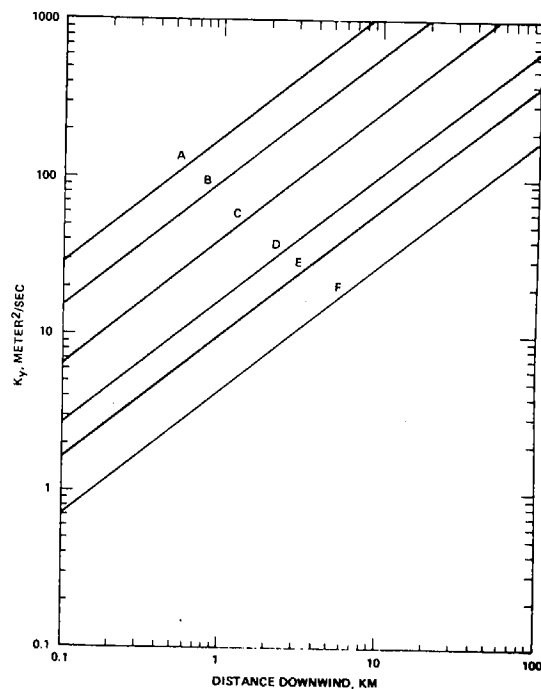
**A. VERTICAL DISPERSION
STANDARD DEVIATIONS**



**B. HORIZONTAL DISPERSION
STANDARD DEVIATIONS**



**C. VERTICAL DIFFUSION COEFFICIENT
(10 MPH MEAN WIND)**



**D. HORIZONTAL DIFFUSION COEFFICIENT
(10 MPH MEAN WIND)**

Figure 4-7. Vertical and Horizontal Diffusion Coefficients, Derived Using the EPA Workbook Dispersion Standard Deviations.

σ_{ϵ} = the standard deviation of the vertical wind vane fluctuation (radians) and is dependent upon stability as follows:

Stability	A	B	C	D	E	F
σ_{ϵ}	.262	.237	.184	.119	.056	.023

z = the turbulence scale length (meters), and depends on both height and stability. This dependence is shown in meters in the following table of turbulence scale lengths:

Z(m)	A	B	C	D	E	F
10	18	15	12	10	8	7
20	30	25	21	18	16	14
30	41	34	29	25	22	20
50	62	52	44	39	35	31
75	84	71	60	52	48	43
100	105	85	74	64	59	54

k = Von Karman's constant, in this case taken to be equal to 0.45.

In homogeneous terrain, the vertical variation in the wind field can be expressed as a function of stability as

$$U = U_0 (z/z_0)^p$$

where

z = the altitude above ground level

U_0 = the wind speed measured at reference altitude z_0

p = determined by stability as follows

Stability	A	B	C	D	E	F
p	.15	.17	.2	.26	.39	.48

Therefore, the vertical diffusivity can be expressed as

$$K_z = k U_o (z/z_o)^p \sigma_\epsilon \ell .$$

Horizontal diffusivities are calculated in a manner similar to Lantz (Intercomp, 1975) using the relation $K_x = \alpha K_z$ where α depends on stability as follows:

Stability	A	B	C	D	E	F
α	.5	.75	.9	1.0	1.7	2.1

Sklarew and Wilson used an empirical approach to develop these coefficients.

4.3.3. Intercomp Diffusion Model

Lantz (Intercomp, 1975) developed a formulation for the turbulent diffusivity based on fitting a finite difference point source dispersion solution to the Turner (EPA Workbook) σ_y and σ_z curves. This empirical approach lead to the following formulation:

$$K_y = K_{y0} (U_o/U_{ref})^\beta$$

$$K_z = \alpha^{-1} K_y$$

$$U = U_o z^\gamma$$

where

$\alpha, \beta, \gamma, K_{y0}$ = a function of stability class, defined as follows (in MKS units)

	A	B	C	D	E	F
1/α	10	2	0.7	0.2	0.05	0.0008
β	1.76	1.38	1.14	1.0	1.0	0.67
γ	.14	.14	.14	0.2	0.3	0.4
K _{yo}	572	340	114	92	75	63

$$U_{\text{ref}} = 1 \text{ (meter/sec).}$$

4.3.4 Myrup/Ranzieri Diffusion Model

Myrup and Ranzieri (1976) developed an approach based on the Monin-Obukhov length for the lower part of the planetary boundary layer and suggested an empirical approach for extending the model to greater altitudes. Given a value of the Monin-Obukhov length and the surface roughness z_o , the vertical diffusivity can be expressed as:

$$K_z = \frac{k U_* z}{(1+4.7 z/L)} \quad L > 0 \text{ stable condition}$$

$$K_z = k U_* z (1-15 z/L)^{1/4} \quad L < 0 \text{ unstable condition}$$

$$z/L \leq -5$$

and

$$K_z = 1.4 k U_* z \left(\frac{-0.4}{k} \frac{z}{L} \right)^{1/3} \quad z/L > -5$$

where

- k = Von Karman's constant, given as 0.35 by Myrup and Ranzieri
- z = the height above the roughness elements (meters)
- z_o = the surface roughness (meters)
- L = the Monin-Obukhov length (meters)
- U_* = the friction velocity which can be approximated as:

$$U_* = k U_o / \ln [z_w/z_o + 2/L (z_w - z_o)]$$

where

U_o = the wind speed measured at height z_w (m/sec).

The relationship between the Monin-Obukhov length, L ; the surface roughness, z_o ; atmospheric stability; and the surface evaporation rate is given in Figure 4-8. The relationship between land use, surface roughness, atmospheric stability, and Monin-Obukhov length was derived from the work by Myrup and Ranzieri and is shown in Table 4-3.

An extension of the theory beyond the lower portion of the boundary layer was made by multiplying the diffusivity as calculated above by a correction factor, q ; with q defined as:

$$\begin{aligned} q &= 1 & z < 0.1 z_i \\ q &= (1.1 - z/z_i) & 0.1 z \leq z \leq 1.0 z_i \end{aligned}$$

where

z_i = the mixing height.

In the current version of the model, provided by the Air Resources Board, the following extensions are added.

- Inside an elevated inversion, the surface wind speed, U_o , is set to 3.0 m/sec; the Monin-Obukhov length, L , is set to 20.0; and Z , the height above the surface, is measured from the bottom of the inversion layer.
- Above an elevated inversion, neutral stability is assumed, $L \rightarrow \infty$, and Z is measured from the top of the inversion.

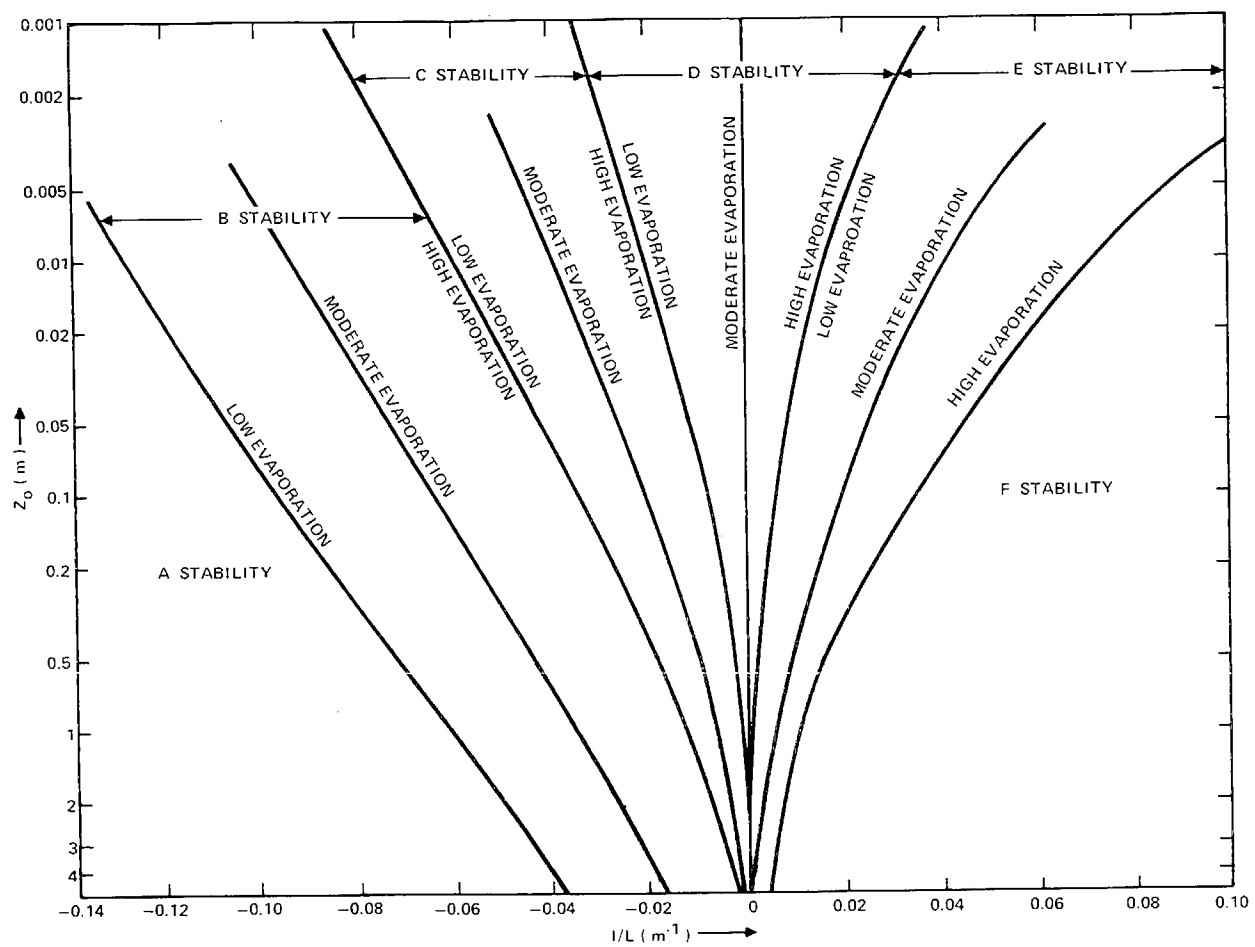


Figure 4-8. $1/L$ as a Function of Pasquill Stability Classes, (Myrup, 1976).

Table 4-3. Relationship of Land Use, Surface Roughness, Atmospheric Stability, and Monin-Obukhov Length.

CATEGORY	SURFACE ROUGHNESS (m)	EVAPORATION	MONIN-OBUKHOV LENGTH STABILITY CLASS					
			A	B	C	D	E	F
CENTRAL* BUSINESS DISTRICT	3.21	L	-14	-14	-33	-200	∞	100
HIGH DENSITY* RESIDENTIAL	3.70	M	-20	-20	-50	-1000	∞	200
OFFICE* BUILDING	1.75	L	-12.5	-12.5	-20	-142	∞	1000
LIGHT DENSITY* RESIDENTIAL	1.08	M	-14	-14	-33	-200	∞	100
PARK*	1.27	H	-18	-18	-100	∞	∞	125
OPEN GREEN	.15	L	-7	-12	-50	-250	400	40
AGRICULTURAL (WHEAT- ALFALFA)	.20	H	-12.5	-50	-333	200	40	12

* BASED ON ONE STABILITY CLASS MORE UNSTABLE DUE TO URBAN HEAT ISLAND EFFECT

4.3.5 Tensor Diffusivity Model

An extension of the work started by Mellor and Yamada (1974) was recently proposed by Freeman (1976) where the second-order closure of the turbulence transport equations in a density-stratified atmosphere can be solved algebraically. The resulting diffusion coefficients display the following properties:

- The local mean fields enter only through the Richardson number, the magnitude of the vertical shear of the horizontal wind, and the horizontal components of the wind shear.
- All transport coefficients contain a length scale which is a function of the height above the surface, the surface roughness, and the height of the planetary boundary layer.
- A diffusivity tensor is obtained in which horizontal and vertical diffusivities can differ substantially. Off-diagonal components are comparable to those on the diagonal.

Unfortunately, only a limited number of examples have been run to date using this approach.

4.3.6 Comparison of Diffusivity Formulations

The comparison of the various eddy diffusivity formulations is facilitated by the fact that all show the vertical diffusivity to be linearly proportional to a reference horizontal wind speed in homogeneous terrain. Thus, the value of K_z/U_0 , a quantity independent of wind speed (i.e., a normalized diffusivity), can be compared. The comparison of the T. B. Smith formulation used in DEPICT and the Myrup-Ranzieri (M/R) model (assuming no correction factor) for the first 100 meters is shown in Figure 4-9. The M/R model uses one stability class more unstable for those land-use categories located within urban areas to account for

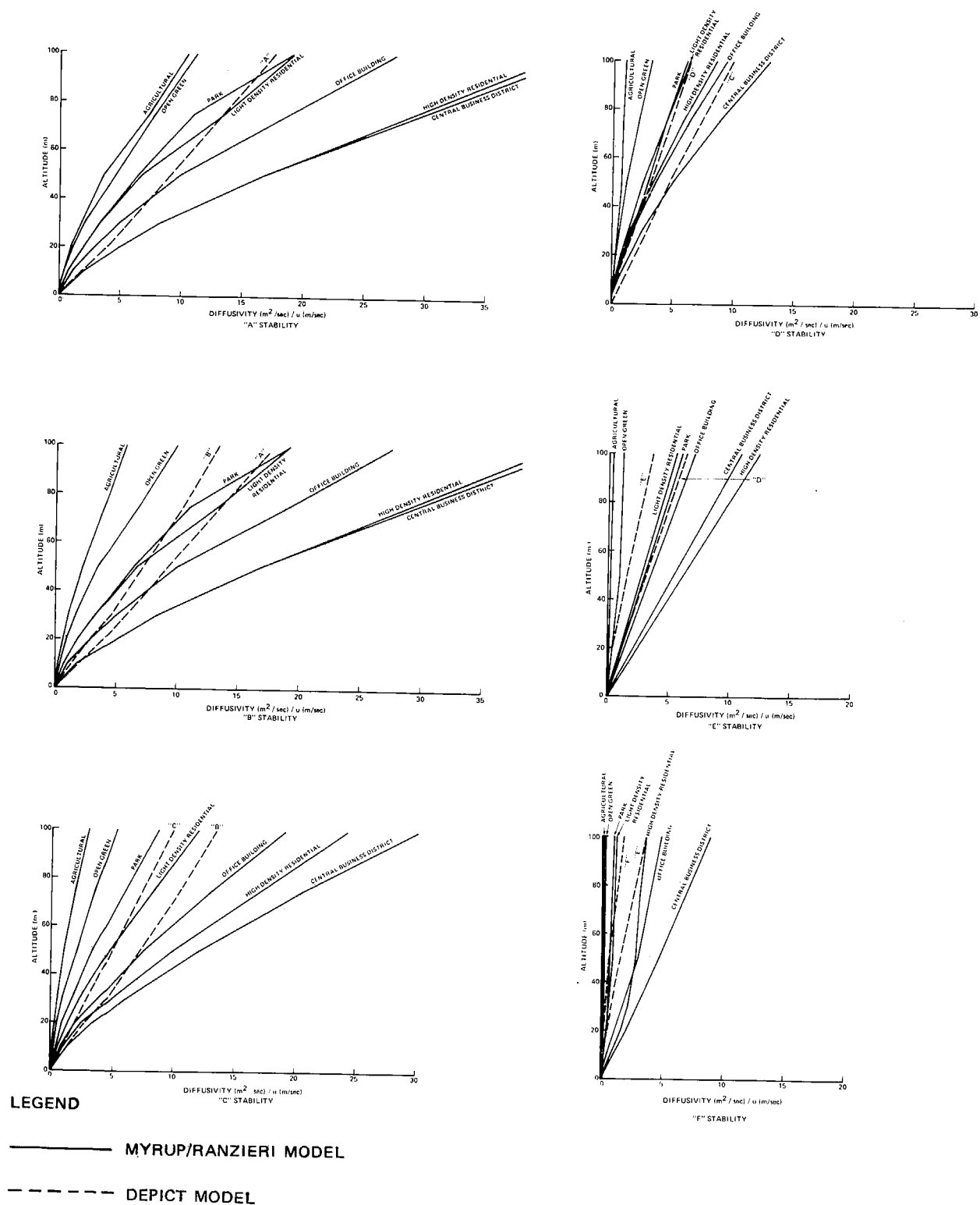


Figure 4-9. Comparison of Myrup/Ranzieri and DEPICT Diffusivities in the Lower Boundary Layer.

the urban heat island effect. Therefore, diffusivities for the actual stability class and one stability class more unstable are shown for the DEPICT formulation to provide a more meaningful comparison. For all stabilities, the values predicted by the DEPICT formulation fall roughly in the center of the values predicted by the M/R model and are similar to values given by the M/R model for the light residential and park land use categories. The M/R model shows a large range of values for various land use categories ranging from over $40 \text{ m}^2/\text{sec}$ (1 mps reference velocity at 100 meters AGL) for A stability, high density residential or central business district land uses, to less than $0.2 \text{ m}^2/\text{sec}$ for F stability, undeveloped open green or agricultural categories. Similar DEPICT values vary from $16 \text{ m}^2/\text{sec}$ for A stability to about $2 \text{ m}^2/\text{sec}$ for F stability.

There are complications when comparing the values of the vertical eddy diffusivities derived from the vertical dispersion standard deviations developed by EPA or Pasquill (see section 3.2), and the values resulting from the DEPICT and M/R models. These complications are caused by the fact that the former are independent of vertical heights above ground and dependent on downwind distance from the source, while the latter are just the opposite, dependent on vertical height and independent of downwind distance. As an approximate comparison appropriate for typical point source dispersion problems, we arbitrarily select a reference datum at a vertical height of 100 meters and a downwind distance of 5 kilometers. The resulting diffusivities values for the various methods are shown in Table 4-4.

Except for the EPA values for A stability (the values of σ_z are probably not valid at 5 km), all the methods show remarkably reasonable agreement. The agreement of most values to within a factor of two is all the more interesting, since the various models are based on significantly different sets of experimental data and theoretical considerations. The selection of another reference datum (if reasonable) is not expected to significantly change this observation.

Table 4-4. Comparison of Normalized Eddy Diffusivities (K_z/U_o , meters) as Derived from EPA and Pasquill Vertical Dispersion Standard Deviation σ_z and the DEPICT and M/R Diffusivity Models, (Datum = 100m AGL, 5 Km Downwind of Source).

STABILITY CLASS	EPA* WORKBOOK (AT 5 km) SURFACE ROUGHNESS		PASQUILL* (AT 5 km) SURFACE ROUGHNESS				DEPICT (100 m)	M/R (100 m)
	3 cm	100 cm	3 cm	10 cm	100 cm	1000 cm		
A	88,000	--	172	212	306	477	16	40 - 10
B	90	162	19	24	34	53	14	40 - 6
C	6	10	5	6	8	13	10	30 - 3
D	1.1	2	1.7	2	3	5	6	13 - 1
E	.4	.72	.7	.8	1.2	1.9	4	12 - .4
F	.2	.36	.3	.4	.5	.8	2	9 - .2

*See Section 3.2 for a Description of the EPA and Pasquill Formulation for Dispersion Standard Derivatives.

4.3.7 Variations of Diffusivity With Height

The variation of diffusivity with height is presented schematically in Figure 4-10 for the M/R, DEPICT, and EPA dispersion σ_z models. In this figure, a slightly unstable layer (Pasquill stability class C) is capped by a strong inversion (class F) with neutrally stable air (class D) above. Note that each model incorporates a different variation of diffusivity with height. Below the inversion, the resulting stabilities are within a factor of two of each other. (It is of interest to note that the typical vertical zoning of IMPACT code for a point source dispersion problem is roughly from 25 to 100 meters.) The difference above the inversions are more significant and could change the predicted air quality impact of plumes that penetrate the inversion.

4.3.8 The Ratio of Horizontal to Vertical Diffusivity

A comparison of the ratio of the horizontal ($K_x = K_y$) to vertical values of diffusivity (K_x/K_z) is shown in Figure 4-11 as a function of atmospheric stability. The ratios for the DEPICT method were selected on the basis of empirical considerations. The ratios for the Intercomp and SIG DIF models are based on a best fit of the EPA Workbook curves with a finite difference dispersion model. The EPA Workbook and the Pasquill ratios are based on calculating the values of K_x and K_z from horizontal and vertical dispersion standard deviations for a range (1 to 10 km) of downwind distances and, in the case of the Pasquill formulation, a range (3 to 100 cm) of surface roughnesses. (The values used for σ_θ are given in Table 3-1.) The maximum and minimum values of K_x/K_z were then plotted. The shape of the curve shown for the Pasquill dispersion sigma's indicates a seeming physical inconsistency where the ratio of horizontal to vertical diffusivity decreases as the atmosphere becomes more stable, suggesting that the approaches for calculating σ_y and σ_z are not consistent.

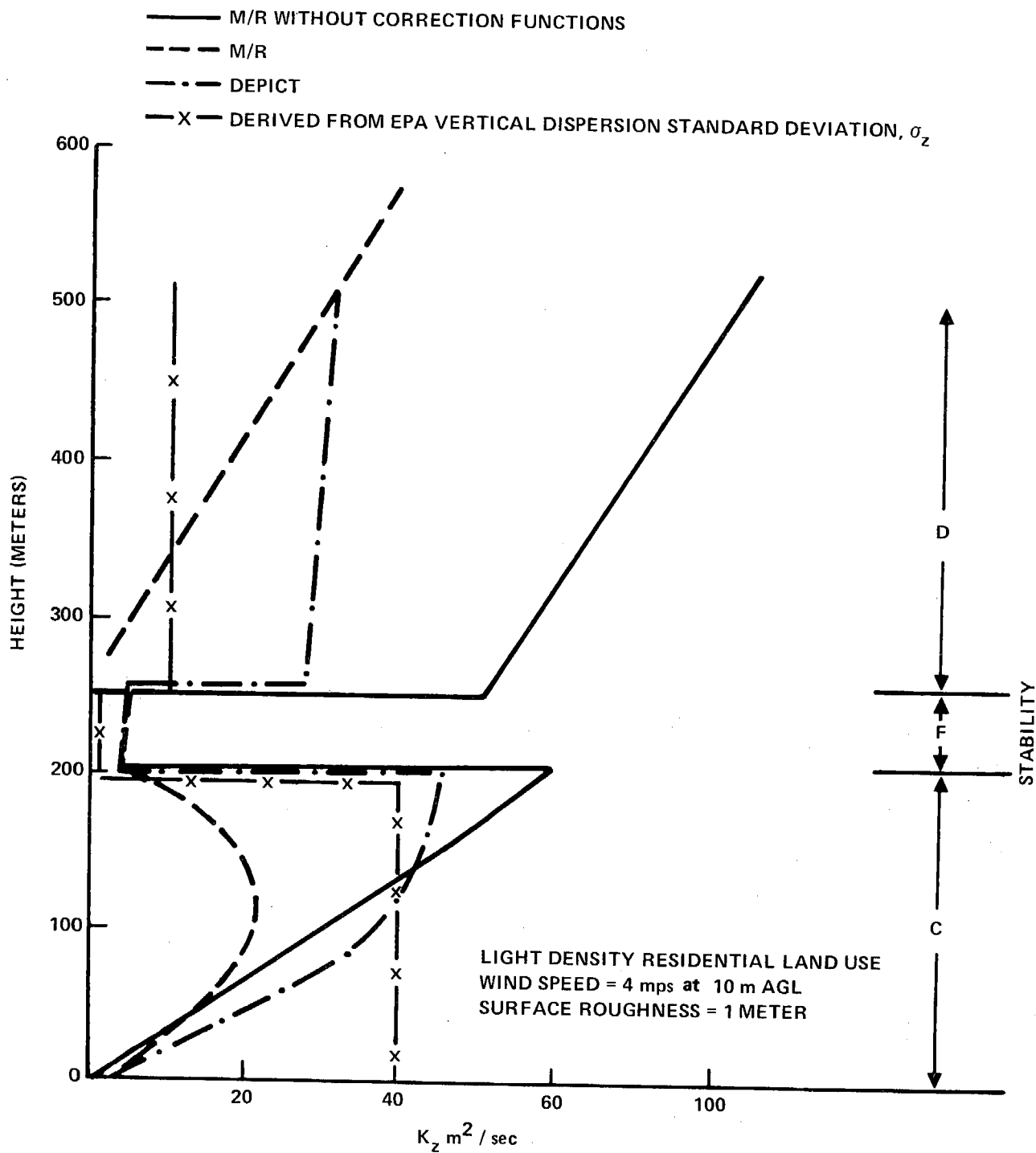


Figure 4-10. Comparison of the Vertical Diffusivities Predicted by the DEPICT Model and the M/R Model.

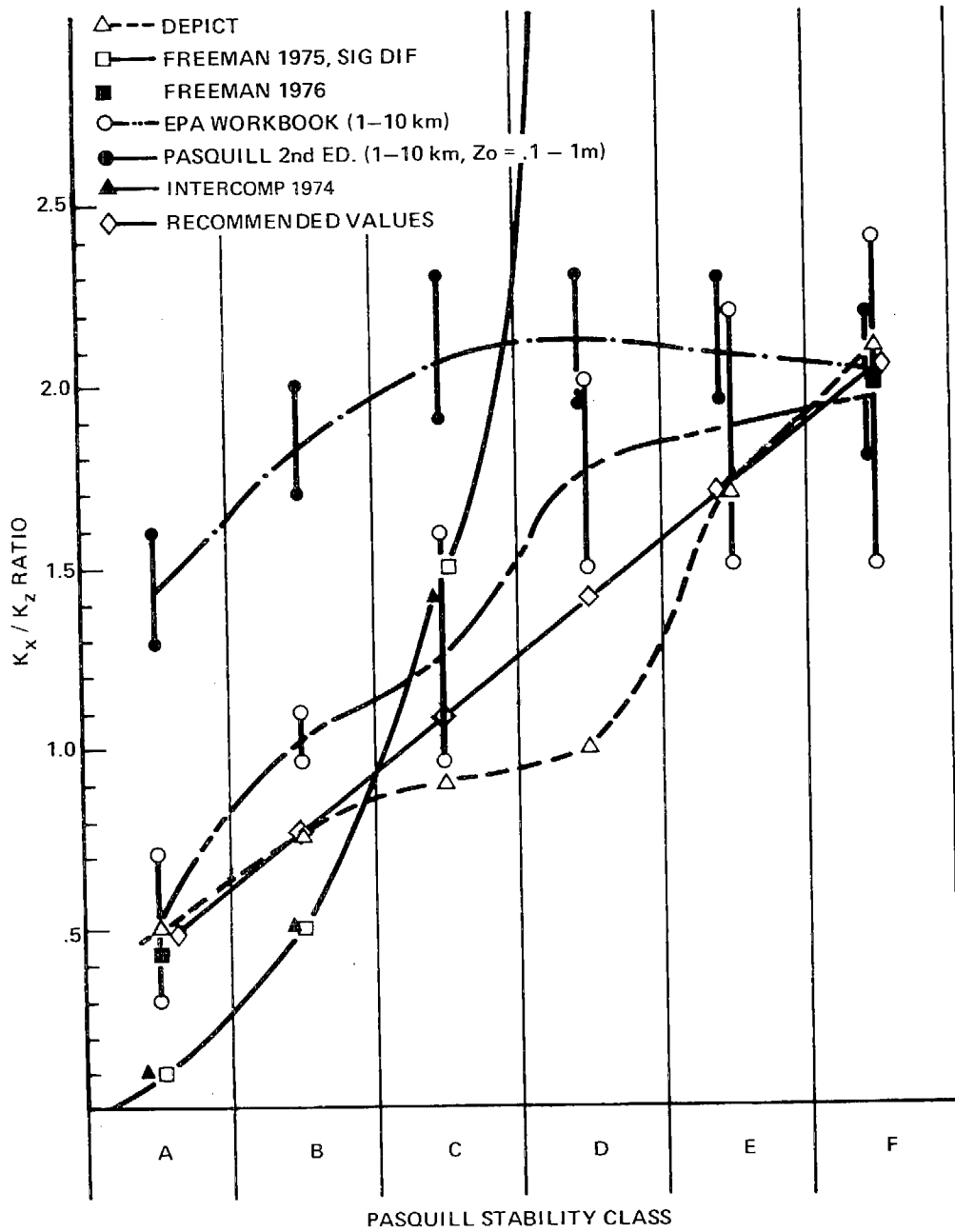


Figure 4-11. Variation of the Ratio of Horizontal to Vertical Diffusivity (K_x/K_z) as a Function of Atmospheric Stability.

It should be noted however, that except for the Intercomp model (Intercomp, 1975) and a similar approach used by Freeman (1975), the ratios derived from all models are roughly the same. Of considerable interest is that the preliminary values given by Freeman's tensor model for very unstable and very stable cases agree with the DEPICT model and the EPA Workbook sigmas. The recommended values indicated in Figure 4-10 are based on a linear fit between the extreme values. At present, there seems no justification for a more precise fit, although thorough parametric studies using detailed models (such as the one prepared by Freeman) and additional experimental data should allow additional refinement.

4.4 Review of Pollutant and Advection/Diffusion Modules

The transport and dispersion of atmospheric pollutants due to advective and diffusive processes are fundamental to the accurate treatment of point source emissions in the atmosphere. The advective/diffusive process can be expressed mathematically as

$$\frac{\partial C}{\partial t} = -\nabla \cdot \vec{U}C + \nabla \cdot \vec{K} \cdot \nabla C$$

where the rate of change of pollutant concentration at a given location, $\frac{\partial C}{\partial t}$, is equal to the increase (or decrease) due to advection, $-\nabla \cdot \vec{U}C$, plus the increase (or decrease) due to eddy diffusion, $\nabla \cdot \vec{K} \cdot \nabla C$.

The solution of this equation usually involves the division of a three-dimensional region of interest into subregions (usually called nodes or cells) with the implicit assumption that these subregions are sufficiently small that the concentration, wind and diffusion fields can be treated as varying linearly inside the subregion. The real problem of simulating atmospheric point sources places a severe strain on this assumption.

As an example, consider the following application of a standard finite difference model (although other numerical solution approaches suffer from the same problem). An estimate is needed of the impact on air quality of the emission from a large power plant in complex terrain. The region of interest is 30 kilometers by 30 kilometers; the terrain varies from sea level to 1000 meters. The cell size (or zoning) which, in the case of most grid models must be uniform, would be typically 1000 meters by 1000 meters in the horizontal by 100 meters in the vertical. This gives a total of 9000 cells; the minimum computer storage requirement to run this problem is about 80,000 words (320k bytes). For the case of photochemical impact (which requires multiple pollutants), the storage requirements would increase to over 180,000 words (720k bytes). This is a large code even for modern virtual-

memory computers. If we wanted to increase the resolution (i.e., decrease the cell size) by a factor of four such that the cell size would be reduced to 250 meters by 250 meters by 25 meters, we would need to increase the storage requirements by a factor of 64, requiring a total of 5 million words for the simple model and a staggering total of 11 million words for the photochemical simulation. In addition, the basic computation time step used for advection and diffusion calculations, which is a function of the cell size, would be reduced by a factor of four. Therefore, the cost of running the computer program (based on the number of operations required) for the fine grid would be at least 256 times the cost of the original program. Typical costs for an inert pollutant impact range from \$5 to \$50, while the photochemical simulation could range from \$50 to \$500 for the coarse grid. The cost for the fine grid would be at least 256 times as much: an obviously impossible situation. Therefore, the user of the grid type models must be reconciled to accept a fairly coarse resolution of the region. This requirement, forced by economics, can be to some extent alleviated by the use of variable zoning techniques, or possibly by finite element or spectral approaches. However, at the current time none of the latter options have been implemented for three-dimensional photochemical simulations.

The coarse resolution in the region for the point source emission results in a highly nonlinear concentration field since the stack radius is rarely more than a few meters (compared with grid cell of 1000 x 1000 x 100 meters). Therefore, the primary requirement for the finite difference solution method is an accurate treatment of point (i.e., delta function) sources.

The numerical solution of the advection/dispersion equations has received considerable attention. A wide range of solution methodologies and analyses have been proposed. A description of some of the more recently reported studies relevant to air quality models are presented in Table 4-5.

Table 4-5. Past Comparisons of Advection Methods.

STUDY	ADVECTION METHODS	TEST PROBLEM	ANALYSIS
BASS, FLOW RESEARCH, 1974	<ul style="list-style-type: none"> • SPECTRAL • 2nd ORDER FINITE DIFFERENCE 	<ul style="list-style-type: none"> • 2D PUFF IN SHEAR WIND • 2D PUFF IN RIGID ROTATION 	<ul style="list-style-type: none"> • ABSOLUTE ERROR • TIME
LONG & PEPPER, DUPONT, 1976	<ul style="list-style-type: none"> • DONOR • IMPLICIT • CRANK NICOLSON • CUBIC SPLINE • GALERKIN FINITE ELEMENT • EGAN-MAHONY 2nd MOMENT 	<ul style="list-style-type: none"> • ANALYTIC • 2D PUFF IN RIGID ROTATION 	<ul style="list-style-type: none"> • CONSERVATION OF MASS • STABILITY • QUADRATIC CONSERVATION
FABRICK & NAKAYAMA, SCIENCE APPLICATIONS INC., 1974	<ul style="list-style-type: none"> • POINT MASS • RANDOM WALK 	<ul style="list-style-type: none"> • 3D PLUME UNIFORM WIND, SIMPLIFIED STEADY STATE PHOTO-CHEMISTRY 	<ul style="list-style-type: none"> • GRAPHIC COMPARISON WITH GAUSSIAN SOLUTION
REYNOLDS et al, SYSTEMS APPLICATION INC., 1975	<ul style="list-style-type: none"> • PRICE • CROWLEY 2nd ORDER • CROWLEY 4th ORDER • SHASTA • GALERKIN FINITE ELEMENT • PARTICLE IN CELL • EGAN & MAHONY 2nd MOMENT 	<ul style="list-style-type: none"> • 1D FIRST ORDER REACTIVE PLUME 	<ul style="list-style-type: none"> • GRAPHIC COMPARISON WITH ANALYTIC SOLUTION • TIME
MEYER & DURRAN, SYSTEMS APPLICATION INC., 1976	<ul style="list-style-type: none"> • PRICE • SHASTA • NON FLUX LIMITED STANDARD • PHOENICAL • EGAN & MAHONY 2nd MOMENT 	<ul style="list-style-type: none"> • 1D ADVECTION • 2D ADVECTION WITH PHOTOCHEMISTRY • AIR SHED SIMULATION • ANALYTIC 	<ul style="list-style-type: none"> • ABSOLUTE ERROR • GRAPHIC COMPARISON WITH ANALYTIC SOLUTION • TIME • COMPARISON WITH DATA
LANTZ, INTERCOMP, 1975	<ul style="list-style-type: none"> • IMPLICIT • PARTICLE IN CELL 	<ul style="list-style-type: none"> • 3D PLUME UNIFORM WIND 	<ul style="list-style-type: none"> • GRAPHIC COMPARISON WITH ANALYTIC SOLUTION
SKLAREW, FABRICK, SYSTEMS SCIENCE AND SOFTWARE, 1971	<ul style="list-style-type: none"> • DONOR • CROWLEY 4th ORDER • FROMM 4th ORDER • PARTICLE IN CELL 	<ul style="list-style-type: none"> • 2D ADVECTION 	

With a myriad of potential methods, a screening procedure was established to limit evaluation to appropriate models. The criteria established were, in order of importance: the ability to simulate three-dimensional problems, the ability to simulate photochemical pollutants, and an existing and verified methodology.

The first criterion eliminated a number of potentially interesting finite element methods, since no three-dimensional finite element advection problem has been successfully treated. The second criterion, the ability to simulate photochemical pollutants, eliminated a number of attractive methods that map the concentration field into other spaces (e.g., spectral). This procedure allows for accurate simulation of advection but becomes unacceptably expensive with the requirement for calculating multiple pollutant concentrations in real space needed to calculate the chemical transformations for every time increment. The final requirement was applied to the list of potential candidates and the schemes remaining were generalized to the following list:

- A semi-implicit, second-order, accurate, cell-centered difference scheme (Phillips, 1974)
- A second-order, accurate, flux-corrected scheme based on Crowley's algorithm (Sklarew, 1976)
- A version of SHASTA (second-order, accurate, non-flux corrected) used by Systems Applications in their point source air quality model, PDM (Meyer, 1976)
- A hybrid, point mass, random-walk method developed at Los Alamos Scientific Laboratories (Hirt, 1972) and applied to reactive point sources at Science Applications (Fabrick, 1974).

The technique of fractional steps, or splitting (Yanenko, 1971) was used in the first three methods to solve the three-dimensional transport/diffusion problem. This technique divides the original problem into a series of three one-dimensional advection problems which are solved sequentially.

A summary of the properties of each of the methods selected is given in Table 4-6 (assuming uniform zoning, winds, and diffusivities). The reader is referred to the cited references for additional information.

As discussed previously, the crux of the advection problem is in utilizing a coarse grid for accurate simulation of concentrations (particularly surface concentrations) due to point source emission. The test problem selected to establish the best scheme for this particular class of problems should simulate (as far as possible) a physically realistic situation while still retaining an analytic solution.

A straightforward test problem would be in the solution of the advection/diffusion equation for the case of uniform wind and diffusion field. The solution of this problem is the Gaussian point source model with the dispersion standard deviations σ_y and σ_z defined as

$$\begin{aligned}\sigma_y^2 &= 2 K_y x/U \\ \sigma_z^2 &= 2 K_z x/U\end{aligned}$$

and the surface concentration is given as

$$C = \frac{Q}{\pi \sigma_y \sigma_z U} e^{-y^2/2\sigma_y^2} e^{-H^2/2\sigma_z^2}$$

where

- σ_y = horizontal dispersion standard deviation (meters)
- σ_z = vertical dispersion standard deviation (meters)
- U = wind speed (m/sec)
- x = downwind distance from source to receptor (meters)
- H = effective plume height (meters)
- y = crosswind distance (meters)
- Q = emission rate ($\mu\text{g/s}$)
- C = the concentration ($\mu\text{g/m}^3$).

Table 4-6. Proposed Advection – Diffusion Methods with Uniform Wind Field and Constant Mesh.

① CROWLEY 2nd ORDER (ADH), FLUX CORRECTED

$$C_j^{n+1} = \left(\beta - \frac{\alpha}{2} + \frac{\alpha^2}{2} \right) C_{j+1}^n + (1 - 2\beta - \alpha^2) C_j^n + \left(\beta + \frac{\alpha}{2} + \frac{\alpha^2}{2} \right) C_{j-1}^n ;$$

$$\text{WHERE } \beta = \frac{K\delta t}{\delta x^2} \quad \alpha = \frac{U\delta t}{\delta x}$$

② SHASTA, NON FLUX LIMITED, NON MASS CONSERVATIVE

$$C_j^{n+1} = \left(-1/64 + \frac{\alpha}{16} - \frac{\alpha^2}{16} \right) C_{j+2}^n + \left(1/16 + \beta - 5/8\alpha + 3/4\alpha^2 \right) C_{j+1}^n + \\ \left(29/32 - 2\beta - 11/8\alpha^2 \right) C_j^n + \left(1/16 + \beta + 5/8\alpha + 3/4\alpha^2 \right) C_{j-1}^n + \\ \left(-1/64 - \frac{\alpha}{16} - \frac{\alpha^2}{16} \right) C_{j-2}^n ; C_j^{n+1} \geq 0$$

③ SEMI-IMPLICIT, NON MASS CONSERVATIVE

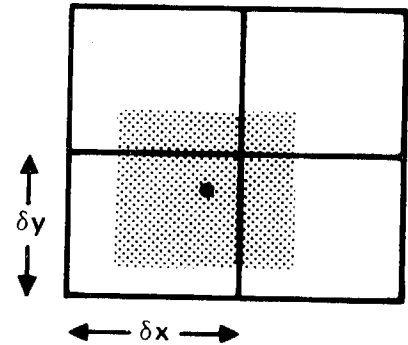
$$C_j^{n+1} = \alpha^2 C_{j+2}^n + (\beta + \alpha) C_{j+1}^n + (1 - 2\beta - 2\alpha^2) C_j^n + \\ + (\beta - \alpha) C_{j-1}^n + \alpha^2 C_{j-2}^n ; C_j^{n+1} \geq 0$$

④ POINT MASS (RANDOM WALK)

$$x^{n+1} = x^n + \alpha \pm (4\beta)^{1/2} W$$

$$\text{WHERE } \zeta = 2\pi^{-1/2} \int_0^W e^{-z^2} dz \quad 0 \leq \zeta \leq 1$$

$$C_j = \sum_{i=1}^M m_i / \delta x \delta y \delta z$$



The Gaussian problem is an initial step, but the actual atmosphere does not have uniform wind and diffusion fields. Thus, a more complex test problem would be preferable. The following solution of the point source problem with the wind and diffusion fields varying in altitude was developed by Smith (1957).

$$C = \frac{Q (zH)^{1/4} U_0^{1/2}}{4\pi^{1/2} K_1^{1/2} K_0 x^{2/3}} \cdot \exp \left[\frac{-K_0/K_1 y^2 + z^2 + H^2}{4K_0 x/U_0} \right] \cdot I_{-1/4} \left[\frac{zH}{2K_0 x/U_0} \right]$$

where

- z = the vertical distance (meters)
- y = the crosswind distance (meters)
- x = the downwind distance (meters)
- U = wind speed = $U_0 z^{1/2}$ (m/s)
- U_0 = the reference velocity at $z = 1$
- K_z = vertical diffusivity = $K_0 z^{1/2}$ (m^2/s)
- K_y = horizontal diffusivity = $K_1 z^{1/2}$ (m^2/s)
- K_0 = the reference vertical diffusivity at $z = 1$
- K_1 = the reference horizontal diffusivity at $z = 1$
- H = effective plume height (meters)
- Q = source strength ($\mu g/s$)
- I = the modified Bessel function of the first kind
- C = the concentration ($\mu g/m^3$).

This test problem introduces wind and diffusivity shear in the vertical but not in the horizontal. A change in coordinates modifies the above equation to a plume in a vertically shearing, horizontally rotating wind field as shown in Figure 4-12.

The problems described above (Gaussian, vertical shear, vertical and horizontal shear) are the three test problems that

were used to evaluate the candidate advection methods. All test problems used a zone size of 1000 meters by 1000 meters by 100 meters, a source height of 350 meters, a source strength 100 grams/sec., a wind speed at the source height of 2.37 meters/sec., and a vertical and horizontal diffusivity at the source height of $5.9 \text{ m}^2/\text{sec.}$ and $59 \text{ m}^2/\text{sec.}$, respectively. A time step of 250 seconds was used in all test problems and the problems were run to steady state (usually about 100 cycles). The results of the test problems are discussed below.

The downwind centerline and crosswind surface concentrations for the Gaussian problem are shown in Figure 4-13. Due to the coarse grid employed, the surface concentrations predicted by the various numerical methods produce an average concentration over the grid cell (in this case from 0 to 100 meters). Therefore, the analytic solution was plotted for heights of 0, 50, and 100 meters to illustrate the effects of cell averaging on the predicted concentrations. Perhaps the most interesting result of this test was the unusual behavior of the semi-implicit space-centered difference method which predicted values twice the actual solution. The reason for this critical inaccuracy is the errors made by the method in calculating the concentration gradient near a delta function source. This problem seems to be common to all space-centered differencing methods and it is therefore recommended that these methods not be used for point source type problems.

Another type of problem was noticed in the case of the particle random-walk method. Due to the fact that only a small percentage of the particles migrate down to the lowest layer of cells, the surface concentrations predicted by this method fluctuate from cycle to cycle. The data plotted in Figure 4-13 are the result of averaging predicted concentrations for 50 cycles after steady state was reached. The emission of 10 particles per cycle produced wide fluctuations in spite of the averaging. While the use of 50 particles per cycle gave acceptable results, the

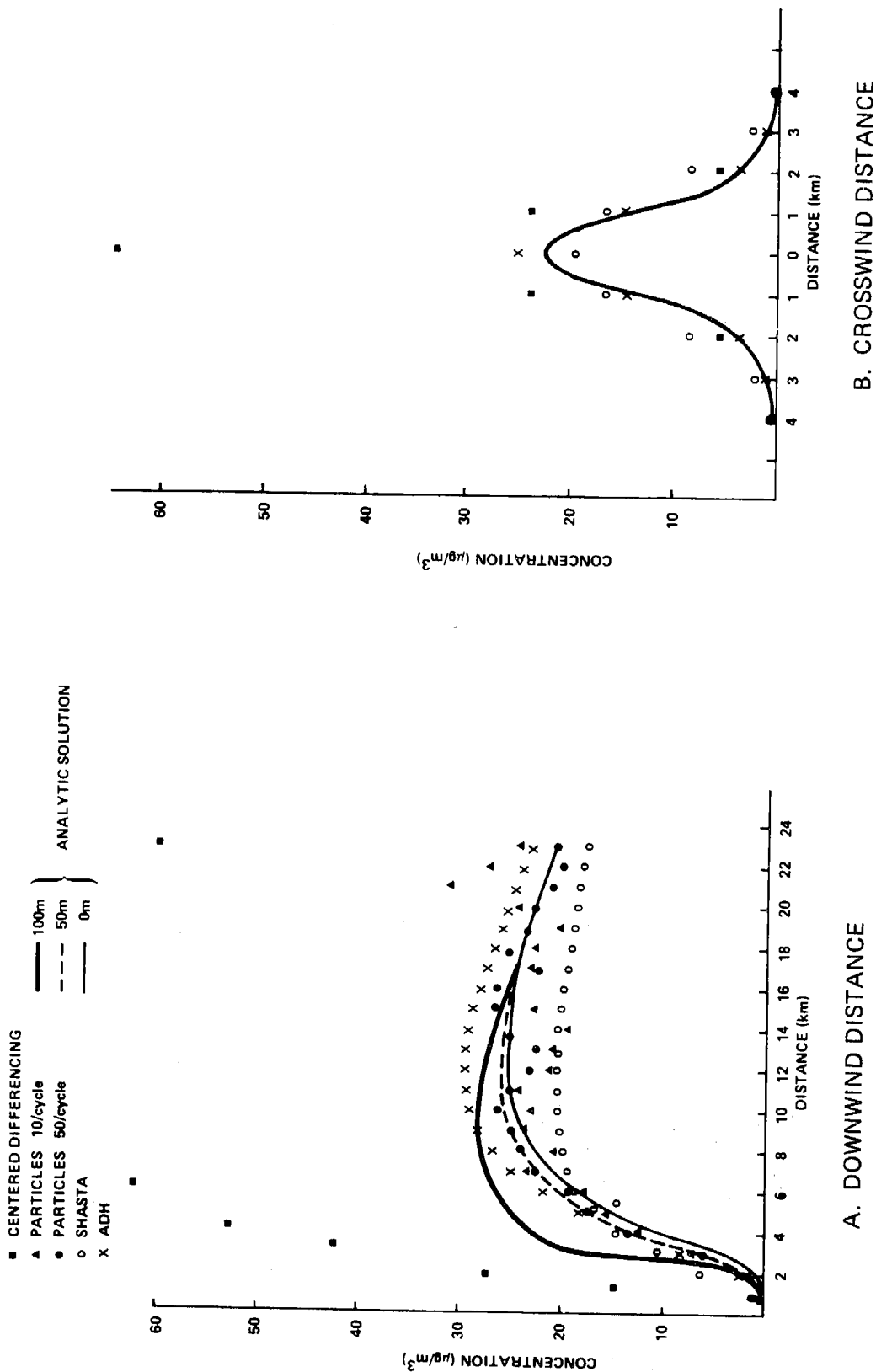


Figure 4-13. Comparison of Surface plus Centerline Concentrations for Finite Difference and Random Walk Solutions of a Three-Dimensional Point Source Plume, Uniform Wind and Diffusion Fields.

fluctuation from cycle to cycle and the large storage requirements make this method inappropriate for the use in a generalized point source air quality model. However, the random-walk method is applicable to situations when precise data is needed for concentration distributions for a single source and the user is willing to incur the computation storage requirements of large numbers of point mass particles.

The underestimate of the centerline surface concentration by the non-flux corrected, non-mass conservative version of the SHASTA method is probably due to the large artificial (i.e., numerical) diffusion in the crosswind direction. Referring to Table 4-6, we note that for the zero velocity case $\alpha = 0$ and the expression for the updated concentration becomes

$$C_j^{n+1} = \left\{ \beta (C_{j+1}^n - 2C_j^n + C_{j-1}^n) \right\} \text{ physical diffusion} \\ + \left\{ 1/64 (-C_{j+2}^n + 4C_{j+1}^n - 6C_j^n + 4C_{j-1}^n - C_{j-2}^n) \right\} \text{ numerical diffusion} \\ + C_j^{n+1}$$

The numerical diffusion is minimal when α approaches one. The overprediction of the surface centerline concentration by the Crowley second-order flux-corrected method used in the DEPICT code (ADH) is caused by the fact that the solution algorithm sweeps from left to right while the physical transport of this problem is from right to left. Thus the flux-corrected part of the algorithm (which works by adjusting the flux going into the next cell) is working against the physical flow of the problem. When the same test problem was run with a positive wind, the centerline concentrations were equal to or slightly less than the 50-m analytic solution.

Both the SHASTA and ADH advection schemes were then compared with the analytic solution for wind and diffusion fields with a vertical shear. The resulting centerline concentrations are

plotted in Figure 4-14. Note that the same trends continue in this test problem with SHASTA underpredicting surface centerline concentrations and ADH overpredicting.

The results of the final test problem are shown in Figure 4-15. The surface concentrations for the analytic, ADH and SHASTA solutions are shown as perspective and contour plots. We note that neither ADH or SHASTA can reproduce the sharp concentration peak near the source (due to the coarse zoning of the test region). It can also be seen that even though both the u and v components of the wind field are non-zero, SHASTA still has some numerical diffusion resulting in an increased plume width. Two cuts across the plume (illustrated in Figure 4-15 at AA and BB) are shown in Figure 4-16. The same trends discussed previously continue here with the exception that at section AA, both ADH and SHASTA overpredict the actual surface concentrations. The difference between the analytic and numerical solutions are illustrated in Figure 4-17 as perspective and contour plots of the analytic solution minus the ADH or SHASTA solutions. After reviewing the results of these tests, it is felt that at the present time the correct selection for the advection-diffusion scheme is the Crowley second-order, flux-corrected algorithm ADH as used in DEPICT. However, the flux-corrected or phoenical version of SHASTA (Meyer, 1976) may warrant additional consideration.

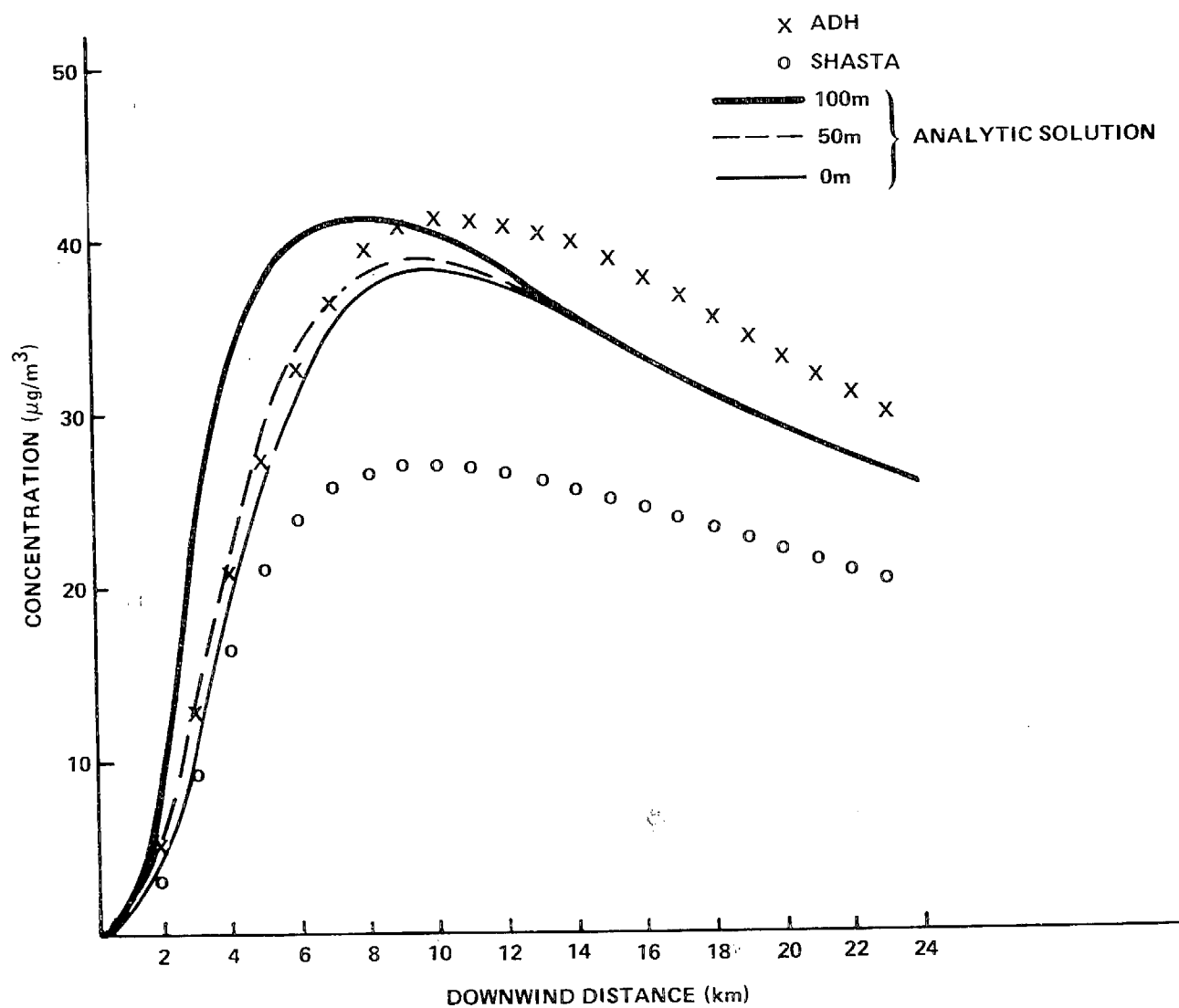


Figure 4-14. Comparison of Surface Concentrations for Finite Difference Solutions of a Three-Dimensional Point Source Plume, Vertically Sheared Wind and Diffusion Fields.

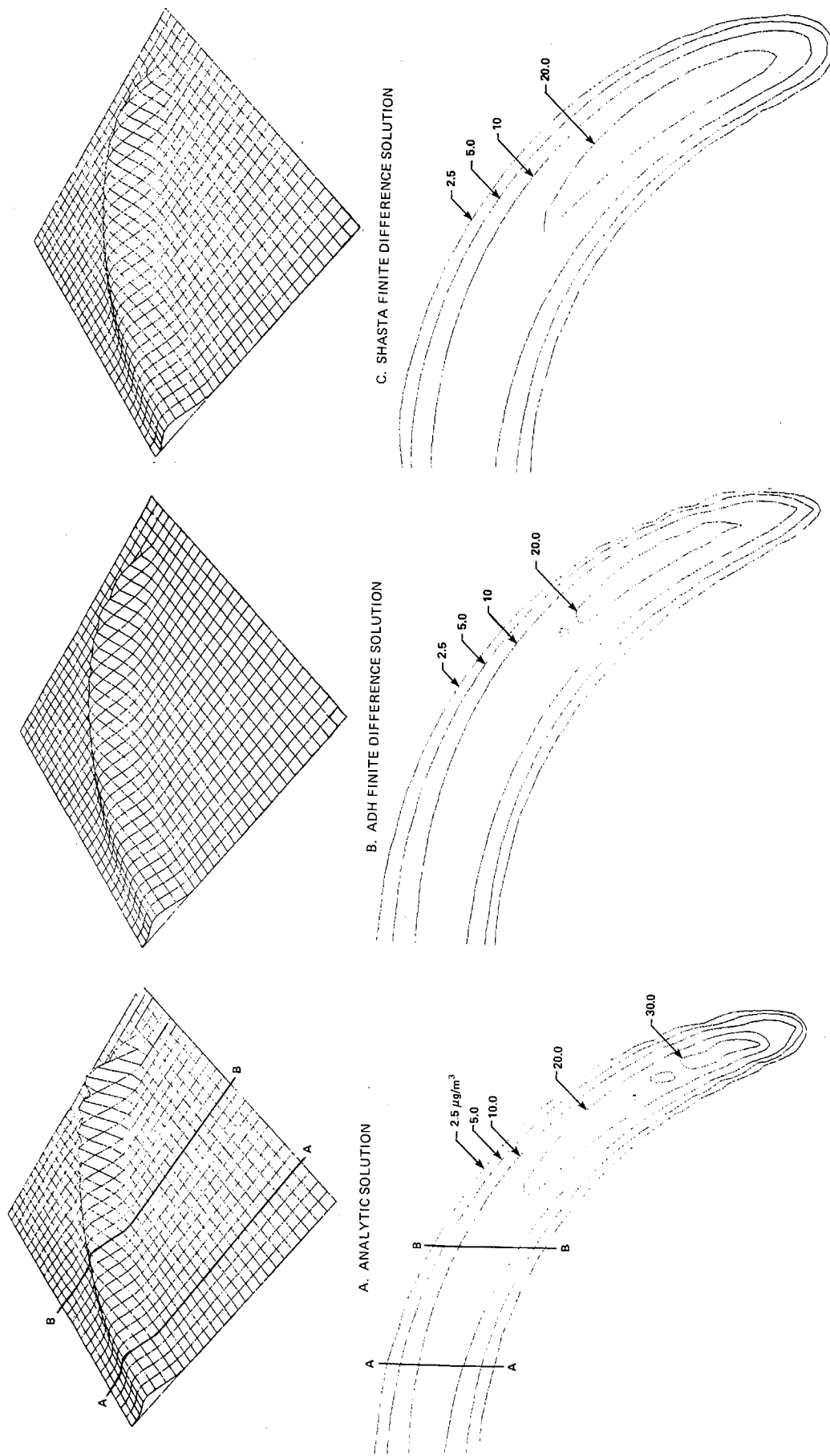
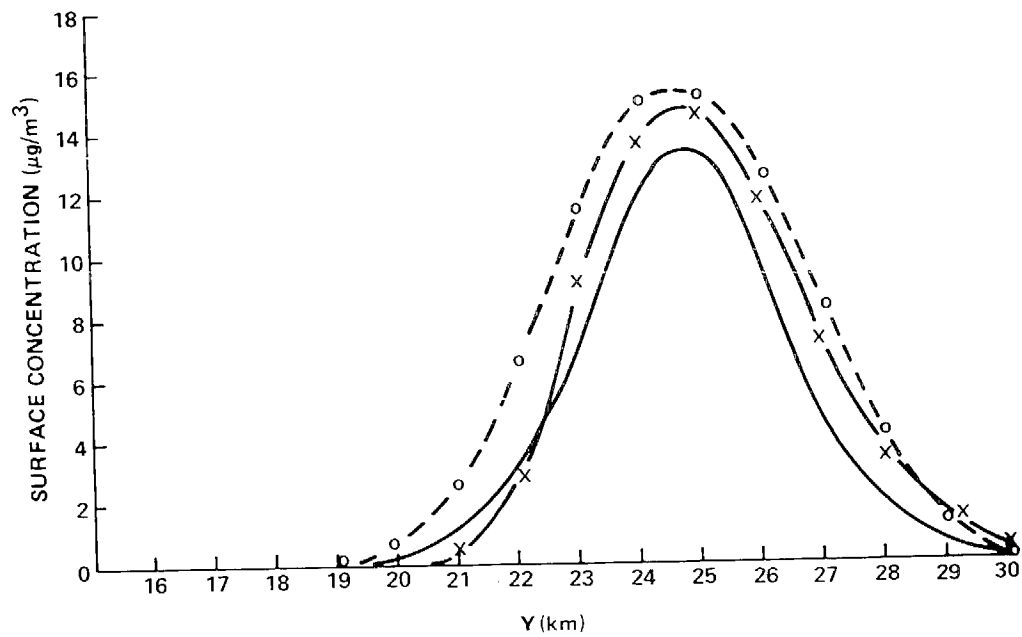
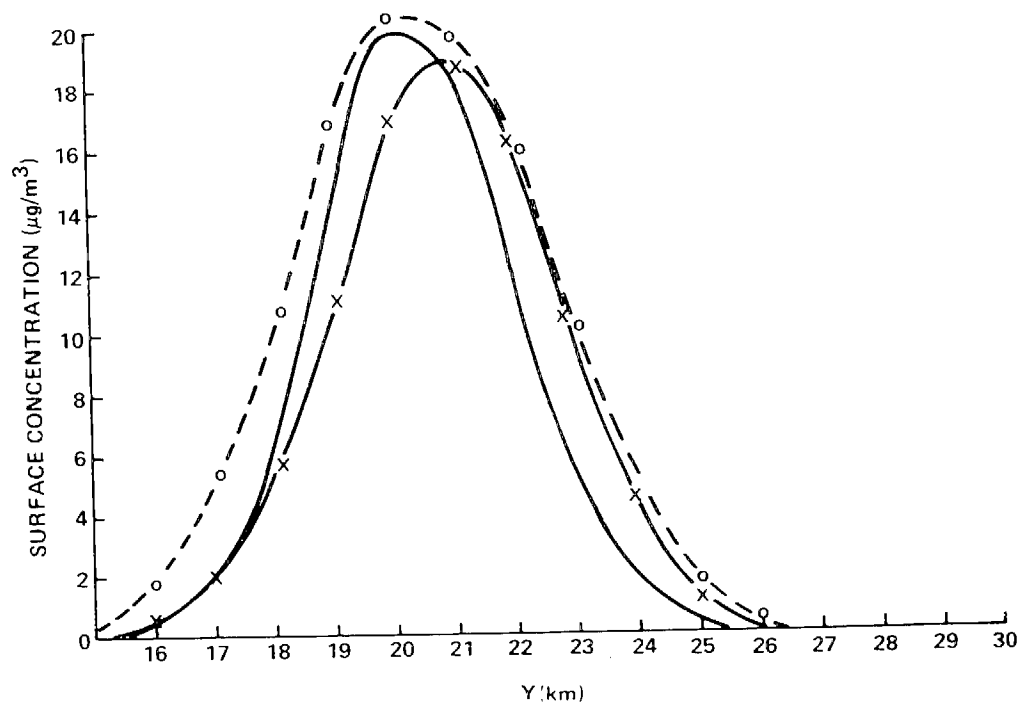


Figure 4-15. Comparison of Perspective (top) and Contour (bottom) Plots of Surface Concentrations for Finite Difference Solutions of Three-Dimensional Point Source Plume, Vertically Sheared Diffusion Field and Horizontally Sheared Wind Field.



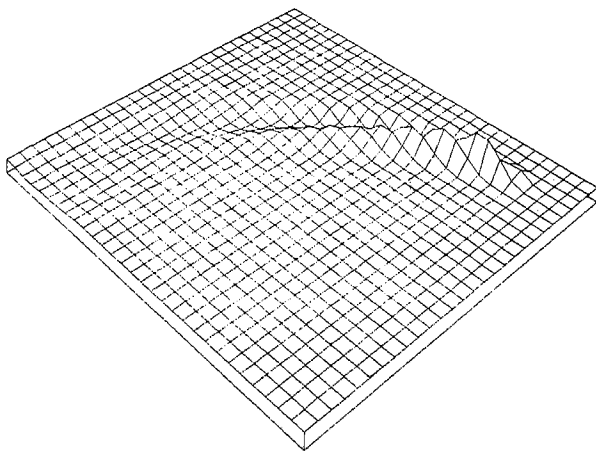
A. SECTION A-A (X = 20 KM)

— x — ADH
 - - o - - SHASTA
 — ANALYTIC

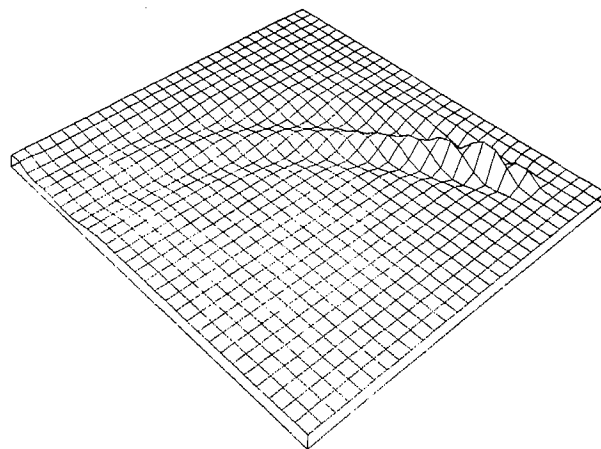


B. SECTION B-B (X = 10 KM)

Figure 4-16. Comparison of Surface Concentrations for Finite Difference Solutions of a Three-Dimensional Point Source Plume, Vertically Sheared Diffusion Field and Vertically and Horizontally Sheared Wind Field.



A. ANALYTIC SOLUTION MINUS ADH



B. ANALYTIC SOLUTION MINUS SHASTA

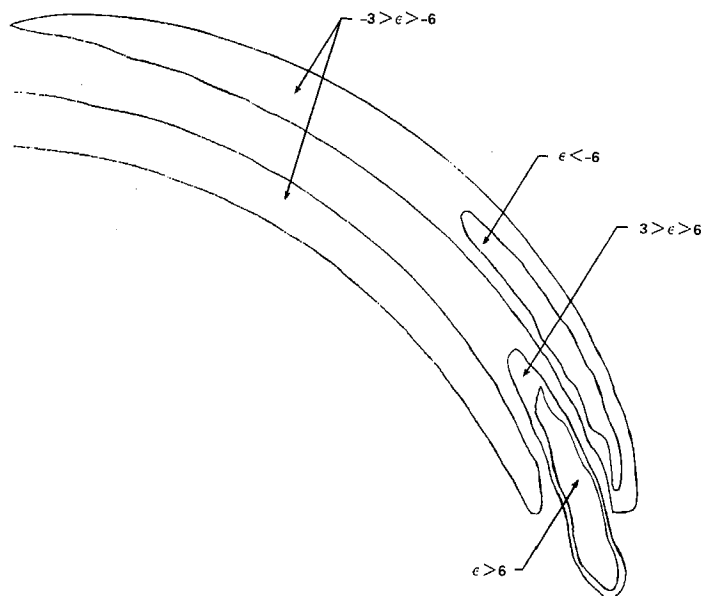
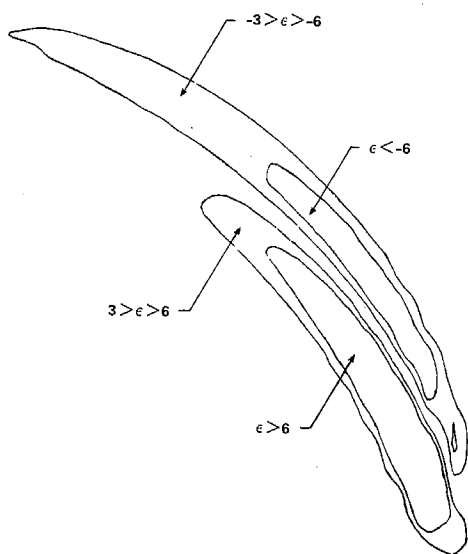


Figure 4-17. Perspective and Contour Plots Showing the Difference Between the Analytic Solutions Less the ADH and SHASTA Solutions (ϵ , $\mu\text{g}/\text{M}^3$).

4.5 Review of Chemistry Options

The IMPACT code is designed to provide the framework for simulating the complex chemical transformations of air pollutants as well as the transport and dispersion of simple inert pollutants. Three chemical reaction mechanisms are available as options in the present version of IMPACT. They provide a representative sampling of the state-of-the-art in air pollutant chemical reactions. Other chemistry mechanisms can easily be incorporated if desired (see Appendix C for detailed information on the incorporation of other chemical mechanisms).

Two chemical reaction mechanisms simulate the transformation of the constituents of photochemical smog. A simple mechanism developed by GRC (Eschenroder, 1972), CHEM6, supports five active species and is limited to simulations of 12 hours or less (see Table 4-7). The other photochemical model, CHEM15, incorporates a more general mechanism (Hecht, 1974) and supports 14 active species. Both CHEM6 and CHEM15 express the effects of chemical reactions and sources by a solution for each cell of a rate equation of the form

$$\frac{\partial C_{\ell}}{\partial t} = A_{\ell} + \sum_{n=1}^N B_{\ell n} C_n + \sum_{n,m=1}^N D_{\ell nm} C_n C_m$$

for the ℓ th pollutant species. The A_{ℓ} is used to enter sources and the net advective/diffusive flux into the cell. The rate equation is recast into

$$\frac{\partial C_{\ell}}{\partial t} = F_{\ell} - R_{\ell} C_{\ell}$$

and an approximate solution, used as a predictor-corrector, is

$$C_{\ell}^{n+1} = -F_{\ell}/R_{\ell} + \left(C_{\ell}^n - F_{\ell}/R_{\ell} \right) \exp(-R_{\ell} \Delta t) .$$

Table 4-7. CHEM6 Reaction Mechanism.

	REACTION MECHANISM	RATE CONSTANT (ppm/min)
1.	$h\nu + \text{NO}_2 \rightarrow \text{NO} + \text{O}$	2.67×10^{-1}
1a.	$\text{O} + \text{O}_2 + \text{M} \rightarrow \text{O}_3 + \text{M}$	2.6×10^6
2.	$\text{NO} + \text{O}_3 \rightarrow \text{NO}_2 + \text{O}_2$	2.67×10
3.	$\text{O} + \text{HC} \rightarrow (b_1) \text{RO}_2$	2.67×10^2
4.	$\text{OH} + \text{HC} \rightarrow (b_2) \text{RO}_2$	$.5 \times 10^4$
5.	$\text{O}_3 + \text{HC} \rightarrow (b_3) \text{RO}_2$	$4. \times 10^{-3}$
6.	$\text{RO}_2 + \text{NO} \rightarrow \text{NO}_2 + (\gamma) \text{OH}$	$1. \times 10^5$
7.	$\text{RO}_2 + \text{NO}_2 \rightarrow \text{PAN}$	$2. \times 10^2$
8.	$\text{OH} + \text{NO} \rightarrow \text{HONO}$	1.5×10^3
9.	$\text{OH} + \text{NO}_2 \rightarrow \text{HNO}_3$	$3. \times 10^3$
10.	$h\nu + \text{HONO} \xrightarrow{\text{H}_2\text{O}} \text{OH} + \text{NO}$	1.0×10^{-3}
11.	$\text{NO} + \text{NO}_2 \rightarrow 2 \text{HONO}$	$1. \times 10^{-3}$
12.	$\text{NO}_2 + \text{O}_3 \rightarrow \text{NO}_3 + \text{O}_2$	$5. \times 10^{-3}$
13.	$\text{NO}_3 + \text{NO}_2 \rightarrow \text{N}_2\text{O}_5$	4.5×10^3
14.	$\text{N}_2\text{O}_5 \rightarrow \text{NO}_3 + \text{NO}_2$	1.4×10
15.	$\text{N}_2\text{O}_5 + \text{H}_2\text{O} \rightarrow 2\text{HNO}_3$	6.05×10
16.	$\text{NO}_2 + \text{PARTICULATES} \rightarrow \text{PRODUCTS}$	0.0

NOTE: $b_1 = 8, b_2 = 8, b_3 = 1, r = 1/8$
 $\text{O}_2, \text{M}, \text{H}_2\text{O}$ concentrations incorporated in rate constants. Rate constant for Reaction 1 normalized to solar flux = 100 watts/m².

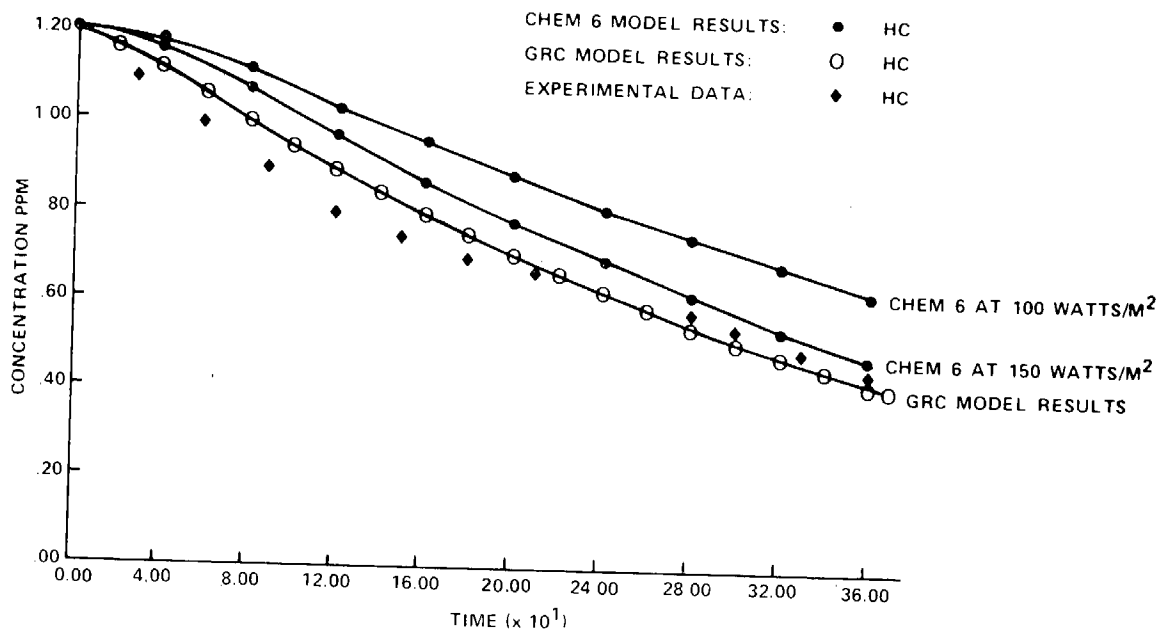
This technique was developed specifically for solving the particular class of equations that describe photochemical reactions (Sklarew, 1971). As such, it is extremely efficient while retaining the accuracy of more generalized solution techniques.

As a test of the CHEM6 routine, the rate constants for a toluene hydrocarbon run as specified in the GRC report (Eschenroder, 1972) were selected and the results of the CHEM6 simulation were compared with the results in the report (Figure 4-18). Because the value of the solar flux was not recorded, runs using the value of 100 and 150 watts/m² were used. These values (which are representative of actual conditions) appear to bracket the GRC model results.

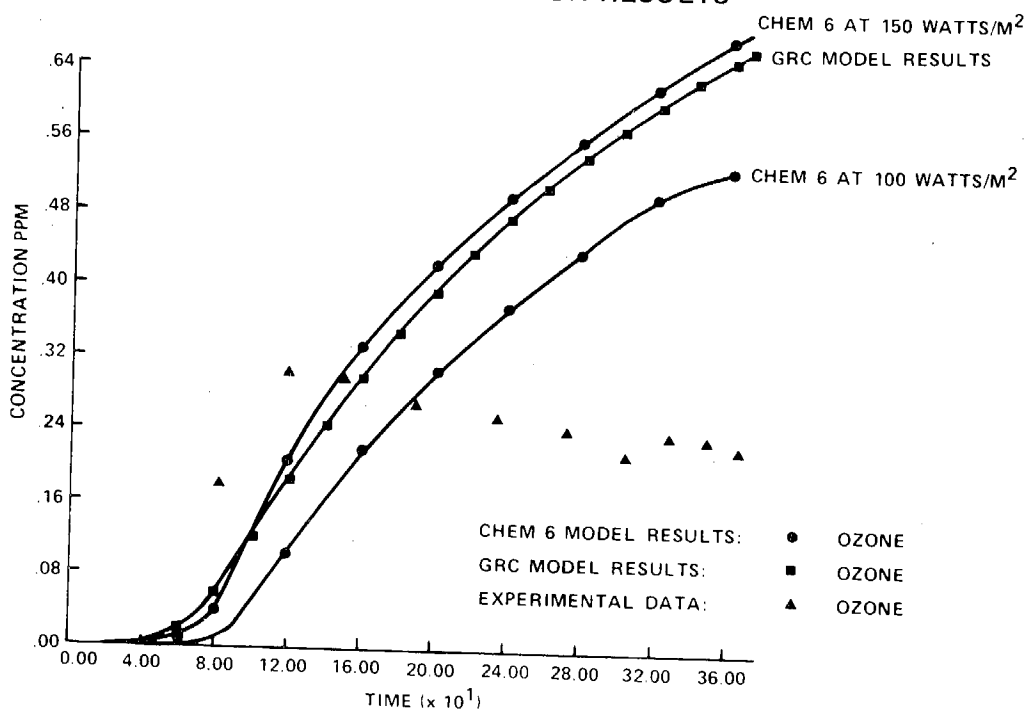
The CHEM15 routine (see Table 4-8) was run for several different cases corresponding to experiments sited by Hecht (1974) and showed generally good agreement with their solution. Table 4-9 illustrates the comparison of the CHEM15 and EPA model for experiment 348 as reported.

The third chemistry option available is a simplified treatment of the oxidation of sulfur dioxide to sulfate. The chemistry of SO₂ in the atmosphere (and for that matter in the smog chamber) is poorly understood relative to the state-of-the-art of ozone chemistry. The SO₂ mechanism currently encoded in IMPACT does not simulate SO₂ photochemistry but rather relies upon empirical observation of atmospheric SO₂ oxidation rates. Observed maximum rates have been found to range from 2 percent per hour (Katz, 1950) to 12 percent per minute (Shirai, 1962).

Recent work sponsored by the ARB (Liu, 1976) suggests that the rate of conversion is related to downwind distance from the SO₂ source. Table 4-10 (taken from this ARB report) summarizes the observed relationship. Presumably the rate variation is related to concentrations of OH, O, NO₃, HO₂, etc. in the ozone depression plume associated with NO stack emissions. In keeping with these results, the SO₂ mechanism in IMPACT employs a



A. HYDROCARBON RESULTS



B. OZONE RESULTS

Figure 4-18. Comparison of CHEM6 Model Results, GRC Model Results, and Experimental Data, Experiment 271, Toluene/NO_x.

Table 4-8. CHEM15 Reaction Mechanism.

REACTION MECHANISM	RATE CONSTANT (ppm/min)
1. $\text{NO}_2 + h\nu \rightarrow \text{NO} + \text{O}$	2.66×10^{-1}
2. $\text{O} + \text{O}_2 + \text{M} \rightarrow \text{O}_3 + \text{M}$	$2. \times 10^{-5}$
3. $\text{O}_3 + \text{NO} \rightarrow \text{NO}_2 + \text{O}_2$	2.08×10^1
4. $\text{O} + \text{NO} + \text{M} \rightarrow \text{NO}_2 + \text{M}$	3.5×10^{-3}
5. $\text{O} + \text{NO}_2 \rightarrow \text{NO} + \text{O}_2$	1.38×10^4
6. $\text{O} + \text{NO}_2 + \text{M} \rightarrow \text{M} \rightarrow \text{NO}_3 + \text{M}$	2.2×10^{-3}
7. $\text{O}_3 + \text{NO}_2 \rightarrow \text{NO}_3 + \text{O}_2$	4.6×10^{-2}
8. $\text{NO}_3 + \text{NO} \rightarrow 2\text{NO}_2$	1.5×10^4
9. $\text{NO}_3 + \text{NO}_2 \rightarrow \text{N}_2\text{O}_5$	4.5×10^3
10. $\text{N}_2\text{O}_5 \rightarrow \text{NO}_2 + \text{NO}_3$	1.5×10
11. $\text{N}_2\text{O}_5 + \text{H}_2\text{O} \rightarrow 2\text{HNO}_3$	$1. \times 10^{-5}$
12. $\text{NO} + \text{HNO}_3 \rightarrow \text{HNO}_2 + \text{NO}_2$	2.5×10^{-4}
13. $\text{HNO}_2 + \text{HNO}_3 \rightarrow \text{H}_2\text{O} + 2\text{NO}_2$	$2. \times 10^{-1}$
14. $\text{NO} + \text{NO}_2 + \text{H}_2\text{O} \rightarrow 2\text{HNO}_2$	2.1×10^{-6}
15. $2\text{HNO}_2 \rightarrow \text{NO} + \text{NO}_2 + \text{H}_2\text{O}$	4.5
16. $\text{HNO}_2 + h\nu \rightarrow \text{OH} + \text{NO}$	1.3×10^{-2}
17. $\text{OH} + \text{NO}_2 \rightarrow \text{HNO}_3$	1.5×10^4
18. $\text{OH} + \text{NO} + \text{M} \rightarrow \text{HNO}_2 + \text{M}$	1.2×10^4
19. $\text{OH} + \text{CO} + (\text{O}_2) \rightarrow \text{CO}_2 + \text{HO}_2$	2.5×10^2
20. $\text{HO}_2 + \text{NO} \rightarrow \text{OH} + \text{NO}_2$	$7. \times 10^2$
21. $\text{H}_2\text{O}_2 + h\nu \rightarrow 2\text{OH}$	2.5×10^2
22. $\text{HC}_1 + \text{O} \rightarrow \text{ROO} + \alpha\text{RCOOO} + (1-\alpha)\text{HO}_2$	6.8×10^3
23. $\text{HC}_1 + \text{O}_3 \rightarrow \text{RCOOO} + \text{RO} + \text{HC}_4$	1.6×10^{-2}
24. $\text{HC}_1 + \text{OH} \rightarrow \text{ROO} + \text{HC}_4$	2.5×10^4
25. $\text{HC}_2 + \text{OH} \rightarrow \text{ROO} + \text{OH}$	1.07×10^2
26. $\text{HC}_2 + \text{OH} \rightarrow \text{ROO} + \text{H}_2\text{O}$	$8. \times 10^3$
27. $\text{HC}_3 + \text{O} \rightarrow \text{ROO} + \text{OH}$	6.5×10
28. $\text{HC}_3 + \text{OH} \rightarrow \text{ROO} + \text{H}_2\text{O}$	3.8×10^4
29. $\text{HC}_4 + h\nu \rightarrow \beta\text{ROO} + (2-\beta)\text{HO}_2$	2.5×10^{-3}
30. $\text{HC}_4 + \text{OH} \rightarrow \beta\text{RCOOO} + (1-\beta)\text{HO}_2 + \text{H}_2\text{O}$	2.3×10^4
31. $\text{ROO} + \text{NO} \rightarrow \text{RO} + \text{NO}_2$	9.1×10^2
32. $\text{RCOOO} + \text{NO} + (\text{O}_2) \rightarrow \text{ROO} + \text{NO}_2 + \text{CO}_2$	9.1×10^2
33. $\text{RCOOO} + \text{NO}_2 \rightarrow \text{RCOOO} + \text{NO}_2$	$1. \times 10^2$
34. $\text{RO} + \text{O}_2 \rightarrow \text{HO}_2 + \text{HC}_4$	2.4×10^{-2}
35. $\text{RO} + \text{NO}_2 \rightarrow \text{RONO}_2$	4.9×10^2
36. $\text{RO} + \text{NO} \rightarrow \text{RONO}$	2.5×10^2
37. $\text{HO}_2 + \text{HO}_2 \rightarrow \text{H}_2\text{O}_2 + \text{O}_2$	5.3×10^3
38. $\text{HO}_2 + \text{ROO} \rightarrow \text{RO} + \text{OH} + \text{O}_2$	$1. \times 10^2$
39. $2\text{ROO} \rightarrow 2\text{RO} + \text{O}_2$	$1. \times 10^2$

HC_1 = olefins, HC_2 = aromatics, HC_3 = parafins, HC_4 = aldehydes

Table 4-9. Comparison of Solutions of the Seinfeld-Hecht-Dodge Photochemical Reaction Model.

TIME (MINUTES)	O ₃		NO ₂		HC1	
	H-S	CHEM 15	H-S	CHEM 15	H-S	CHEM 15
0	0	0	0	.0600	.44	.44
40	0	.0013	.04	.12	.4	.42
80	0	.0028	.2	.23	.35	.40
120	0	.0064	.4	.41	.30	.37
160	0	.0161	.6	.67	.25	.32
200	.04	.0633	.8	.94	.2	.27
240	.30	.30	.7	.93	.15	.20
280	.55	.52	.55	.66	.10	.13
320	.6	.66	.45	.38	.08	.08
360	.7	.74	.2	.2	.05	.04

Table 4-10. Rate of SO₂-Sulfate Conversion as Estimated From the Predictions of the Reactive Plume Model, (Liu, 1976).

<u>September 10, 1974 (Moss Landing)</u>	
< 10 km from stack	0.6%/hr
> 10 km	4.0%/hr
<u>September 11, 1974 (Moss Landing)</u>	
< 10 km	0.46%/hr
> 10 km	4.0%/hr
<u>October 1, 1974 (Haynes)</u>	
< 10 km	0.20%/hr
> 10 km	6.0%/hr
<u>October 11, 1974 (Haynes)</u>	
< 10 km	0.3%/hr
> 10 km	6.0%/hr
<u>October 17, 1974 (Haynes)</u>	
< 10 km	0.3%/hr
> 10 km	22.0%/hr
<u>October 25, 1974 (Los Alamitos)</u>	
< 10 km	0.1%/hr
> 10 km	3.0%/hr
<u>October 30, 1974 (Los Alamitos)</u>	
< 10 km	0.05%/hr
> 10 km	3.0%/hr
<u>November 7, 1974 (Los Alamitos)</u>	
< 10 km	0.02%/hr
> 10 km	1.0%/hr

spatially-dependent SO_2 conversion rate that depends upon the plume concentration at the point under consideration. Figure 4-19 describes the relationship between conversion rate and plume concentration.

Values of FAST and SLOW correspond to estimates of the conversion rate distal and proximal to the stack, (where a SO_2 concentration in the neighborhood of 200 ppm might be expected). From Table 4-9, reasonable values of FAST and SLOW could be taken as 10 percent and 1.0 percent, respectively.

Other models such as augmented photochemical SO_2 mechanism (Liu, 1976) modifications of the LIRAQ photochemical mechanism (Galenis, 1977) warrant consideration as additional sulfur-sulfate chemistry options.

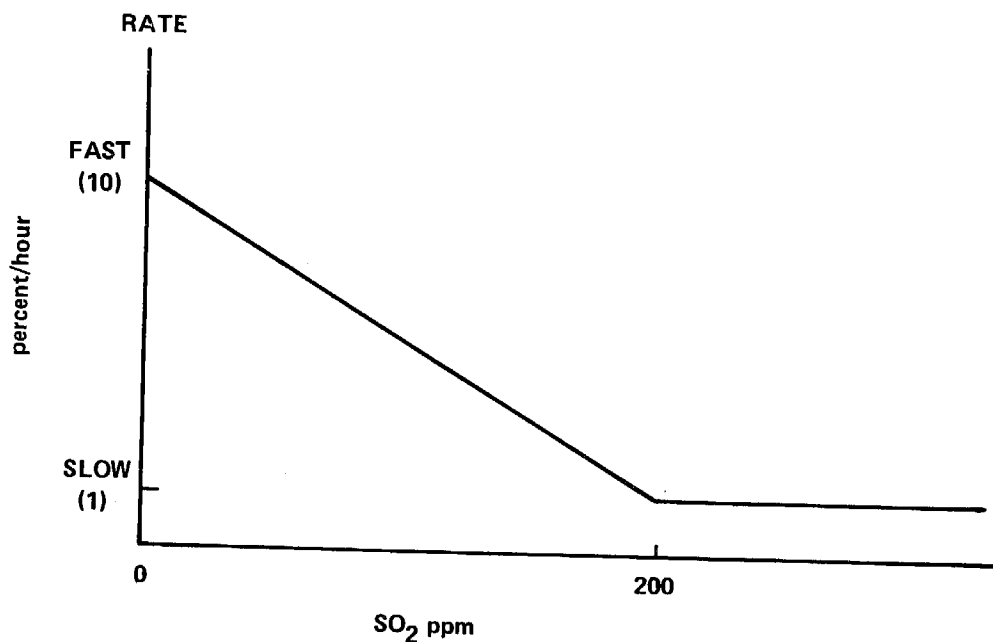


Figure 4-19. SO_2 Conversion to SO_4 .

5.0 VALIDATION OF DISPERSION MODELS

The development and use of a mathematical model requires that the accuracy of the model be substantiated with actual field measurements so that the user may have confidence in the model results. This procedure is usually termed model validation or model verification.

Because of the complexity of the air pollution dispersion problem, the best approach to validation is to focus on each key submodel separately (e.g., plume rise, transport, etc.). Thus, key experiments can be devised to differentiate between a number of alternate submodels. An example of this procedure is the review of the plume rise options used in both the Gaussian and grid models, in which a comparison is made of predicted values with actual field tests (see section 3.1.3).

Unfortunately, the paucity of data and the uncertainty of the required realism of each submodel severely limits this step-by-step ideal approach. In practice, the entire model is usually validated as a unit. This is partially due to the fact that in typical field studies the measurement of surface concentrations at specific locations is the most important objective and is usually the most accurately measured data in the field program. The use of aerial sampling in some programs does provide an indication of plume rise and structure; however, sufficient detailed data are typically lacking on pollutant dispersion and on wind and diffusivity fields.

5.1 Discussion of Validation Options

As discussed above, the usual focus of the validation of air quality dispersion models is how well the model predicts pollutant surface concentrations. In theory this procedure would seem to provide sufficient validation for the user to implement the model. In practice, however, the complexity of the physical phenomenon involved requires a further discussion as to the applicability of the model to differing topographies and meteorologies. In fact, there are three concepts which should be incorporated into model validation efforts. These three concepts are: precision, realism, and generality.

- Precision refers to the deviation of the model's predicted value from the population mean. This generally refers to the ability of the model to predict the value of a variable measured in the field. In defining the required performance of the model in terms of precision, the investigator must predetermine acceptable error limits.
- Realism refers to two characteristics of the model: first, the correspondence between simulated subsystems and real world subsystems, and secondly, the extent to which the model is based on the physics and chemistry of the phenomena, as opposed to statistically simulating the variation of a parameter. In defining how realistic the model must be, the investigator must identify those systems which may be represented by probability functions and tables of input data, and those systems which are defined by physio-chemical relationships. The level of realism is defined by the number of subsystems included in the simulation whose dynamics are actually simulated, expressed as a percent of the total number of subsystems.
- Generality refers to the range of applicability of the model. The model may be very precise and realistic for a given region but may not be applicable to another region,

due to limitations on boundary conditions or to system components (which could be assumed constant in other field situations) that vary from region to region. The generality of the model can be defined in terms of time and space. For example, the number of days, weeks or years, and the areas of terrain (e.g., mountains versus level ground, etc.) to which the model does apply need to be compiled. Generality of a model can be defined by the number of environments for which it is applicable, expressed as a percentage of the number of environments which are found in the real world.

To fulfill the requirement of model validation, all three issues must be specifically addressed and answered.

5.1.1 Precision

Precision refers to deviation of the model's predicted value from the population mean and, therefore, the statistics which measure this quantity are appropriate. Mean error, maximum error, mean error as a function of population variance (Z - score), and correlation are all measures of precision for relatively large sample sizes (i.e., 30 or more receptors). In the case of smaller sample sizes, however, the statistics of Wilcoxon Signed Rank test, Wilcoxon Two Sample test, or the Spearman's Rank correlation could be used. A problem which usually arises is that μ , the true population mean, is frequently not measured due to cost or time constraints. So \bar{X}_s or a representative sample mean is used in its place.

There are some dangers in using these statistics blindly without accompanying graphic displays and plots. Figure 5-1 shows some of the problems which can arise by using standard statistical procedures. This figure represents a simplified model validation test for a Gaussian point source model. Consider a point source with an effective stack height of 190 meters, an elevated inversion at 200 meters, neutral atmospheric stability from the surface to the elevated inversion, an emission rate of 10 grams/sec., and a

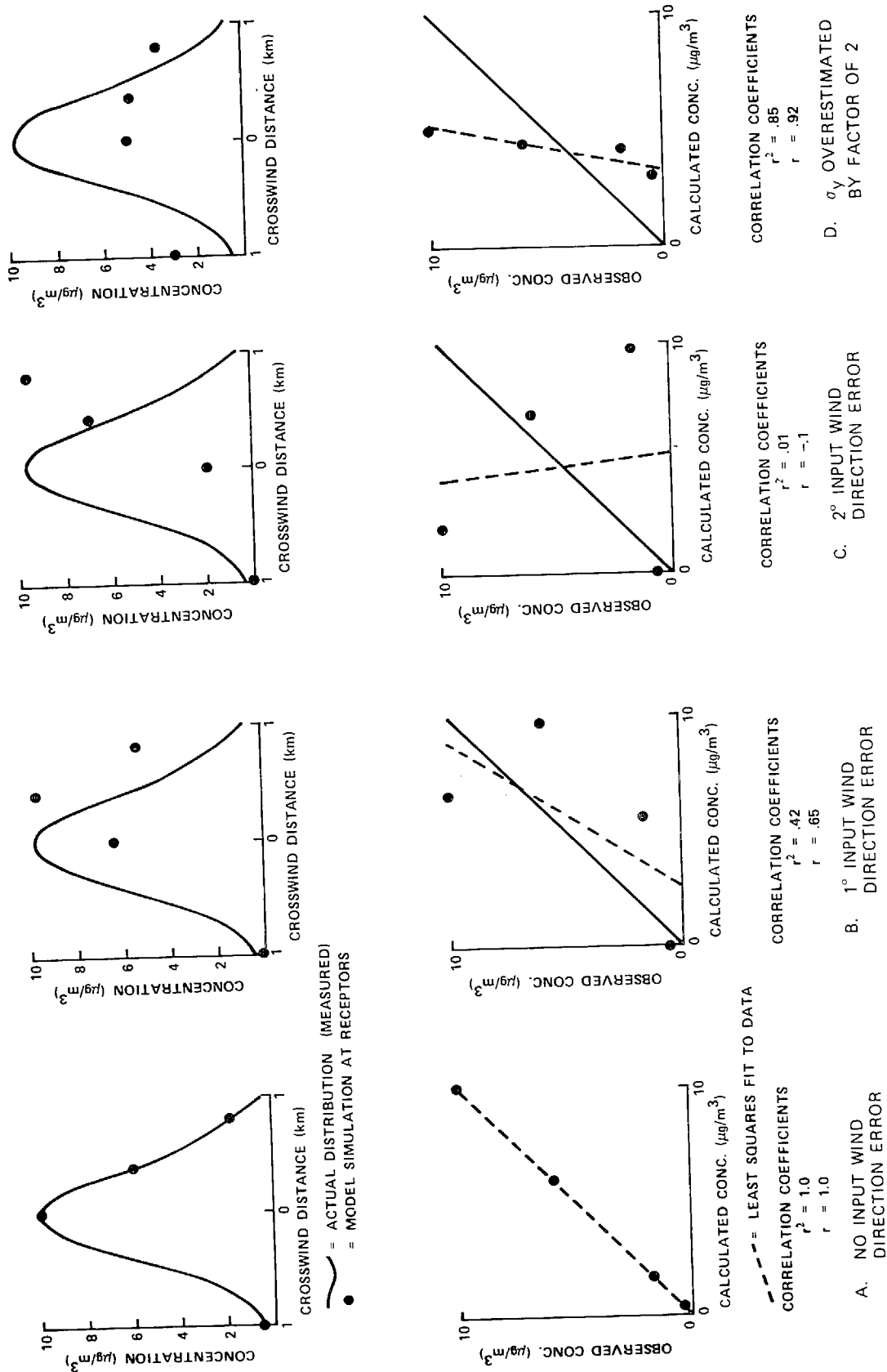


Figure 5-1. Illustration of the Problems in Using Statistical Measures in Assessing Model Validation for Point Source Models.

wind speed of 5 meters/sec. Assume that the Gaussian model provides a completely accurate description of pollutant dispersion and that we have an array of receptor stations 20 kilometers downwind of the source. The plots shown in the upper portion of Figure 5-1 represent the actual surface concentrations distribution and the concentrations predicted by the Gaussian model assuming various errors in the data-input wind direction. The lower portion of the figure illustrates the scatter plots and the correlation coefficient associated with the distributions illustrated above.

From this figure we note that a 100% precise model with an input error in wind direction of only two degrees (which is not an unreasonable mean error in the field) would result in a correlation coefficient of 0.01, while a model with an error of a factor of two in horizontal dispersion standard deviation with no wind error would produce a correlation coefficient of 0.85. Although this case is admittedly contrived, it is not unrealistic and clearly shows the danger of only relying on standard statistical procedures.

Of course, errors in measured wind direction are only one possible source of uncertainty in the model validation procedure. A more complete list is presented in Figure 5-2. The errors associated with each element in these validation procedure processes are rough estimates based on insight gained by the authors from many years of experience in model validation and the examination of numerous sets of field data; the reader is cautioned against considering these estimates to be exact.

In spite of these uncertainties involved in the validation procedure, model validation is possible. Graphic displays (e.g., pollutant isopleths and wind streamlines) can reveal patterns in spite of rotational (or more complex) transformations due to errors in wind measurements. Although difficult to quantify, the comparison of predicted and observed isopleths and wind streamlines is likely to remain the best model validation procedure.

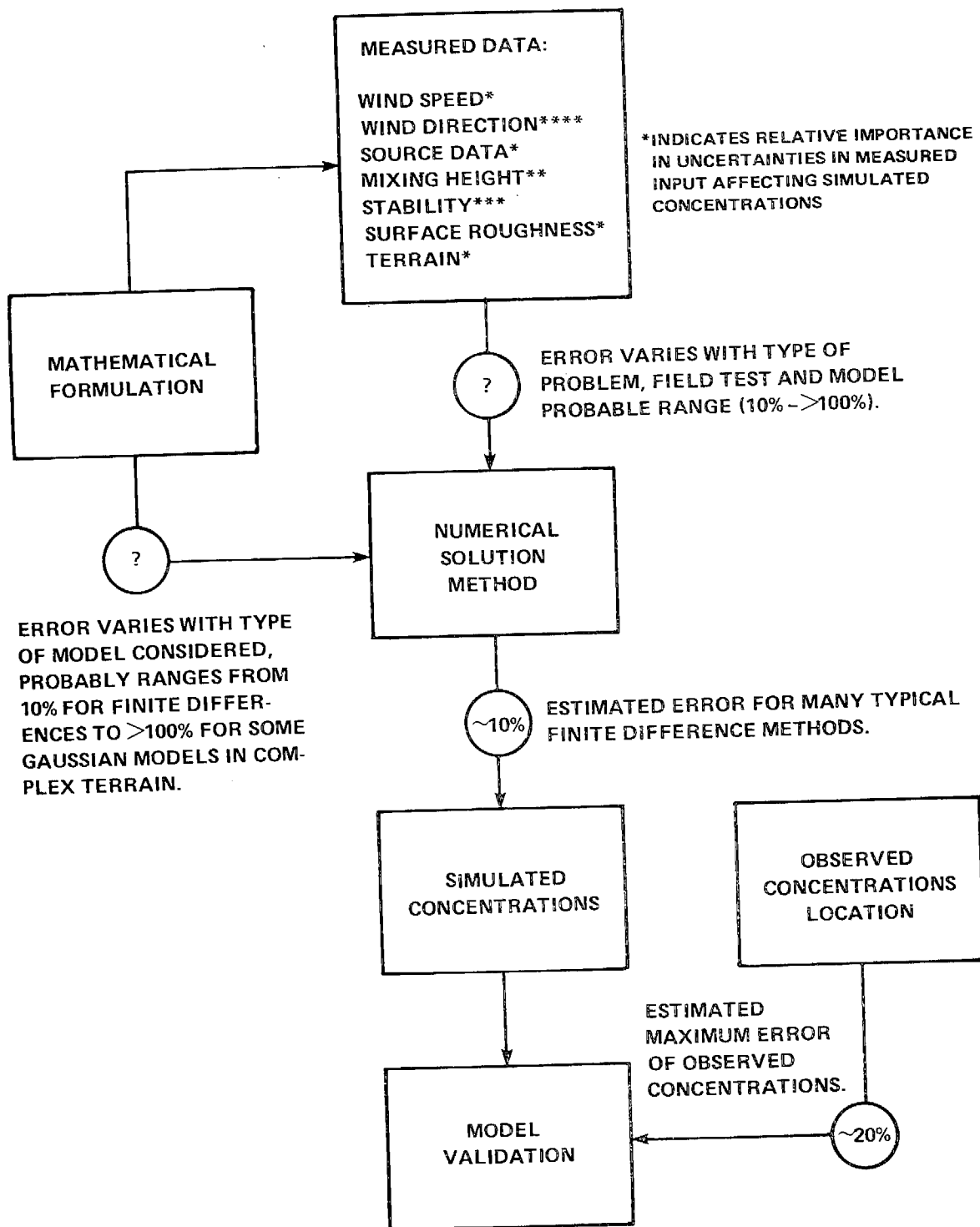


Figure 5-2. Areas of Uncertainty and Possible Sources of Error Associated with Each Step in the Model Validations Procedure.

Also, other model parameters such as the maximum pollutant concentration and the downwind distance at which it occurs are less likely to be as severely affected by errors in model input as overall concentration distributions. Therefore, the approach used to define the precision of the GEM and IMPACT models will be as follows:

- GEM:
 - Graphical display of representative predicted isopleths overlaid with field measurements.
 - Scatter plots of standard and mean error of predicted vs. observed maximum concentrations and the downwind distance of the maximum concentrations.
- IMPACT:
 - Graphical streamlines of predicted and observed wind fields.
 - Scatter plots of predicted vs. observed wind speed and wind direction.
 - Isopleths of predicted pollutant concentrations overlaid with field measurements.
 - Time-dependent plots of predicted vs. observed secondary pollutant (e.g., ozone) concentrations.

5.1.2 Realism

The precise quantification of the degree of realism is not practical since all submodels are to some degree based on simplification of the real world. However, qualitative comparisons can be made between the various submodels (or options) available in GEM and IMPACT and between the two codes themselves.

5.1.3 Generality

As with realism, the precise quantification of the generality of the GEM and IMPACT models is not practical. However, the general areas of applicability can be tabulated.

The following section (5.2) contains a description of the field tests used for model validation. Estimates of model precision based on the field tests discussed above are presented in section 5.3. A summary of the model validation, precision, realism, and generality for both GEM and IMPACT is presented in section 5.4.

5.2 Field Data Description

Ideally, one would like sufficient field programs to provide data bases for all possible environments that occur in California. For example, field programs should be undertaken in coastal regions (both urban and rural) for stable, neutral, and unstable atmospheric conditions, and in inland valley and mountainous terrain over a similar range of atmospheric stabilities. Additionally, the air quality impact should be measured, both locally and regionally. In order to validate photochemical point source models, both primary and secondary pollutants must be measured upwind and downwind of the source, as well as measuring such parameters as insolation and relative humidity.

Unfortunately, the cost and complexity of executing a field study which provides the data needed as input to the model and provides sufficient data for comparison between model simulation and reality is such that few reference studies are available.

A summary of the bases considered for this study is shown in Table 5-1. The selection of the data bases used was based on the following criteria:

- The data base should be readily available in reduced form (i.e., the reduction of raw data would be beyond the scope of this study).
- The number and distribution of meteorological and pollutant measurements must be sufficient to allow accurate input data and model validation information.
- The data base should represent typical situations found in California.

After review of the candidate data bases and consultation with the project sponsors, the following three field studies were selected as meeting the criteria for an adequate data base: the NOAA program in Garfield, Utah which investigated the dispersion of an inert pollutant in complex terrain; a field program sponsored by the

Table 5-1. Summary of Candidate Model Validation Data Bases.

	PLUME RISE	COMPLEX TERRAIN WINDS	TRACER	PHOTOCHEMICALLY REACTIVE POLLUTANTS	COMMENTS
ARB PLUME STUDY	YES	NO	SF ₆	YES (NO HC)	COASTAL PLAIN
GARFIELD	YES	NO	SF ₆	NO	PLUME IMPACT IN COMPLEX TERRAIN
NAVAJO	YES	YES	SO ₂	NO	LIMITED METEOROLOGICAL DATA
DUGWAY	NO	YES	FLUORESCENT PARTICLES	NO	MOUNTAIN VALLEY
ORMOND BEACH	YES	NO	SF ₆	YES (THC)	COASTAL PLAIN 4-HOUR AVERAGE CONCENTRATIONS
SAVANNAH RIVER	NO	YES	SF ₆	NO	ROLLING TERRAIN RECIRCULATING FLOW
EPRI PLUME STUDY	NO	NO		YES (MINIMAL HC SAMPLES)	AIRCRAFT AND PIBAL DATA
MARYLAND PLUME STUDIES	YES	NO	SULFUR	YES (NO HC)	LIMITED DATA ROLLING TERRAIN
OAK RIDGE: EASTERN TENNESSEE TRAJECTORY EXPERIMENT					DATA NOT READILY AVAILABLE
VANDENBERG TRACER STUDY	NO	NO	YES	NO	DATA NOT READILY AVAILABLE
HUNTINGTON CANYON	NO	YES	SF ₆	NO	MOUNTAIN CANYON LIMITED METEOROLOGICAL DATA
EPA: CRSTER VERIFICATION DATA	YES	YES	SF ₆	YES (NO, NO ₂ ONLY)	ANNUAL AVERAGE ONLY
PORTLAND GENERAL ELECTRIC CO. WHITE SANDS	NO	YES	NO	NO	LIMITED DATA METEOROLOGICAL DATA ONLY

ARB to determine the impact of large power plants on the air quality in rural and urban areas; and the field program sponsored by Southern California Edison to determine the impact of a large power plant located at Ormond Beach in Ventura County.

Although these field programs represent a combined investment of millions of dollars, they provide only a fraction of the data needed to cover the full spectrum of possible environmental conditions. A summary of the validation data bases represented by these studies is shown in Table 5-2. The need for additional data is graphically illustrated in Table 5-3. This table is meant to be illustrative only; the relative importance of each element of the matrix must be determined by the agencies or organizations using the models.

Table 5-2. Summary of Model Validation Data Bases.

GARFIELD

- COMPLEX TERRAIN – RURAL
- UNSTABLE ATMOSPHERE
- INERT POLLUTANT (SF_6)
- HIGH RESOLUTION (12–16 EFFECTED RECEPTORS)
- LOCAL CONCENTRATION (< 5 KM)

MOSS LANDING

- FLAT TERRAIN – RURAL
- STABLE ATMOSPHERE – ELEVATED INVERSION
- INERT POLLUTANT (SF_6) PLUS SOME REACTIVE POLLUTANTS (NO_x , SO_x , O_3) NO HYDROCARBON DATA
- LOW RESOLUTION (4–5 EFFECTED RECEPTORS)
- LONG RANGE CONCENTRATION (10–40 KM)

ORMOND BEACH

- FLAT TERRAIN – LIGHT URBAN, RURAL
- UNSTABLE TO STABLE ATMOSPHERE WITH ELEVATED INVERSION
- INERT POLLUTANT (SF_6) PLUS REACTIVE POLLUTANTS
- HIGH RESOLUTION ~ 10 EFFECTED RECEPTORS
- INTERMEDIATE RANGE CONCENTRATION (5–20 KM)

ADDITIONAL DATA BASE NEEDS

- STABLE ATMOSPHERE – COMPLEX TERRAIN
- URBAN AREAS – INERT AND PHOTOCHEMICAL
- NON-COASTAL RURAL AND URBAN AREAS

Table 5-3. Validation Data Base Matrix.

<div> <div>LOCATION AND ATMOSPHERIC STABILITY</div> <div>POLLUTANT TYPE AND IMPACT REGION</div> </div>		COASTAL						INLAND								
		URBAN			RURAL			URBAN			RURAL TERRAIN					
											LEVEL-ROLLING			COMPLEX		
		STABLE	NEUTRAL	UNSTABLE	STABLE	NEUTRAL	UNSTABLE	STABLE	NEUTRAL	UNSTABLE	STABLE	NEUTRAL	UNSTABLE	STABLE	NEUTRAL	UNSTABLE
INERT	LOCAL < 5 KM															
	INTERMEDIATE 5 TO 20 KM															
	LONG RANGE 10 TO 40 KM															
PHOTO-CHEMICAL	LOCAL < 5 KM															
	INTERMEDIATE 5 TO 20 KM															
	LONG RANGE 10 TO 40 KM															

 Garfield Data Base

 Moss Landing Data Base

 Ormond Beach Data Base

5.2.1 The NOAA Garfield, Utah Field Program Description

This field program was conducted by the Air Resources Laboratory of the National Oceanographic and Atmospheric Administration (NOAA) in 1973 near Garfield, Utah (Start, 1974). A 122-m smelter stack was used for sulfur hexafluoride (SF_6) injection. The SF_6 was detected by a number of bag samplers (approximately 20 per test). The relationship of the smelter stack, sampler sites, and terrain is shown in Figure 5-3. Of the seven tests, the data sets from Tests 3 and 7 were selected as providing the maximum data for model validation.

Test 3 was conducted on 19 June 1973 under slightly unstable conditions (Pasquill stability class C). This test consisted of:

- SF_6 injection from 1649 to 1749 MST
- 17 ground-level integrated SF_6 samples
- 5 local surface sites with winds every half-hour
- One pibal sounding
- Helicopter sampling of 1/2 to 1-minute duration at each of 14 locations.

Test 7 was conducted on 27 June 1973 under unstable conditions (Pasquill stability class B). This test consisted of:

- SF_6 injection from 1438 to 1538 MST
- 12 ground-level integrated SF_6 samples
- 7 local surface sites with winds every half-hour
- One pibal sounding
- Helicopter sampling of 1/2 to 1-minute duration at each of 11 locations.

The grid used for both the Gaussian (GEMGAR) and grid model (IMPACT) validation had a cell size of one-third kilometer by one-third kilometer. Figure 5-4 illustrates the grid coordinates

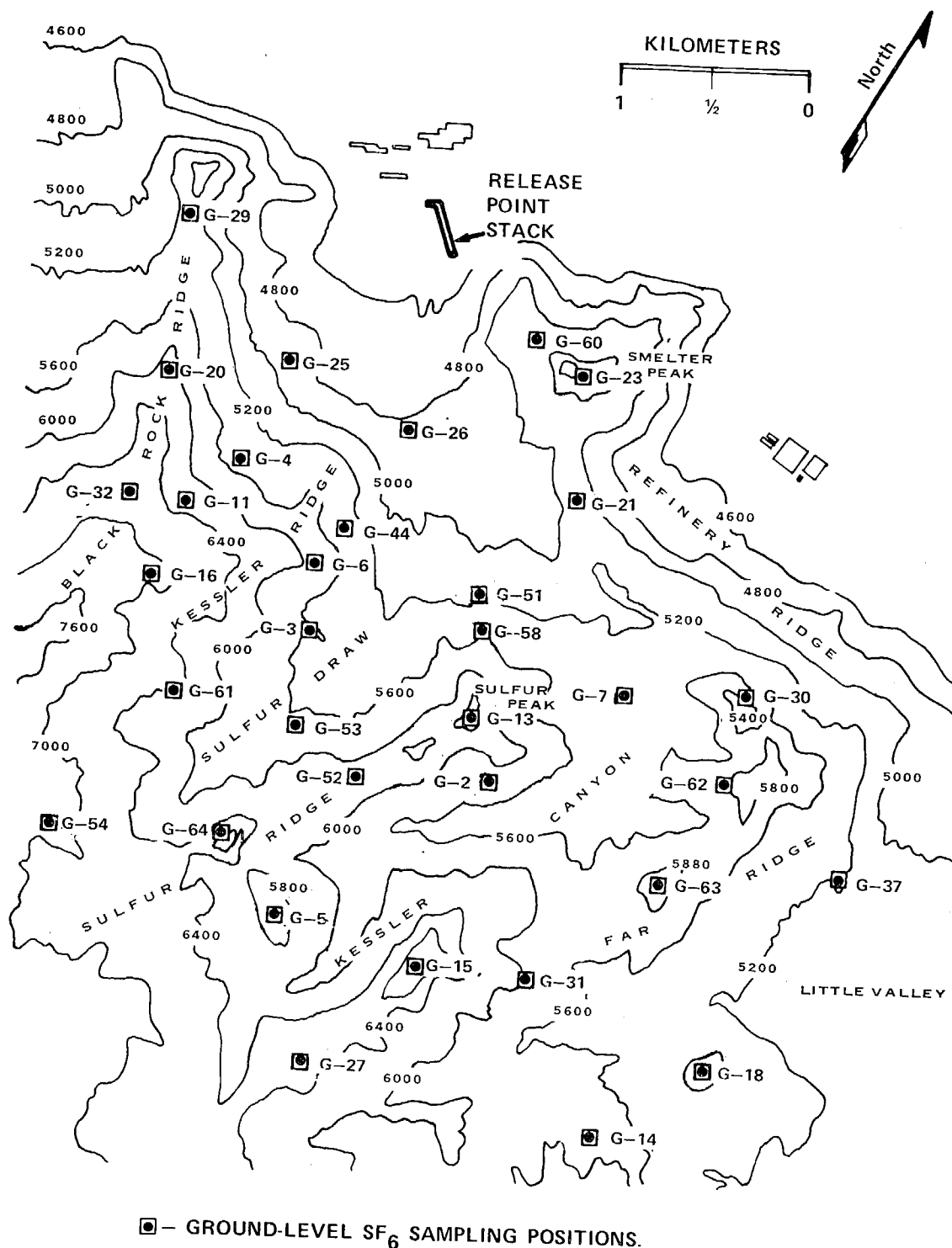


Figure 5-3. Garfield Test Site, Distribution of Ground Level Samplers and Terrain Heights (feet above mean sea level) for Tests 1 through 7.

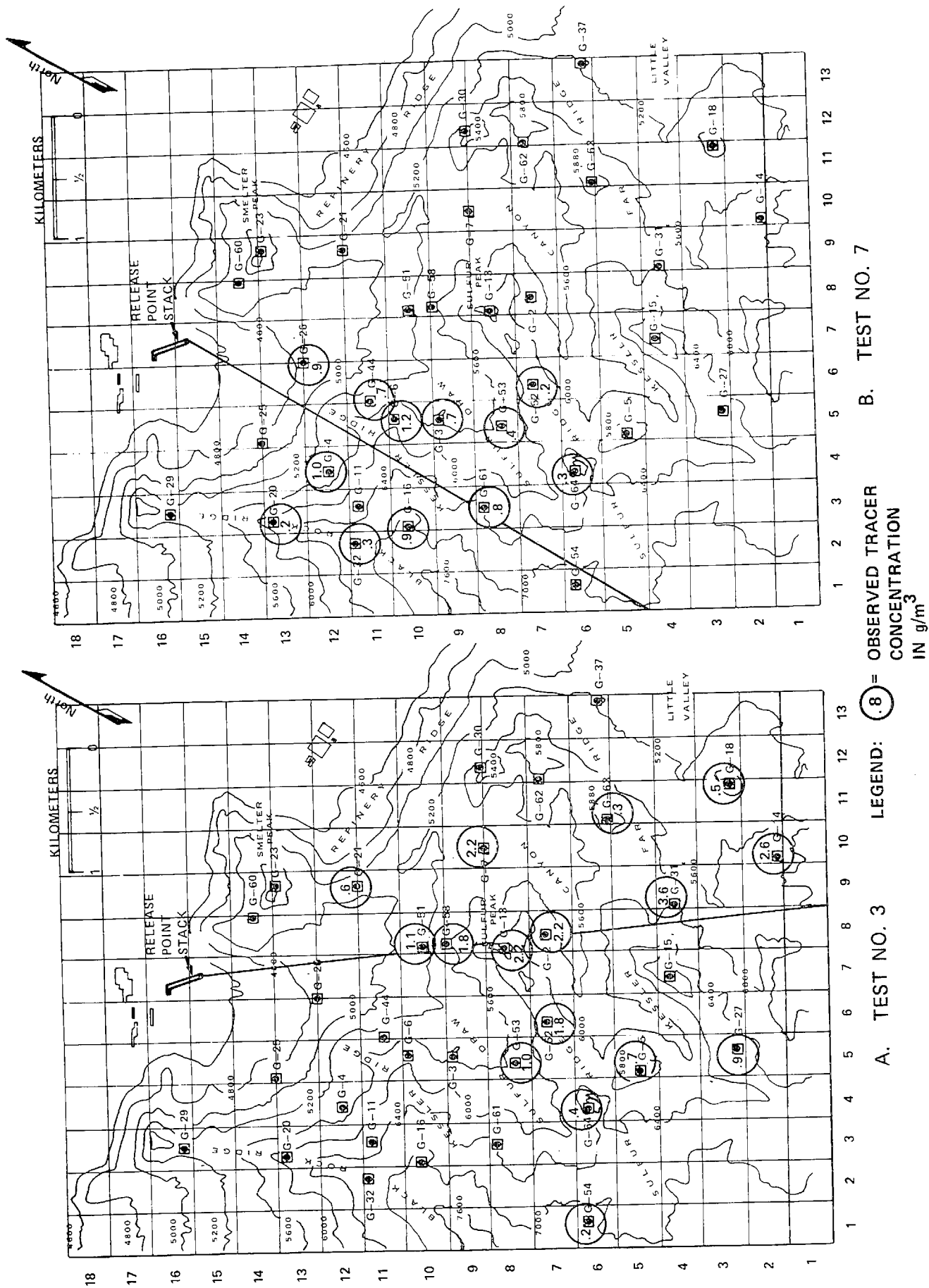


Figure 5-4. The Garfield Grid, Two Examples.

together with the approximate plume trajectory and the location and magnitude of the observed tracer concentrations ($\mu\text{g}/\text{m}^3$). The relationship between the plume trajectory and the topography of the test region is illustrated in Figure 5-5.

In terms of the density of the receptor network and number of meteorological sites, this field program is perhaps one of the best validation data bases for an inert pollutant. However, there are some serious deficiencies. Due to the lack of temperature sounding data, the Pasquill stability class procedure (modified by Turner, 1970) was used. This procedure, which defines atmospheric stability as a function of wind speed and insolation (solar angle, cloud cover, and cloud ceiling), is approximate and can differ by several stability classes from other more exact procedures (Chock, 1977). Another problem with the Garfield data base is the way in which surface concentrations were measured. Instead of a continuous emission of a plume tracer (SF_6), usually only one-hour releases were made. Because the sampler devices collected samples (i.e., clean air) both before and after the release period, it was necessary to normalize the measured calculations by:

$$C = C' \frac{\tau}{t}$$

where C = the concentration if there had been a continuous release

C' = the measured concentration

τ = the sampling duration

t = the trace release duration.

If steady state winds were assumed, then C would represent the correct concentrations for a continuous release. However, if the wind were not steady, the normalization procedure could result in considerable error. Inspection of the wind data taken during the tests indicates that the winds were not steady. However, the magnitude of the error caused by the renormalization is not known. Additionally, no indication was given as to the accuracy or instrument threshold of the SF_6 measurements.

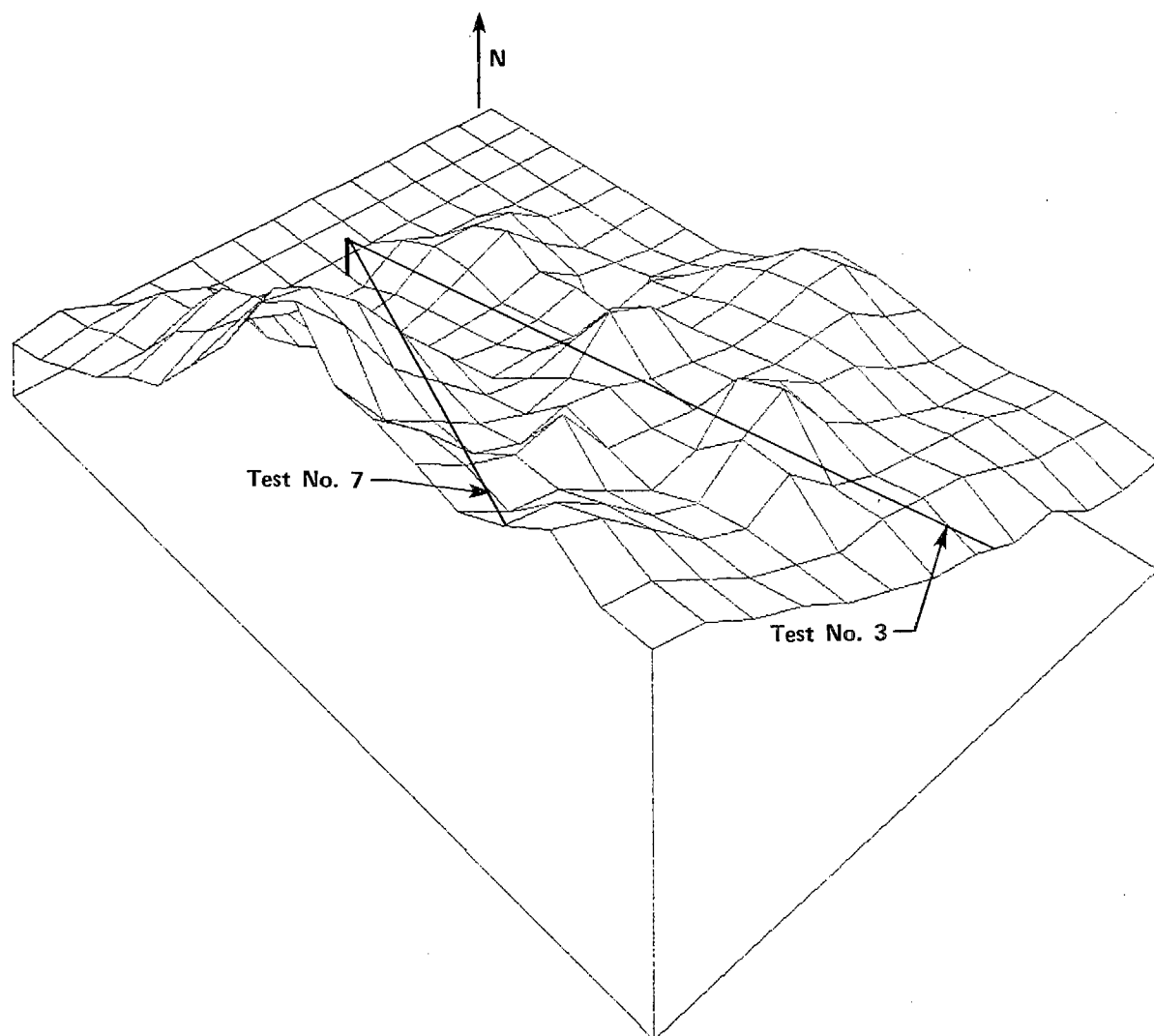


Figure 5-5. Representative Plume Trajectories for the Garfield Tests, Illustrated in Relation to the Area's Terrain.

5.2.2 The ARB Point Source Field Program Description

A multi-organizational program was initiated by the California Air Resources Board in 1974 to consider the effects of several fossil fuel power plants on air quality in California. The objective of the program was to examine the chemistry, dispersion, and transport of pollutants from these plants. Operational variations consisting of the use of oil vs. gas and differences in the background pollutant environment were incorporated into the program design. A key factor in assuring proper interpretation of the pollutant measurements was the release of a tracer gas, SF_6 , from each plant.

Areas of responsibility in the multi-organizational program included the following:

- SF_6 release, sampling, and analysis - Caltech (CIT), (Drivas, 1975)
- Ground observations of SO_2 and sulfates - Rockwell Air Monitoring Center, (Richards, 1976)
- Sulfate analyses - Air and Industrial Hygiene Laboratory, (Appel, 1976)
- Correlation spectrometer measurements of SO_2 - Environmental Measurements, Inc. (EMI)
- Airborne sampling and meteorological measurements - Meteorology Research, Inc. (MRI), (Smith, 1975)

The program consisted of 9 days of sampling: 3 days each at the Moss Landing (Pacific Gas and Electric Co.), Haynes (Los Angeles Water and Power), and Los Alamitos (Southern California Edison Co.) plants. The Moss Landing plant is located on the coast north of Monterey, while the Haynes and Los Alamitos plants are located at Long Beach, California.

The detailed airborne plume measurements (horizontal and vertical traverses) performed by MRI included measurements of

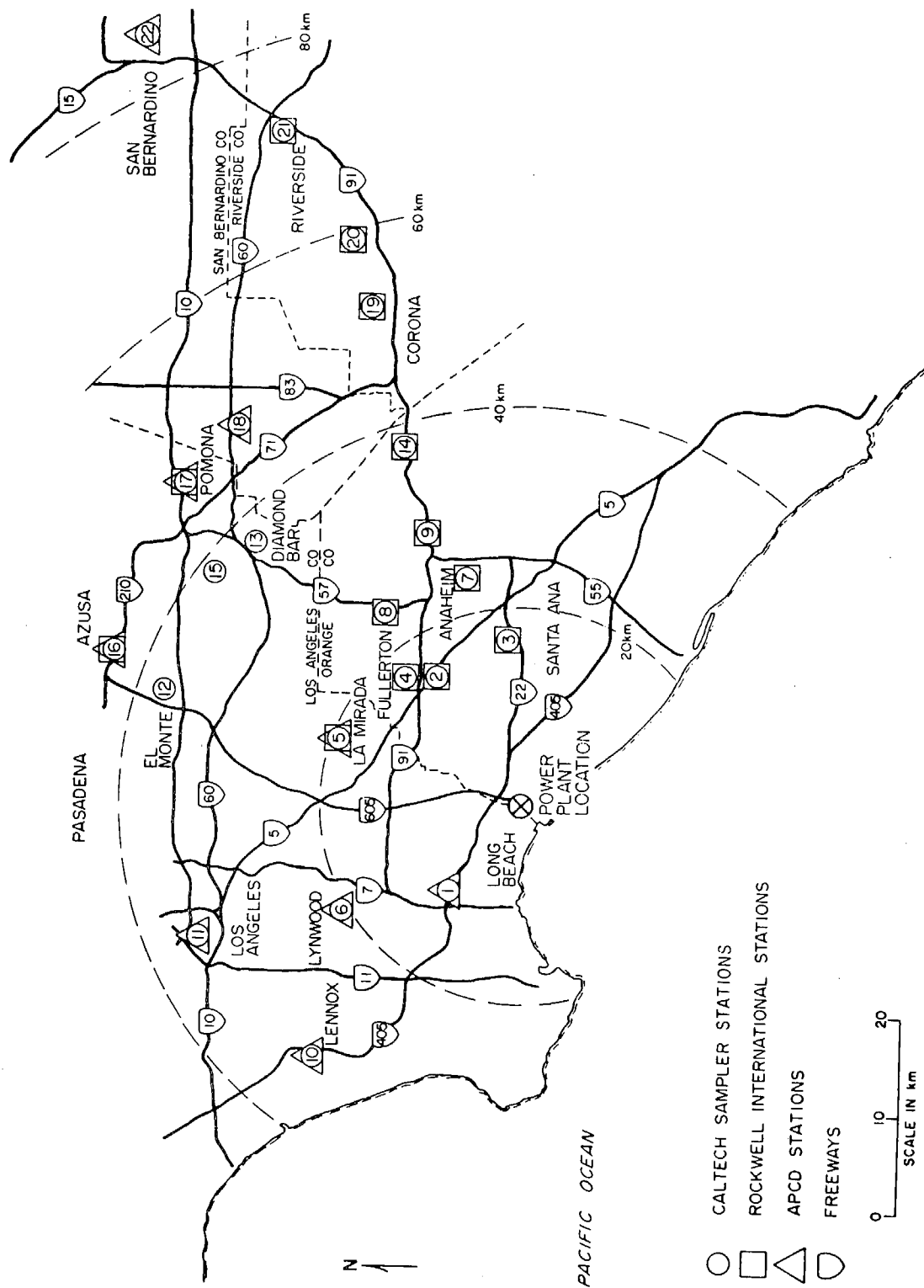
carbon monoxide (CO), ozone (O_3), light scattering coefficient (b_{scat}), turbulence, condensation nuclei (CN), temperature, humidity, oxides of nitrogen (NO_x), nitric oxide (NO), sulfur dioxide (SO_2), and traverse-averaged sulfur hexafluoride (SF_6) data. These measurements were useful in determining plume rise and are used for the preliminary assessment of the various plume rise submodels (section 3.1.3).

However, there were several deficiencies in the test program that reduced the usefulness of the program as a model validation data base. The data base could not be used for validating point source photochemical models since the lack of detailed hydrocarbon data (both plume and ambient concentrations) meant that a major input parameter in these models could not be accurately determined.

The extent of the surface to be sampled and the limited number of sampling stations in the Los Angeles area, involving 13 to 18 operating stations spread over approximately 2000 square miles, meant that only two to four stations showed significant plume impact during any one-hour test period. Figure 5-6 gives the locations of the stations at which pollutants emitted by the Long Beach power plants were sampled.

The locations of surface sampling stations for the Moss Landing test were less scattered, with the result that as many as five stations showed significant plume impact for some wind directions. A serious concern in the use of tracer data taken in this program was the accuracy of measurements. On page 6 of their Final Report, CIT states: "Consequently, the data points tabulated in Appendices A-4, A-7 and A-8 are within at least $\pm 30\%$ of the true values, with most of the data accurate to $\pm 15\%$." (Appendices A-4, A-7 and A-8 contain all the data collected during the study.)

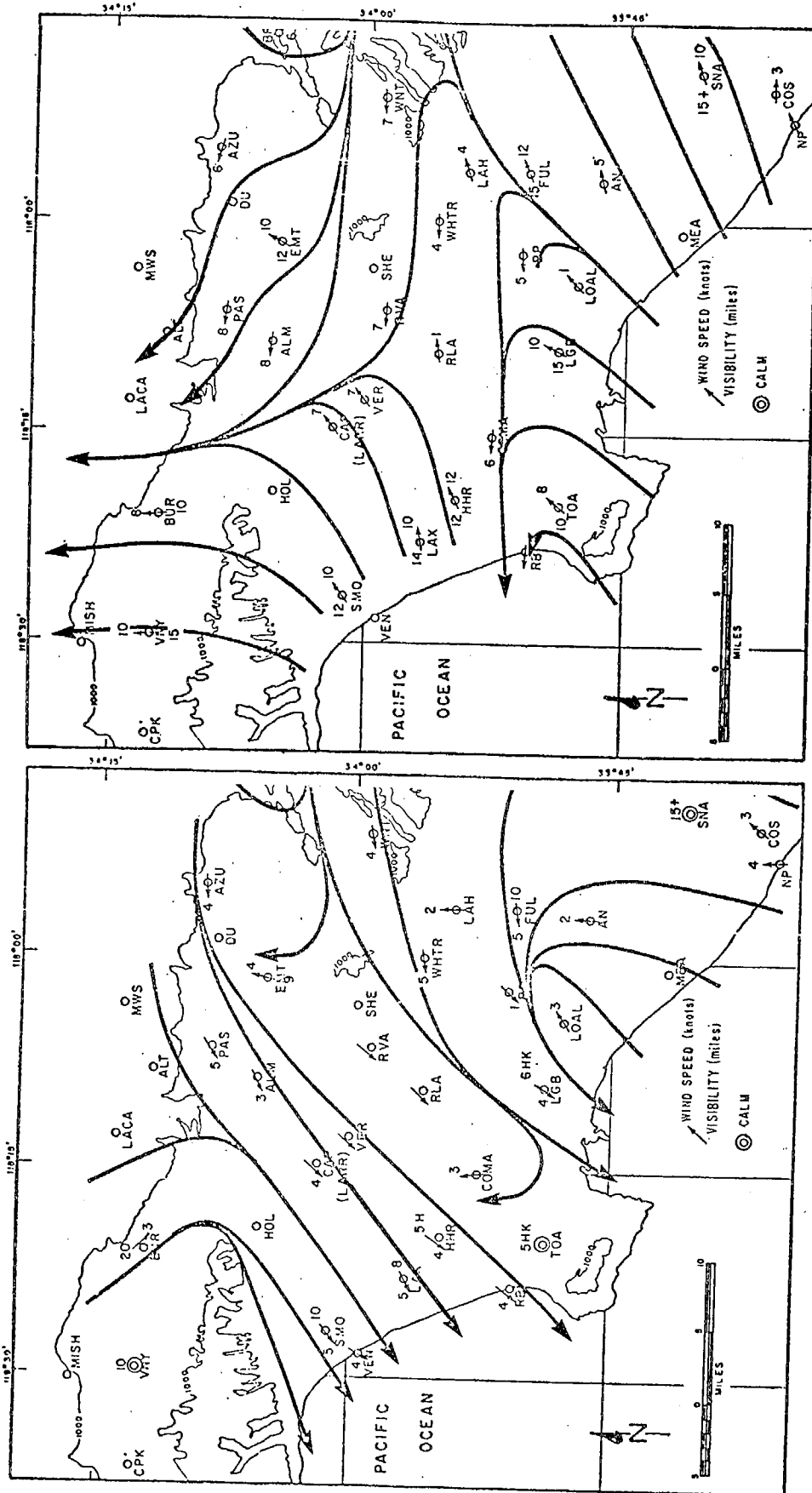
Investigations of the surface SF_6 measurements also revealed significant ground level concentrations of SF_6 before the SF_6 release could have reached the receptor location. These concentrations were believed to be due to local sources of SF_6 , possibly from high



voltage circuit breakers. The anomalous values in the Los Angeles region varied from 10 ppt to over 40 ppt, while the Moss Landing data showed anomalous values ranging from about 2 to 15 ppt.

An extensive number of surface meteorological locations were combined with pibal and aircraft upper air observations in the Los Angeles area by MRI (Figure 5-7) to provide a detailed description of the regional meteorology during the field test period. However, the coverage was less extensive for the Moss Landing program and only minimal data were available. In spite of some reservations about the precision of the Los Angeles wind data, the data collected on 30 October 1974 in support of the field program were used to evaluate the wind field submodel of the IMPACT code. After careful consideration of both the available tracer and meteorological data and after reviewing this data with field program personnel (Shair, 1976), it was decided that a three-hour average concentration (1400 to 1700 hours, PST) taken on 11 September 1974 (Moss Landing Test 2) would provide the best data for model validation. A summary of meteorological data and plume centerline locations for the Moss Landing tests are shown in Figure 5-8. As noted by the project principals (Drivas, 1975), the absence of significant plume impact during Test 1 was due to the trapping of the plume in an elevated inversion. Although not directly supported by aerial data, it is probable that (for Tests 2 and 3) the plume was trapped below the inversion, thus producing significant surface concentrations.

The location of the air samplers for Test 2 is shown in Figure 5-9 with an overlay of test grid used by GEMGAR and IMPACT validation simulations. A detailed breakdown of the actual data recorded during Test 2 is shown in Table 5-4. The tracer release period is noted at the bottom of the table and the dashed lines indicate the estimated arrival time of the initial tracer concentrations at each station.



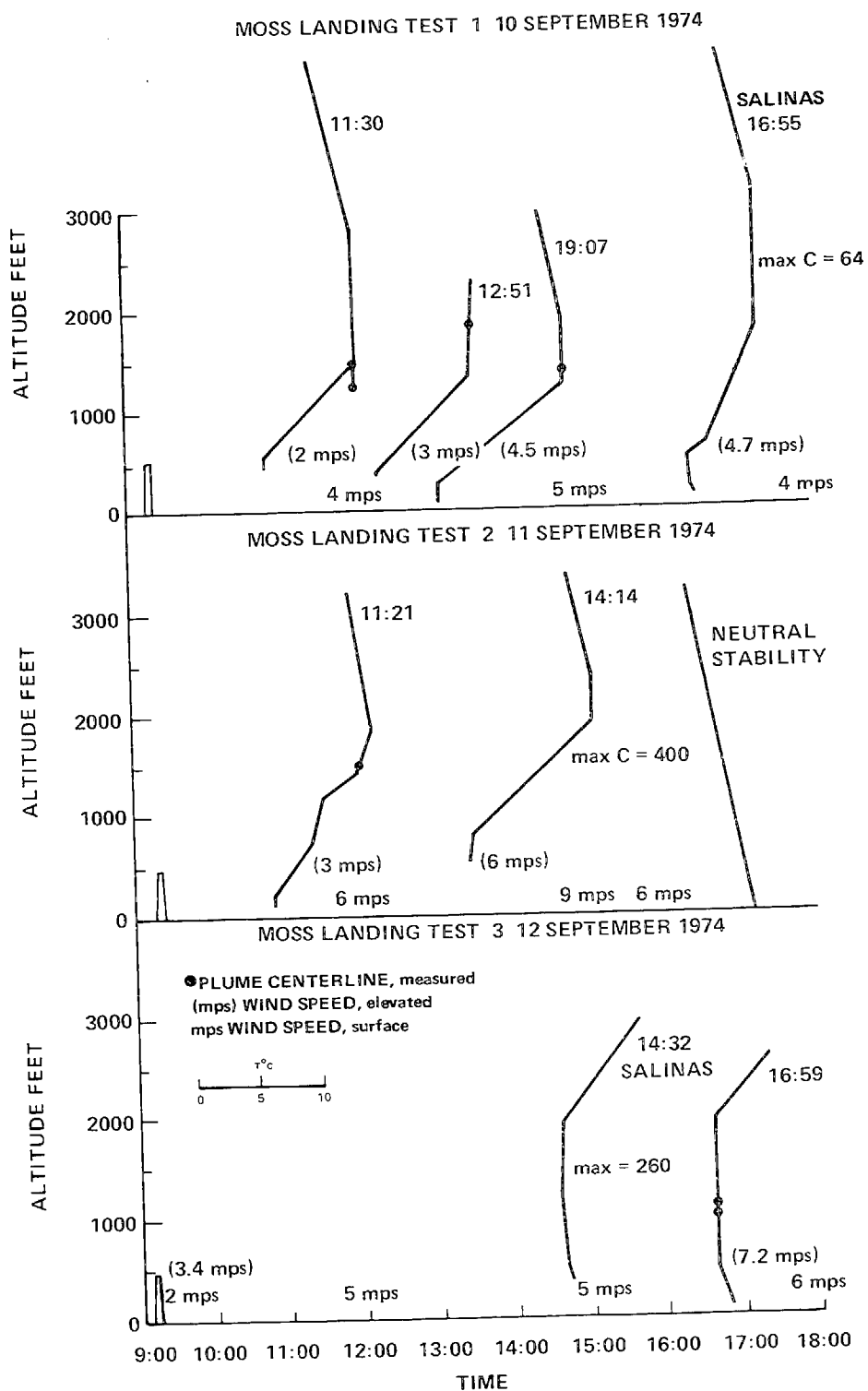


Figure 5-8. Summary of Meteorological Data Taken at Moss Landing Test Site.

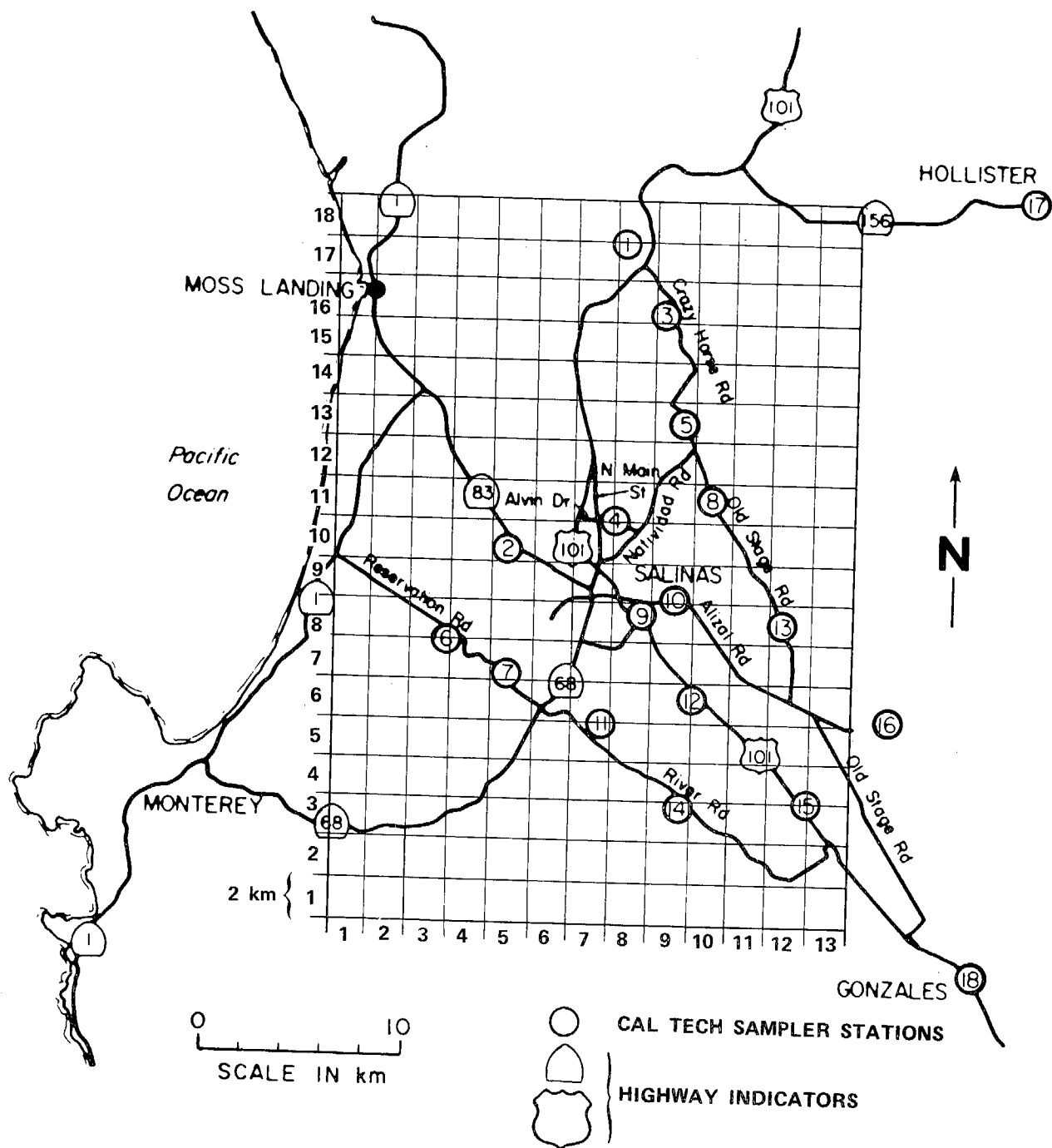


Figure 5-9. Location of Air Samplers and the Test Grid for the Moss Landing Field Program.

Table 5-4. One-Hour Averaged SF₆ CIT Tracer Data (ppt)
for Moss Landing Test No. 2, 11 August 1974.

LOCATION NUMBER	DISTANCE IN KILOMETERS	TIME OF DAY - PACIFIC DAYLIGHT SAVINGS TIME															
		A.M.								P.M.							
		8-9	9-10	10-11	11-12	12-1	1-2	2-3	3-4	4-5	5-6	6-7	7-8	RELEASE PERIOD			
1	12.7	0.0	1.7	3.2	3.9	0.0	0.0	0.0	0.0	0.0	0.0	0.0	0.0				
2	13.1	3.4	1.9	1.8	0.0	4.8	1.2	0.0	0.0	1.5	0.0	0.0	0.0				
3	14.7	0.0	2.1	7.7	2.2	3.9	0.0	0.0	0.0	0.0	0.0	0.0	0.0				
4	16.0	5.4	1.1	51.0	3.0	66.0	100.0	420.0	290.0	160.0	10.0	0.0	2.2				
5	16.4	0.0	2.8	3.2	6.6	0.0	0.0	0.0	1.6	1.4	20.0	0.0	0.0				
6	16.9	0.0	0.0	3.1	0.0	2.1	3.0	0.0	0.0	0.0	0.0	0.0	0.0				
7	19.3	4.4	0.0	0.0	4.9	0.0	2.3	0.0	3.0	0.0	0.0	0.0	0.0				
8	20.4	2.8	0.0	3.6	3.8	7.9	1.8	1.3	1.4	1.4	63.0	2.0	0.0				
9	21.1	5.9	5.4	16.5	5.2	10.5	363.0	246.0	338.0	187.0	14.0	0.0	n.d.				
10	23.3	4.1	0.0	0.0	0.0	7.8	5.0	63.0	180.0	280.0	130.0	n.d.	96.0				
11	25.2	0.0	0.0	0.0	0.0	1.9	2.5	0.0	0.0	0.0	0.0	0.0	0.0				
12	25.6	4.9	1.0	8.7	3.3	2.1	260.0	230.0	300.0	160.0	41.0	1.7	3.5				
15	32.3	0.0	0.0	5.5	10.0	12.0	170.0	260.0	n.d.	150.0	110.0	1.2	0.0				
17	33.3	1.8	8.1	9.3	12.0	6.5	2.5	1.4	0.0	0.0	0.0	0.0	0.0				
18	43.7	3.6	2.4	5.7	9.1	5.1	42.0	170.0	40.0	76.0	150.0	6.6	1.7				

5.2.3 The SCE Ormond Beach Field Program Description

This field program was conducted in 1973 to determine the photochemical impact of the Southern California Edison Ormond Beach generating station. The data collected consisted of:

- Pollutants monitored on a network of 25 ground stations which recorded 4-hour averages of NO_2 , NO_x and SO_2 by bubbler and of CO , THC and SF_6 tracer by bagged sample.
- Ground level winds at eleven sites, up to three pibal soundings per hour, up to three aircraft temperature soundings per hour, and up to two Rawindsondes per day.
- Continuous pollutant monitoring at six Ventura County Air Pollution Control District (VAPCD) stations.
- Miscellaneous data including
 - NO , NO_2 and SO_2 overburden
 - Mobile, short-term SF_6 samples, both aerial and ground level.

The relationship of these monitoring sites, the generating station, and terrain is shown in Figure 5-10. Data from the afternoon of 14 August 1973 were selected for the validation data base since previous analysis (Sklarew, 1975) showed significant air quality impact as well as consistency in the relationship among measured data (e.g., winds, SF_6 , and NO_x). The impact on the ground station network was evident for SF_6 , NO , and NO_2 , as shown in Figure 5-11. In addition, the plume swept past the Camarillo VAPCD station, providing an hourly record of NO , NO_2 and O_3 impacts.

Previous analysis of the data (Sklarew, 1975) has shown that the NO_x measured by the ground station network is proportional to the coincidentally measured SF_6 and the proportionality constants agree with the NO_x to SF_6 ratio observed in the stack. However, the VAPCD measurements of NO_x were consistently higher by approximately a factor of two. In addition, much of the meteorological

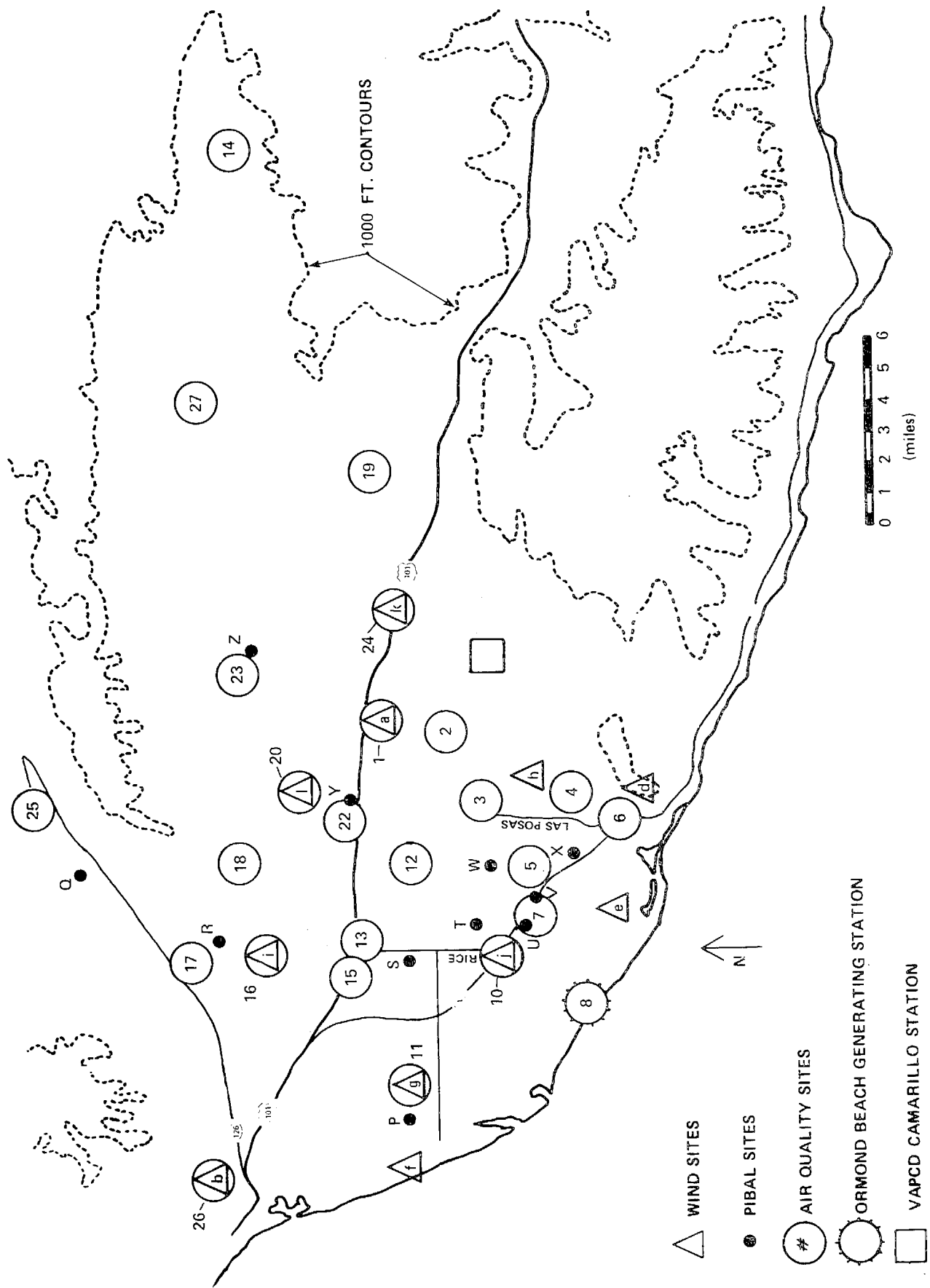


Figure 5-10. Wind, Pibal, and Air Quality Sites.

as well as pollutant data were obtained from cooperating agencies and differed in averaging time, time base (PST or PDT), and assigned time (0900 hour average could mean the data was taken from 0830 to 0930, from 0900 to 1000, or from 0800 to 0900). Thus, there is an uncertainty of ± 1 hour for the temporal location of much of the supporting meteorological data.

Additionally, although hydrocarbon concentrations were measured, no attempt was made to differentiate hydrocarbons by reactivity class. Therefore, an important input requirement, the ambient concentration of hydrocarbons by reactivity class, could not be satisfied. Finally, only limited estimates of the error range or uncertainty of the variables measured in this program were made, making it impossible to distinguish between errors due to the model, errors due to model input, and errors in observed surface measurements.

5.3 Estimates of Model Precision

5.3.1 GEM, Gaussian Evaluation Model

Because of the range of options available in the GEM, a large number of runs were required for each data set in order to assess the accuracy and sensitivity of the Gaussian model.

A summary of the input data required by GEM for each of the test cases is given in Table 5-5. The height above the surface for all meteorological observations was taken to be 10 meters. Additional data required by GEMGAR is the elevation of each grid cell and the height of each receptor above the surface. The terrain height data used for the Garfield test is tabulated in Table 5-6. The values given are in hundreds of feet and were converted internally by the code to meters. The height of terrain for the Moss Landing and Ormond Beach tests were taken to be sea level since most receptors were located on the level terrain adjacent to the coast. The height of each receptor above the surface was taken to be one meter for all tests (varying the receptor height from 0.1 to 10 meters resulted in little or no change in the observed concentrations).

Roughness data for each test were derived from considerations of land use (Myrup, 1976) or from reported data (Liu, 1976). Wind speed and direction data were obtained from the findings of the surface meteorological stations nearest the source (Garfield Tests 3 and 7, and Ormond Beach) or by an average of available data (Moss Landing). Stability data were derived either from the Pasquill procedure (Turner, 1970) or by the use of temperature sounding to determine the temperature gradient at the stack height, using the pre-established relationship in Table 5-7.

Table 5-5. Input Data used for Gaussian Evaluation Tests.

TEST	METEOROLOGICAL DATA							POINT SOURCE DATA						
	WIND SPEED (m/sec)	WIND DIREC- TION (deg.)	MIXING HEIGHT (meters)	SUR- FACE TEMP. (°C)	STABIL- ITY CLASS	REGION TYPE	SUR- FACE ROUGH- NESS (cm)	SOURCE STRENGTH (g/sec)	ELE- VATION (meters)	HEIGHT (meters)	TEMP. (°C)	EXIT VELOC- ITY (mps)	EXIT DIAM- ETER (meters)	SPECIFIED PLUME RISE PARA. $\mu\Delta h$ or Δh
GARFIELD #3	3.5	355	--	20	B/C	RURAL	100	2.194	1372	128	165	4	8.2	1036
GARFIELD #7	1.5	30	--	20	B/C	RURAL	100	3.222	1372	122	165	4	8.2	150
ORMOND BEACH	5.8	240	350	22	E	RURAL	3	2.6	0.	72	124	vol flow rate / π = 262.6		
	4.5	235	305	22	E									
	3.0	235	457	22	A to D									
	8.0	250	305	22	E									
MOSS LANDING #2	7.0	325	260	20	E	RURAL	5	9.76	1.	152	100	vol flow rate / π = 1305.5		
	7.0	325	260	20	E									
	7.0	325	260	20	E									

Table 5-6. Height of Terrain Matrix for Garfield Test Site,
Height in Hundreds of Feet.

18	46	47	45	45	45	45	45	45	45	45	45	45	45
17	47	48	48	46	45	45	45	45	45	45	45	45	45
16	49	50	52	50	46	45	45	45	45	45	45	45	45
15	51	51	53	50	46	45	45	48	46	46	45	45	45
14	54	56	58	50	47	46	47	50	50	49	46	45	45
13	56	59	60	52	49	47	48	50	52	48	45	45	45
12	61	63	61	55	53	49	49	49	50	47	46	45	45
11	66	69	65	60	56	51	50	50	51	40	47	46	45
10	73	72	68	62	57	52	52	51	51	52	50	48	47
9	76	71	64	60	56	55	56	57	54	53	54	52	50
8	71	65	62	59	57	58	62	60	55	55	56	56	53
7	71	67	62	60	61	60	58	57	56	56	57	57	53
6	70	67	65	66	60	59	58	58	57	57	57	54	52
5	69	66	65	62	59	60	64	61	58	57	54	52	51
4	71	70	67	63	61	64	66	60	57	55	53	52	51
3	74	72	68	64	62	64	60	58	57	56	55	53	52
2	71	70	67	64	62	60	60	59	58	56	54	53	52
1	71	70	67	65	62	60	58	57	55	55	52	51	51
	1	2	3	4	5	6	7	8	9	10	11	12	13

Table 5-7. Stability Class as Determined
by Temperature Stratification.

STABILITY CLASS	TEMPERATURE GRADIENT (°C/100m)
A	<-1.9
B	-1.9 to -1.7
C	-1.7 to -1.5
D	-1.5 to -0.5
E	-0.5 to 1.5
F	>1.5

U.S. Atomic Energy Commission Safety Guide 23, 1972

Since data on the wind direction fluctuation (σ_θ) and change in mean wind direction over the vertical extent of the plume ($\Delta\theta$) were not measured, these parameters which are used in the EPA 1976 and Pasquill dispersion sigma formulations were set to default values (i.e., σ_θ given in Table 3-1, $\Delta\theta = 0$). Data on stack parameters were taken from the field program reports and the specified plume rise parameter ($u\Delta h$) was adjusted to fit the observed apparent plume rise for each test case as measured by aerial sampling. The magnitude of the specified plume rise parameter for the Moss Landing test was set such that the final plume rise was just below the elevated inversion, since relevant plume sampling data were not available.

A summary of the Gaussian test runs is given in Tables 5-8 through 5-11. Each test is specified by the atmospheric stability class used along with the dispersion σ and plume rise options. In addition, the Garfield tests have a plume trajectory/complex terrain option specified, while the Moss Landing and Ormond Beach tests specify a limited mixing option. Furthermore, a tabulation of maximum predicted concentration, the downwind distance from the

Table 5-8. Garfield Test No. 3.

RUN NUMBER	STABILITY CLASS	DISPERSION σ OPTION	PLUME RISE OPTION	COMPLEX TERRAIN OPTION	MAX. CONC. $\mu\text{g}/\text{m}^3$	DOWNWIND DISTANCE TO MAX. CONC.	PLUME WIDTH ($\frac{1}{2}$ PEAK) AT MAX. CONC.	COMMENTS
			OBSERVED		3.6	4 km	>1 km	MAX. CONCENTRATIONS ON PLUME CENTERLINE, ON HIGH RIDGE
3.1	C	TURNER	BRIGGS '74 ($\Delta h = 170$ m)	NOAA	0.69	5 km	~1 km	MAX. CONC. AT END OF GRID, VALUES MUCH TOO LOW
3.2	C	EPA '76	BRIGGS '74	NOAA	1.33	~2 km	~ $\frac{1}{2}$ km	CONCENTRATIONS FALL OFF TOO FAST
3.3	C	PASQUILL	BRIGGS '74	NOAA	0.61	3.5 km	2 km	CONCENTRATIONS TOO LOW (FACTOR OF 4 TO 6)
3.4	C	TURNER	BRIGGS '74	ERT	2.92	2.5 km	<1 km	CONCENTRATIONS FALL OFF TOO FAST, CONC. AT OBSERVED PEAK ARE $\sim 2 \mu\text{g}/\text{m}^3$
3.5	C	EPA '76	BRIGGS '74	ERT	2.38	2 km	~1 km	CONCENTRATIONS PEAK TOO EARLY, CONC. AT OBS. PEAK ARE $1 \mu\text{g}/\text{m}^3$
3.6	C	PASQUILL	BRIGGS '74	ERT	2.00	2 km	~1 km	CONCENTRATIONS PEAK TOO EARLY, CONC. AT OBS. PEAK ARE $1.2 \mu\text{g}/\text{m}^3$
3.7	C	TURNER	BRIGGS '74	CRAMER	6.66	2.5 km	<1 km	CONCENTRATIONS GENERALLY TOO HIGH, CLOSE TO SOURCE, CONC. AT OBS. PEAK ARE $2 \mu\text{g}/\text{m}^3$
3.8	C	EPA '76	BRIGGS '74	CRAMER	3.13	1.5 km	~1 km	CONCENTRATIONS FALL OFF TOO FAST, CONC. AT OBS. PEAK ARE $1 \mu\text{g}/\text{m}^3$
3.9	C	PASQUILL	BRIGGS '74	CRAMER	3.27	1.5 km	1.5 km	CONC. FALL OFF TOO FAST, CONC. AT OBS. PEAK ARE $1.25 \mu\text{g}/\text{m}^3$
3.10	C	EPA '76	USER DATA ($\Delta h = 180$ m)	ERT	2.35	2 km	~1 km	CONCENTRATIONS PEAK TOO EARLY, CONC. AT OBS. PEAK ARE $1 \mu\text{g}/\text{m}^3$
3.11	C	PASQUILL	USER DATA ($\Delta h = 180$ m)	ERT	1.93	2 km	~1 km	CONCENTRATIONS PEAK TOO EARLY, CONC. AT OBS. PEAK ARE $1.2 \mu\text{g}/\text{m}^3$

Table 5-9. Garfield Test No. 7.

RUN NUMBER	STABILITY CLASS	DISPERSION σ OPTION	PLUME RISE OPTION	COMPLEX TERRAIN OPTION	MAX. CONC. $\mu\text{g}/\text{m}^3$	DOWNWIND DISTANCE TO MAX. CONC.	PLUME WIDTH ($\frac{1}{2}$ PEAK) AT MAX. CONC.	COMMENTS
			OBSERVED		1.2	~1.5 km	~1.75 km	MAX. CONCENTRATION OFF CENTERLINE ~100 METERS ON EDGE OF CANYON
7.1	C	TURNER	BRIGGS '74 ($\Delta h = 390$ m)	NOAA	0.08	~4 km	<1 km	VALUES MUCH TOO LOW (FACTOR OF 10 TO 100), MAX. VALUE AT EDGE OF GRID
7.2	C/B	EPA '76	BRIGGS '74	NOAA	1.78	~3 km	<1 km	VALUE AT 11 km TOO LOW BUT GENERALLY WITHIN 50% OF OBSERVED DATA
7.2B	B/A	EPA '76	BRIGGS '74 ($\Delta h = 430$ m)	NOAA	3.04	1 km	<1 km	MAX. OBSERVED ON PLUME CENTERLINE, GOOD AGREEMENT WITH OBSERVED DATA
7.3	C	PASQUILL	BRIGGS '74	NOAA	0.41	~4 km	<1 km	VALUES TOO LOW, CONCENTRATIONS AT OBSERVED PEAK ~.01 g/m^3
7.5	C/B	EPA '76	BRIGGS '74	ERT	6.14	~2 km	<1 km	VALUES TOO LARGE (FACTOR OF 2 TO 4)
7.5B	B/A	EPA '76	BRIGGS '74	ERT	3.86	~2 km	<1 km	VALUES TOO LARGE
7.5+5	C/B	EPA '76	BRIGGS '74	ERT	5.26	~2 km	~1 km	5° CHANGE IN WIND ANGLE, LESS THAN 20% CHANGE IN CONCENTRATIONS COMPARED TO RUN 7.5
7.6	C	PASQUILL	BRIGGS '74	ERT	2.66	3 km	~1 km	VALUE AT RECEPTOR LOCATION TOO LOW
7.6B	B	PASQUILL	BRIGGS '74	ERT	2.44	~2 km	1.5 km	MOST POINTS LOOK GOOD, SOME EXCEPTIONS
7.8	C/B	EPA '76	BRIGGS '74	CRAMER	10.33	1.5 km	~1 km	CENTERLINE VALUE MUCH TOO HIGH

Table 5-10. Moss Landing Test No. 2.

RUN NUMBER	STABILITY CLASS	DISPERSION σ OPTION	PLUME RISE OPTION	LIMITED MIXING OPTION	MAX. CONC. $\mu\text{g}/\text{m}^3$	DOWNWIND DISTANCE TO MAX. CONC.	PLUME WIDTH ($\frac{1}{2}$ PEAK) AT MAX. CONC.	COMMENTS
			OBSERVED		1.74	16 km	?	MAX. CONC. AT RECEPTOR CLOSEST TO SOURCE, APPARENT- LY ON PLUME CENTERLINE
2.0	E/D	EPA '76	BRIGGS '74 $\Delta h > 260$	TURNER	0.0			PLUME ABOVE BOTTOM OF INVERSION ($H = 260$), THEREFORE NO SURFACE CONCENTRATION
2.1	E/D	EPA '76	USER DATA $\Delta h = 260$	TURNER	3.75	20 km	< 1 km	PLUME MAX. AT 20 km, VALUE AT OBSERVED MAX. = $.71 \mu\text{g}/\text{m}^3$
2.2	E	PASQUILL	USER DATA	TURNER	0.22	> 30 km	~ 5 km	PLUME MAX. AT EDGE OF GRID, VALUES MUCH TOO LOW
2.3	E	TURNER	USER DATA	TURNER	1.73	> 30 km	~ 3 km	PLUME MAX. NEAR EDGE OF GRID, VALUES AT MOST RECEPTORS ARE MUCH TOO LOW

Table 5-11. Ormond Beach, 4-Hour Averages.

RUN NUMBER	STABILITY CLASS (EACH HOUR)	DISPERSION σ OPTION	PLUME RISE OPTION	LIMITED MIXING OPTION	MAX. CONC. $\mu\text{g}/\text{m}^3$	DOWNWIND DISTANCE TO MAX. CONC.	PLUME WIDTH ($\frac{1}{2}$ PEAK) AT MAX. CONC.	COMMENTS
					.36	5 km	~4 km ?	MAXIMUM OBSERVED AT CLOSEST RECEPTOR, HIGH VALUES (.31) OUT TO 12.5 km
1.1	EEDE	TURNER	BRIGGS '74 (130 - 190)	NONE	.08	25 km	~2 km	MAXIMUM AT EDGE OF GRID, VALUES MUCH TOO LOW
1.2	EEDE	TURNER	BRIGGS '74	TURNER	.08	25 km	~2 km	SAME AS FOR RUN NUMBER 1.1
1.4	EEDE	EPA '76	BRIGGS '74	TURNER	.31	25 km	~2 km	MAXIMUM AT EDGE OF GRID, CONC. AT 5 km ABOUT .06 $\mu\text{g}/\text{m}^3$
1.5	EEDE	PASQUILL	BRIGGS '74	TURNER	.33	25 km	~2 km	ROUGHLY THE SAME RESULTS AS FOR RUN NUMBER 1.4
1.5-A	EEAE	PASQUILL	BRIGGS '74	TURNER	.22	25 km	~4 km	VALUE AT 5 km IS 0.01 $\mu\text{g}/\text{m}^3$
1.3-A	EEAE	PASQUILL	BRIGGS '74	REFLECTION	.15	25 km	~4 km	SAME RESULTS AS IN 1.5-A, SLIGHTLY LOWER AT LONG DISTANCES
1.4-A	EEAE	EPA '76	BRIGGS '74	REFLECTION	.09	~20 km	~2 km	LARGE VALUES (0.08 AS CLOSE AS 12 km), VALUES GENERALLY TOO LOW
1.6-A	EEAE	EPA '76	BRIGGS '74	TURNER	.10	25 km	~1 km	SAME AS FOR RUN NUMBER 1.4-A
1.7-A	EEAE	EPA '76	TVA (30 - 240)	TURNER	.31	~20 km	~1 - 2 km	IF WINDS ROTATED 10, REASONABLY GOOD CORRELATION BETWEEN OBSERVED DATA AND MODEL

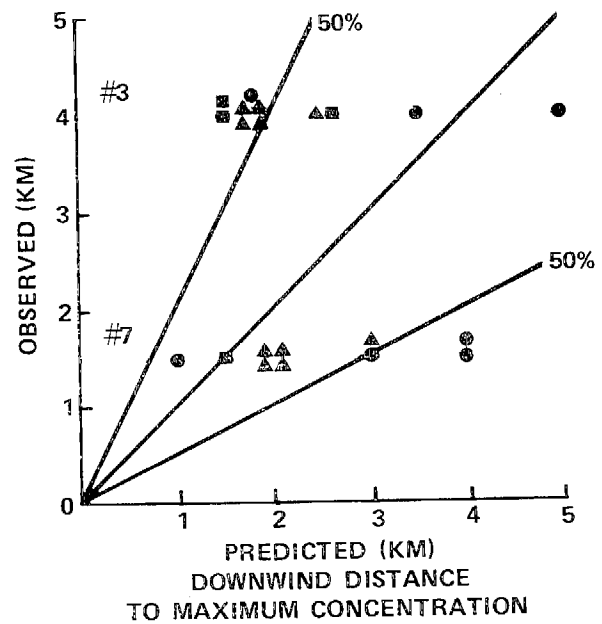
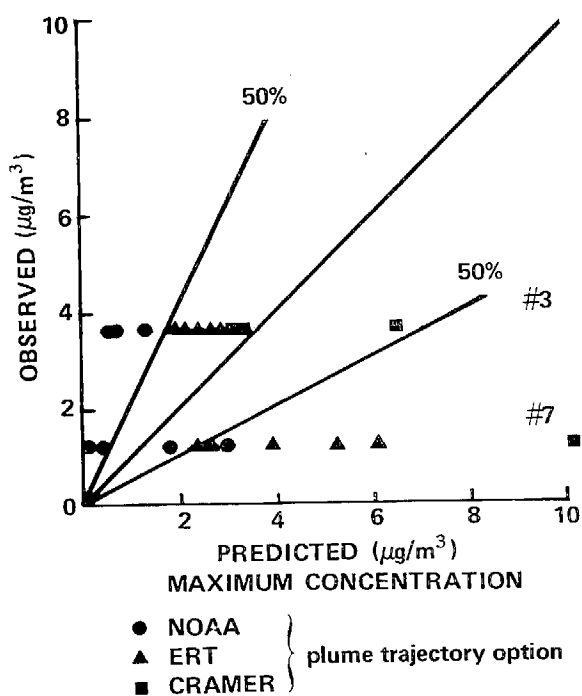
source to the predicted maximum concentration, and an approximation of the half-width of the plume at the concentration maximum are presented along with general comments on the surface concentration patterns. Scatter plots of the predicted vs. observed maximum concentration and distance to maximum concentration stratified by region (coastal vs. complex terrain) are presented in Figure 5-12.

Representative examples of the better validation runs are presented in Figures 5-13 to 5-17. The predicted values are shown in the computer print-out for each grid cell, while the location and values of the observed concentration, as well as the source location and plume trajectory, are shown as an overlay.

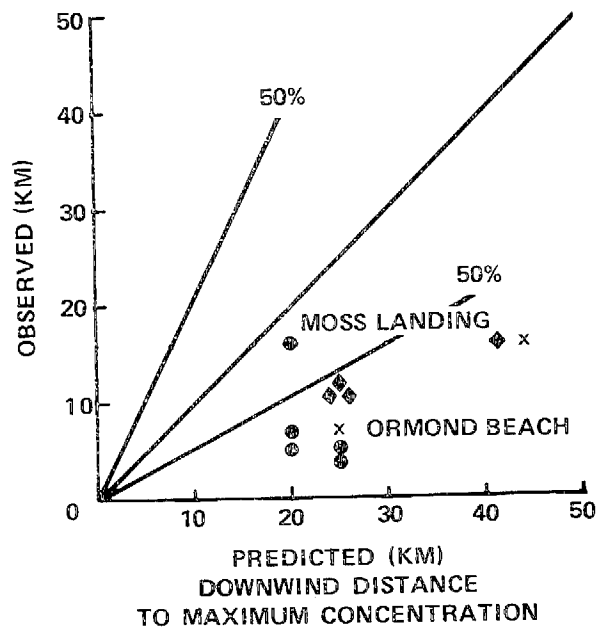
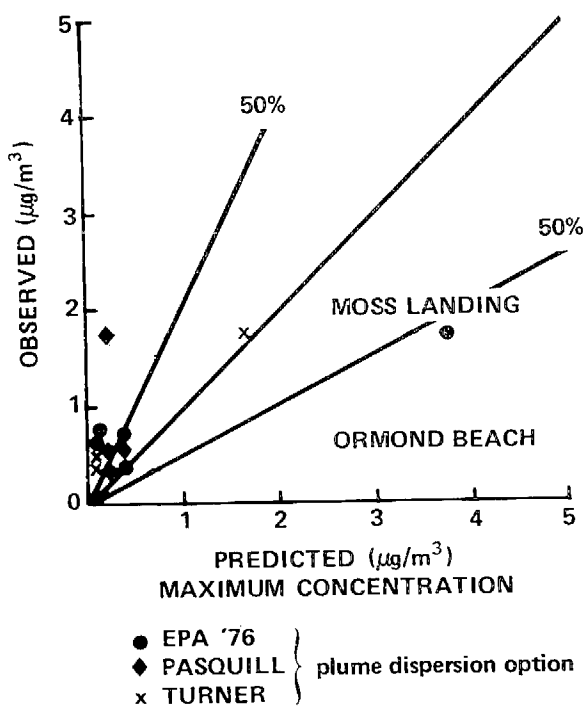
After careful review of the Gaussian evaluation tests, one reaches the inescapable conclusion that almost any desired result can be obtained, given the range of options for the dispersion parameters; plume trajectory in complex terrain, etc.; and the range of experimental uncertainty in the observed wind speed, wind direction, and atmospheric stability.

In general, it appears that the coastal regions are more difficult for the Gaussian models to handle than the complex terrain situations (at least for the limited test cases considered in this study). Among the factors contributing to this situation are:

- Unsteady shifting winds result in curved plume trajectories which cannot be treated by the straight-line steady-state Gaussian model. In complex terrain, the wind flow for slightly unstable atmospheric conditions results in an approximate potential flow and more-or-less straight trajectories.
- The large sources tested in the coastal regions impact a large surface area. Therefore, the Gaussian assumption of constant winds and atmospheric stability may not be valid.



A. COMPLEX TERRAIN: GARFIELD TEST NOS. 3 AND 7



B. COASTAL REGION: MOSS LANDING TEST NO. 2, ORMOND BEACH

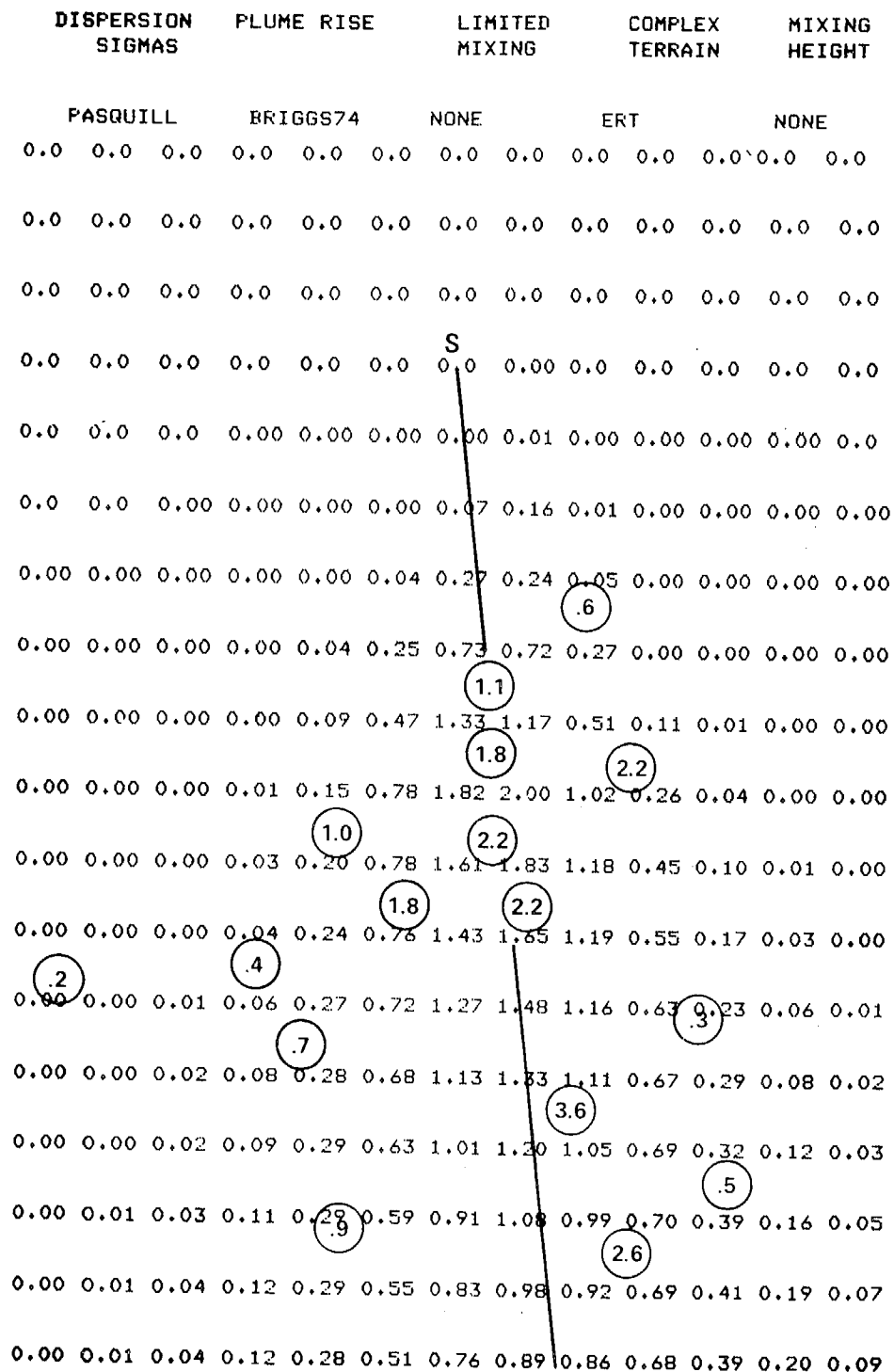
Figure 5-12. Summary of GEM Validation Tests.

GEM TEST : G A R F I E L D R U N 13X18 3.6

GAUSSIAN POINT SOURCE MODEL EVALUATION PROGRAM

GARFIELD TEST # 3

OPTIONS SELECTED:



LEGEND:

S SOURCE

PLUME CENTERLINE TRAJECTORY

(1.8) OBSERVED CONCENTRATION, $\mu\text{g}/\text{m}^3$

Scale

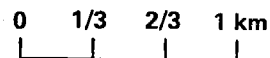


Figure 5-13. Representative GEM Validation Using Garfield Test No. 3 Data.

GEM TEST : G A R F I E L D R U N 13X18 7.2B

GAUSSIAN POINT SOURCE MODEL EVALUATION PROGRAM

GARFIELD TEST # 7

OPTIONS SELECTED:

DISPERSION SIGMAS			PLUME RISE			LIMITED MIXING			COMPLEX TERRAIN			MIXING HEIGHT		
EPA 1976			BRIGGS74			NONE			NOAA			NONE		
0.0	0.0	0.0	0.0	0.0	0.0	0.0	0.0	0.0	0.0	0.0	0.0	0.0	0.0	0.0
0.0	0.0	0.0	0.0	0.0	0.0	0.0	0.0	0.0	0.0	0.0	0.0	0.0	0.0	0.0
0.0	0.0	0.0	0.0	0.0	0.0	0.0	0.0	0.0	0.0	0.0	0.0	0.0	0.0	0.0
0.00	0.00	0.00	0.00	0.00	0.00	0.00	0.00	0.00	0.00	0.00	0.00	0.00	0.00	0.00
0.00	0.00	0.00	0.00	0.06	0.80	0.05	0.00	0.0	0.0	0.0	0.0	0.0	0.0	0.0
0.00	0.00	0.01	0.20	1.55	2.81	0.10	0.00	0.0	0.0	0.0	0.0	0.0	0.0	0.0
0.00	0.02	0.20	1.15	3.04	1.88	0.07	0.00	0.00	0.0	0.0	0.0	0.0	0.0	0.0
0.03	0.15	0.65	1.79	2.37	0.92	0.04	0.00	0.00	0.00	0.0	0.0	0.0	0.0	0.0
0.10	0.37	0.98	1.63	1.35	0.40	0.02	0.00	0.00	0.00	0.0	0.0	0.0	0.0	0.0
0.23	0.56	1.01	1.15	0.70	0.17	0.01	0.00	0.00	0.00	0.00	0.0	0.0	0.0	0.0
0.34	0.63	0.84	0.73	0.36	0.08	0.01	0.00	0.00	0.00	0.00	0.00	0.00	0.00	0.0
0.40	0.58	0.62	0.44	0.19	0.04	0.00	0.00	0.00	0.00	0.00	0.00	0.00	0.00	0.0
0.40	0.48	0.43	0.26	0.10	0.02	0.00	0.00	0.00	0.00	0.00	0.00	0.00	0.00	0.00
0.36	0.37	0.29	0.16	0.06	0.01	0.00	0.00	0.00	0.00	0.00	0.00	0.00	0.00	0.00
0.30	0.27	0.19	0.09	0.03	0.01	0.00	0.00	0.00	0.00	0.00	0.00	0.00	0.00	0.00
0.24	0.19	0.12	0.06	0.02	0.00	0.00	0.00	0.00	0.00	0.00	0.00	0.00	0.00	0.00
0.19	0.14	0.08	0.04	0.01	0.00	0.00	0.00	0.00	0.00	0.00	0.00	0.00	0.00	0.00
0.14	0.10	0.05	0.02	0.01	0.00	0.00	0.00	0.00	0.00	0.00	0.00	0.00	0.00	0.00

LEGEND:

S SOURCE

PLUME CENTERLINE TRAJECTORY

7 OBSERVED CONCENTRATION, $\mu\text{g}/\text{m}^3$

Scale
0 1/3 2/3 1 km

Figure 5-14. Representative GEM Validation Using Garfield Test No. 7 Data.

GAUSSIAN POINT SOURCE MODEL EVALUATION PROGRAM

OPTIONS SELECTED:

LEGEND:

S SOURCE

**TRAJECTORY BASED ON
OBSERVED SURFACE
CONCENTRATIONS**

**TRAJECTORY BASED ON
WIND DIRECTION AT
SOURCE**

1.07 OBSERVED
CONCENTRATIONS,
 $\mu\text{g}/\text{m}^3$

Scale
0 2 4 6 km

Figure 5-15. Representative GEM Validation Using Moss Landing No. 2 Data.

GEM TEST : ORMOND BEACH 8/14/73 18X18 1.4

GAUSSIAN POINT SOURCE MODEL EVALUATION PROGRAM

OPTIONS SELECTED:

DISPERSION SIGMAS	PLUME RISE	LIMITED MIXING	COMPLEX TERRAIN	MIXING HEIGHT
EPA 1976	BRIGGS74	TURNER	NONE	PLANAR

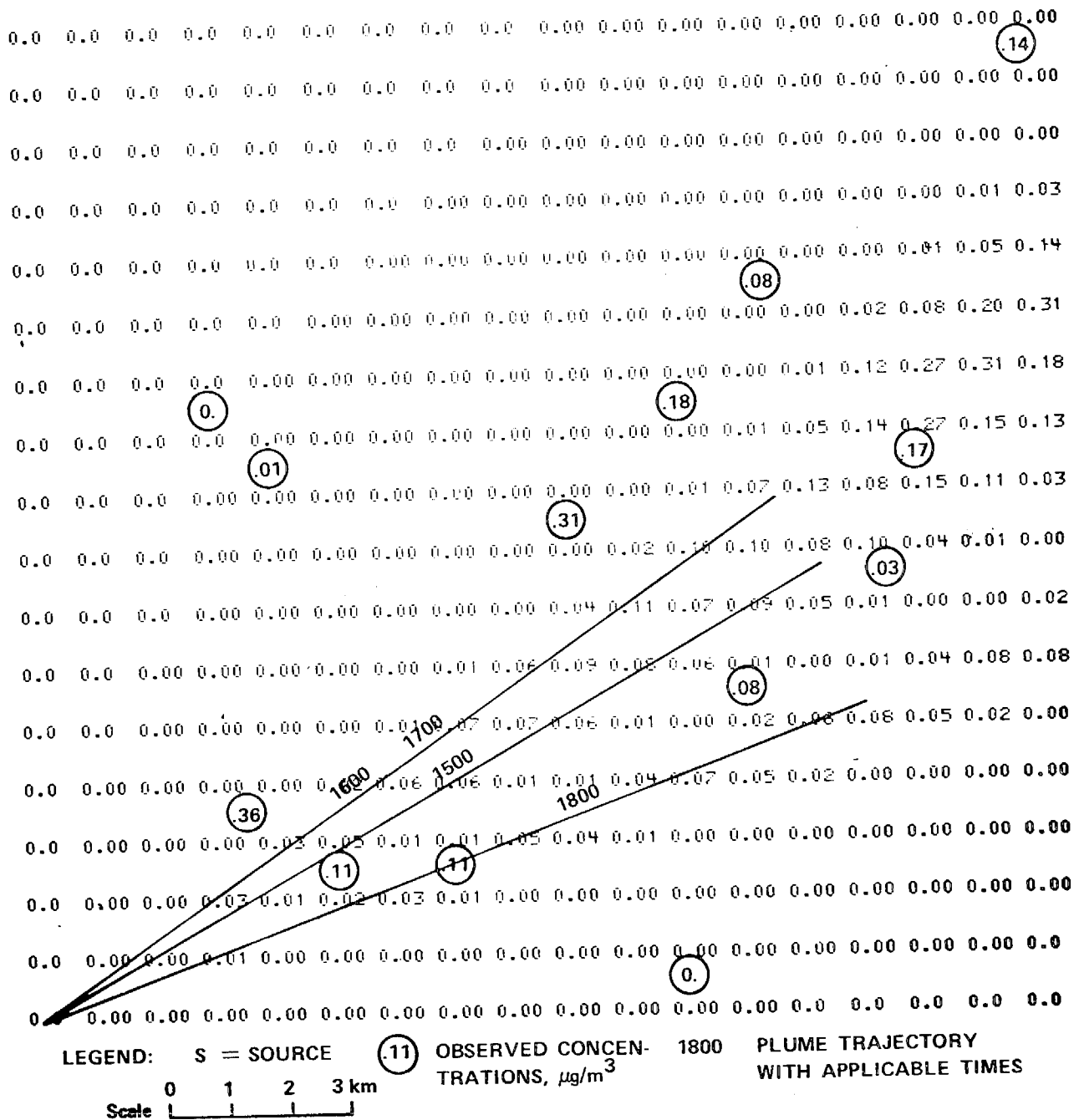
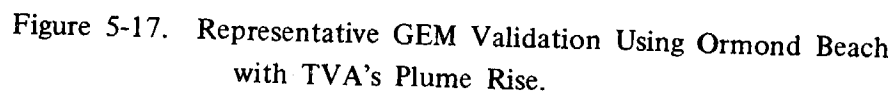


Figure 5-16. Representative GEM Validation Using Ormond Beach with Briggs' Plume Rise.

GAUSSIAN POINT SOURCE MODEL EVALUATION PROGRAM

MINING
HEIGHT

PLÄNE:



- Due to the lack of measured wind fluctuation data (σ_θ), parameterized values had to be used as input to the proposed EPA and Pasquill horizontal dispersion standard deviation (σ_y) formulations.

If the parameterized values for σ were more appropriate for complex terrain than coastal regions, the accuracy of predictions of surface concentrations in coastal locations would be degraded.

A rough estimate of Gaussian model precision (based on the test data available) would be that in complex terrain and unstable atmospheric conditions, the Gaussian models can predict the hour-average maximum surface concentration and the downwind distance to the maximum to within about a factor of 2. For coastal regions with elevated inversions, the Gaussian models underpredict the three to four-hour average maximum concentration and overpredict the downwind distance to the maximum. The meteorology affecting the dispersion of pollutants on the coast is apparently not parameterized correctly in the current Gaussian models.

5.3.2 IMPACT, Integrated Model for Plumes and Atmospheric in Complex Terrain

The validation effort for the more sophisticated finite difference grid model can be separated into the following three categories: the validation of the wind field submodel, the validation of the code for inert (or tracer) pollutants, and the validation of the code for reactive (photochemical) pollutants. In spite of some reservations as to the adequacy and sufficiency of the meteorological data collected for the purpose of validating the wind field submodel, it was felt that a validation effort should be undertaken because of the key importance of this submodel. Data collected for the Garfield tracer Test 3 and for the ARB point source tracer program in Los Angeles were selected as representative of complicated wind fields in complex terrain and coastal regions.

The approach followed for validation of the wind field models was to compare the measured (observed) data with the model predictions as the number of specified interior wind points were reduced. This procedure must be used with some caution since the measure of model accuracy is determined by the nature of the wind field (i.e., highly complex eddying flow or simple stream flow) and by which data measurements are eliminated. The results of the Garfield data are shown in Figure 5-18 where only a single data point was used to initialize the flow. The channeling effects of terrain accounted for the variation in the flow field at the other locations.

The scatter plots and data shown in Figure 5-18 indicate that the wind field submodel can accurately treat flow in complex terrain on a scale of 10 km for slightly unstable atmospheric conditions.

The results of the validation tests for the Los Angeles area are shown in Figures 5-19, 5-20, 5-21 and 5-22. The first two figures illustrate the flow field and streamlines as a function of the number of data points used. The locations of the data are indicated by the shaded cells. Comparing the streamlines generated by using all stations (26) with the streamlines drawn by the field program meteorologists (Figure 5-7), it is apparent that the flow fields generated by using all stations are realistic. The flow fields generated using half the available data stations are also reasonable with the exception of the flow around the Palos Verdes Peninsula for 0900 hours. Even with only 7 of the 26 sites, the major patterns of the flow field remain although some details are filtered out. Because a neutral atmospheric stability was used in the wind field simulation (based on available sounding data), the channeling effects of terrain on the surface wind field are not as pronounced as if stable atmospheric conditions had been simulated.

SITE LOCATION		WIND PARAMETERS			
		OBSERVED		CALCULATED	
I	J	SPEED	DIRECTION	SPEED	DIRECTION
6	17	2.2	20	2.9	349
9	13	3.8	4	3.6	349
11	8	3.6	355	3.6	355
7	8	4.9	355	4.8	353
5	5	2.5	0	3.6	0

NOTE: SHADING INDICATES USE OF OBSERVED WIND VALUES
AT LOCATION 11, 8

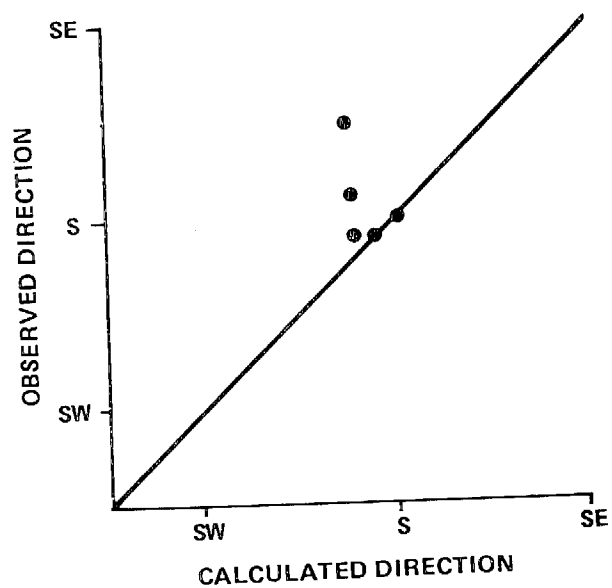
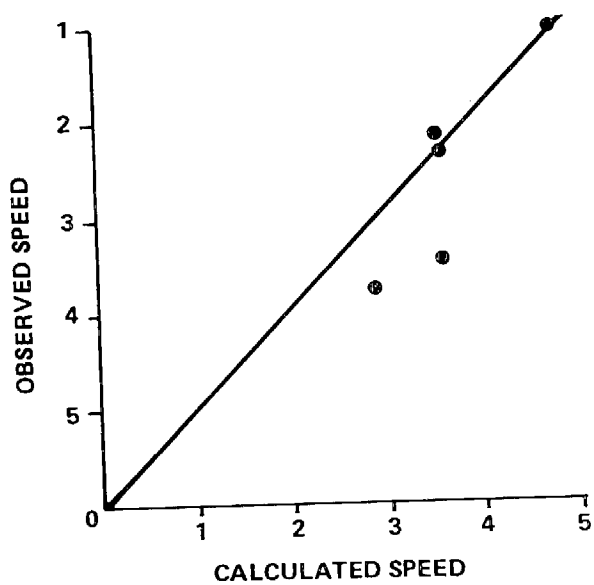
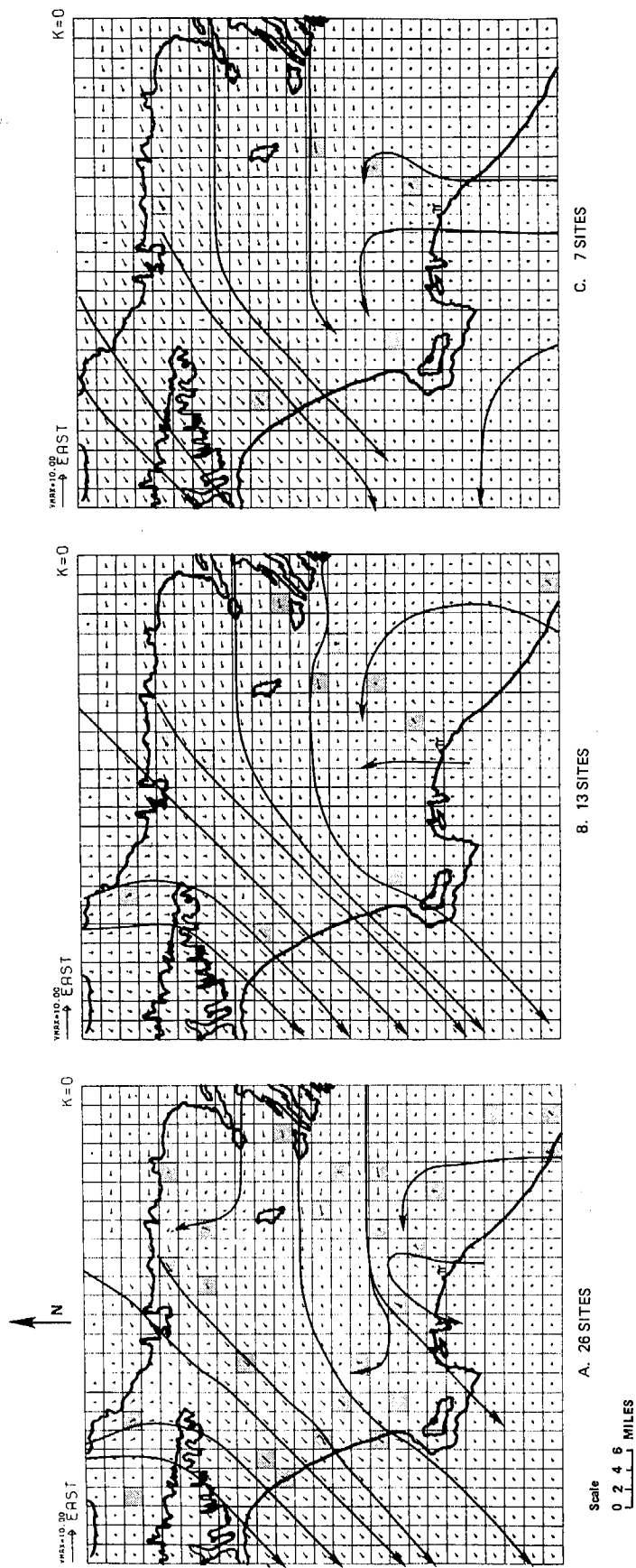


Figure 5-18. West Validation Test Using Garfield Test No. 3.



LEGEND: SURFACE METEOROLOGICAL DATA
 PIBAL SITE

Figure 5-19. WEST Validation Test Using Los Angeles Data (0900 Hours, 30 October 1974), Comparing Streamline Patterns as a Function of the Number of Meteorological Inputs.

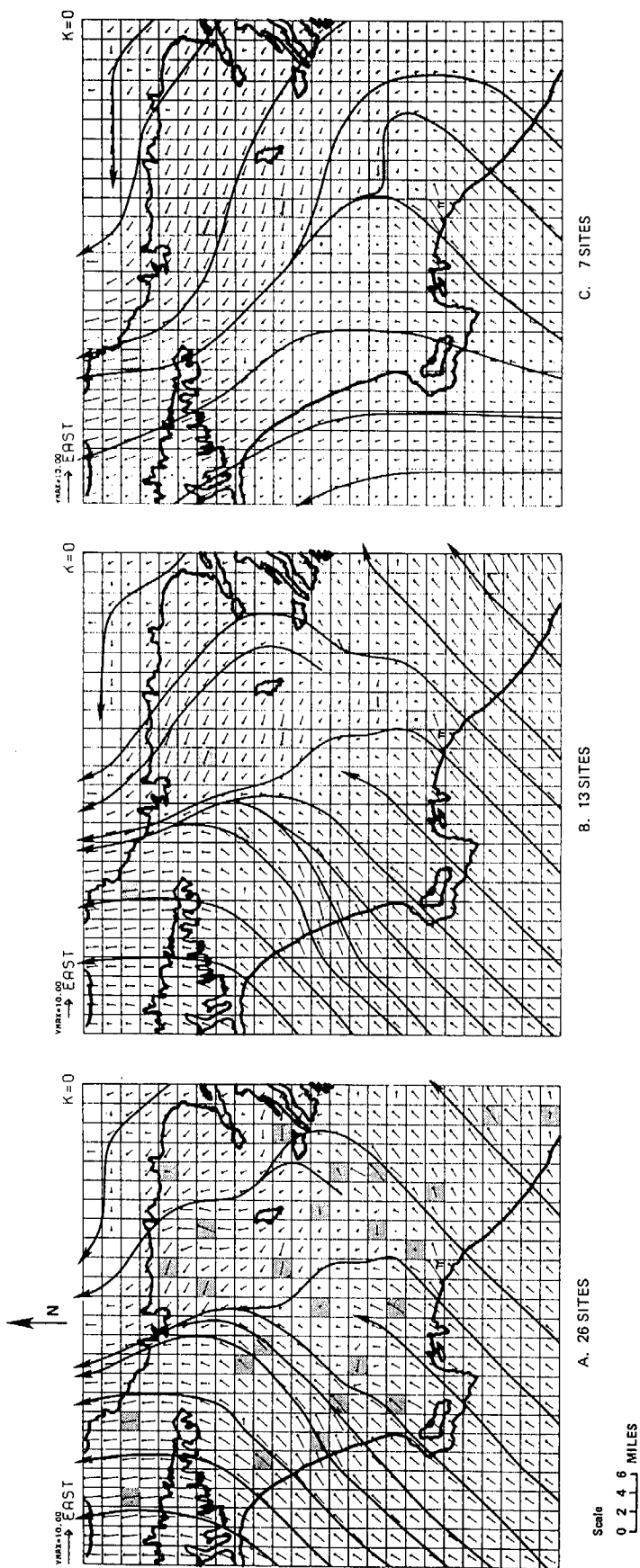
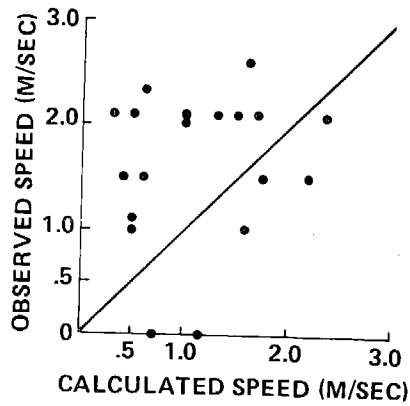
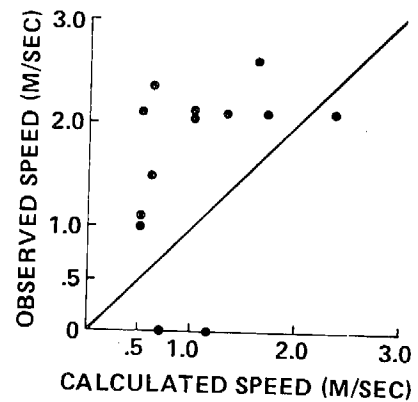


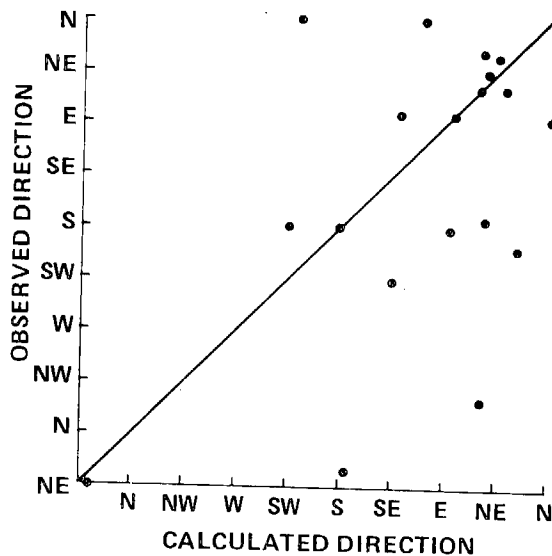
Figure 5-20. WEST Validation Test Using Los Angeles Data (1500 Hours, 30 October 1974), Comparing Streamline Patterns as a Function of the Number of Meteorological Inputs.



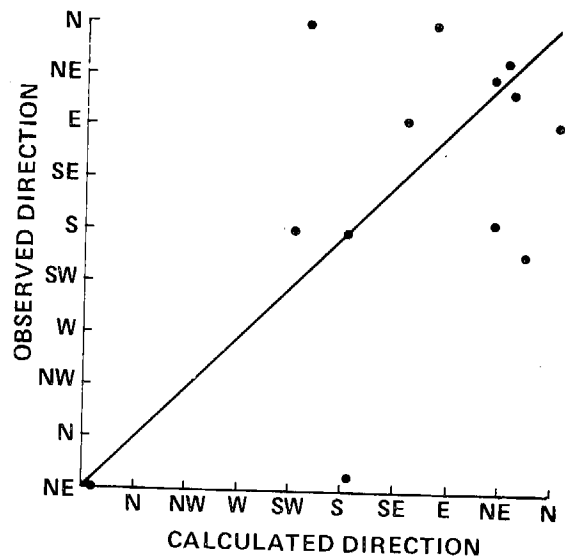
A. SPEED (CALCULATED BASED ON 7 SITES VS. OBSERVED AT THE OTHER 19 SITES).



B. SPEED (CALCULATED BASED ON 13 SITES VS. OBSERVED AT THE OTHER 13 SITES).

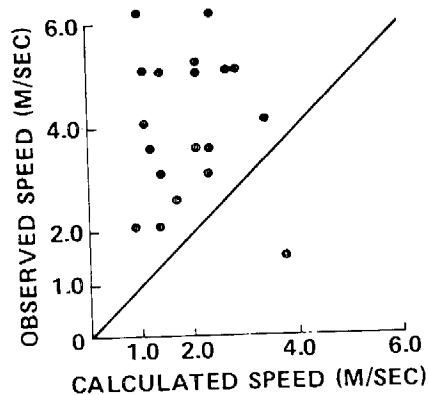


C. DIRECTION (CALCULATED BASED ON 7 SITES VS. OBSERVED AT THE OTHER 19 SITES).

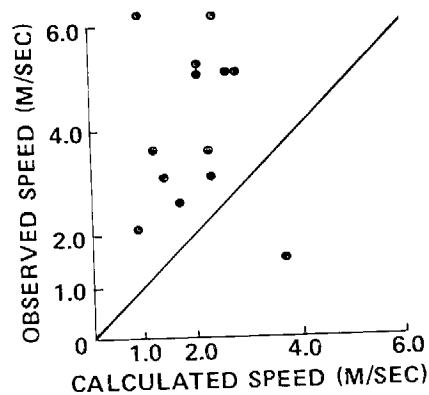


D. DIRECTION (CALCULATED BASED ON 13 SITES VS. OBSERVED AT THE OTHER 13 SITES).

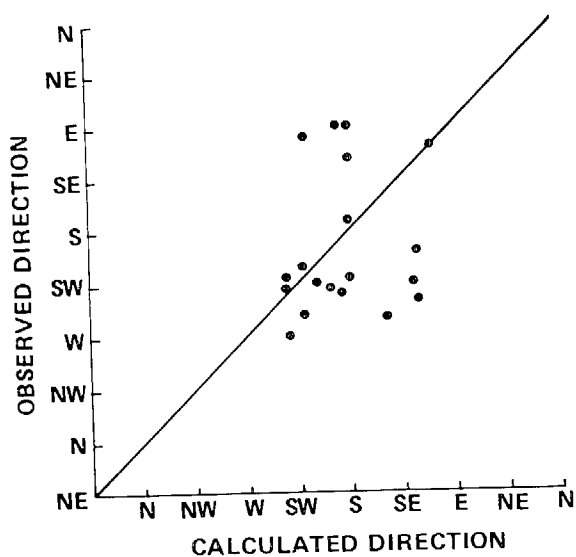
Figure 5-21. West Validation Test Using Los Angeles Data Taken at 0900 Hours on 30 October 1974, Comparing Calculated and Observed Data.



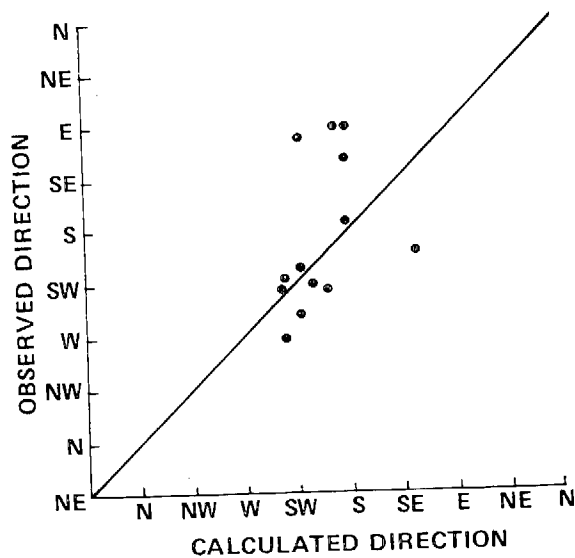
A. SPEED (CALCULATED BASED ON 7 SITES VS. OBSERVED AT THE OTHER 19 SITES).



B. SPEED (CALCULATED BASED ON 13 SITES VS. OBSERVED AT THE OTHER 13 SITES).



C. DIRECTION (CALCULATED BASED ON 7 SITES VS. OBSERVED AT THE OTHER 19 SITES).



D. DIRECTION (CALCULATED BASED ON 13 SITES VS. OBSERVED AT THE OTHER 13 SITES).

Figure 5-22. West Validation Test Using Los Angeles Data Taken at 1500 Hours on 30 October 1974, Comparing Calculated and Observed Data.

Inspection of the scatter plots (Figures 5-21, 5-22) reveals that WEST correctly predicts the correct wind direction at 50% of the sites to within one sector (22.5°) and over 70% of the sites to within two sectors (45°). Since the accuracy of the observed data (some taken at small airports) is probably plus or minus one or two sectors, the agreement of the WEST calculation is close to the maximum accuracy that can be expected. The agreement between calculated and observed wind speed is quite good for the simulation of 0900 hours, considering that the accuracy of the hour-average speed observations are probably between plus or minus one to two meters per second (2 to 4 mph). The simulation for 1500 hours, however, shows a considerable underprediction of maximum wind speeds. A comparison of the observed data, Figure 5-7, and the WEST calculations, Figure 5-20, indicates that the random selection of observed data used as input to the WEST model resulted in the higher wind speed locations not being used as input. This result illustrates the dependence of the objective analysis wind models (such as WEST or MATHEW) to the selection of representative input data conditions.

The approach followed for the validation of the IMPACT code for inert (i.e., tracer) pollutants was to use available data as input to the model and to compare the model results with the observed measurements of surface concentrations. Calculations using both the Myrup/Ranzieri and the DEPICT diffusivity models were run in order to compare the sensitivity of the model results to the selection of a particular diffusivity model. Since the plume rise options employed in IMPACT are identical with those used in GEM, IMPACT required no additional sensitivity tests for plume rise. Instead, the observed (or, in the case of Moss Landing, the inferred) plume rise was specified.

The results of the Garfield Test 3 are shown in Figure 5-23. The Garfield tests used a 13 by 18 by 10 grid with a .33 km by .33 km by 133.33 meter cell size and assumed an atmospheric stability class C with an unlimited mixing height. Under these

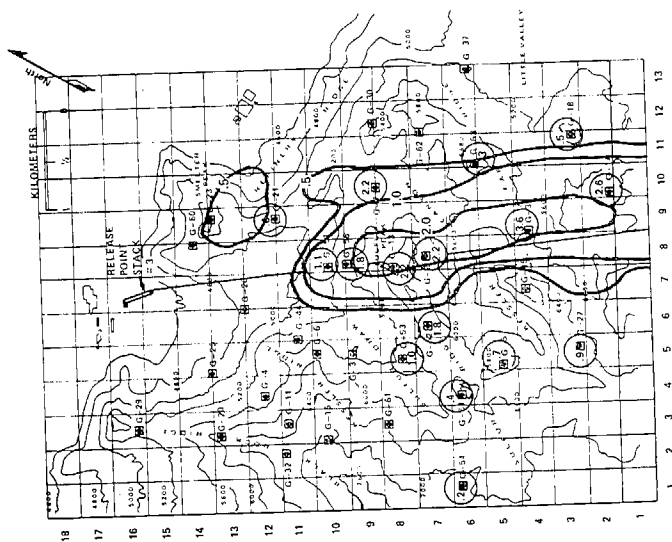


Figure 5-23. Results of IMPACT Validation Using Garfield Test 3 Data, Surface Concentrations SF₆ μg/m³.

conditions, the M/R diffusivity model calculates a vertical diffusion coefficient on the order of $200 \text{ m}^2/\text{sec.}$, while the DEPICT diffusivity model calculates a diffusion coefficient almost one order of magnitude lower (i.e., on the order of $20 \text{ m}^2/\text{sec.}$). This change in diffusivity results in about a 30% change in the predicted surface concentrations. Another run using an average vertical diffusivity of $2 \text{ m}^2/\text{sec.}$ resulted in surface concentrations most closely approximating the observed values. It is of interest to note that for this application the use of one-hour average winds did not provide sufficient information to correctly predict the surface concentrations to the left of the plume centerline. Inspection of the original wind data (one-half hour averages) indicates that the wind field was not steady state but varied significantly; it is reasonable to assume that the meandering of the wind field was responsible for the observed values not correctly predicted by the code using hour-averaged wind data.

The inclusion of pibal data taken during the tracer release and/or the reduction of the vertical cell size from 133.33 meters to 100 meters did not significantly affect the predicted surface concentrations.

The results of the Garfield Test 7 are shown in Figure 5-24. Notice the difference in predicted surface concentrations as a function of inclusion of the pibal data. Since the pibal data is instantaneous, there is a great deal of uncertainty as to how well a particular pibal represents the mean wind field aloft. In this particular case, the inclusion of the pibal data does increase the similarity between the observed and calculated surface concentrations. The use of the DEPICT diffusivity model instead of the M/R model results in an increase of predicted surface concentrations of about 30 to 40% due to the reduced vertical diffusivity. Since there was no independent field measurements of turbulent diffusivity, there is no way to select the correct diffusivity except by comparison of the simulation results to the observed data, an unreliable method for such a complex test.

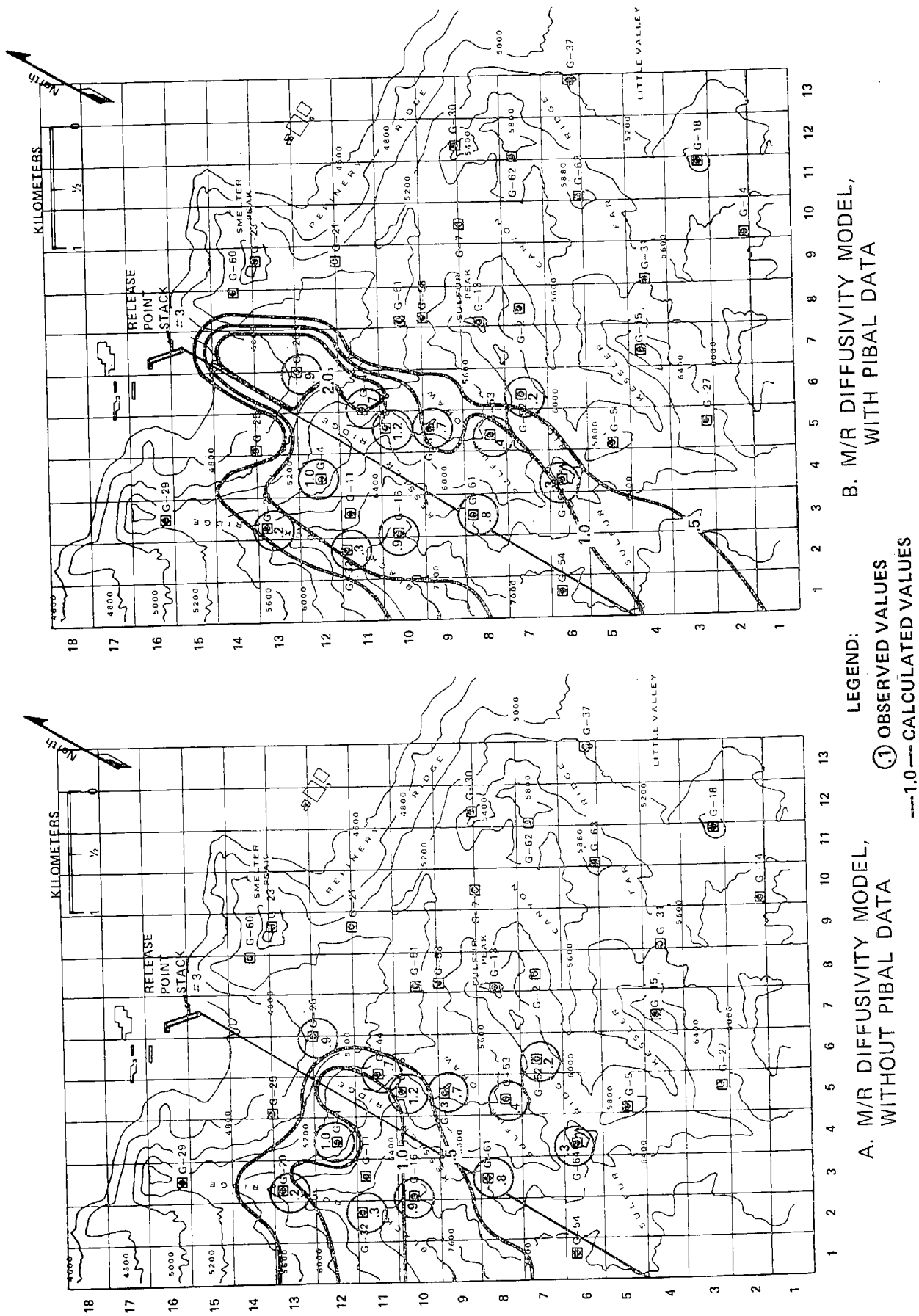
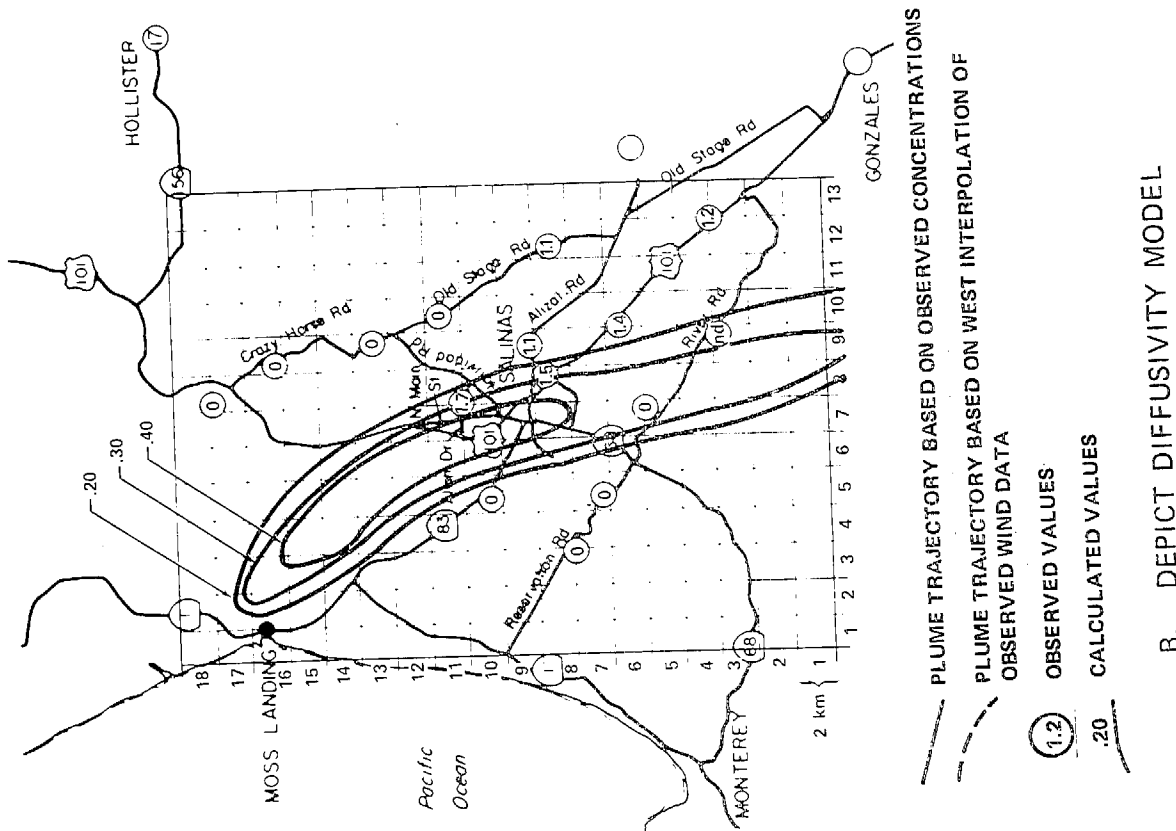


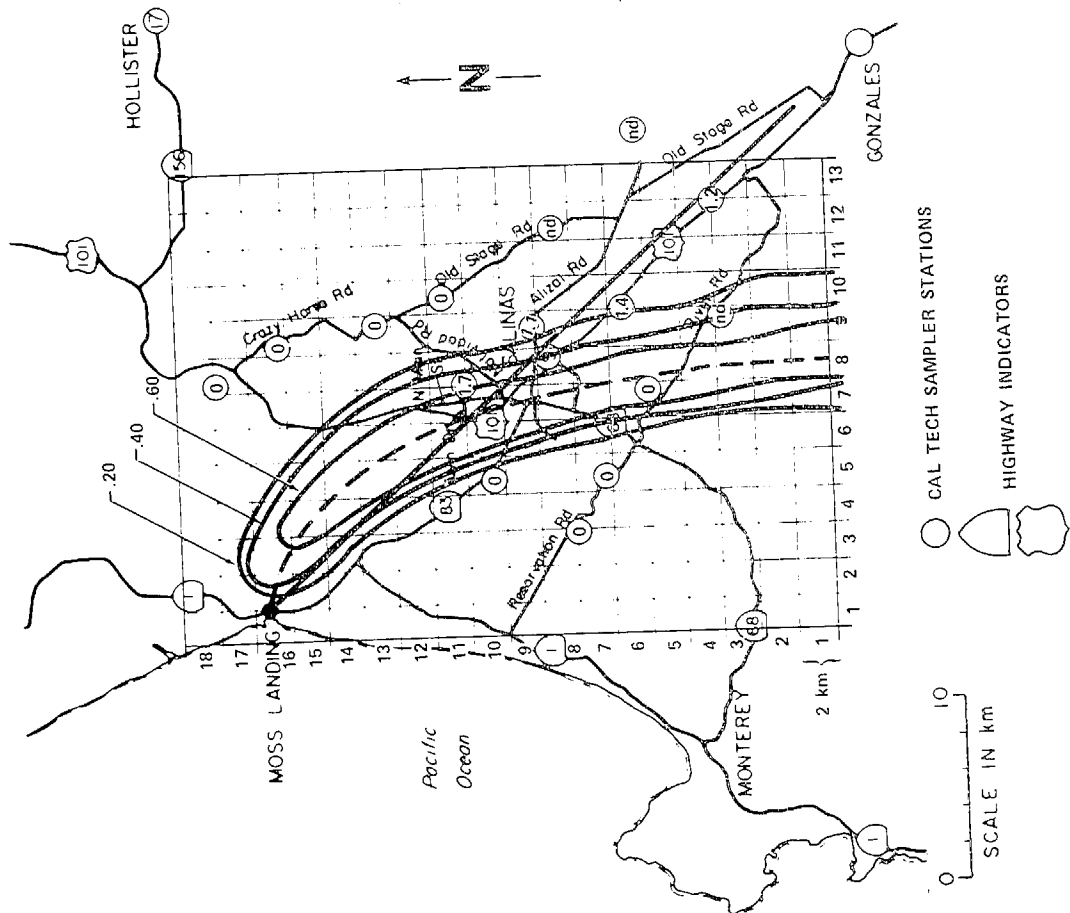
Figure 5-24. Results of IMPACT Validation Using Garfield Test 7 Data, Surface Concentration SF_6 $\mu\text{g}/\text{m}^3$.

The simulation of the Moss Landing Field Test 2 was performed using a 13 by 18 by 7 grid with a 2 km by 2 km by 50 meter cell size. Since a minimal amount of meteorological field data was available, the height of the inversion was set to a constant 250 meters. An atmospheric stability class E was assigned below the inversion and stability class F assigned in the inversion (see Figure 5-8). Six hours were simulated using IMPACT (1100 to 1700); the first 3 hours to initialize the concentration field and the final 3 hours to produce the 3-hour average surface concentration fields shown in Figure 5-25.

The differences between the plume trajectory based on observed surface concentrations and the trajectory based on wind field created by WEST using observed wind data cannot be reconciled due to the limited amount of both observed tracer concentrations and wind data. However, the trajectory produced by WEST does agree with the streamlines developed by MRI (Smith, 1975), the meteorological consultants for the ARB Point Source Field Program. Apparently the minimal number of wind sites is not sufficient to correctly characterize the wind field for this particular test. The difference between the calculated concentrations using the DEPICT and M/R diffusivity models can be best explained by the differences in the two models' treatment of the inversion. In the DEPICT model, the variation of diffusivity from the cell below the inversion to the cell above the inversion is about $25 \text{ m}^2/\text{sec}$ to $10 \text{ m}^2/\text{sec}$; for the M/R model, this variation is $23 \text{ m}^2/\text{sec}$ to $0.11 \text{ m}^2/\text{sec}$. The M/R model describes the inversion as an impermeable lid, while in the DEPICT model the inversion is treated as a barrier that still allows considerable upward diffusion. Therefore, in the run using the DEPICT diffusivity model, a considerable amount of the tracer is diffused into the inversion layer resulting in lower surface concentrations. Drivas and Shair report good agreement with data using a Gaussian plume model and assuming neutral (D) stability. However, the limited amount of sounding data does not support this choice of atmospheric stability.



B. DEPICT DIFFUSIVITY MODEL



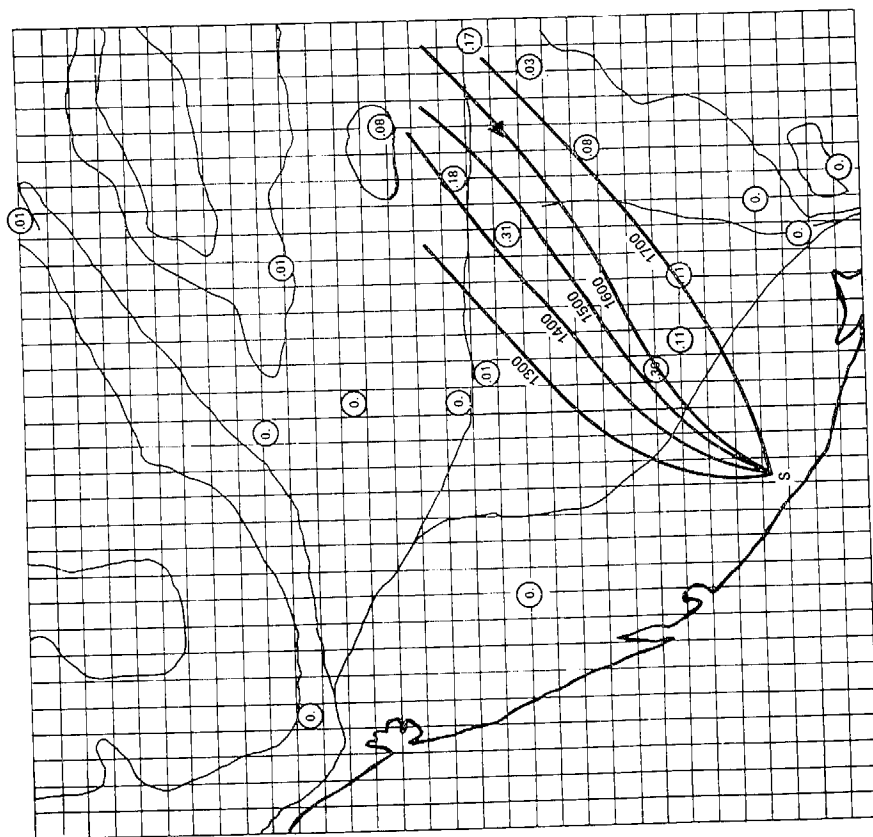
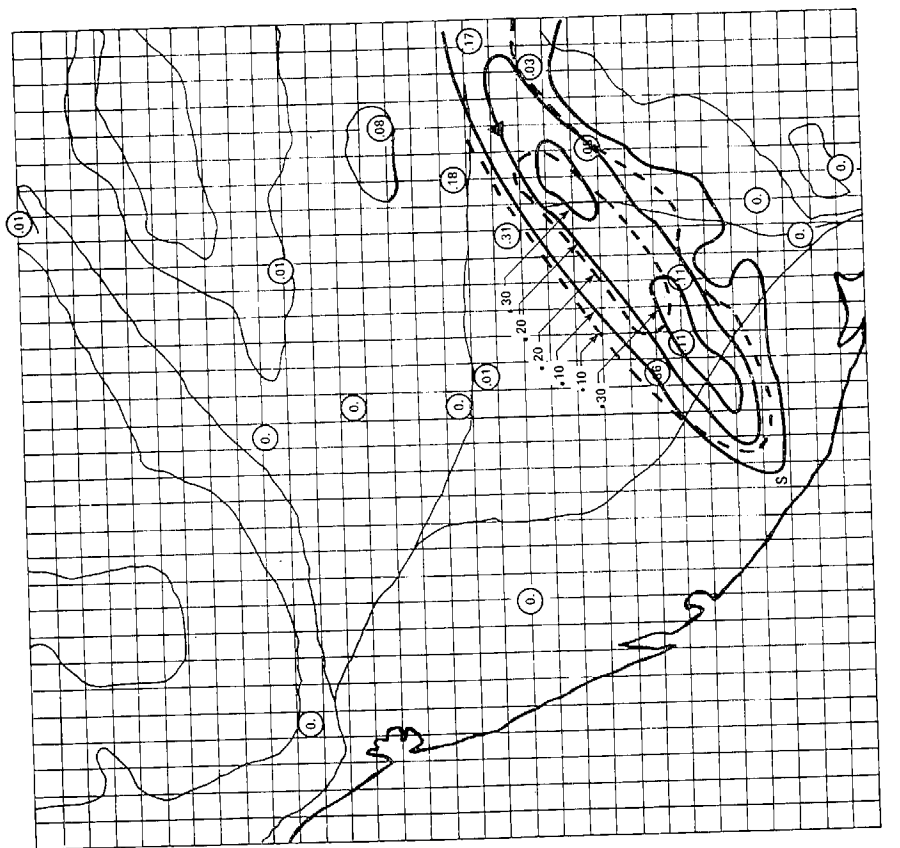
A. M/R DIFFUSIVITY MODEL

Figure 5-25. Results of IMPACT Validation Using Moss Landing Test 2 Data, Surface Concentration SF_6 $\mu\text{g}/\text{m}^3$.

The coarse horizontal resolution of the calculational grid (2 km by 2 km) was partially responsible for the relatively low values of the predicted concentrations, as compared with the observed values. (Instantaneous tracer measurements indicate a plume width of approximately 1 km at 10 km downwind distance.) However, additional simulations using finer resolution were not possible in this study.

The simulation of tracer surface concentration by IMPACT at Ormond Beach was run with a 30 by 30 by 7 grid with each cell 1 km by 1 km by 100 meters. For each hour, all available meteorological data was used to develop the wind and diffusion fields. The simulation was run for 5 hours; the first hour was used to initialize the concentration distribution and the surface concentrations were averaged for the last 4 hours in order to compare with measured data. (The DEPICT diffusivity model was used to develop the diffusion field.) The hour-averaged plume concentration analyzed for ground level centerline, clearly shows the rotation of the wind fields over a period of 4 hours. The major contribution to the 4-hour average occurred at hour 1600 when unstable atmospheric conditions under the inversion brought the high concentrations in the plume to the surface. Thus, the contour of the 4-hour average concentrations lies approximately along the 1600-hour plume centerline as seen in Figure 5-26. A rotation of the simulated surface concentrations of about ten degrees would bring the predicted concentrations into close agreement with the observed values. In view of the uncertainty of the accuracy of the meteorological data (see section 5.2.3), an error of this magnitude is not unreasonable. Once again the question of model precision cannot be adequately assessed because of the lack of precise data.

The photochemical simulation for the Ormond Beach data base was run on a 10 by 7 by 7 grid with each cell 2 km by 2 km by 100 meters, in order to reduce computer storage requirements. A comparison of the 4-hour average tracer concentration for the 1-km



SCALE

0 2 4 6 KM

▲ CAMARILLO APCD STATION

NOTE: CIRCLED VALUES INDICATE MEASURED VALUES

— 1 km RESOLUTION

- - - 2 km RESOLUTION

B. FOUR-HOUR AVERAGE (1400 to 1700)
SF₆ SURFACE CONCENTRATIONS, $\mu\text{g}/\text{m}^3$

A. PLUME CENTERLINE INFERRED FROM
HOUR-AVERAGE TRACER CONCENTRATIONS
BY MEANS OF IMPACT CALCULATIONS

Figure 5-26. Results of IMPACT Validation Using Ormond Beach Test Tracer Data.

and 2-km horizontal resolution simulations is shown in Figure 5-26. The patterns are very similar; however, the high values ($>.30 \mu\text{g}/\text{m}^3$) of the 1-km resolution simulation have been smeared out in the 2-km resolution simulation. The maximum 4-hour average surface concentration for the 1-km resolution simulation was $0.34 \mu\text{g}/\text{m}^3$, while the maximum surface concentration for the 2-km resolution was $0.25 \mu\text{g}/\text{m}^3$, a 26% decrease in maximum surface concentration. An increase in resolution from 1 km to 1/2 km is expected to result in less than a 10% increase in the maximum surface concentrations due to the finite width of the plume and the rotating nature of the wind field. IMPACT was used with a constant pollutant background everywhere outside the plume. Thus, it is possible to simulate the impact of the Ormond Beach power plant without an extensive emissions inventory, but at a reduction in fidelity. Photochemical reactions are only simulated in the cells impacted by the plume; other cells remain at background concentrations. Input pollutant background values were chosen from measurements outside the plume. Background values selected were as follows: $\text{NO}_2 = 2$ pphm, $\text{NO} = 1$ pphm, $\text{O}_3 = 9$ pphm, and reactive HC = 25 pphm. The total measured hydrocarbons were 2 to 3 ppm. However, the GRC photochemistry reaction (CHEM6) mechanism needs reactivity-weighted hydrocarbon (with methane weighted by zero). The fraction of total hydrocarbons which are ARB class III (high reactivity) is exceedingly small. Values less than 10% of total hydrocarbons are typical, so the concentration of reactive HC was set to 25 pphm. The calculated 4-hour averaged NO_2 and NO surface concentrations are shown in Figure 5-27. Power plant emissions, air temperature, and insolation are shown in Table 5-12. The major differences between the calculated and measured concentrations can most likely be attributed to other NO_x sources, particularly traffic along Highway 101. The observed and predicted values show good agreement, and the overall pattern corresponds to the SF_6 tracer concentrations.

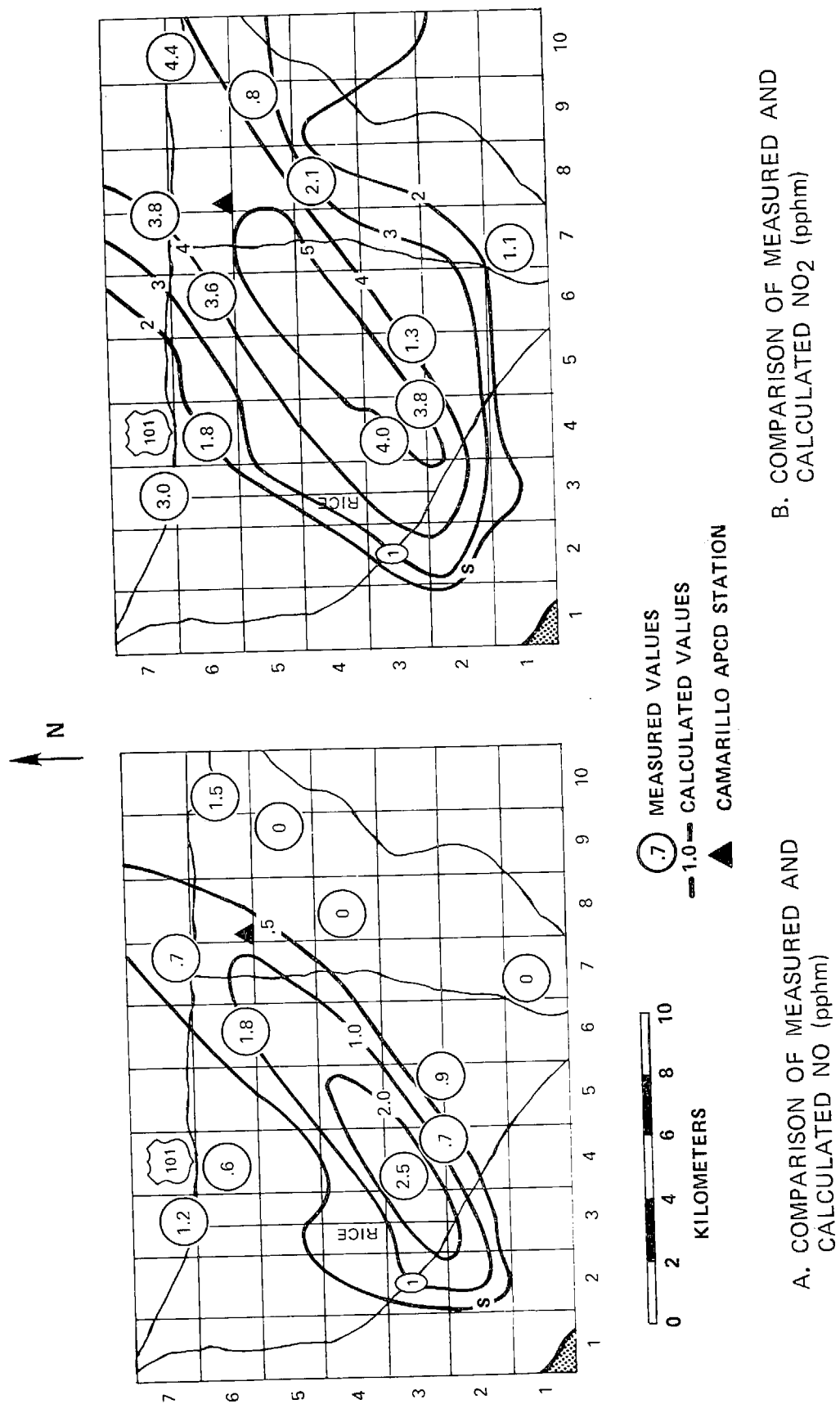


Figure 5-27. NO and NO₂ Concentrations, Comparing 4-Hour Average of Measured and Calculated Values.

Table 5-12. Hourly Data Used in IMPACT Photochemical
Simulation of the Ormond Beach Power Plant

HOUR	POWER PLANT EMISSIONS (G/SEC)		AIR TEMPERATURE AT SURFACE (°C)	SOLAR INSOLATION (WATTS/M ²)
	SF ₆	NO		
14	2.6	609	22	135
15	2.6	609	22	125
16	2.6	609	23	97
17	2.6	609	18	60

The simulation of photochemically produced ozone is perhaps the most demanding test of the model. The NO emitted from the power plant stack reacts with the ambient ozone producing NO₂ and a marked decrease in ozone concentrations. The ozone depression can be easily seen in Figure 5-28, illustrating the hour-averaged ozone concentrations for each hour. The increasingly deeper ozone depression each hour is due to higher plume impact at the surface and decreased insolation which retards the formation of additional ozone.

Although ozone concentrations were not measured as part of the field program, the calculated ozone impact can be corroborated by measurements taken at the Camarillo Ventura Air Pollution Control District (APCD) station. The plume has a major impact at this site only for hour 1600 as shown in Figure 5-29. The ratio of SF₆ at Camarillo to maximum SF₆ at the same radius as Camarillo can be viewed as a measure of the proximity of the plume centerline of Camarillo. The effect on ozone is dramatic: a reduction of 8 ppm in hour 1500 to 5 pphm in hour 1600 and back to 8 in hour 1700; or 9 pphm to 5 pphm to 9 pphm as calculated by IMPACT. The temporal variation of NO_x at Camarillo also confirms the plume impact in hour 1600.

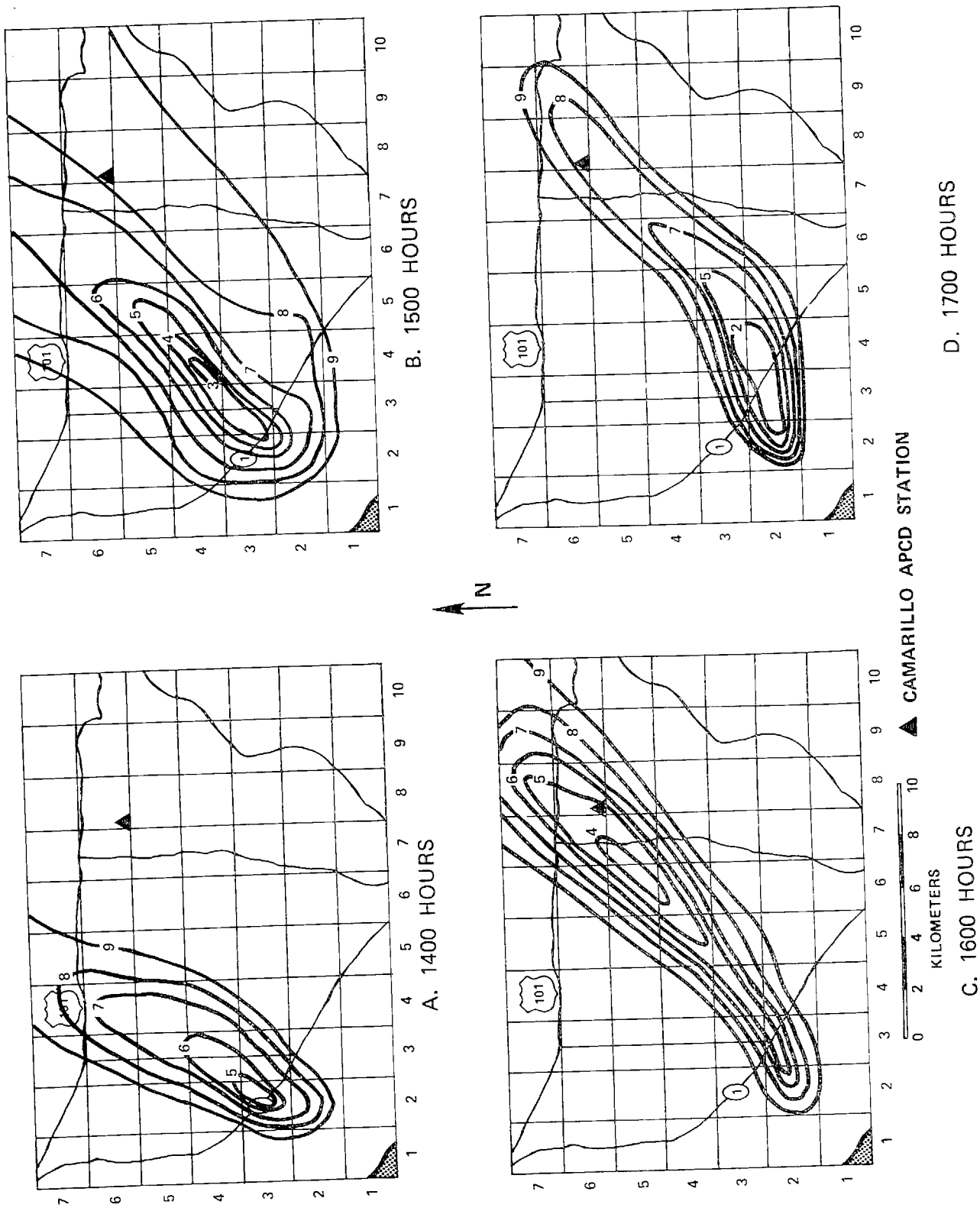


Figure 5-28. Hour-Averaged Ozone Contours (pphm) in Relation to Camarillo APCD Station.

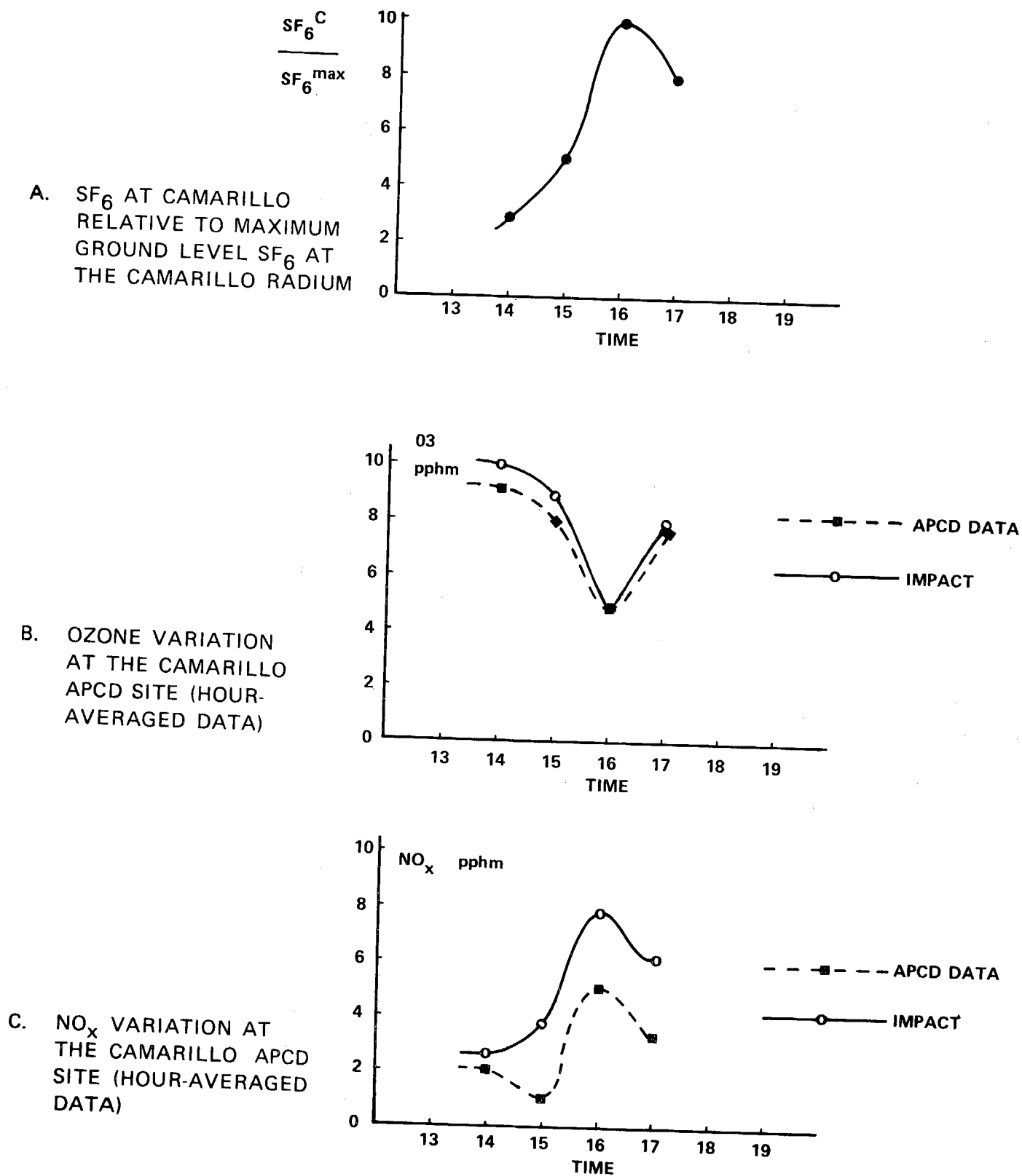


Figure 5-29. Temporal Variation of Pollutant Concentrations at the Camarillo APCD Station in Ventura County.

5.4 Summary of Model Precision, Realism and Generality

As can be seen in the previous discussions, the volume of accurate comprehensive field data from varied locations (needed to thoroughly evaluate point source air quality models) is not yet available. This should not be taken as a discouraging view, however, since it really means that major progress must be based on our understanding of the underlying physical phenomena of the transport and dispersion of air pollutants. Further field programs should be undertaken with clear specification of the physical phenomena being measured.

The framework to establish priorities in field programs and model development can be seen in a review of the discussion of precision, realism, and generality of the two models developed for this program.

Because of limited data available for validation, a precise statement as to model accuracy (complete with confidence limits) cannot be made. However, it is possible to state in a general way the expected accuracy of the Gaussian and grid models. In Table 5-13 the model accuracy is shown as a matrix of the region types and averaging periods of the measurement. Of the 3 x 4 matrix, only two elements have been investigated during this study. In complex terrain, the expected accuracy for short-term (1-hour), maximum pollutant measurement is about a factor of 2 to 3 for the Gaussian model and about a factor of 2 for the grid model, provided that the quality of the input data is at least as good as that taken for the test data.

In coastal regions for medium-term (3 to 4-hour) pollutant measurements, the Gaussian model is accurate to about a factor of 3 to 4 while the grid model is accurate to a factor of 2. Because of the limited resolution of the coastal data, model accuracy for a one-hour averaging time was not investigated. However, it is expected to be worse than the accuracy for the three-hour average. Model accuracy for longer measurement times (i.e., 24 hours, one year) was not examined as it was beyond the scope of this study.

Table 5-13. Summary of Model Precision.

REGION \ AVERAGING PERIOD	1-HOUR	3-HR.	24-HR.	ANNUAL
	1-HOUR	3-HR.	24-HR.	ANNUAL
FLAT OR ROLLING	NOT TESTED IN THIS PROGRAM; SHOULD BE MORE ACCURATE THAN THE OTHER REGIONS HOWEVER			REQUIRES MODIFICATION FOR USING STAR-TYPE DATA OR THE USE OF METEOROLOGICAL REGIME ANALYSIS
COMPLEX TERRAIN	<u>GEM</u> FACTOR OF 2 TO 3 FACTOR OF ~2 <u>IMPACT</u>	NOT TESTED IN THIS PROGRAM	NOT TESTED IN THIS PROGRAM	
COASTAL	NOT EXAMINED IN THIS PROGRAM, BUT LIKELY TO BE WORSE THAN 3-HR AVERAGE	<u>GEM</u> FACTOR OF 3 TO 4 FACTOR OF 2 4-HR AVG <u>IMPACT</u>		

Predictions of annual average concentrations would require modification of both types of models due to the excessive costs of data collection and computer time that would be incurred if the existing models were to be used hour-by-hour for a whole year.

The degree of realism of the various models (pollutant, transport, dispersion, plume rise and chemistry) used in air quality models varies from assumed constant values and curves derived from field data, to complex solutions of coupled non-linear differential equations. A summary of model realism is shown in Table 5-14 where representative examples of the relative realism of the various submodels are used to estimate pollutant transports, dispersion plume rise, and chemistry. Submodels that are included in the GEM and IMPACT models are indicated. It is apparent that, in general, to increase realism means to increase the complexity and, hence, cost of the model. Thus, while the submodels used in the grid model are more realistic (and by inference more accurate), they are also more expensive than the modules used in the Gaussian models.

The coincidence of model realism, accuracy, and cost indicates that a hierarchy of models would provide the most cost-effective method for the evaluation of point source impact.

A diagram of this hierarchical method to investigate the impact of a point source on air quality is indicated in Figure 5-30. In practice, the impact of a point source could involve a number of separate pollutants, each of which could have a number of air quality standards (i.e., maximum allowed concentrations for a specified averaging time). However, a single pollutant is assumed in this example. Since the cost of each succeeding step is greater than the previous, this type of screening practice is very cost-effective. It is also of interest to note that the improvement of model accuracy at any level (i.e., decreasing the uncertainty factor, μ) would produce a considerable cost-savings since the screening procedure could eliminate marginal cases from additional consideration. Therefore, the incentive to increase model accuracy for both Gaussian and grid models still exists even though the grid models are considerably more precise than the Gaussian models.

Table 5-14. Summary of Model Realism by Submodel.

TRANSPORT	DISPERSION	PLUME RISE	CHEMISTRY
<p>STANDARD GAUSSIAN</p> <p>CURVED WIND GAUSSIAN</p> <p>CRAMER</p> <p>EPA</p> <p>NOAA</p> <p>ERT</p> <p>SPECIFIED WIND FIELD</p> <p>TWO-DIMENSIONAL WIND FIELD THERMALLY DRIVEN</p> <p>MATHEW</p> <p>WEST</p> <p>THREE-DIMENSIONAL FINITE DIFFERENCE SOLUTION OF NAVIER-STOKES EQUATION</p>	<p>SPECIFIED K_x, K_y CONSTANTS</p> <p>σ_y, σ_z TURNER</p> <p>σ_z PROPOSED EPA</p> <p>σ_z PROPOSED PASQUILL SMITH</p> <p>σ_y EPA, PASQUILL</p> <p>DEPICT</p> <p>M/R MODEL</p> <p>HIGHER ORDER CLOSURE MODEL</p>	<p>SPECIFIED</p> <p>TVA</p> <p>BRIGGS</p> <p>BRIGGS' ANALYTIC CONTINUATION</p> <p>LAGRANGIAN-EULERIAN FINITE DIFFERENCE HYDRODYNAMIC</p> <p>THREE-DIMENSIONAL FINITE DIFFERENCE HYDRODYNAMIC</p>	<p>INERT POLLUTANT</p> <p>EXPONENTIAL DECAY</p> <p>WILSON SULFATE MODEL</p> <p>GRC 14-STEP PHOTOCHEMISTRY</p> <p>HECHT-SEINFELD - DODGE PHOTOCHEMISTRY</p> <p>DETAILED PHOTOCHEMISTRY PLUS SO_2, SO_4</p>

LEGEND:

IN GEM

IN IMPACT

IN BOTH GEM AND IMPACT

NOT IMPLEMENTED

ZEROth ORDER APPROXIMATION, USUALLY A SPECIFIED CONSTANT

REALISM

CONTAINS ALL KNOWN RELEVANT PHYSICS

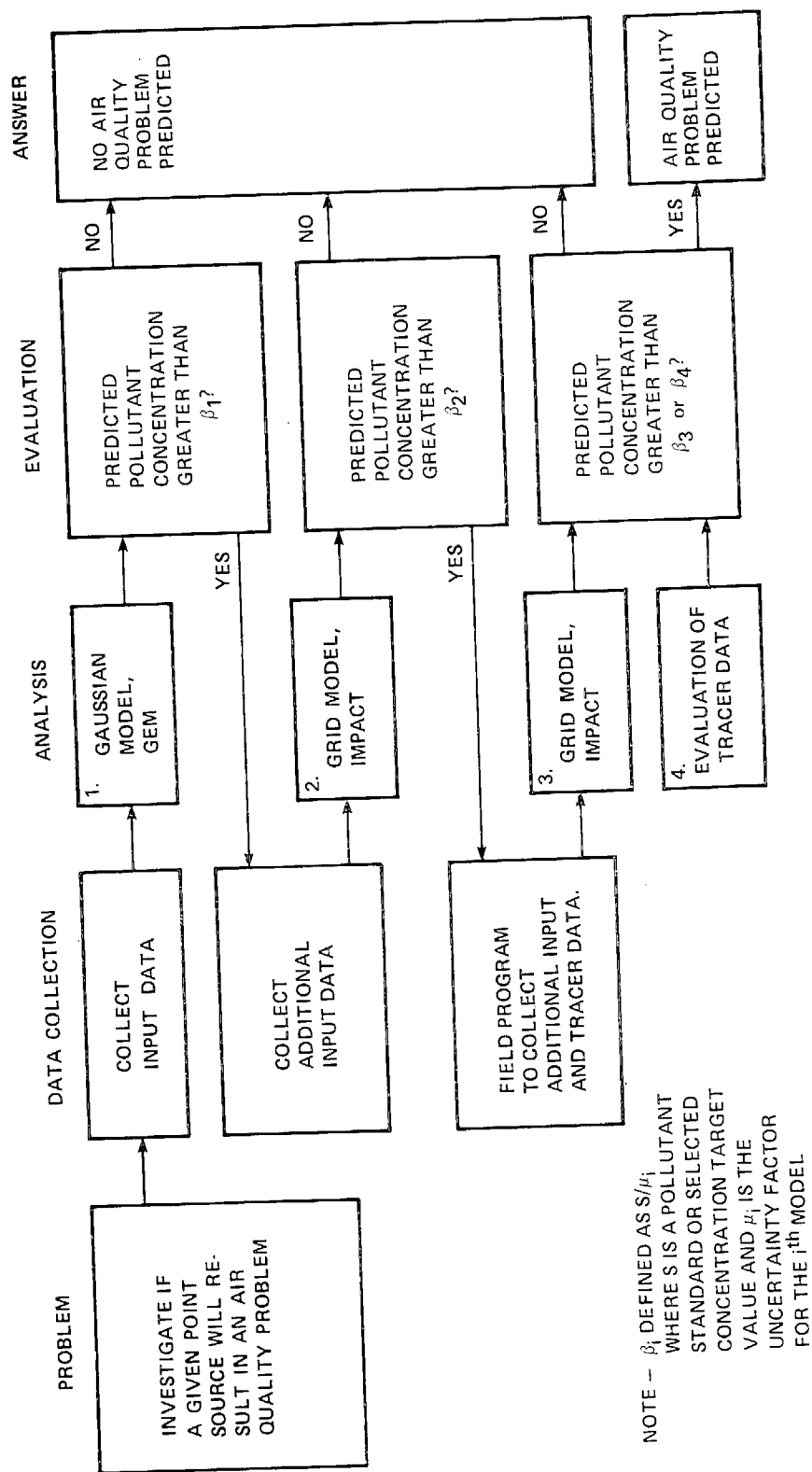


Figure 5-30. Hierarchical Analysis of Air Quality Impact from Point Sources.

The final consideration for model validation, the generality of the model, has been partially answered by the discussion of model precision and realism. A summary of model generality in terms of the applicability of the model for various pollutant averaging periods, source location, and type of pollutant is indicated in Table 5-15. Both Gaussian and grid models can be used for 1, 3 and 24-hour averaging times, for flat or rolling terrain, and for inert pollutants. The Gaussian model cannot be used for photochemical pollutants and its use is problematic for sulfur oxide pollutants or in complex terrain or coastal regions.

Table 5-15. Summary of Model Generality.

MODEL TYPE EVALUATION CRITERIA		GEM	IMPACT
TIME PERIOD	1-HOUR	YES	YES
	3-HOUR	YES	YES
	24-HR.	YES	YES
	ANNUAL	REQUIRES MODIFICATION FOR STAR DATA	REQUIRES THE DEVELOPMENT OF METEOROLOGICAL REGIME METHODOLOGY
REGION	FLAT OR ROLLING	YES	YES
	COMPLEX	FOR INITIAL EVALUATION ONLY	YES
	COASTAL		YES
POLLUTANT TYPE	INERT POLLUTANT	YES	YES
	SULFATES	ONLY WITH EXPONENTIAL DECAY	SIMPLIFIED SO ₂ CONVERSION MODEL
	PHOTO-CHEMICAL	NO	YES

6.0 REFERENCES

- Anderson, G. E., "Mesoscale Influences on Wind Fields." The Center for the Environment and Man, December, 1970.
- Appel, B. R., and others. "Sulfate Formation from Stationary SO₂ Sources in Clean and Polluted Air." Air Resources Board, Interagency Agreement ARB-948, February, 1976.
- Arakawa, A. "Computational Design for Long-Term Numerical Integration of the Equations of Fluid Motion: Two-Dimensional Incompressible Flow. Part 1." U.C.L.A. Department of Meteorology, Contribution No. 122, 1966.
- Bass, A. Principal scientist at Meteorology Laboratory, Flow Research, Inc., Personal communication with Dr. K. Caulder.
- Boris, J. P. "SHAS2D: A Fully Compressible Hydrodynamics Code in Two Dimensions." Naval Research Laboratory, Memorandum Report No. 2542, December, 1972.
- Briggs, G. A. Plume Rise. AEC Critical Review Series, 1969.
- Briggs, G. A. "Plume Rise Predictions." National Oceanic and Atmospheric Administration, June, 1975.
- Busse, A. D., and J. R. Zimmerman. "User's Guide for the Climatological Dispersion Model." Washington: Environmental Protection Agency Report EPA-R4-73-024, January, 1973.
- Cadle, S. H., and others. "General Motors Sulfate Dispersion Experiment." General Motors Research, January, 1977.

Carpenter, S. B., and others. "Principal Plume Dispersion Models: TVA Power Plants." APCA Journal, XXI, No. 8 (August, 1971).

"The Chemistry, Dispersion, and Transport of Air Pollutants Emitted from Fossil Fuel Power Plants: Moving Laboratory Support for Plume Analysis." Environmental Measurements, Inc. (EMI), Air Resources Board Contract No. 4-187, April, 1975.

Chock, D. P. "General Motors Sulfate Dispersion Experiment: Assessment of the EPA HIWAY Model." Journal of the Air Pollution Control Association, XXVII, No. 1 (January, 1977).

Cramer, H. E., and others. Diffusion-Model Calculations of Long- and Short-Term Ground Level Concentrations Produced by the Major SO₂ Stationary Sources in Allegheny County, Pennsylvania. H. E. Cramer Co., 1971.

Cramer, H. E., and others. Assessment and Updating of Particulate Emissions. H. E. Cramer Co., January, 1976.

Drivas, P. J., and F. H. Shair. "The Chemistry, Dispersion, and Transport of Air Pollutants Emitted from Fossil Fuel Power Plants in California: Plume Tracer (SF₆) Measurement and Analyses." California Institute of Technology, June, 1975.

Egan, B. A. "Turbulent Diffusion in Complex Terrain." Paper presented at the American Meteorological Society, September, 1975.

Eschenroeder, A. Q. "Evaluation of a Diffusion Model for Photochemical Smog Simulation." Environmental Protection Agency Publication EPA-R4-73-012, 1972.

- "Evaluation of Selected Air Pollution Dispersion Models Applicable to Complex Terrain." INTERCOMP. Environmental Protection Agency Publication EPA-450/3-75-059, 1975.
- Fabrick, A. J. "Mathematical Modeling of Reactive Point Sources." Air Pollution Control Association Publication 74-120, June, 1974.
- Fabrick, A. J., and others. "A Methodology for Treating Large Localized Emissions of Reactive Pollutants." Environmental Protection Agency Publication EPA-650/4-74-006, February, 1974.
- Fabrick, A. J., and R. C. Sklarew. "Oregon/Washington Diffusion Modeling Study." Xonics, Inc., June, 1975.
- Fosberg, M. A. "Estimating Airflow Patterns Over Complex Terrain." USDA Forest Service, March, 1976.
- Freeman, B. E. "Tensor Diffusivity of a Trace Constituent in a Stratified Boundary Layer." Pending publication of Journal of Atmospheric Sciences (1976).
- Freeman, B. E., and J. R. Taft. "Three-Dimensional Windfield and Diffusivity Models for Atmospheric Dispersion Over Complex Terrain." Science Applications, Inc., June, 1975.
- Galenis, R. (senior scientist, Science Applications, Inc.) Personal communication. January, 1977.
- Gifford, F. A. "Atmospheric Dispersion Models for Environmental Pollution Applications." Paper presented at the American Meteorological Society, September, 1975.

- Haugen, D. A. "Lectures on Air Pollution and Environmental Impact Analyses." American Meteorological Society, 1975.
- Hecht, T. A., and J. H. Seinfeld. "Further Development of Generalized Kinetic Mechanism for Photochemical Smog." Environmental Science and Technology, LXXXIV, No. 327, (1974).
- Hirt, C. W., and R. S. Hotchkiss. "Particulate Transport in Highly Distorted Three-Dimensional Flow Fields." University of California, Los Alamos, Scientific Laboratory, June, 1972.
- Intercomp Resources Development and Engineering, Inc., "Evaluation of Selected Air Pollution Dispersion Models Applicable to Complex Terrain." EPA-450/3-75-059, June 1975.
- Katz, M. "Photoelectric Determination of Atmospheric SO₂ Employing Dilute Starch-Iodine Solution." Anal. Chem., XXII, 1040-1047 (1950).
- Lantz, R. B. "Application of a Three-Dimensional Numerical Model to Air Pollutant Calculations." Paper No. 72-141 presented at the 65th Annual Meeting of APCA, June, 1972.
- Lissaman, P. B. S. "A Simple Unsteady Concentration Model Explicitly Incorporating Ground Roughness and Heat Flux." Air Pollution Control Association Publication No. 73-129, June, 1973.
- Liu, M. K., and others. "Assessment of the Feasibility of Modeling Wind Fields Relevant to the Spread of Brush Fires." Science Applications, Inc., December, 1974.

- Liu, M. K., and others. "The Chemistry, Dispersion, and Transport of Air Pollutants Emitted from Fossil Fuel Power Plants in California: Data Analysis and Emission Impact Model." Systems Applications, Inc., September, 1976.
- Long, P. E., and D. W. Pepper. "A Comparison of Six Numerical Schemes for Calculating the Advection of Atmospheric Pollution." E. I. duPont de Nemours & Co.
- Lyons, W. A. "Turbulent Diffusion and Pollutant Transport in Shoreline Environments." Paper presented at the American Meteorological Society, September, 1975.
- Martin, B. Numerical Representations Which Model Properties of the Solution to the Diffusion Equation. Academic Press, Inc., 1975.
- Mellor, G., and T. Yamada. "A Hierarchy of Turbulence Closure Models for Planetary Boundary Layers." Journal of Atmospheric Science, XXXI, 1791-1806, 1974.
- Meyer, J. P., and D. R. Durran. "Evaluation of the Suitability of the Shasta, Price, and Egan and Mahoney Integration Schemes in Photochemical Simulation Programs." Systems Applications, Inc. Report ER76-140A, 1976.
- Molenkamp, C. R. "Accuracy of Finite-Difference Methods Applied to the Advection Equation." Journal of Applied Meteorology, VII (April, 1968), 160-167.
- Montgomery, T. L. Summary of Tennessee Valley Authority Atmospheric Dispersion Modeling. Tennessee Valley Authority, October, 1974.

- Moore, D. "A Comparison of the Trajectories of Rising Buoyant Rising Plumes with Theoretical/Empirical Models." Atmospheric Environment, VIII, 441-457, 1974.
- Moses, H., and G. H. Strom. "A Comparison of Observed Plume Rises with Values Obtained from well-known Formulas." Journal of the Air Pollution Control Association, II, 455-466, 1961.
- Myrup, L. O., and A. J. Ranzieri. "A Consistent Scheme for Estimating Diffusivities to be Used in Air Quality Models: Interim Report." California Department of Transportation, June, 1976.
- Pasquill, F. Atmospheric Diffusion. Second Edition. John Wiley & Sons, 1974.
- Pasquill, F. "The Dispersion of Material in the Atmospheric Boundary Layer - The Basis for Generalization." Paper presented at the American Meteorological Society, September, 1975.
- Pasquill, F. "Atmospheric Dispersion Parameters in Gaussian Plume Modeling - Part II: Possible Requirements for Change in the Turner Workbook Values." Environmental Protection Agency Publication EPA-600/4-76-0306, June, 1976.
- Phillips, G. T., and others. "A Numerical Model for non-linear Waves." Science Applications, Inc. Publication SAI-76-605-LJ, 1974.
- Phillips, G. T. "Semi-annual Progress Report - Wind Energy Siting Program." Energy Resources and Development Administration (ERDA) Publication, January, 1977.

- Reynolds, S. D., and others. "Model Development and Refinement Final Report, Vol. II." Environmental Protection Agency Publication, July, 1975.
- Richards, L. W., and others. "The Chemistry, Dispersion, and Transport of Air Pollutants Emitted from Fossil Fuel Power Plants in California: Ground Level Pollutant Measurement and Analysis." Rockwell International, February, 1976.
- Sasaki, Y. "Some Basic Formalisms in Numerical Variational Analysis." Monthly Weather Review, XCVIII, No. 875 (1970).
- Shair, F. H. (California Institute of Technology). Personal communication. December, 1976.
- Sherman, C. A. "A Mass-Consistent Model for Wind Fields Over Complex Terrain." Unpublished report of Lawrence Livermore Laboratory, UCRL-76171, 1976.
- Shirai, T., and others. "Photooxidation of SO₂ in Air." Koggo-Kagaku Zasshi, LXV, No. 1906 (1962).
- Sklarew, R. C., and A. J. Fabrick. "HAIFA: Hydrodynamics using the Almost Incompressible Flow Approximation." Systems Science and Software, (December, 1970).
- Sklarew, R. C., and others. "A Particle-in-Cell Method for Numerical Solution of the Atmospheric Diffusion Equation, and Applications to Air Pollution Problems." Systems, Science and Software (November, 1971).
- Sklarew, R. C., and J. C. Wilson. "Study of Data from the Ormond Beach Generating Station Impact Field Program 1972-1973." Report to Southern California Edison Company, March, 1975.

Sklarew, R. C., and J. C. Wilson. "Air Quality Models Required Data Characterization." Science Applications, Inc., May, 1976.

Sklarew, R. C., and J. C. Wilson. "Applications of DEPICT to the Garfield, Navajo, and Ormond Beach Air Quality Data Bases." Science Applications, Inc., July, 1976.

Slade, D. Meteorology and Atomic Energy. U.S. Atomic Energy Commission, 1968.

Smith, F. B. "The Diffusion of Smoke from a Continuous Elevated Point-Source into a Turbulent Atmosphere." Journal of Fluid Mechanics, II, No. 49 (1957).

Smith, T. B., and S. M. Howard. "Methodology for Treating Diffusivity." Meteorology Research, Inc. (MRI) Publication FR-1020, 1972.

Smith, T. B., and others. "The Chemistry, Dispersion, and Transport of Air Pollutants Emitted from Fossil Fuel Power Plants in California: Airborne Pollutant Measurement and Analysis." Meteorology Research, Inc. (MRI), November, 1975.

Start, G. E., and others. "Effluent Dilutions Over Mountainous Terrain." National Oceanographic and Atmospheric Administration (NOAA) Technical Memorandum ERL ARL-51, Idaho Falls, Idaho, December, 1974.

Turner, D. B. Workbook of Atmospheric Dispersion Estimates. Environmental Protection Agency (Revised), 1970.

Winiarski, L., and W. Frick. Cooling Tower Plume Model. Environmental Protection Agency, 1975.

Winiarski, L., and W. Frick. A Simple Numerical Plume Model.
Environmental Protection Agency, June, 1976.

Yanenko, N. N. Method of Fractional Steps. New York: Springer-
Verlag, 1971.

00004349



ASSET